Universitat Politècnica de València
Departamento de Máquinas y Motores Térmicos


# Theoretical and experimental study on the autoignition phenomena of homogeneous reactive mixtures

Doctoral Thesis
Presented by:
Darío López Pintor
Directed by:
Prof. José María Desantes Fernández
and
Dr. José Javier López Sánchez

Valencia, September 29, 2017

# Doctoral Thesis

## Theoretical and experimental study on the autoignition phenomena of homogeneous reactive mixtures


Presented by: Darío López Pintor
Directed by: Prof. José María Desantes Fernández
Dr. José Javier López Sánchez


Examining Board:

President: Prof. Jesús Vicente Benajes Calvo
Secretary: Prof. Juan José Hernández Adrover
Examiner: Dr. Ezio Mancaruso

Reviewing Board:

Prof. Octavio Armas Vergel
Dr. Paul C. Miles
Dr. Ezio Mancaruso

Valencia, September 29, 2017

**Resumo.** O autoencendido é unha modalidade de combustión con especial relevancia en todo tipo de motores de combustión interna alternativos (MCIA). O seu estudo ten interese non só porque sexa o principio de funcionamento básico dos motores de encendido por compresión, senon tamén porque é necesario evitalo autoencendido nos motores de ignición forzada, onde este pode ter consecuencias catastróficas. A relevancia deste fenómeno viuse recentemente incrementada debido ás novas tendencias de combstión en MCIA. Como resposta ás normativas anticontaminación cada vez máis rigorosas e á preocupación cada vez maior polo consumo de combustíbeis fósiles, apareceron novos modos de combustión con potencial para xerar motores con cero emisións de óxidos de nitróxeno e de borralla, así coma de mante-lo alto rendemento. Moitos destos novos modos de combustión baséanse precisamente no autoencendido controlado dunha mestura reactiva, máis ou menos homoxénea, nun ambiente con certo déficit de osíxeno.

O obxectivo de devandita Tesis Doutoral é o estudo do fenómeno do autoencendido de mesturas reactivas dende un punto de vista teórico e experimental. Realizouse un amplo estudo paramétrico nunha Máquina de Compresión-Expansión Rápida (RCEM polas súas siglas en inglés) barrendo diversas temperaturas iniciais, relacións de compresión, dosados relativos e fraccións molares de osíxeno (mediante o uso de EGR sintético) para distintos combustíbeis. O tempo de retraso do fenómeno de chamas frías (no caso de se atoparen), así coma o tempo de retraso da etapa de alta temperatura, obtivéronse experimentalmente, sendo as súas tendencias explicadas mediante cinética química.

Estudáronse os diferentes efectos das distintas especies involucradas no EGR sintético sobre o tempo de retraso, deslindando aqueles de carácter termodinámico dos efectos puramente químicos. Tivéronse en conta distintas composicións para definir devandito EGR, chegando a establecer limites de validez para candasúa mistura. Os efectos termodinámicos e químicos resultaron ser opostos, sendo dominante un ou outro a distintos rangos de temperatura de traballo.

Validáronse varios mecanismos de cinética química grazas ós resultados experimentais obtidos. Ademáis dun mecanismo detallado para mesturas PRF de iso-octano máis n-heptano, levouse a cabo a análise doutro mecanismo simplificado para o n-dodecano. Porén, validouse un submodelo de xeración e decaemento de OH* excitado contra resultados de quimioluminiscencia e espectroscopía.

Estudáronse as distintas fontes de radiación do proceso de autoencenido para o iso-octano e o n-heptano por medio da aplciación de técnicas de espectroscopía. Asemade, realizáronse medidas de quimioluminiscencia filtrada a 310 $nm$ (lonxitude de onda de emisión do radical OH*) para a análise da xeneralización e da velocidade de propagación da fronte de autoencendido. A propagación do encendido mostrou ser dependente das condicións termodinámicas achadas na cámara de combustión no intre de ignición máis que da reactividade da mistura. Ademáis, atopáronse dúas fontes distintas de radiación a 310 $nm$ mediante espectroscopía, dependendo da intensidade do encendido: o decaemento do radical OH* de estado excitado a natural e a oxidación de CO a $CO_2$ (contínuo do CO). Nembargantes, estas técnicas tan so foron utilizadas

para os dous combustíbeis de referencia da escala de octanaxe debido a limitacións técnicas.

Á fin, un novo modelo preditivo foi desenvolvido teóricamente partindo do modelo de Glassman para o autoencendido. Este método basease en modelar primeiro a tasa de acumulación de portadores de cadea até a súa concentración crítica (obtendo así o tempo de retraso referido a etapa de chamas frías) e, tras ese intre, modelar a tasa de consumo dos mesmos portadores de cadea até a súa completa desaparición (intre no cal se da a máxima exotermia de proceso, predicindo o tempo de retraso referido á etapa de alta temperatura). Comprobouse a capacidade preditiva do modelo para cada un dos seis combustíbeis ensaiados. Asemade, dita capacidade preditiva foi comparada ca de outros métodos existentes na literatura, coma é a integral de Livengood & Wu. De feito, analizouse a validez de cada un dos métodos, definindo unha metodoloxía de uso para obter predicción razoables do tempo de retraso.

**Resumen.** El autoencendido es una forma de combustión de especial relevancia en todo tipo de motores de combustión interna alternativos (MCIA). Su estudio tiene interés no solo porque sea el principio de funcionamiento básico de los motores de encendido por compresión, sino también porque es necesario evitar el autoencendido en motores de ignición forzada, donde éste tiene consecuencias catastróficas. La relevancia de este fenómeno se ha visto incrementada enormemente en los últimos años debido a las nuevas tendencias de combustión en MCIA. Como respuesta al endurecimiento de las normativas anti-contaminación y a la preocupación cada vez mayor por el consumo de combustibles fósiles, han aparecido nuevos modos de combustión con potencial para conseguir motores de cero emisiones de óxidos de nitrógeno y de hollín, así como de elevado rendimiento. Muchos de estos nuevos modos de combustión se basan precisamente en el autoencendido controlado de una mezcla reactiva, más o menos homogénea, en un ambiente con cierto déficit de oxígeno.

El objetivo de esta Tesis Doctoral es el estudio del fenómeno de autoencendido de mezclas reactivas desde un punto de vista teórico y experimental. Se ha realizado un amplio estudio paramétrico en una Máquina de Compresión-Expansión Rápida (RCEM por sus siglas en inglés) barriendo diversas temperaturas iniciales, relaciones de compresión, dosados relativos y fracciones molares de oxígeno (mediante el uso de EGR sintético) para distintos combustibles. El tiempo de retraso del fenómeno de llamas frías (en el caso de existir), así como el tiempo de retraso de la etapa de alta temperatura, han sido obtenidos experimentalmente y sus tendencias explicadas mediante cinética química.

Se han estudiado los diferentes efectos de las distintas especies involucradas en el EGR sintético sobre el tiempo de retraso, desligando aquellos de carácter termodinámico de los efectos puramente químicos. Se han tenido en cuenta distintas composiciones para definir dicho EGR, estableciendo límites de validez para cada una de las mezclas propuestas. Los efectos termodinámicos y químicos resultaron ser opuestos, siendo dominante uno u otro a distintos rangos de temperatura de trabajo.

Varios mecanismos de cinética química han sido validados gracias a los resultados experimentales obtenidos. Además de un mecanismo detallado para mezclas PRF de iso-octano y n-heptano, se ha llevado a cabo la validación de otro mecanismo simplificado para el n-dodecano. Por otro lado, un submodelo de formación y decaimiento de OH* excitado ha sido validado contra resultados de quimioluminiscencia y espectroscopía.

Se han estudiado las diferentes fuentes de radiación del proceso de autoencendido para el iso-octano y el n-heptano mediante técnicas de espectroscopía. Además, se han realizado medidas de quimioluminiscencia filtrada a 310 $nm$ (longitud de onda de emisión del radical OH*) para el análisis de la generalización y velocidad de propagación del frente de autoencendido. La propagación del encendido ha mostrado ser dependiente de las condiciones termodinámicas alcanzadas en la cámara de combustión en el instante de ignición más que de la reactividad de la mezcla. Se han encontrado dos fuentes de radiación distintas a 310 $nm$ mediante espectroscopía, dependiendo de la intensidad del encendido: el decaimiento del radical OH* de estado excitado a estado natural y la oxidación del CO a $CO_2$ (continuo del CO). No obstante,

estas técnicas han sido utilizadas solamente para los dos combustibles de referencia de la escala de octanaje debido a limitaciones técnicas.

Finalmente, se ha desarrollado un nuevo modelo predictivo de manera teórica partiendo del modelo de Glassman para el autoencendido. Este método se basa en modelar primero la tasa de acumulación de portadores de cadena hasta su concentración crítica (obteniendo así el tiempo de retraso referido a la etapa de llamas frías) y, tras dicho instante, modelar la tasa de consumo de dichos portadores de cadena hasta su completa desaparición (instante en el cual se produce la máxima exotermia del proceso, prediciendo el tiempo de retraso referido a la etapa de alta temperatura del encendido). La capacidad predictiva del modelo ha sido comprobada para cada uno de los seis combustibles ensayados. Además, dicha capacidad predictiva ha sido comparada con la de otros métodos existentes en la literatura, como la integral de Livengood & Wu. La validez de cada uno de los métodos ha sido analizada, definiendo una metodología de uso para obtener predicciones razonables del tiempo de retraso.

**Resum.** L'autoencesa és una forma de combustió d'especial rellevància en tot tipus de motors de combustió interna alternatius (MCIA). El seu estudi té interès no solament perquè és el principi de funcionament bàsic dels motors d'encesa per compressió, sinó també perquè és necessari evitar l'autoencesa en motors d'ignició forçada, on aquest té conseqüències catastròfiques. La rellevància d'aquest fenomen s'ha vist incrementada enormement en els últims anys a causa de les noves tendències de combustió en MCIA. Com a resposta a l'enduriment de les normatives anti-contaminació i a la preocupació cada vegada major pel consum de combustibles fòssils, han aparegut noves maneres de combustió amb potencial per a aconseguir motors de zero emissions d'òxids de nitrogen i de sutge, així com d'elevat rendiment. Moltes d'aquestes noves maneres de combustió es basen precisament en l'autoencesa controlada d'una mescla reactiva, més o menys homogènia, en un ambient amb cert dèficit d'oxigen.

L'objectiu d'aquesta Tesi Doctoral és l'estudi del fenomen d'autoencesa de mescles reactives des d'un punt de vista teòric i experimental. S'ha realitzat un ampli estudi paramètric en una Màquina de Compressió-Expansió Ràpida (RCEM per les seues sigles en anglès) cobrint diverses temperatures inicials, relacions de compressió, dosatges relatius i fraccions molars d'oxigen (mitjançant l'ús de EGR sintètic) per a diferents combustibles. El temps de retard del fenomen de flames fredes (en el cas d'existir), així com el temps de retard de l'etapa d'alta temperatura, han sigut obtinguts experimentalment i les seues tendències explicades mitjançant cinètica química.

S'han estudiat els diferents efectes de les diferents espècies involucrades en l'EGR sintètic sobre el temps de retard, deslligant aquells de caràcter termodinàmic dels efectes purament químics. S'han tingut en compte diferents composicions per a definir aquest EGR, establint límits de validesa per a cadascuna de les mescles proposades. Els efectes termodinàmics i químics van resultar ser oposats, sent dominant un o un altre a diferents rangs de temperatura de treball.

Diversos mecanismes de cinètica química han sigut validats gràcies als resultats experimentals obtinguts. A més d'un mecanisme detallat per a mescles PRF d'iso-octà i n-heptà, s'ha dut a terme la validació d'un altre mecanisme simplificat per al n-dodecà. D'altra banda, un submodel de formació i decaïment d'OH* excitat ha sigut validat contra resultats de quimioluminescència i espectroscopía.

S'han estudiat les diferents fonts de radiació del procés d'autoencesa per a l'iso-octà i l'n-heptà mitjançant tècniques d'espectroscopía. A més, s'han realitzat mesures de quimioluminescència filtrada a 310 $nm$ (longitud d'ona d'emissió del radical OH*) per a l'anàlisi de la generalització i velocitat de propagació del front d'autoencesa. La propagació de l'encesa ha mostrat ser depenent de les condicions termodinàmiques aconseguides en la cambra de combustió en l'instant d'ignició més que de la reactivitat de la mescla. S'han trobat dues fonts de radiació diferents a 310 $nm$ mitjançant espectroscopía, depenent de la intensitat de l'encesa: el decaïment del radical OH* d'estat excitat a estat natural i l'oxidació del CO a $CO_2$ (continu del CO). No obstant açò, aquestes tècniques han sigut utilitzades solament per als dos combustibles de referència de l'escala de octanaje a causa de limitacions tècniques.

Finalment, s'ha desenvolupat un nou model predictiu de manera teòrica partint del model de Glassman per a l'autoencesa. Aquest mètode es basa a modelar primer la taxa d'acumulació de portadors de cadena fins a la seua concentració crítica (obtenint així el temps de retard referit a l'etapa de flames fredes) i, després d'aquest instant, modelar la taxa de consum d'aquests portadors de cadena fins a la seua completa desaparició (instant en el qual es produeix la màxima exotermia del procés, predient el temps de retard referit a l'etapa d'alta temperatura de l'encesa). La capacitat predictiva del model ha sigut comprovada per a cadascun dels sis combustibles assajats. A més, aquesta capacitat predictiva ha sigut comparada amb la d'altres mètodes existents en la literatura, com la integral de Livengood & Wu. La validesa de cadascun dels mètodes ha sigut analitzada, definint una metodologia d'ús per a obtenir prediccions raonables del temps de retard.

**Abstract.** Autoignition is a combustion mode specially relevant in the frame of reciprocating internal combustion engines (ICE). Its study has great interest not only because autoignition is the operating principle for the start of combustion in compression ignition (CI) engines, but also because it is a phenomenon to avoid in spark ignition (SI) engines, where it can cause catastrophic effects. The relevance of autoignition has been increased during the last years due to the new combustion trends in ICE. More restrictive anti-pollutant regulations, as well as the concern associated to fossil fuels consumption, have favored the development of new combustion modes, which show virtually zero emissions of soot and nitrogen oxides, as well as the capability to reach high efficiencies. Most of these new combustion modes are based on the controlled autoignition of a reactive mixture, with a higher or lower degree of homogeneity, in an environment with low oxygen content.

The main objective of this Thesis is the study of the autoignition phenomenon of reactive mixtures from a theoretical and experimental point of view. A wide parametric study has been carried out in a Rapid Compression-Expansion Machine (RCEM) for different initial temperatures, compression ratios, equivalence ratios and molar fractions of oxygen (by using synthetic EGR) for different fuels. The ignition delay referred to cool flames (if it can be identified), as well as the ignition delay referred to the high-temperature stage of the ignition, have been experimentally obtained and their trends have been explained regarding the chemical kinetics of each fuel.

The different effects of the species that compose the synthetic EGR on the ignition delay have been studied, decoupling the thermodynamic effects from the chemical ones. Different compositions have been taken into account to generate the synthetic EGR, and validation limits have been obtained for each mixture. The thermodynamic and the chemical effects have shown to be opposed, while the dominant one is different depending on the working temperature.

Several chemical kinetic mechanisms have been validated by comparison to the experimental results. A detailed mechanism for iso-octane and n-heptane blends and a reduced mechanisms for n-dodecane have been analyzed. Moreover, a sub-model for the generation and decay of excited $OH^*$ has been validated by comparison to chemiluminescence and spectroscopy results.

The different radiation sources have been studied for iso-octane and n-heptane by means of spectroscopy techniques. Besides, chemiluminescence measurements filtered at 310 $nm$ ($OH^*$ emission wavelength) have been performed in order to analyze the generalization and propagation velocity of the autoignition front. The ignition propagation has shown to depend on the thermodynamic conditions reached in the combustion chamber when the first ignition spot occurs and not on the global reactivity of the mixture. Furthermore, two different radiation sources have been found at 310 $nm$ in the spectroscopic analysis depending on the ignition intensity: the decay of the $OH^*$ radical from excited to ground state and the oxidation of CO to $CO_2$ (CO continuum). However, these optical techniques have been applied only in the experiments carried out with iso-octane and n-heptane due to technical limitations.

Finally, a new predictive model has been theoretically developed starting from the Glassman's model for autoignition. This method is based on modeling the accumulation rate of chain carriers up to reach their critical concentration (obtaining the ignition delay referred to cool flames) and, afterwards, modeling the disappearance rate of such chain carriers up to their consumption (when the maximum heat release rate is reached, obtaining the ignition delay referred to the high-temperature stage of the process). The predictive capability of the model has been compared to the ability of other methods that can be found in the literature, such as the Livengood & Wu integral method. The validity of each method has been tested, defining a working methodology to obtain reasonable predictions for the ignition delay.

*á miña dona, Cris*
*ó meu irmán, Hugo*
*ós meus pais, Concha e Manolo*

## Agradecimientos

Quiero agradecer a mis directores de Tesis, *Pepe Desantes* y *Javi López*, todo su apoyo y ayuda ofrecidos durante el desarrollo del presente trabajo. Además de directores sois buenos amigos de los que he aprendido mucho y que siempre habéis tenido la puerta de vuestro despacho abierta para ayudarme y apoyar mi trabajo. A ambos os debo muuuchos cafés por todo el tiempo que os he robado. ¡Los consejos que me habéis dado tienen un valor incalculable!

Me gustaría extender este agradecimiento al director del Instituto Universitario de Investigación CMT - Motores Térmicos, *Francisco Payri*. Además, no puedo olvidarme de los responsables del departamento, que me han facilitado los medios necesarios para llevar a cabo los trabajos de investigación que se presentan en la Tesis, así como del personal de secretaría e informática por su trato cuando he necesitado su ayuda. También quiero incluir en estos agradecimientos a toda la línea de Combustión, que han sido mis compañeros en el día a día. Siempre he encontrado vuestras puertas abiertas para mis consultas. Y quiero dar las gracias de forma muy especial a *José Enrique*, *Omar*, *Borja*, *Sergi* y *Jose*, porque sin vosotros el laboratorio sería un completo caos. ¡Gracias por vuestra paciencia! Finalmente, me gustaría agradecer a *Joaquín* que haya puesto a mi disposición los medios del Instituto de Tecnología Química todas las veces que los he necesitado, ¡y no han sido pocas!

Mi agradecimiento también a mis compañeros de despacho *Dani* y *Jorge* porque siempre habéis estado ahí cuando os he necesitado. Gracias por vuestras ideas y, sobre todo, por hacer cada jornada más amena. Y no puedo olvidarme de todos los compañeros con los que he colaborado a lo largo de este período: *Elisabet*, *Vicente*, *Esther*, *Sergio*, *Victor*, *Marcos*, *Shravaan*, *Lorène*, *Antoni*, *Álvaro* y *Vincenzo*. Vuestra ayuda ha sido clave en la realización de este trabajo.

I would like to thank to the director of the Aerothermochemistry and Combustion Systems Laboratory from ETH - Zürich, *Konstantinos Boulouchos*, for welcoming me as academic guest and for putting at my disposal all the facilities of the laboratory. I would like also to thank *Bruno Schneider* for his help and support during my stay. I have felt like a member of the lab!

Quero darlle o meu agradecemento ós meus amigos (por estrita orde alfabética, que non quero líos) *Alan*, *Alberto*, *David* e *Roger*, porque case non me tiverades en conta todo o tempo que non vos puiden adicar e pola parte que vos toca na morriña e saudade que temos os que estamos fóra da terra.

Á miña *nai* e a o meu *pai* porque non poderei agradecerlles nunca o seu apoio. Quérovos! E ó meu irmán, *Hugo*, por mor de tódolos bos momentos que temos pasado xuntos. Tan só agardo que estes tan orgulloso de mim coma eu o estou de ti.

Non hai verbas cas cales darlle as grazas á miña dona, *Cris*. Ela é quen estivo ó meu lado en todo momento, aturando as xornadas interminábeis no choio, as estancias, as vacacións sen vacacións... Só podo dicirche que te quero e que nos agarda unha nova etapa que pasaremos coma sempre, xuntos.

# Table of Contents

# Index of Figures

# Index of Tables

# Nomenclature

***Latin***

| | |
|---|---|
| $a$ | Speed of sound |
| | Piston acceleration |
| $a_{st}$ | Oxygen-to-fuel molar ratio under stoichiometric conditions |
| $A$ | Area |
| $A_f$ | Area of the reaction front |
| $B$ | Spalding's transfer number |
| $C$ | Heat capacity |
| | Courant number |
| $C_{11}$ | Characteristic constant of the heat losses model |
| $C_{12}$ | Characteristic constant of the heat losses model |
| $C_{1\epsilon}$ | Dissipation rate of turbulent kinetic energy constant of the $k-\epsilon$ turbulence model |
| $C_2$ | Characteristic constant of the heat losses model |
| $C_{2\epsilon}$ | Dissipation rate of turbulent kinetic energy constant of the $k-\epsilon$ turbulence model |
| $C_m$ | Mean piston speed |
| $C_p$ | Heat capacity at constant pressure |
| $C_v$ | Heat capacity at constant volume |
| $C_\mu$ | Turbulent viscosity constant of the $k-\epsilon$ turbulence model |
| $d$ | Piston bore |
| $D$ | Mass diffusivity |
| $Da$ | Damköhler number |
| $Da_1$ | Damköhler number referred to the expansion velocity |
| $Da_2$ | Damköhler number referred to the speed of sound |

| | |
|---|---|
| $Da_3$ | Damköhler number referred to the turbulent combustion velocity |
| $E_a$ | Activation energy |
| $f$ | Focal length |
| $f_{ac}$ | Acquisition frequency |
| $f_c$ | Cutoff frequency |
| $F$ | Fuel |
| | Force |
| | Fuel-to-oxygen mass ratio |
| $F_r$ | Equivalence ratio |
| $h$ | Convection coefficient |
| $I_{back}$ | Background noise level of radiation |
| $I_{max}$ | Maximum pixel intensity for a certain image |
| $k$ | Turbulent kinetic energy |
| $K$ | Characteristic constant of the deformations model |
| $k_b$ | Backward specific reaction rate |
| $k_f$ | Forward specific reaction rate |
| $k_i$ | Specific reaction rate of reaction $i$ |
| $K_v$ | Vaporization constant |
| $m$ | Mass |
| | Number of hydrogen atoms of a hydrocarbon |
| $M$ | Third body species |
| | Mach number |
| $n$ | Engine speed |
| | Number of carbon atoms of a hydrocarbon |
| $N$ | Number of repetitions of each experiment |
| $Nu$ | Nusselt number |
| $p$ | Percentage of intensity used as threshold for the filtering of the images |
| | Number of oxygen atoms of a hydrocarbon |
| $P$ | Pressure |
| | Product |
| $P_{ref}$ | Reference pressure (1 $bar$) |
| $Q_{accumulated}$ | Accumulated heat release |
| $\dot{Q}_{lost}$ | Heat losses |
| $R$ | Universal gas constant |

| | |
|---|---|
| | Reactant |
| $R_g$ | Specific gas constant of a certain gas |
| $R^2$ | Coefficient of determination |
| $S$ | Stroke |
| $Se_R$ | Sensitivity of a certain parameter to a certain reaction, $R$ |
| $t$ | Time |
| $t_{1-\alpha/2,N-1}$ | Student's t-distribution for a level of confidence of $1-\alpha$ and $N-1$ degrees of freedom |
| $T$ | Temperature |
| $T_a$ | Activation temperature |
| $t_{filling}$ | Filling time of the RCEM |
| $t_{heating}$ | Heating time of a fuel droplet |
| $t_i$ | Time of ignition. Ignition delay under transient conditions |
| $t_{i,1}$ | Ignition delay under transient thermodynamic conditions referred to the maximum pressure rise caused by cool flames |
| $t_{i,2}$ | Ignition delay under transient thermodynamic conditions referred to the maximum pressure rise caused by the high-temperature stage of the combustion process |
| $t_{i,CC}$ | Ignition delay under transient thermodynamic conditions referred to the critical concentration of chain carriers |
| $t_{i,CO}$ | Ignition delay under transient thermodynamic conditions referred to the maximum oxidation rate of CO to $CO_2$ |
| $t_{i,OH}$ | Ignition delay under transient thermodynamic conditions referred to the maximum $OH^*$ decay rate |
| $t_{vap}$ | Vaporization time of a fuel droplet |
| $T_w$ | Wall temperature |
| $u$ | Velocity |
| $u_b$ | Expansion velocity of the burned gases |
| $u_{chem}$ | Chemical velocity |
| $u_{comb}$ | Combustion velocity of the autoignition front |
| $u_{crit}$ | Critical propagation velocity from which diffusive effects are negligible |
| $u_{LC}$ | Laminar combustion velocity |
| $u_{prop}$ | Propagation velocity of the autoignition front |
| $u_{TC}$ | Turbulent combustion velocity |
| $u_{wave}$ | Propagation velocity of the pressure front |
| $u_{swirl}$ | Swirl velocity |

| | |
|---|---|
| $V$ | Volume |
| $V_d$ | Displacement volume |
| $x$ | Piston position |
| $X_j$ | Molar fraction of the species $j$ |
| $Y_j$ | Mass fraction of the species $j$ |

***Greek***

| | |
|---|---|
| $\alpha$ | Multiplicative factor for chain carriers in Glassman's autoignition model |
| $\alpha_T$ | Turbulent thermal diffusivity |
| $\gamma$ | Adiabatic coefficient |
| $\delta$ | Linear deformation of the combustion chamber |
| $\epsilon$ | Ignition delay deviation |
| | Dissipation rate of turbulent kinetic energy |
| $\lvert\bar{\epsilon}\rvert$ | Average of the ignition delay deviations in absolute value |
| $\theta$ | Crank angle |
| $\lambda$ | Thermal conductivity |
| | Lineal density of the piston tube |
| $\lambda_{st}$ | $O_2$-to-fuel ratio under stoichiometric conditions |
| $\mu$ | Semi-amplitude of the confidence interval |
| $\nu$ | Laminar kinematic viscosity |
| $\nu_T$ | Turbulent kinematic viscosity |
| $\xi$ | Ignition delay deviation between different EGR mixtures |
| $\rho$ | Density |
| $\sigma$ | Standard deviation |
| $\sigma_k$ | Turbulent kinetic energy constant of the $k-\epsilon$ turbulence model |
| $\sigma_\epsilon$ | Dissipation rate of turbulent kinetic energy constant of the $k-\epsilon$ turbulence model |
| $\tau$ | Ignition delay |
| $\tau_1$ | Ignition delay under constant thermodynamic conditions referred to the maximum pressure rise caused by cool flames |
| $\tau_2$ | Ignition delay under constant thermodynamic conditions referred to the maximum pressure rise caused by the high-temperature stage of the combustion process |

| | |
|---|---|
| $\tau_{CC}$ | Ignition delay under constant thermodynamic conditions referred to the critical concentration of chain carriers |
| $\upsilon_j$ | Stoichiometric coefficient for the species $j$ |
| $\phi$ | Diameter of a fuel droplet |
| | Auxiliary equivalence ratio to determine the EGR composition |
| $\dot{\omega}$ | Reaction rate |
| $\Delta t$ | Time step |
| $\Delta x$ | Cell size |

**Superscripts**

| | |
|---|---|
| $*$ | Excited species |

**Subscripts**

| | |
|---|---|
| 0 | Initial conditions |
| 1 | Referred to cool flames |
| 2 | Referred to the high-temperature stage of the autoignition process |
| $\infty$ | Referred to ambient conditions far away of a fuel droplet |
| | Referred to ambient conditions far away of the reaction front |
| $b$ | Referred to the burned gases |
| $CC$ | Relative to chain carriers |
| $crit$ | Relative to a critical concentration of chain carriers |
| | Referred to critical conditions in a throat |
| $i$ | Referred to conditions behind the incident pressure wave |
| $ICE$ | Referred to data obtained from CHEMKIN using the internal combustion engine reactor |
| $Int$ | Referred to the new predictive integral method proposed in this Thesis |
| $LW$ | Referred to the Livengood & Wu predictive integral method |
| $max$ | Relative to a maximum value |
| $motored$ | Referred to motoring conditions (without combustion) |
| $osc$ | Referred to the in-cylinder pressure oscillations |
| $r$ | Referred to conditions behind the reflected pressure wave |
| $RCCC$ | Referred to the predictive method based on the Relative Concentration of Chain Carriers |

| | |
|---|---|
| $RCEM$ | Referred to data experimentally obtained in a Rapid Compression-Expansion Machine |
| $realEGR$ | Referred to the synthetic EGR mixture formed by $O_2$, $N_2$, $CO_2$, $H_2O$ and Ar |
| $ref$ | Relative to a reference conditions |
| $st$ | Relative to stoichiometric conditions |
| $TDC$ | Referred to Top Dead Center |
| $throat$ | Referred to conditions in the throat |
| $u$ | Referred to the unburned mixture |

**Initials and acronyms**

| | |
|---|---|
| $BDC$ | Bottom dead center |
| $CAD$ | Computer-Aided Design |
| | Crank Angle Degrees |
| $CAI$ | Controlled Auto-Ignition |
| $CC$ | Chain Carrier |
| $CI$ | Compression Ignition |
| | Confidence Interval |
| $CFD$ | Computational Fluid Dynamics |
| $CR$ | Compression Ratio |
| $CV$ | Coefficient of Variation |
| $DBIEI$ | Diffused Back-Illumination Extinction Imaging |
| $DNS$ | Direct Numerical Simulations |
| $DRG$ | Directed Relation Graph |
| $ECU$ | Electronic Control Unit |
| $EGR$ | Exhaust Gas Recirculation |
| $FVM$ | Finite Volume Method |
| $FWHM$ | Full Width at Half Maximum |
| $HC$ | Hydrocarbon |
| $HCCI$ | Homogeneous Charge Compression Ignition |
| $HRR$ | Heat Release Rate |
| $ICE$ | Internal Combustion Engine |
| $LEI$ | Light Extinction Imaging |
| $LHV$ | Lower Heating Value |

| | |
|---|---|
| $LIF$ | Laser-Induced Fluorescence |
| $LII$ | Laser Induced Incandescence |
| $LTC$ | Low Temperature Combustion |
| $MDM$ | Moment Distribution Method |
| $MW$ | Molecular Weight |
| $NTC$ | Negative Temperature Coefficient |
| $ON$ | Octane Number value |
| $PCCI$ | Premixed Charge Compression Ignition |
| $PHM$ | Photomultiplier |
| $PIV$ | Particle Image Velocimetry |
| $PLIF$ | Planar Laser-Induced Fluorescence |
| $PLII$ | Planar Laser Induced Incandescence |
| $PM$ | Particulate matter |
| $PRF$ | Primary Reference Fuel |
| $PSR$ | Perfectly Stirred Reactor |
| $RANS$ | Reynolds-averaged Navier-Stokes equations |
| $RCCC$ | Relative Concentration of Chain Carriers |
| $RCEM$ | Rapid Compression-Expansion Machine |
| $RCM$ | Rapid Compression Machine |
| $SCR$ | Selective Catalytic Reduction |
| $SI$ | Spark Ignition |
| $TDC$ | Top Dead Center |
| $TWC$ | Three-Way Catalyst |
| $UHC$ | Unburned Hydrocarbons |

# Chapter 1

# Introduction

**Contents**



## 1.1 Justification and background

Internal Combustion Engines (ICE) have demonstrated to have a main role in the frame of propulsive systems for transport media. Reciprocating internal combustion engines have been used for years as the best solution for passenger and merchandise mobility because of their unbeatable power-to-weight ratio, their well-know technology and their easily storable energy source [1]. Engine efficiency has been improved during the last years up to reach hardly improvable values. Thus, nowadays the engine research is focused on reducing pollutant emissions but keeping, or even improving, the high efficiency reached in modern engines.

Regulations about pollutant emissions in internal combustion engines have become increasingly restrictive during the last years. Fig. 1.1 shows the evolution of the European emission standars for passenger cars and light-duty commercial vehicles ($\leqslant$1305 $kg$) for both Compression-Ignition (CI) and Spark-Ignition (SI) engines. It can be seen that the trend from Euro III (January, 2000) to Euro VI (September, 2014) is to decrease the

limits of unburned and pollutant species, specially for nitrogen oxides ($NO_x$) and particulate matter (PM). Moreover, this trend is not only present in automotive engines, but also for naval and stationary engines. New European emission standards (Euro VI) for heavy-duty vehicles equipped with diesel engines, for instance, have reduced the $NO_x$ limits in 80%, while the maximum soot emissions have been reduced in 50% [2]. In conventional CI-engines, both $NO_x$ and soot emissions cannot be simultaneously reduced due to the opposite effects of the conventional diesel combustion strategies on these pollutant species. As for SI-engines, the combustion efficiency is limited by quenching effects that appear near to the walls because of temperature gradients, which imply the existence of a volume of fuel that cannot be burned by the flame front [3].

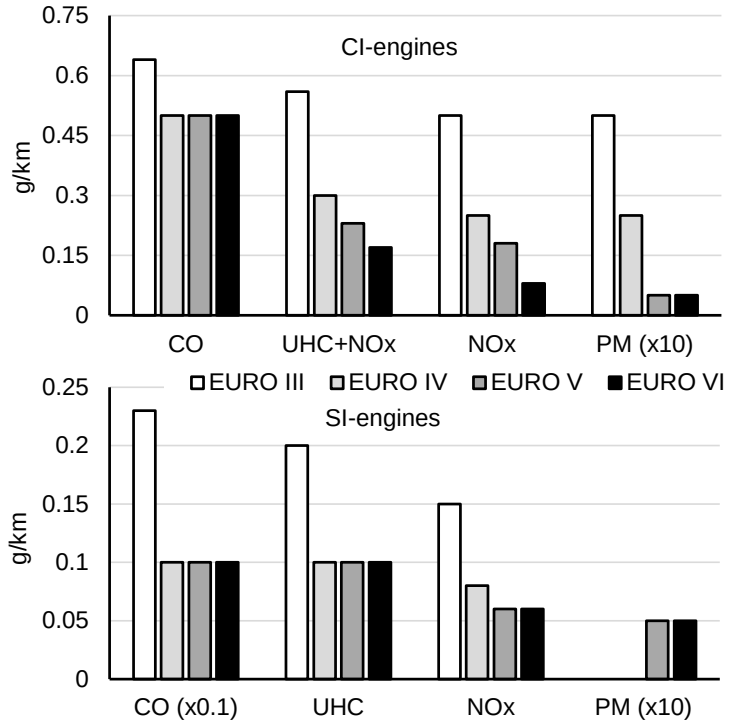


***Figure 1.1.*** *Evolution of the European emission standars for passenger cars and light-duty commercial vehicles (⩽1305 kg) for both CI and SI-engines from Euro III (January, 2000) to Euro VI (September, 2014).*

There are two ways to reduce pollutant emissions in internal combustion engines. On the one hand, pollutant emissions can be reduced by means of after-treatment systems located in the exhaust line. Despite the fact that after-treatment systems for unburned hydrocarbons (UHC), carbon monoxide (CO) and PM are well-known and highly efficient techniques, $NO_x$ reduction methods have shown some limitations. Three-way catalytic converters (TWC) have the advantage of working as both oxidation and reduction catalysts. However, their operating range is limited to stoichiometric air-fuel ratios, which precludes the optimization of the equivalence ratio in terms of fuel consumption. Selective Catalytic Reduction (SCR) after-treatment systems for the reduction of $NO_x$ species have shown to have some disadvantages, including high cost and high maintenance. SCR systems need additional injection systems to supply a reductant (typically urea) to the exhaust flow, which increase the complexity of the engine. Moreover, the reductant, which has to be replenished, as well as the reduction products, can cause corrosion in the injector, reducing the useful life of the system [4]. On the other hand, the formation of pollutant emissions can be avoided directly during the combustion process itself. In this sense, Exhaust Gas Recirculation (EGR) is a widely used technique to reduce the formation of $NO_x$ through the thermal pathway [5]. The working principle of EGR is to recirculate a certain amount of exhaust gases to the intake manifold, mixing them with the fresh air. The burned gases act as a diluent of the unburned mixture, thus a lower initial oxygen molar fraction is reached and lower combustion temperatures are obtained. In fact, the absolute temperature reached after combustion varies inversely with the exhaust gas mass fraction. Hence increasing the exhaust gas fraction reduces $NO_x$ emissions levels. This is a compulsory strategy for conventional CI-engines and its use is also widespread in current SI-engines. Moreover, the relevance of EGR is even higher in the frame of new combustion modes, which use massive amounts of EGR to reduce the maximum temperature reached in the cycle.

Advanced combustion modes based on the autoignition of an air-fuel mixture with a certain degree of homogeneity and high EGR rates, such as Homogeneous Charge Compression Ignition (HCCI), Premixed Charge Compression Ignition (PCCI), Controlled Autoignition (CAI) and others, have been studied for the simultaneous reduction of soot and $NO_x$ in CI-engines and for the improvement of the combustion efficiency in SI-engines. Their working principle is based on Low Temperature Combustion (LTC) and their effectiveness has been widely proved in previous studies [6]. Fig. 1.2 shows the conditions reached in these new combustion strategies, as well as in conventional diesel and spark-ignition combustion, in an equivalence

ratio - temperature diagram [7], where it can be seen that the simultaneous reduction of soot and $NO_x$ is possible by avoiding the soot and $NO_x$ formation peninsulas. Regarding CI-engines, LTC modes show virtually zero emissions of soot and $NO_x$, but high UHC and CO emissions that can be easily eliminated with well-known low-cost after-treatment techniques. Since the maximum temperature reached in the cycle is low and it decreases further after Top Dead Center (TDC), most of the fuel located in the thermal boundary layer and in other crevice volumes cannot diffuse out into the bulk gas and burn, which results in products of incomplete combustion [8]. As for SI-engines, CAI mode is based on the autoignition of a premixed air-fuel mixture to avoid the establishment of a flame front, leading to higher combustion efficiencies and lower UHC, CO and $NO_x$ emissions [9].

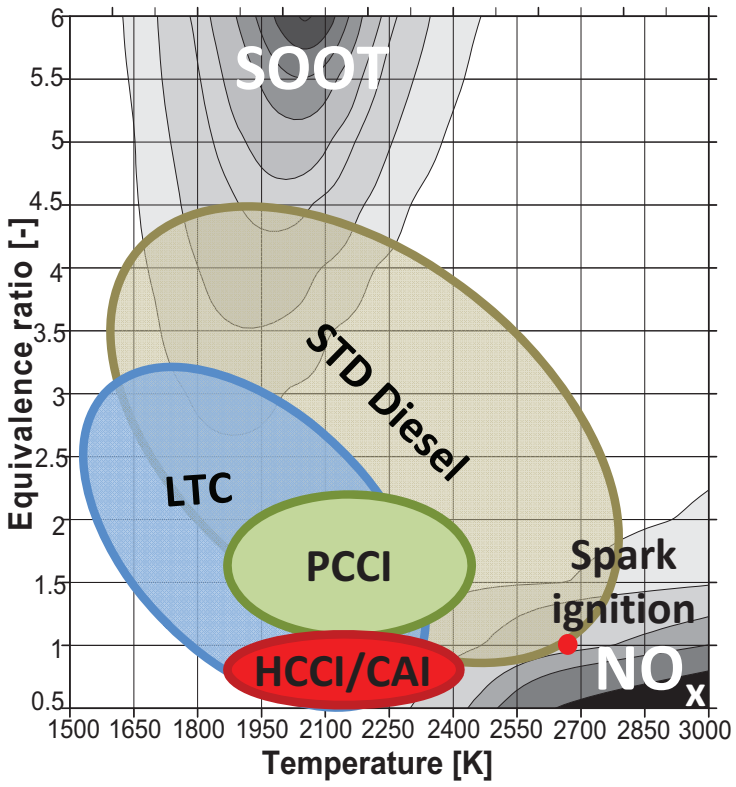


***Figure 1.2.*** *Operating conditions reached in different combustion modes represented in an equvalence ratio versus temperature diagram, the soot and $NO_x$ formation peninsulas are also represented (from [7]).*

Two main challenges appear with the implementation of these combustion strategies in commercial reciprocating internal combustion engines: the lack of control over the autoignition process and, therefore, over the heat release rate [10]; and the operating range, which is limited to low-to-medium loads [11]. On the one hand, ignition is controlled by the chemical kinetics of the charge in these combustion modes. This control entails higher complexity because of the absence of an explicit ignition-controlling event, such as a spark or an injection process, when very reactive conditions are reached in the combustion chamber (near TDC). The reactivity of the mixture can be modified by adjusting the engine operating parameters, such as the EGR rate and the inlet temperature. Therefore, improving the knowledge about the autoignition phenomenon under low temperature conditions and the capability of predicting the autoignition event is mandatory to properly modify the operating conditions of the engine in order to control the heat release. On the other hand, the operating range in LTC modes is restricted to low-to-medium loads due to the fast combustion velocity of the autoignition process when the engine load is increased, which results in high pressure rise rates and, therefore, in high combustion noise and mechanical strains.

Dual-fuel combustion based on diesel/gasoline mixtures has shown to be a good method to increase the operating range of LTC modes. Bessonette et al. [12] showed that different in-cylinder reactivities are required for a proper LTC operation under different operating conditions. Specifically, low octane fuels are required at low loads, while high octane fuels are needed at medium-to-high loads. A wide range of octane numbers can be provided by using premixed gasoline mixtures in which a direct diesel injection causes an stratification of reactivities. Thus, a flexible operation over a wide operating range is possible by modifying both the blend ratio between fuels and the direct injection settings. Therefore, the control over the autoignition event should be improved not only for diesel and gasoline surrogate fuels, but also for a wide range of reactivities (i.e. of octane numbers).

Although ignition can be reasonably well-predicted by using advanced Computational Fluid Dynamics (CFD) codes with detailed chemistry, the required computing time is too long to be solved in real time. In fact, simple numerical methods with very short computing time are the only ones that can be implemented in an Engine Control Unit (ECU). If the chemical kinetics of the mixture is characterized, the engine settings can be modified to control the heat release rate and optimize the engine efficiency. Thus, low computing time methods with enough accuracy to predict ignition delays are the only ones that allow improving the control of the engine, since decisions in real time can be taken.

Finally, there is great interest in simulating with accuracy the phenomena that take place inside the cylinder of an internal combustion engine. CFD simulations are very useful at the design stage, since they reduce the number of experiments, prototypes and cost of developing new engines. Computing time is the key parameter when CFD simulations are carried out, and it can be highly increased by linking the physical models with detailed chemical kinetic mechanisms. This is the reason why the higher the spatial resolution, the simpler the chemical mechanism employed to solve the reaction paths. Therefore, the use of detailed chemical kinetic mechanisms coupled with CFD codes is limited by the physical discretization of the domain. The computational cost of solving detailed chemistry in cases with a high number of cells could be unacceptable, imposing the use of simplified mechanisms. The total computing time can be reduced by implementing predictive numerical methods to determine the ignition delay instead of solving the involved reaction rates. Thus, some CFD applications can be solved with simple numerical methods that characterize the autoignition and combustion processes with quite a reasonable computing cost.

It should be noted that the existing predictive numerical methods for the ignition delay can be summarized in the classic Livengood & Wu integral method [13]. This procedure has been developed in 1955 and its hypotheses should be revised. Moreover, this predictive method is indiscriminately applied nowadays, regardless the meaning of the different variables involved. Thus, a revision about the limits of application of the method is needed, as well as the development of new predictive methods that can extend these limits.

## 1.2 Objectives and methodology

Regarding the background shown in the previous paragraphs, the main objective of this Thesis can be summarized as follows:

- *To improve the knowledge about the autoignition phenomenon under LTC conditions by developing an alternative numerical method to predict ignition delays under transient thermodynamic conditions and by studying the ignition propagation under working conditions with real applications.*

This global objective can be decoupled in different goals:

i To design a criterion to define the proper composition of the synthetic EGR for autoignition studies.

The use of synthetic EGR is mandatory in the typical facilities where autoignition studies are carried out due to the absence of enough flow of exhaust gases. In order to define the EGR composition for a proper replication of the processes that occur in real engines, the effects of the different species that can compose the synthetic mixture on the ignition delay is intended to be studied. The thermodynamic and chemical effects are isolated in order to distinguish which one is the dominant depending on the temperature regime. To do so, a wide range of operating conditions want to be simulated solving a fully-validated chemical kinetic mechanism and the chemical paths that involve the EGR species want to be analyzed. Finally, a criterion to define the species that should be taken into account for autoignition studies under realistic conditions wants to be established.

ii To develop a new alternative procedure to predict ignition delays under transient thermodynamic conditions.

A theoretical development based on more sophisticated models for the autoignition process than the classic Livengood & Wu expression is intended to be performed. The resulting procedure should be able to predict not only the ignition delay referred to cool flames, but also the ignition delay referred to the high-exothermic stage of the combustion process. Furthermore, the validity of this alternative predictive method has to be proved for different octane numbers, in order to be able to apply the procedure to any fuel.

iii To validate different chemical kinetic mechanisms, as well as different predictive methods for the ignition delay, by comparison to experimental data.

Every model has to be compared to experimental data to ensure its validity. Thus, an experimental database of ignition delays referred to cool flames and to the high-temperature stage is intended to be generated under a wide range of operating conditions, including different initial temperatures, compression ratios, oxygen molar fractions and equivalence ratios in a Rapid Compression-Expansion Machine (RCEM). The aforementioned database will be available for the scientific community and it could be used for the validation of different combustion models. Besides, the validity of the hypotheses of the Livengood & Wu integral method and its limits of application should be studied. A wide analysis about the theoretical development to obtain the classic Livengood & Wu expression is intended to be performed and the main hypotheses of the method want to be revised. To do so, alternative predictive methods that

avoid such hypotheses have to be developed and then compared to the integral method. Moreover, the validity of all the different predictive procedures involved in this investigation wants to be evaluated along the octane number reference scale versus experimental data, defining their limits of application. Finally, it should be noted that if chemical kinetic mechanisms want to be used for the generation of the ignition characteristics under constant conditions used in the predictive methods, such mechanisms have to be also validated in the working range.

iv To study the generalization of the autoignition event and the propagation of the autoignition front in experimental facilities under realistic conditions.

The accuracy of measuring the ignition delay by means of optical techniques wants to be studied. Besides, the consistence between the in-cylinder pressure evolution, the luminous intensity signal and the heat release rate will be discussed. An analysis about the generalization of the autoignition is intended to be performed by measuring the area occupied by the radiation as well as the velocity of propagation of the autoignition front. Moreover, since the OH* radiation can be outshone by other luminous reactions under LTC conditions, a spectroscopic analysis wants to be performed in order to study how the working conditions affect to this phenomenon and the chemical kinetics involved in the process. Finally, a complete diagnosis of the autoignition and combustion processes wants to be done regardless of the source of radiation (the decay of OH* or other excited species).

Despite the fact that a detailed description about the methodological approach can be found in Chapter 3, the methodology followed in this work is summarized in the following paragraphs.

A wide experimental parametric study has been carried out in a RCEM in order to be able to accomplish with the objectives of this Thesis. The ignition characteristics of six different fuels have been obtained for different initial temperatures, compression ratios, oxygen molar fractions and equivalence ratios, and the resulting data have been used for the validation of chemical kinetic mechanisms and predictive procedures for the ignition delay. Besides, different optical techniques have been applied for the analysis of the autoignition promotion and propagation. The ignition delay referred to the combustion luminosity has been obtained by recording the integrated radiation from chemilumescence of radicals present in the process. Furthermore, the spatial distribution of the radiation emitted by different reactions has been also recorded for the analysis of the propagation of the autoignition front.

Finally, a complete diagnosis of the ignition and combustion processes has been performed by means of spectroscopy.

The experiments have been replicated in CHEMKIN, which is a widespread numerical tool to perform chemical kinetic simulations developed by Reaction Design (ANSYS). The simulated ignition delays have been compared to the experimental ones, and the relative deviations between both have been studied as a method to validate the chemical kinetic mechanisms. Finally, a new procedure to predict the ignition delay under transient conditions has been developed and validated by comparison to the experimental data, while its predictive capability has been compared to the accuracy of other existing predictive methods.

## 1.3 Thesis structure

This Thesis tries to deepen the knowledge about the autoignition phenomenon under LTC conditions. The development of a new alternative procedure to predict the ignition delay of a certain air-fuel mixture under variable thermodynamic conditions is intended to be solved in this work. To do so, a theoretical analysis of the autoignition event is required. The development process and details of the final model are presented in this document. Moreover, an optical analysis about the ignition propagation is also presented, as well as a full diagnosis of the autoignition process.

After this brief introduction (Chapter 1), an extensive review about the autoignition phenomenon is described in Chapter 2. It starts describing the fundamentals about chemical kinetics and autoignition theory, as well as the phenomena that take place during the ignition delay, such as accumulation and consumption of chain carriers and competence of chemical paths depending on the temperature regime. Besides, the experimental facilities and numerical tools to characterize the autoignition event are presented, highlighting their advantages and disadvantages. A literature survey about the current challenges in experimental autoignition studies is discussed; and not only about the challenges related to the experimental methodology, but also the ones related to the research gaps present in this phenomenon. It should be mentioned that this is a pioneering Thesis in autoignition investigations using an RCEM at CMT - Motores Térmicos, where this work has been carried out.

The experimental facilities involved in this investigation, as well as the working methods, are described in Chapter 3. The facilities and tools with which the experiments are carried out are presented, highlighting the

capabilities of the different setups. Besides, the parametric study performed is shown. Finally, the methodological approach is described in detail. Different working methodologies can be distinguished: related to the RCEM used in this study and the post-processing of the experimental data, related to the optical measurements, and related to the chemical kinetic modeling. A full description about the models involved in the Thesis can be found in this section. Moreover, the chemical kinetic mechanisms used in this study are also validated in this chapter. Since this is the first research work carried out in the RCEM available at CMT - Motores Térmicos, a validation of the experimental facility is also included as an appendix.

On the one hand, the theoretical results derived from this work are presented in Chapter 4, which can be decoupled in two different items:

i Design of synthetic EGR for autoignition studies.

A wide analysis about the thermodynamic and chemical effects of the different species that compose the synthetic EGR on the ignition delay is shown, resulting in a criterion to define the proper composition of the synthetic air-fuel mixture for autoignition studies.

ii Theoretical development of an alternative procedure to predict ignition delays.

The theoretical aspects related to the new predictive procedure proposed in this work are described in detail, including the main hypotheses and assumptions to be able to predict both cool flames and high-temperature ignition delays.

On the other hand, the experimental results derived from this work are presented in Chapter 5, which can be decoupled in two more items:

iii Validation of the Livengood & Wu integral and the new predictive method proposed.

Different predictive methods are evaluated by comparing their predictive capability to direct chemical kinetic simulations and experimental results. The physical sense of each method, as well as its limits of application, are discussed.

iv Generalization of the autoignition event. Ignition delay measurements by means of optical techniques.

The establishment and propagation of the autoignition front is analyzed. Moreover, the capability of optical techniques to measure ignition delays and to describe the autoignition phenomenon is studied.

It should be noted that each item is related to an objective of the Thesis.

Finally, the conclusions of this Thesis are presented in Chapter 6. Moreover, some future works or research topics are also proposed.

# References

[1] Heywood John B. *Internal combustion engine fundamentals*. McGraw-Hill series in mechanical engineering. McGraw-Hill, New York, 1988.

[2] Union Eurpoean. "On type-approval of motor vehicles and engines with respect to emissions from heavy duty vehicles (Euro VI) and on access to vehicle repair and maintenance information and amending Regulation (EC) No 715/2007 and Directive 2007/46/EC and repealing Directives 80/1269/EEC and 2005/78/EC.". *Official Journal of the European Union. Regulation*, 2009.

[3] Taylor Charles Fayette. *The internal combustion engine in theory and practice*. M.I.T. Press, Cambridge, Mass, 2nd ed., rev edition, 1985.

[4] Floyd R., Kotrba A., Martin S. and Prodin K. "Material corrosion investigations for urea SCR diesel exhaust systems". *SAE Technical Paper 2009-01-2883*, 2009.

[5] Payri F. and Desantes J.M. *Motores de combustión interna alternativos*. Reverté, 2012.

[6] Li T., Wu D. and Xu M. "Thermodynamic analysis of EGR effects on the first and second law efficiencies of a boosted spark-ignited direct-injection gasoline engine". *Energy Conversion and Management*, Vol. 70, pp. 130–138, 2013.

[7] Desantes J.M., López J.J., Redón P. and Arrégle J. "Evaluation of the thermal NO formation mechanism under low temperature diesel combustion conditions". *International Journal of Engine Research*, Vol. 13, pp. 531–539, 2012.

[8] Bendu H. and Murugan S. "Homogeneous charge compression ignition (HCCI) combustion: Mixture preparation and control strategies in diesel engines". *Renewable and Sustainable Energy Reviews*, Vol. 38, pp. 732–746, 2012.

[9] Milovanovic N. and Chen R. "A review of experimental and simulation studies on Controlled Auto-Ignition Combustion". *SAE Technical Paper 2001-01-1890*, 2001.

[10] Bahlouli Keyvan, Atikol Ugur, Khoshbakhti Saray R. and Mohammadi Vahid. "A reduced mechanism for predicting the ignition timing of a fuel blend of natural-gas and n-heptane in HCCI engine". *Energy Conversion and Management*, Vol. 79, pp. 85–96, 2014.

[11] Benajes J., Pastor J. V., García A. and Monsalve-Serrano J. "An experimental investigation on the influence of piston bowl geometry on RCCI performance and emissions in a heavy-duty engine". *Energy Conversion and Management*, Vol. 103, pp. 1019–1030, 2015.

[12] Bessonette P.W., Schleyer C.H., Duffy K.P., Hardy W.L. and Liechty M.P. "Effects of fuel property changes on heavy-duty HCCI combustion". *SAE Technical Paper 2007-01-0191*, 2007.

[13] Livengood J. C. and Wu P. C. "Correlation of autoignition phenomena in internal combustion engines and rapid compression machines". *Symposium (International) on Combustion*, Vol. 5, pp. 347–356, 1955.

# Chapter 2

# The autoignition phenomenon

Contents

## 2.1 Introduction

Autoignition is the spontaneous combustion of an air-fuel mixture under certain thermodynamic conditions. It is a phenomenon with high relevance in the propulsive systems for transport media and, specifically, in internal combustion engines. In fact, autoignition is the operating principle of the start of combustion in CI-engines and it is a phenomenon to avoid in SI-engines, where it can cause catastrophic damages [1]. Moreover, the relevance of autoignition is even higher in the frame of new combustion modes. Autoignition is present in most of the operating principles of these new combustion strategies [2], which are based on the autoignition of a reactive mixture, with a higher or a lower degree of homogeneity, in an environment with low oxygen content (much less than in the atmosphere) to reduce the maximum temperature reached in the cycle [3]. In this way, the soot and $NO_x$ formation peninsulas, which can be seen in equivalence ratio - temperature diagrams, can be avoided [4]. Thus, these modes show virtually zero emissions of soot and $NO_x$, but high emissions of UHC and CO [5]. The main challenge to implement these new combustion strategies in commercial engines is the lack of control over the autoignition process and over the heat release rate, which leads to low engine efficiencies when they work at low temperature regimes [6]. Therefore, improving the knowledge about the auto-ignition phenomenon of reactive mixtures in low temperature conditions is necessary to reach clean, efficient and commercial engines.

In this chapter, the fundamentals of the autoignition phenomenon, as well as some fundamental concepts of chemical kinetics, are described highlighting the oxidation reactions previous to the exothermic combustion. The following paragraphs try to be a short summary of the autoignition theories, starting with simplified mechanisms to explain this phenomenon and finishing with an overview of the main oxidation reactions present during the ignition delay. The trends of the different phenomena present in the autoingition process are also explained. Then, some of the experimental facilities used to study autoignition are described underlining their capabilities according to the thermodynamic conditions that they are able to provide and describing the challenges to overcome in the working methodology. Also the most common criteria to experimentally define the start of combustion are shown. Finally, the numerical tools used in autoignition analyses are presented, describing the

challenges to be able to successfully implement these models and mechanisms in 0-D and CFD simulations.

## 2.2 Chemical kinetics and autoignition theory

The autoignition phenomenon is a process characterized by the existence of a time interval between the instant where the appropriate thermodynamic conditions are reached and the start of combustion. This time is called ignition delay, $\tau$, and it is composed by two different characteristic times: a physical time (time of fuel evaporation, time of the air - fuel mixing and time of other transport phenomena occurring in the system) and a chemical time (time defined by chemical reaction rates) [7]. The relevance of each one of these times is quantified by the Damköhler number ($Da$), which is defined by Eq. 2.1, and that describes the nature of the dominant phenomena in a combustion process. The autoignition event that usually occurs in direct-injection CI internal combustion engines is characterized by low Damköhler numbers, which means that the autoignition phenomenon is mainly controlled by chemical kinetics [8]. In fact, a homogeneous air - fuel mixture in vapor phase under constant thermodynamic conditions is defined by $Da = 0$ (null physical time).

$$Da = \frac{t_{physical}}{t_{chemical}} \tag{2.1}$$

Despite the fact that there is not any important energetic activity, high chemical activity occurs during the ignition delay [9]. Moreover, the reactions that define the chemical characteristic time are not very exothermic, can even be endothermic, but their importance is extremely high because they control the start of the ignition and the subsequent heat release. Autoignition is produced by accumulation of chain carriers (active radicals) up to reach a critical concentration that promotes the combustion process [10]. In a simple way, the autoignition phenomenon can be schematized as follows: the formation of chain carriers is produced by slow and not very exothermic reactions. And once the critical concentration of chain carriers is reached, fast and highly exothermic reactions occur, leading to the formation of combustion products and to the decomposition of these active radicals. Therefore, the critical concentration of chain carriers corresponds to a maximum concentration of such species and its characteristic time corresponds to the ignition delay [11].

Theoretically, the autoignition of a homogeneous mixture is a combustion process that implies a temporal, but not spatial, discontinuity. Ignition occurs at the same time in the whole chamber, so that no flame front is established. Besides, the heat release rate is an infinitely fast event and the thermodynamic conditions during the ignition delay can be considered constant with respect to chemical effects. Thus, the autoignition of ideal homogeneous mixtures is characterized by a sudden exothermic stage with the absence of flame front [12]. However, in case of heterogeneous mixtures, as well as in real *homogeneous* mixtures in which gradients of temperature and composition can be present, autoignition starts in a specific point (ignition spot) and it is rapidly propagated through the chamber. This concept is known as *most reactive mixture fraction* and it arises due to the balance of reactivities between the fuel - air ratio distribution and the temperature distribution [13]. An autoignition front can be seen in these cases, the propagation of which is caused by a flame front that increases the temperature of the surrounding areas, promoting new autoignition spots [14].

Since the ignition delay, $\tau$, is defined as the time needed to reach the critical concentration of chain carriers, this time must be dependent on the chemical kinetics of the air - fuel mixture, which implies a non-linear dependence on temperature and pressure. Thus, contour graphs can be obtained from P versus T plots, where the iso-ignition delay curves are presented. These plots are known as autoignition maps [15]. An example of an autoignition map for stoichiometric n-heptane - air mixtures can be seen in Fig. 2.1 at the top. As it can be seen, the iso-ignition delay curves can show inflection points that correspond to the Negative Temperature Coefficient (NTC) behavior (long chain hydrocarbons are more prone to show these inflection points). This phenomenon is referred to the loss of reactivity when the temperature is increased due to the promotion of formation of long-chain stable olefins by the alkyl radicals, which competes with the formation of chain-carriers, retarding the ignition [16]. Therefore, the ignition delay increases when the temperature is increased in a certain range (NTC zone). Fig. 2.1 at the bottom shows the effects of the NTC behavior on the temperature path during the ignition process. The temperature increases after a certain time under constant thermodynamic conditions (point A). Thus, the thermodynamic conditions change up to reach point B, where the ignition delay is longer, causing a freezing effect on the ignition event. Finally, point C is reached and the combustion of the mixture occurs. As it is shown in Fig. 2.1, the main effect of a pronounced NTC behavior is the appearance of a first brief exothermic stage, which is known as *cool flames* phenomenon, leading to a two-stage ignition pattern [17].

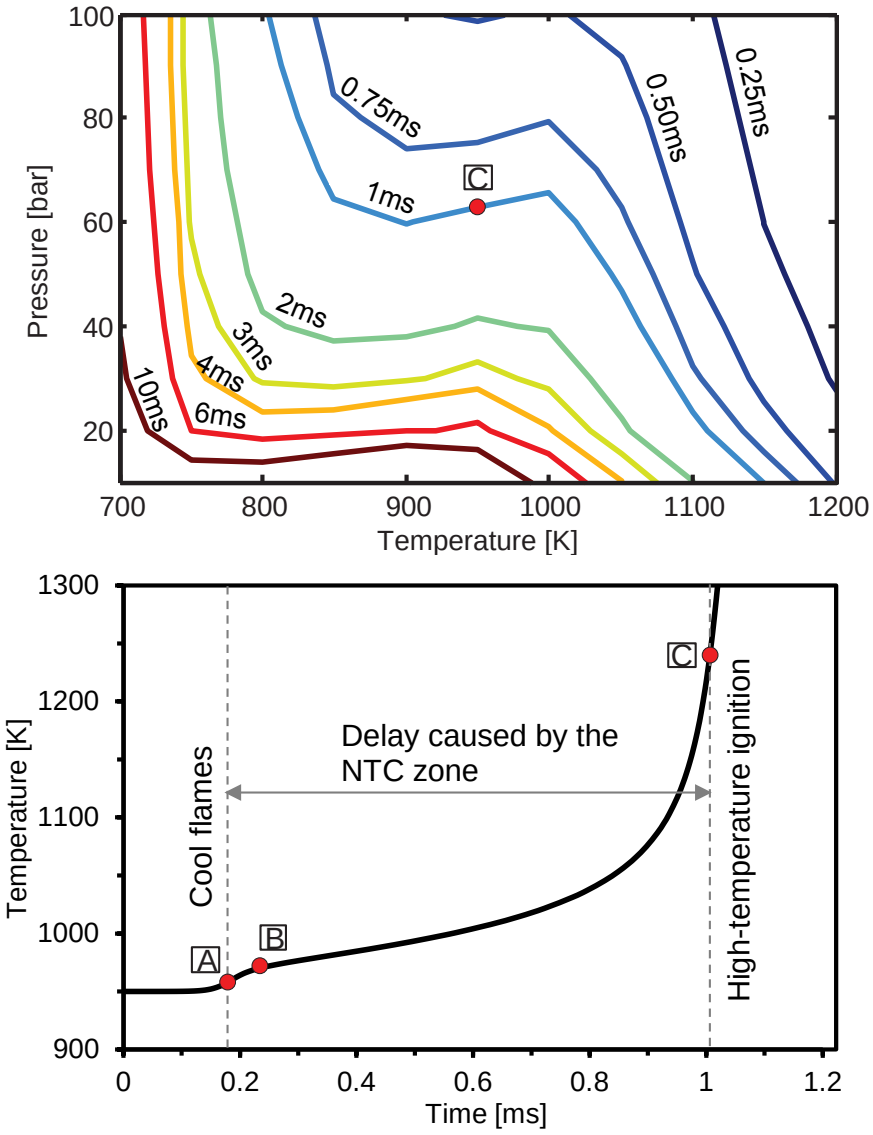


***Figure 2.1.*** *Top.- Autoignition map for stoichiometric n-heptane - air mixtures. Bottom.- Temperature path of an autoignition process of a n-heptane - air mixture under stoichiometric conditions at 950 K and 65 bar (constant pressure).*

It should be taken into account that all fuels ignite following a chemical kinetics that includes the NTC behavior. However, if the characteristic time of the delay between cool flames and the high-temperature ignition is very short (smooth NTC behavior), cool flames and the high-temperature combustion are indistinguishable events, leading to a single-stage ignition pattern [10]. Furthermore, Fig. 2.2 shows three different characteristic times of the ignition process: one referred to cool flames, another referred to a maximum concentration of chain carriers and other referred to the high-exothermic stage of the combustion event. The ignition delay referred to a critical concentration of chain carriers defines the end of the delay caused by the NTC zone and, therefore, this time is always placed between cool flames and the high-temperature stage. Thus: $\tau_{cool\ flames} < \tau_{CC} < \tau_{high\ temperature}$. If the NTC behavior is smooth enough all times are very close to each other, leading to the absence of cool flames as an independent event.

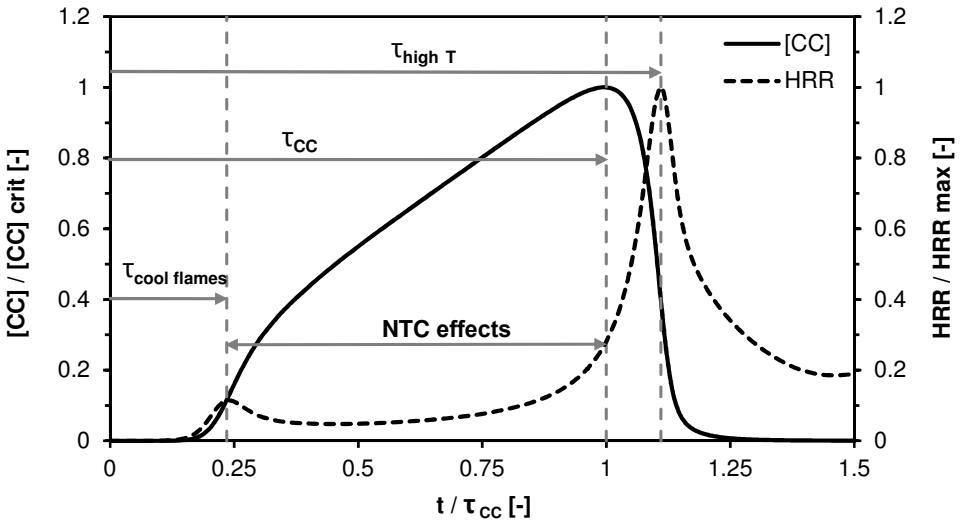


***Figure 2.2.*** *Different characteristic times of the ignition process.*

Finally, it should be noted that any active radical with chain behavior can be assumed as chain carrier. The characteristics that a chain carrier must satisfy include: accumulative behavior during the ignition delay, multiplier effect on its reaction rate and it must be consumed when the ignition occurs.

### 2.2.1 Chemical kinetics of the autoignition phenomenon

The oxidation of a hydrocarbon is extremely complex due to the huge amount of reactions that are involved in the process. In fact, detailed chemical kinetic mechanisms are only available for some pure fuels and their blends, and their predictive capabilities can be limited only to certain boundary conditions. This is the reason why the chemical formulations of the different chemical kinetic mechanisms are always under revision [18, 19]. Here, a simple scheme of the reactions involved in the oxidation of a hydrocarbon under different temperature conditions is presented. The scheme presented, despite of being simple, is able to explain the reactions that cause cool flames and the NTC zone.

The main chemical paths followed by the fuel during the ignition delay are highly dependent on temperature. Thus, the dominant decomposition path will be different for different instants of a process under transient thermodynamic conditions, as in an engine compression stroke. The oxidation scheme of a certain fuel - air mixture is quite well known in the range of temperature with practical applications [20]. However, the reactivity of some long-chain hydrocarbons at really low temperature (600 $K$ - 700 $K$) follows unknown chemical kinetics [21].

Fig. 2.3 shows the chemical paths involved in the autoignition process of a certain hydrocarbon, RH, at different temperature regimes. As it can be seen, the scheme can be divided in two different independent paths: the low-temperature chain branching and the high-temperature cracking [22].

i) Low-temperature chain branching mechanism.

At low temperature conditions, the chemical mechanisms are based in chain reactions in which hydroperoxide ($H_2O_2$) and hydroperoxyl ($HO_2$) radicals are the main active radicals, and keto hydroperoxides ($HOOCH_2OCHO \rightarrow OOQOOH$) and the carbonyl group are the intermediate species, which result in organic acids [23]. As described by several authors [16, 24, 25], the oxidation reactions start with the dehydrogenation of the fuel (RH) by the molecular oxygen ($O_2$) and by other radicals such as $HO_2$ and OH. The high activation energy of other fuel decomposition paths causes that only dehydrogenation is really important at low temperature. Moreover, due to the endothermic character of the $RH + O_2$ reaction, this path becomes not very important when enough radicals are generated. Alkyl radicals (R) and other important intermediate species as $H_2O$, $HO_2$ or $H_2O_2$ are formed directly by the fuel. The $\beta$-scission of alkyl radicals is very slow under low

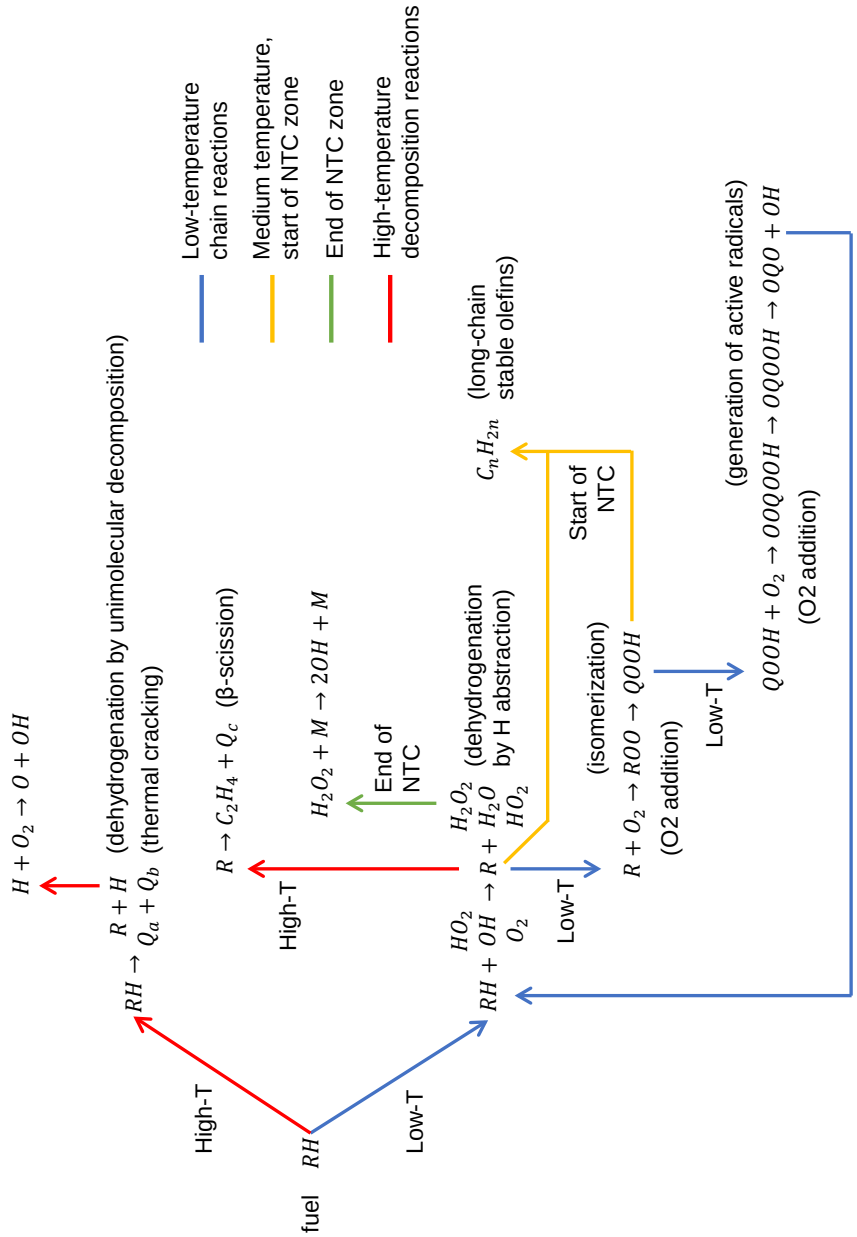


***Figure 2.3.*** *Autoignition mechanism of hydrocarbon - air mixtures.*

temperature conditions ($T \leqslant 900\ K$) due to its high activation energy. So that, the combination of alkyl radicals with the molecular oxygen is favored, forming alkylperoxy species (ROO). These species suffer an isomerization, which implies an internal movement of an atom of hydrogen from its original position to the end of the chain, and form alkyl hydroperoxides (QOOH). Thanks to the low temperature, the alkyl hydroperoxide reacts with the molecular oxygen to form carbonylhydroperoxide (OOQOOH), which finally degenerates to the OQOOH and OQO species, forming OH radicals. These species are atacked by oxygen and other radicals and the cycle starts again. The fuel is decomposed in short-chain hydrocarbons following the low-temperature chain branching mechanism, including formaldehyde ($CH_2O$), which is a typical tracer of the autoignition phenomenon and that can be considered as chain carrier of the process [26]. The chain reactions described above are slightly exothermic, causing a small increase in temperature (cool flames) that implies the competence of new decomposition paths.

Once the temperature reaches medium values, the formation of alkylperoxy species (ROO) competes with the formation of long-chain stable olefins ($C_nH_{2n}$) by the alkyl radicals (R). Moreover, alkyl hydroperoxides (QOOH), the concentration of which decreases due to the lower production rate of ROO species, also form more olefins, reducing the formation of carbonylhydroperoxide. This lower reaction rate of the chain branching results, consequently, in a lower production of active radicals and chain carriers that causes a loss of reactivity and originates the NTC zone. The exothermic reactions become much less relevant, causing a previous peak of heat release that corresponds to cool flames. Thus, the NTC behavior is promoted by the activation energy of the intermediate products, which causes the competition between radicals.

It is known that the third body reaction $H_2O_2 + M \rightarrow OH + OH + M$ controls the global reaction rate at the end of the NTC zone [27]. The third body $M$ is any species that can stabilize the reaction by absorbing part of the energy emitted. In the case of that specific reaction, $M$ could be, for instance, $H_2$, $H_2O$, CO or $CO_2$, among others, and the resulting reaction rate is different for each one of these species. During the NTC zone, the disappearance rate of $H_2O_2$ is much lower than its production rate, so that an accumulative behavior on the concentration of $H_2O_2$ occurs. Once the temperature is slightly increased up to a critical value, $H_2O_2$ is rapidly decomposed through the third body reaction previously mentioned, forming OH that consumes the remaining hydrocarbons very fast and causes the sudden heat release. At the same time, the accumulative behavior of $H_2O_2$ and $CH_2O$ ends and a critical concentration of such species is reached. Intermediate species are irreversibly

decomposed in $H_2O$ and CO, being the oxidation of formaldehyde to CO particularly relevant, which consumes most of the OH radicals generated [28]. Finally, CO is oxidized to $CO_2$. The temperature interval in which the NTC zone appears is very sensitive to changes in the other working conditions, such as pressure, oxygen concentration and equivalence ratio. The trends of the NTC zone depend on the global reactivity of the fuel, which can be controlled by different radicals depending on the temperature regime [29]. It should be noted that not all fuels show a two-stage autoignition pattern. Moreover, fuels do not present autoignition in two stages under all thermodynamic conditions. However, this does not mean that the chemistry related to cool flames and to the NTC behavior had not occurred. Actually, the NTC timescale is really small and cool flames and the high-temperature stage are virtually simultaneous.

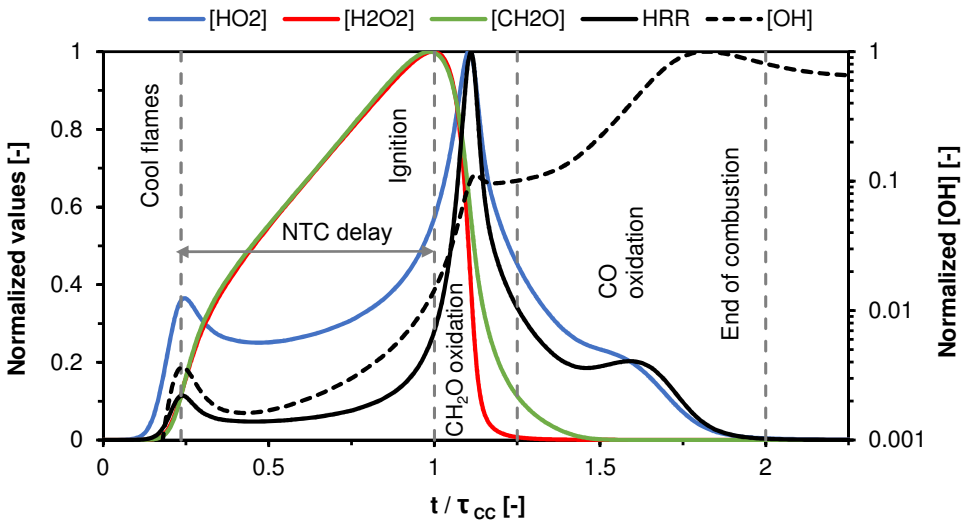


***Figure 2.4.*** *Evolution of the main active radicals during the autoignition process under low temperature. OH is plotted in logarithmic scale.*

Fig. 2.4 shows the evolution of different species during the ignition delay and the combustion process. The OH radical is plotted in logarithmic scale in order to identify the different relative maximum values. As can be seen, any peak of heat release rate corresponds to peaks of OH and $HO_2$. The exothermic peak caused by cool flames coincides with a maximum generation rate of $CH_2O$ and $H_2O_2$, meanwhile the exothermic peak caused by high-temperature reactions coincides with a maximum consumption rate of the

same two species. The NTC zone starts when the temperature is increased by cool flames and ends when $H_2O_2$ reaches a maximum. The oxidation of formaldehyde to CO defines the transition between low and high temperature reactions. This disappearance rate is controlled by the decomposition of $H_2O_2$, which generates the necessary OH radicals for the $CH_2O$ oxidation [30]. Thus, hydrogen peroxide and formaldehyde disappear almost together. Not much OH is accumulated during this stage because almost all this radical is consumed during the $CH_2O$ oxidation. As can be tested experimentally, the concentrations of formaldehyde and of hydrogen peroxide are good estimators of the ignition delay. In fact, these species can be taken as chain carriers, so that ignition occurs when a maximum concentration of such species is reached (the critical concentration). Finally, $HO_2$ is completely consumed during the oxidation of CO to $CO_2$.

As can be seen in Fig. 2.4, $HO_2$ radical is the key specie to generate the intermediate species after the dehydrogenization of the fuel by $O_2$. In fact, the accumulation behavior of $CH_2O$ and $H_2O_2$ starts when the maximum generation rate of $HO_2$ during the cool flames stage is reached. Moreover, $HO_2$ seems to be a good tracer of the cool flames heat release rate. Finally, OH seems to be a good tracer of the high-temperature stage of the process, since high temperature is needed for the accumulative behavior of this radical. Therefore, by tracing the concentrations of these species it is possible to know when the low and the high temperature stages occur [31].

Regarding the combustion products, Fig. 2.5 shows that small amounts of $H_2O$ and CO are generated during cool flames and the NTC zone. Almost all the $H_2O$ and CO are formed at the same time than the $H_2O_2$ decomposition and the $CH_2O$ oxidation. In fact, the maximum generation rates of water and carbon monoxide coincides with the maximum disappearance rates of hydrogen peroxide and formaldehyde. Besides, the maximum concentration of CO is reached when the $H_2O_2$ is completely consumed [32]. The oxidation of CO to $CO_2$ starts just after the end of the delay caused by the NTC zone, but it is not relevant until the appearance of the temperature increment caused by the $CH_2O$ oxidation. Finally, the maximum concentration of $CO_2$ coincides with the full consumption of $HO_2$, and this event defines the end of the combustion process.

ii) High-temperature chain branching mechanism.

It should be noted that the mechanism previously explained also occurs at high temperature conditions. However, high temperature causes changes in the relevance of the different decomposition reactions, and other chemical paths

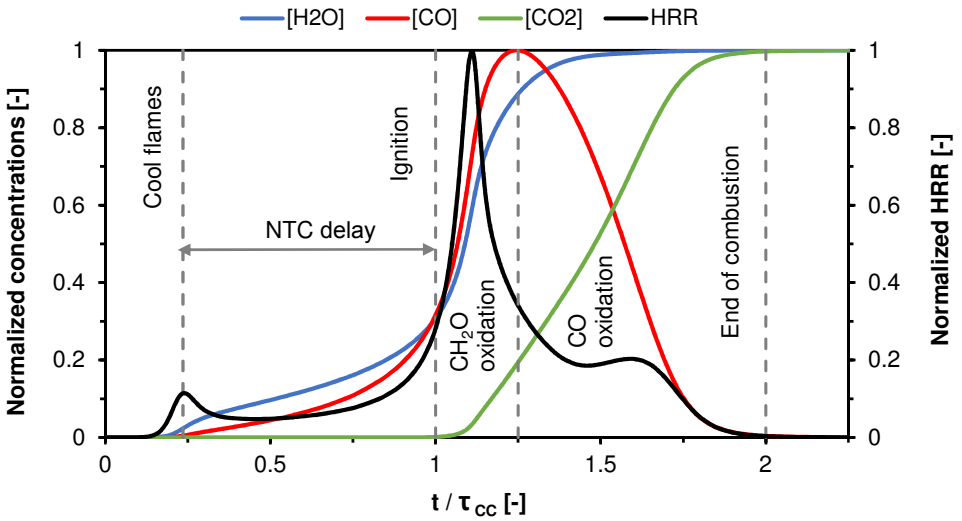


***Figure 2.5.*** *Evolution of the main combustion products during the autoignition process under low temperature.*

become dominant for the oxidation of the fuel. Fuel dehydrogenation is an important fuel decomposition path even at high temperature. Nevertheless, fuel thermal cracking gains relevance when the temperature increase above 1000 $K$ due to its high activation energy. Uni-molecular fuel decomposition produces two alkyl radicals ($RH \rightarrow Q_a + Q_b$) or one alkyl radical and atomic hydrogen ($RH \rightarrow R + H$). Alkyl radicals follow two main decomposition paths at high temperature conditions. First, it can form olefins or react with oxygen to form alkylperoxy species, as it has been explained previously. However, while under low temperature conditions the olefins formed are long and stable, for high temperature the alkyl radicals form short chain olefins, which are rapidly decomposed [24]. Secondly, $\beta$-scission of the alkyl radicals is fast enough to be relevant at high temperature. When an alkyl radical undergoes a $\beta$-scission, the radical breaks two carbons away from the charged carbon, producing an olefin ($C_nH_{2n}$) and a primary free radical, which has fewer carbon atoms. Meanwhile the ignition is controlled by the decomposition of $H_2O_2$ at low temperature, $H + O_2 \rightarrow O + OH$ is the most important high-temperature chain branching reaction that controls the formation of OH radicals [33]. After the fuel decomposition and the generation of active

radicals, olefins, short-chain hydrocarbons and other intermediate species are irreversibly decomposed in $H_2O$ and CO and, finally, CO is oxidized to $CO_2$.

Thereby, the autoignition process that takes place in an CI-engine can be described in four different consecutive stages [29]:

- Cool flames: they are controlled by the production of $HO_2$, which is necessary to form the most important intermediate species such as $CH_2O$ and $H_2O_2$. The initial fuel is decomposed in alkyl radicals by means of a dehydrogenization process in this stage. Brief exothermic activity and, simultaneously, a peak of concentration of $HO_2$ can be seen; and the temperature rise caused by these reactions leads to the next stage of the process.
- NTC zone: the reactivity of the mixture decreases, as well as the exothermic activity. The accumulation of formaldehyde and hydrogen peroxide occurs during this stage, the end of which is controlled by the $H_2O_2$ decomposition that triggers the conversion of formaldehyde to CO. A critical concentration of $H_2O_2$ is reached at the end of the NTC zone.
- CO formation: when the temperature is slightly increased by the slow reactions that take place during the NTC zone, all $H_2O_2$ is decomposed. The decomposition of $H_2O_2$ generates lots of OH, leading to the $CH_2O$ oxidation. Thus, CO is the main product of this stage.
- High temperature chemical reactions: They are controlled by the formation of OH radicals, which follow an accumulation behavior. These OH radicals oxidize the CO to $CO_2$, which is the main product of this stage. Finally, once the temperature starts to decrease, OH is recombined with atomic oxygen to form $O_2$ and atomic hydrogen, since OH is stable only at high temperature.

Taking into account the previous stages of the process, four types of autoignition events can be considered depending on the reached stage [30]:

- Misfire: not any stage is completed at all.
- Only low temperature chemical reactions are completed: high emissions of unburned hydrocarbons are produced, since formaldehyde is not able to decompose to CO.
- Cool flames and the NTC zone are completed: high emissions of CO, which is not able to oxidize to $CO_2$, are produced.

- Cool flames, the NTC zone and the high-temperature chemical reactions are completed: high emissions of $CO_2$. This case corresponds to a complete combustion.

### 2.2.2 Ignition delay trends

The experimental trends shown by the ignition delay are described in this section. Besides, these trends are justified following the previous reactions scheme, since the autoignition phenomenon is controlled by the chemical kinetics of the fuel. The trends of the NTC behavior are also analyzed, taking into account different operating conditions (temperature, pressure, oxygen content and equivalence ratio) and different fuels. Similar results than the following ones have been obtained by several authors in various studies [34–36]

A simple expression to characterize the ignition delay can be easily obtained starting from the conservation of species equation for the concentration of chain carriers:

$$\frac{d[CC]}{dt} + \nabla \cdot (\vec{u}[CC]) - \nabla \cdot (D\nabla[CC]) = \dot{\omega}_{CC} \tag{2.2}$$

where $[CC]$ represents the concentration of chain carriers and the different terms of the equation represent, respectively: the accumulative term, the convective term, the diffusive term (Fick's law) and the source term (global reaction rate).

Assuming a homogeneous mixture under static conditions, the convective and diffusive terms are null and Eq. 2.2 results:

$$\frac{d[CC]}{dt} + \cancel{\nabla \cdot (\vec{u}[CC])} - \cancel{\nabla \cdot (D\nabla[CC])} = \dot{\omega}_{CC} \tag{2.3}$$

Thus, a characteristic time of the process up to reach the critical concentration of chain carriers will be an estimator of the ignition delay and can be obtained as follows:

$$\frac{d[CC]}{dt} = \dot{\omega}_{CC} \rightarrow \tau \approx \frac{[CC]_{crit}}{\dot{\omega}_{CC}} \tag{2.4}$$

And taking into account the dependence of the global reaction rate on the working conditions:

$$\tau \approx \frac{[CC]_{crit}}{k_i \left[O_2\right]^a \left[F\right]^b} = \frac{[CC]_{crit}}{AT^n P^m exp\left(\frac{-E_a}{RT}\right) \left[O_2\right]^a \left[F\right]^b} \tag{2.5}$$

where $[O_2]$ and $[F]$ represent the concentration of reactants: oxidizer and fuel, respectively; and $k_i$ represent the specific reaction rate of the process. The expression to characterize the specific reaction rate can be deduced by the collision theory for bi-molecular reactions [37], where $A$ is the coefficient that imposes the units of $k_i$, $n$ and $m$ are dimensionless experimental coefficients, $E_a$ is the activation energy and $R$ is the universal gas constant. This expression coincides with the Arrhenius' empirical expression, which can be extrapolated to reactions with an order different from two. Following a qualitative interpretation of the Arrhenius' expression, $AT^n P^m$ depends on the reactant molecules and it is an estimator of the collision frequency, meanwhile the exponential term is an estimator of the percent of collisions that have energy enough to react. Eq. 2.5 describes a classical correlation for the ignition delay that has been experimentally adjusted by several authors for different fuels [17, 35, 38].

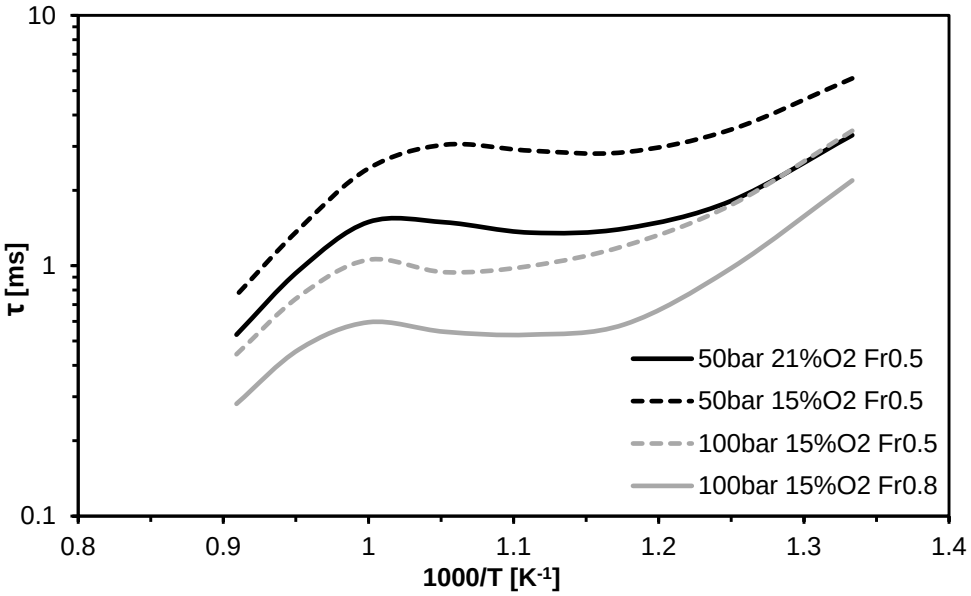


***Figure 2.6.*** *Ignition delay versus temperature under different working conditions for n-heptane (logarithmic scale).*

Fig. 2.6 shows the dependence of the ignition delay on temperature. As it can be seen, the ignition delay is decreased if the temperature is increased except in the NTC zone. Despite the fact that the NTC behavior can be smooth enough to avoid an increase of the ignition delay, the ignition delay decreasing rate is usually affected by this phenomenon, changing the slope of the curve. Taking into account that ignition depends on the chemical kinetics of the mixture, higher temperature implies higher specific reaction rates. In fact, regarding Eq. 2.5, higher temperature means higher collision frequency and collision energy and, therefore, shorter ignition delay. According to cool flames, this phenomenon has shown to be highly dependent on temperature. The ignition delay referred to cool flames is always shorter if the temperature is increased. Obviously, cool flames are not affected by the loss of reactivity of the NTC behavior since it occurs before the NTC zone.

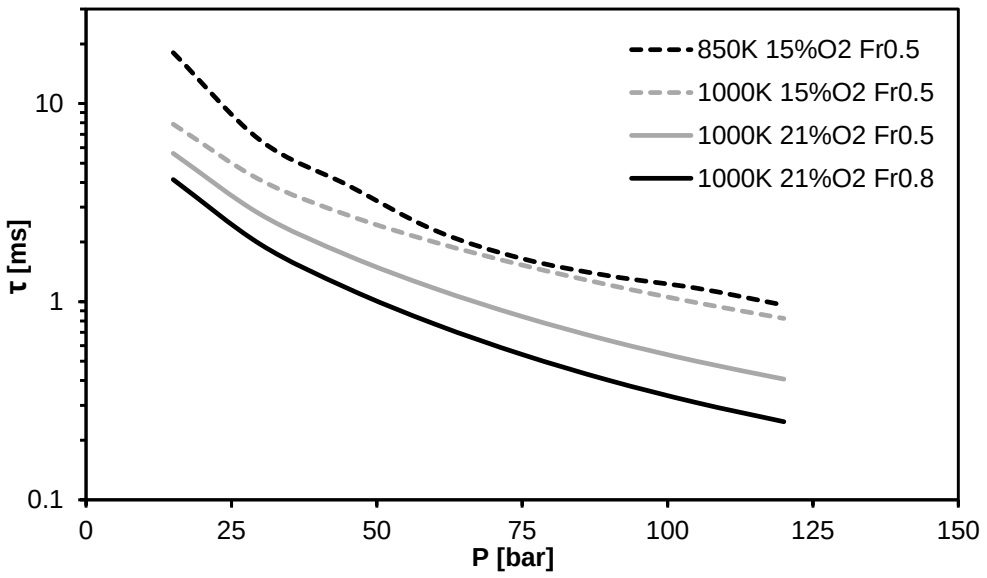


***Figure 2.7.*** *Ignition delay versus pressure under different working conditions for n-heptane (logarithmic scale).*

Fig. 2.7 shows the dependence of the ignition delay on pressure. Ignition delay decreases when the pressure is increased for the hydrocarbons typically used in real applications. Regarding Eq. 2.5, higher pressure means a higher collision frequency and, therefore, shorter ignition delay. Moreover, it can be seen in Fig. 2.6 that the NTC zone is moved to higher temperature and it

becomes less pronounced if the pressure is increased. This behavior depends exclusively on the competence between the formation of long-chain olefines at medium temperature and the chain branching at low temperature, since both global reaction rates are affected by the pressure. The ignition delay referred to cool flames is slightly shorter if the pressure is increased. However, this phenomenon shows small dependence on pressure.

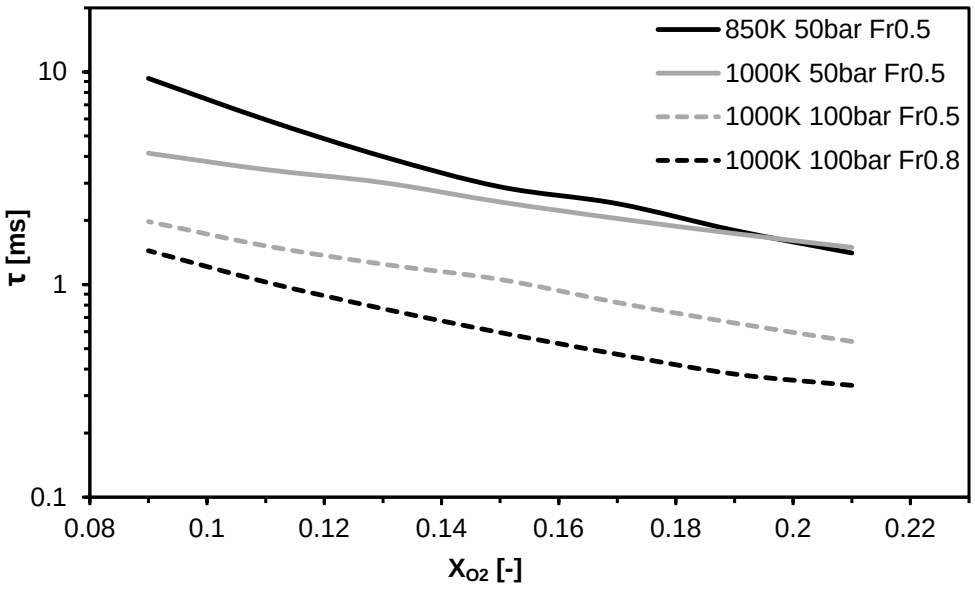


***Figure 2.8.*** *Ignition delay versus molar fraction of oxygen under different working conditions for n-heptane (logarithmic scale).*

Fig. 2.8 shows the dependence of the ignition delay on the oxygen concentration. Ignition delay increases when the oxygen molar fraction of the mixture is decreased, since lower amount of oxidizer implies lower reactivity. In the same way, it can be seen in Fig. 2.6 that the NTC zone is moved to lower temperature and it becomes more pronounced if the oxygen proportion is reduced. Moreover, the ignition delay referred to cool flames is also shorter if the percent of oxygen is increased.

Fig. 2.9 shows the dependence of the ignition delay on the equivalence ratio under two different scenarios. First, the ignition delay behavior under low temperature conditions is plotted in Fig. 2.9-Top. Both ignition delays (referred to cool flames and referred to the high-exothermic stage of the process) decrease when the equivalence ratio is increased in that particular

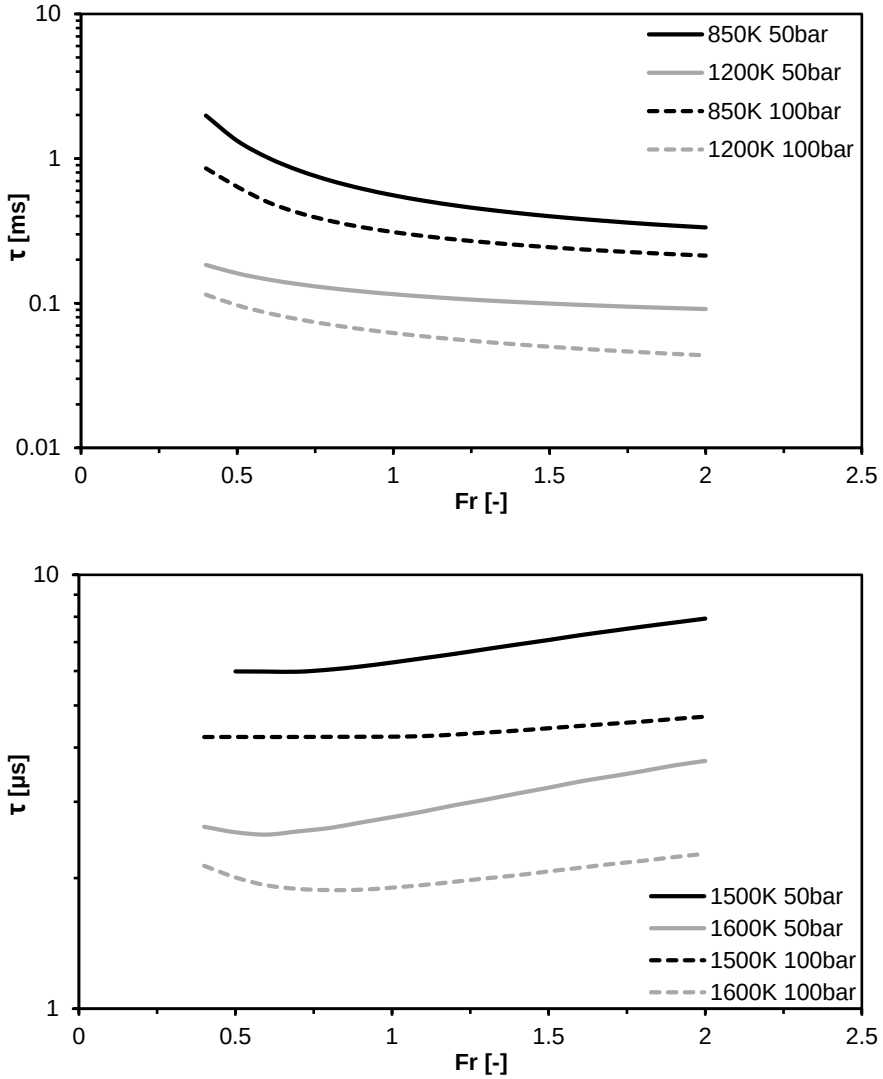


***Figure 2.9.*** *Ignition delay versus equivalence ratio under different working conditions for n-heptane - dry air mixtures (logarithmic scale). Top.- Low-temperature chain branching conditions. Bottom.- High-temperature thermal cracking conditions.*

case, since ignition occurs when a critical concentration of chain carriers is reached. The accumulation of chain carriers depends on the amount of fuel, so that, the higher the equivalence ratio the higher the generation rate of chain carriers and the shorter the ignition delay. Besides, Fig. 2.6 shows that the NTC zone is moved to higher temperature and it becomes less pronounced if the equivalence ratio is increased. Secondly, the ignition delay behavior under high temperature conditions is plotted in Fig. 2.9-Bottom. Ignition delay increases when the equivalence ratio is increased, since the ignition event depends on the decomposition of the fuel by thermal cracking. The lower the equivalence ratio, the lower the amount of fuel to be decomposed and, therefore, the shorter the decomposition time and the ignition delay [24].

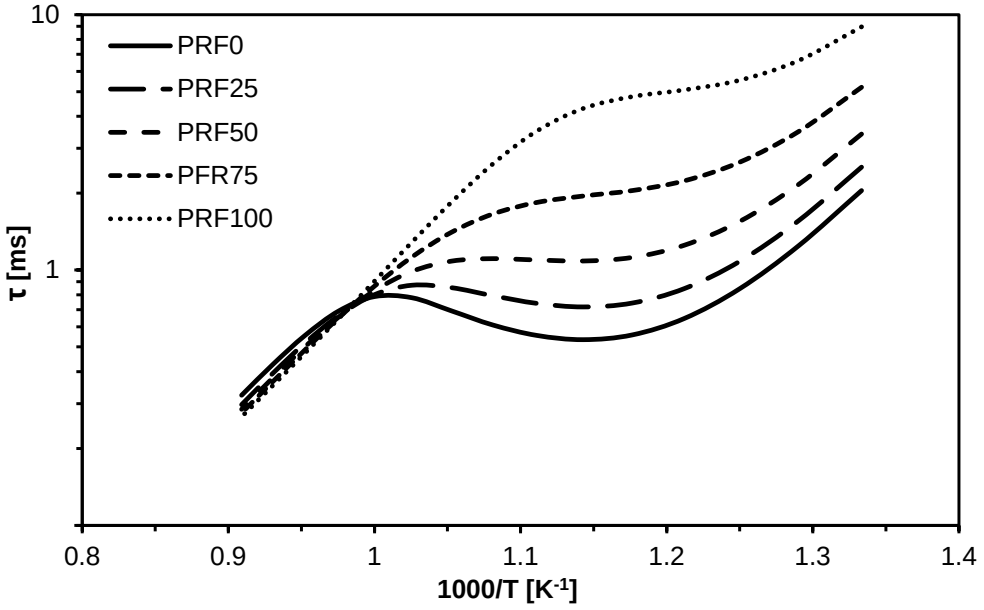


***Figure 2.10.*** *Ignition delay versus temperature for different PRF blends mixed with dry air under stoichiometric conditions at 50 bar.*

Finally, Fig. 2.10 shows the dependence of the ignition delay on the type of fuel. Ignition delay variations with the octane number are described by plotting five different PRF mixtures (n-heptane and iso-octane blends). Obviously, the higher the octane number, the longer the ignition delay, since the octane number represents, with strong non-linearity, the resistance of a certain fuel to be autoignited. Differences in octane number are reflected

in differences in cool flames intensity. Higher amounts of low-temperature heat release and higher quantities of $H_2O_2$ are correlated with earlier ignition and lower octane number values [39]. Furthermore, the NTC zone is more pronounced and it is moved to lower temperature if the octane number is decreased. The existence of a NTC behavior smooth enough to avoid a two-stage ignition pattern is very sensitive to the composition of the fuel. In fact, there are some species that can inhibit this behavior when they are added, resulting in single-stage ignition processes, e.g. toluene or methyl tert-butyl ether [40].

Finally, the sensitivity of both ignition events (cool flames and the high-exothermic stage of the process) with the operating conditions can be studied by analyzing the results of the different experimental adjustments of Eq. 2.5 [17, 35, 38]. The constants $m$, $a$ and $b$, which respectively affect to pressure, oxygen and fuel concentration, are higher in case of the high-exothermic ignition delay. Therefore, cool flames are less dependent on these operating conditions than the high-temperature heat release rate. Otherwise, the activation energy involved in Eq. 2.5 is higher for cool flames, which proves that this phenomenon is mainly controlled by temperature instead of other working parameters.

In summary, the dependence of the ignition delay on the typical working conditions presented in internal combustion engines is as follows:

- The ignition delay decreases if the reactivity of the mixture is increased: higher temperature (with the exception of the NTC zone), higher pressure, higher oxygen concentration or higher equivalence ratio (under conditions with practical application).
- The NTC zone is smoother and it is moved towards higher temperature if the reactivity of the mixture is increased: higher pressure, oxygen content or equivalence ratio (but not with the octane number).
- If the octane number of the fuel is increased the ignition delay is longer, the NTC zone is smoother and it is placed at lower temperature, and the fuel is less prone to show a two-stage ignition pattern.

### 2.2.3 Ignition delay under transient conditions. The Livengood & Wu integral method

From a theoretical point of view, the autoignition phenomenon is usually studied under constant thermodynamic conditions, since the chemical kinetics

can be easily traced and the effects of the different operating conditions can be also easily compared. Thus, if an air-fuel mixture is submitted to certain conditions of temperature and pressure, which remain constant to physical effects and that can be changed only by chemical reactions, the autoignition of the mixture will occur after a certain time, $\tau$, which is called ignition delay under constant conditions. The contour plots of $\tau$ versus these thermodynamic conditions (autoignition maps) are widely used to study the autoignition characteristics of a given fuel, but they are not able to provide enough information when a process under transient conditions of temperature and pressure occurs, e.g. the compression stroke of an engine.

Despite the fact that the ignition delay of a homogeneous air-fuel mixture under constant and full-controlled thermodynamic conditions can be obtained by means of several experimental facilities [41, 42], the parameter of interest in applied studies is the ignition delay under transient conditions of pressure and temperature, $t_i$. There are different numerical tools (see Section 2.3.3) and experimental facilities (see Section 2.3.1.4) to study the ignition delay, $t_i$, of a mixture. However, from a phenomenological point of view, a process under transient conditions of pressure and temperature can be discretized in a series of thermodynamic states that remain constant during a time step. According to this idea, the Livengood & Wu hypothesis [43], also known as the Livengood & Wu integral or, simply, the integral method, allows to obtain ignition delays of processes under variable conditions of temperature and pressure by using the ignition characteristics under constant thermodynamic conditions, which are much easier to obtain. The expression proposed by these authors is the following:

$$\int_0^{t_i} \frac{1}{\tau} dt = 1 \tag{2.6}$$

where $t_i$ is the ignition delay of the process and $\tau$ is the ignition delay under constant conditions of pressure and temperature for the successive thermodynamic states.

The Livengood & Wu integral assumes that the oxidation process during the ignition delay can be described by a single zero-order global reaction and, therefore, the reaction rate does not depend on time under constant thermodynamic conditions. It should be noted that it is not possible to describe the NTC behavior by means of that type of reaction. Moreover, the authors assumed that the autoignition occurs when a critical concentration of chain carriers is reached, being this critical concentration constant for a given air-fuel mixture. Therefore, the ignition delay function, $\tau$, and the ignition

time that appears in the upper limit of Eq. 2.6 should be referred to a critical concentration of chain carriers.

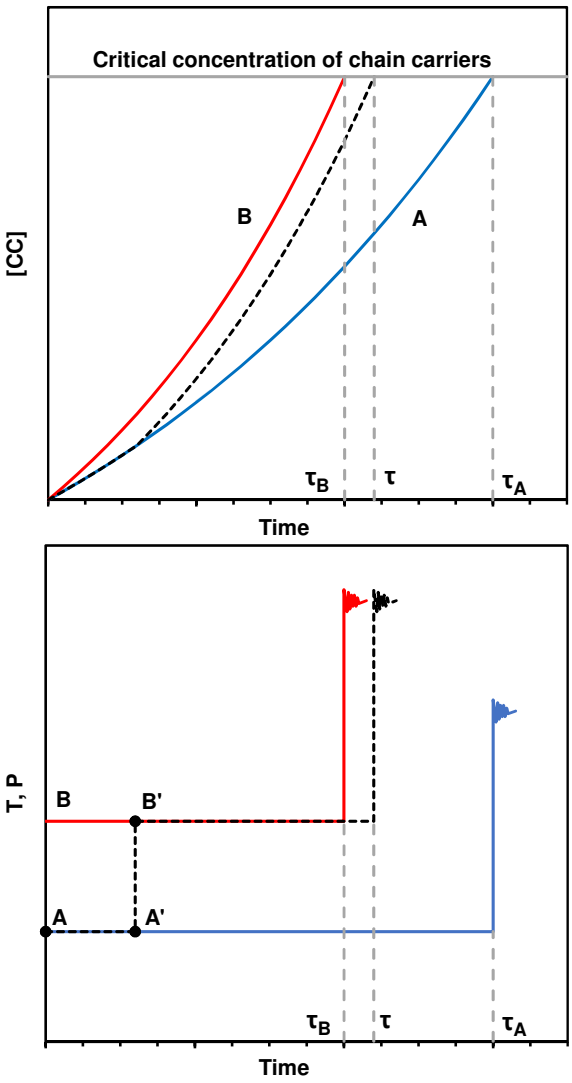


***Figure 2.11.*** *Schematic of the law of conservation of the ignition delay. Top.- Concentration of chain carriers. Bottom.- Thermodynamic paths.*

Taking into account the two previous hypotheses, Livengood & Wu enunciated the law of conservation of the ignition delay, which can be described

based on the schematic presented in Fig. 2.11. Two experiments were performed at different thermodynamic states, A and B, in the figure. If a third experiment is performed employing a stepped compression path $A - A' - B'$, then the overall reaction time will be:

$$\tau = n\tau_A + (1 - n)\tau_B \tag{2.7}$$

where $n$ is the time fraction of $t/\tau$ which elapsed at state A before the next step of the compression to state B. Eq. 2.7 can be obtained only if the critical concentration of active radicals is constant for an equivalence ratio and a type of fuel, whatever the temperature and pressure (Fig. 2.11 - Top). Furthermore, the previous relationship can be discretized and integrated, resulting in Eq. 2.6, only if the global reaction rate does not change with time during a fixed state process (zero order reaction). A priori, these assumptions seem rather unlikely. The critical concentration depends on the decomposition of $H_2O_2$, which depends on temperature and pressure, and a zero-order reaction cannot describe the NTC behavior. Therefore, a study about the validity of the Livengood & Wu hypotheses is required.

The integral method has been traditionally enunciated as a method to predict the occurrence of knock in SI-engines [44]. However, it has been extended to CI-engines as a way to predict the ignition delay of homogeneous air-fuel mixtures as the ones used in HCCI engines [45]. The method has great interest for the prediction of autoignition due to its simplicity and low computational cost, but this simplicity is a consequence of the hypotheses assumed for its development. In fact, as Fig. 2.12 shows, if the $\tau$ function is known, the autoignition process can be characterized by calculating the upper limit of Eq. 2.6 that makes the area indicated in the figure equal to 1.

As it has been shown in Section 2.2.2, it is easy to obtain expressions for $\tau$ as the following one:

$$\tau = AT^n P^m exp\left(\frac{T_a}{T}\right)[O_2]^a [F]^b \tag{2.8}$$

where $T_a$ is the activation temperature. This type of expressions must be adjusted experimentally in order to obtain the values of $A$, $n$, $m$, $T_a$, $a$ and $b$, which are constants for a range of temperature, pressure, equivalence ratio and for a type of fuel [46]. However, it is not possible to reproduce the NTC zone with the previous correlation [47].

Weisser [48] originally proposed a 3-Arrhenius model to parameterize the ignition delay under constant conditions taking into account the NTC

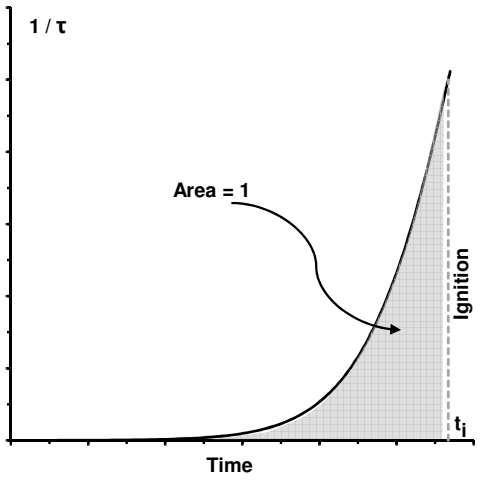


***Figure 2.12.*** *Schematic of the Livengood & Wu integral method.*

behavior. This model was further extended by Vandersickel [42] to include the influence of the oxygen concentration on $\tau$, resulting the following equation:

$$\frac{1}{\tau} = \frac{1}{\tau_1 + \tau_2} + \frac{1}{\tau_3} \tag{2.9}$$

where the three characteristic times $\tau_1$, $\tau_2$ and $\tau_3$ can be correlated as follows:

$$\tau_j = A_j \left(\frac{P}{P_{ref}}\right)^{\beta_j} T^{b_j} exp\left(\frac{T_{a,j}}{T}\right) F_r^{c_j} \left(\frac{[inert]}{[O_2]}\right)^{d_j} exp\left(\frac{[inert]}{[O_2]}\frac{e_j}{T}\right) \tag{2.10}$$

where $j \in \{1, 2, 3\}$. The reference pressure $P_{ref}$ is equal to 1 $bar$ and $F_r$ represents the equivalence ratio, while $[inert]$ represents the EGR rate in volume. $A_j$, $\beta_j$, $b_j$, $T_{a,j}$, $c_j$, $d_j$ and $e_j$ are constants that should be experimentally adjusted.

In Eq. 2.9, the low temperature reactions (represented by $\tau_1$) and the NTC reactions (represented by $\tau_2$) occur sequentially, leading to a two-stage ignition pattern. Therefore, they are directly added to one another. The high temperature reactions (represented by $\tau_3$) lead to a parallel single-stage ignition pattern, so that it is an independent term. Fig. 2.13 (from [49]) shows the coupling of the three characteristic times. $\tau_1$ represents the ignition delay referred to cool flames, and it can be used coupled with the

Livengood & Wu integral method to predict this phenomenon. Otherwise, the global characteristic time $\tau$ is referred to the high-temperature stage of the combustion and can be also linked to the integral method for the prediction of the ignition delay. It should be noted that ignition is defined as the time at which a maximum concentration of chain carriers occurs in the Livengood & Wu predictive method, so that the validity of using a $\tau$ function referred to other stages of the ignition process should be studied.

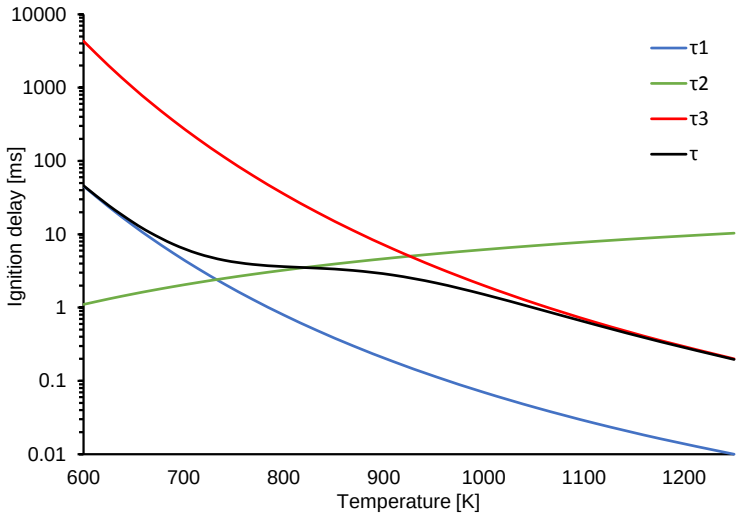


***Figure 2.13.*** *Schematic of the 3-Arrhenius model to parametrize the ignition delay. $\tau_1$ (blue) represents the cool flames, $\tau_2$ (green) represents the NTC zone, and $\tau_3$ (red) represents the high-temperature reactions. The ignition delay $\tau$ (black) is obtained by composition of the other characteristic times.*

The integral method has been used in several CFD studies as the model to predict the autoignition time. For example, Imamori et al. [50] coupled the Livengood & Wu integral with Star-CD and KIVA 3 to improve the performance of a low speed two-stroke Diesel engine. And Li et al. [51] linked the integral method with the CFD code VECTIS to study the effects of heterogeneities on a two-stroke HCCI engine fueled with gasoline.

A new use of the Livengood & Wu integral is its implementation in an engine control unit. Several authors, such as Ohyama [52], Rausen et al. [53], Choi et al. [54] and Hillion et al. [55], used the integral method to predict the start of combustion under HCCI conditions. This method can

be combined with other simple models to obtain global parameters of the combustion process allowing the control of the engine in real time.

Bradley et al. [56, 57] used the Livengood & Wu hypothesis to obtain the octane number of non-PRF fuels by predicting the ignition delay of PRF fuels under engine conditions, with the aim of relating the octane number with the ignition delay. Reyes et al. [58] measured the knock time of n-heptane and of a mixture of 50% n-heptane - 50% toluene in a constant volume vessel. Knock times, which correspond to ignition delays under variable thermodynamic conditions, were used with the Livengood & Wu integral to obtain correlations for the ignition delay under constant conditions, $\tau$. Finally, these correlations were used with the integral method to predict ignition delays under engine conditions. In fact, different correlations for $\tau$ have been proposed by several authors in order to take into account the effect of EGR or of the equivalence ratio, such as the works of Swan et al. [45] or Hoepke et al. [46].

The validity of the Livengood & Wu integral when a two-stage ignition occurs has been wondered by several authors [59]. The integral method is not able to accurately predict the ignition delay because it is based on a single global reaction mechanism that ignores the cool flames. Some of these authors, as Liang and Reitz [60] or Edenhofer et al. [61], show the need to create simple algorithms, but more sophisticated than the integral method, to characterize the autoignition process at low temperature without using any chemical kinetic mechanism (due to simplicity and low computational cost). However, few alternatives to the Livengood & Wu integral can be found in the literature.

Hernandez et al. [62] analyzed the validity of the Livengood & Wu integral by simulations performed with CHEMKIN for several fuels and with various chemical kinetic mechanisms. They proved that the predictions of the method are accurate if the fuel do not show a two-stage ignition pattern. These authors also proposed two different alternatives, one with better and another with worse results than the integral method. However, the validity of the Livengood & Wu integral should be not only analyzed, but also justified. Moreover, most of the alternatives proposed to improve the integral method are based on the integral method itself or assume the same hypothesis, which are too simplified. Numerical expressions based on more sophisticated autoignition mechanisms are needed in order to extend the range of validity of the methods. Moreover, both exothermic stages should be predicted in the case of fuels that show two-stage ignition: cool flames and the high-exothermic heat release. In fact, these research gap is intended to be solved in this Thesis.

## 2.3 Experimental facilities and numerical tools to characterize the autoignition phenomenon

Advances in chemical kinetics allow to improve the knowledge about the in-cylinder combustion process. Better predictive capability about the different ignition events enables the use of advanced LTC modes [63], mixed-mode combustion regimes (dual-fuel technology) [64] or the use of alternative fuels [65]. All these strategies are focused on reducing the pollutants formation and emissions, while keeping a high engine efficiency. There are several experimental facilities designed to study autoignition that are focused in points of view other than the chemical kinetics one, most of which are based on bringing an air-fuel mixture under certain thermodynamic conditions and measuring the time interval between the instant at which these conditions are reached and the start of combustion [19, 66, 67].

In the following paragraphs the experimental facilities usually used to study the autoignition phenomenon are presented. Moreover, their advantages and disadvantages are described, as well as the main challenges to overcome when experimental autoignition studies are carried out. Finally, some numerical tools to analyze the ignition and combustion processes are also shown.

### 2.3.1 Experimental facilities

The main experimental facilities used to study autoignition are described in this section, highlighting their capabilities according to the thermodynamic conditions that they are able to reach and their capability of working with homogeneous and/or heterogeneous mixtures. It should be noted that autoignition studies are not typically carried out in single-cylinder engines but in facilities like Rapid Compression Machines (RCM) [68], shock tubes [69] or combustion vessels [70]. For chemical kinetics studies a quiescent, isothermal, adiabatic combustion zone is desirable with complete control on the gas composition, which are impossible to achieve in internal combustion engines [71]. The facilities described in this section can work under fully controlled initial and boundary conditions by avoiding the complexities associated to engines, such as the valves, lubrication and cooling systems; and by means of adding hardware such as heaters, simpler geometry or extra sensors. Thus, a cleaner environment than the one present in a traditional engine is guaranteed, without residual gases and knowing the initial pressure and temperature, the volume and the mass trapped. Experimental data obtained from such facilities

are extremely useful for the development of detailed chemical kinetics for combustion modeling, since even a detailed chemical kinetic mechanism needs to be validated by comparison to high fidelity experimental results over a wide range of operating conditions.

#### 2.3.1.1 Combustion vessels

A combustion vessel is a constant volume combustion chamber, usually optically accessible [72], which can work under high pressure and high temperature conditions. Many combustion aspects are usually studied by using this facility, such as atomization and other spray parameters [73], spark ignition of air-fuel mixtures [74], flame propagation and combustion velocities [75], or pollutants formation [76]. However, combustion vessels are described in this paragraph according to their capability to study autoignition.

Depending on how the facility reaches the desired thermodynamic conditions, combustion vessels can be divided in two different groups:

i) Closed test chambers that can simulate steady conditions thanks to high pressure gas tanks and electric heaters. Ambient gas temperature and pressure up to 1000 $K$ and 150 $bar$, respectively, can be reached in these facilities [77]. They work under constant thermodynamic conditions, which is a perfect environment to perform chemical kinetic analysis. However, long time is required to reach the desired temperature and pressure, so that it is not possible to directly study the autoignition of homogeneous mixtures, the characteristic time of which is very short. Thus, these test chambers are limited to measure the ignition delay of sprays when they work without a preburn stage [78]. Another usage of these combustion vessels is the study of knocking [58]. A homogeneous air-fuel mixture is ignited thanks to a spark, creating a flame front. The fuel that remains unburned increases its temperature and pressure due to such flame and, finally, it ignites. Ignition delays can be measured by tracing the pressure signal in the chamber, since these facilities correspond with a constant volume closed reactor [79].

ii) Preburn combustion vessels that generate hot gases to reach the desired thermodynamic conditions. The ambient pressure, temperature and species composition at the time of the experiment are varied by igniting a premixed fuel-gas mixture that is completely burned. The combustion products cool over a relatively long time ($\approx$500 $ms$) after the spark-ignited premixed combustion due to heat transfer to the vessel walls, so that the

vessel pressure slowly decreases. However, quasi-steady thermodynamic conditions are kept during a period of time, which defines the time of the experiment [80]. Moreover, most of these vessels include fans to create a stirred environment that guarantees homogeneity [81]. It is not possible to work with homogeneous mixtures in this facility, since the experiment conditions are reached after a pre-combustion. Therefore, only the ignition characteristics of a fuel spray can be studied [82]. In this case, ignition delays can be also measured by tracing the pressure signal in the chamber, since this facility also corresponds to a constant volume closed reactor.

The constant flow test rig is a particular case of combustion vessel that consists on a constant volume open reactor working under constant pressure conditions. The desired thermodynamic conditions to perform the experiments are reached thanks to high flow compressors and electric heaters. The continuous flow improves the temperature homogeneity and ensures steady state thermodynamic conditions inside the chamber [83]. However, this facility is limited to work with direct injection of fuel. Moreover, the ignition delay of the spray cannot be measured by using criteria based on the pressure signal, since pressure remains constant during the experiment. Therefore, the application of optical techniques to determine the time of ignition is mandatory, which leads to more difficult measurements [84]. A picture of the constant flow test rig available at CMT - Motores Térmicos is shown in Fig. 2.14.

It should be noted that the thermodynamic conditions reached in an engine cannot be simulated in these facilities, since they work under constant pressure and temperature. Moreover, transient conditions cannot be replicated because of the long characteristic time of heating.

#### 2.3.1.2 Shock tubes

A shock tube is a tube in which a gas at low pressure (driven gas) and a gas at high pressure (driver gas) are separated using some form of diaphragm, which suddenly bursts under predetermined conditions to produce a wave propagating through the low pressure section. This facility has been used for years due to its simplicity and high capabilities to study combustion phenomena. In fact, the first studies in shock tubes were performed in France in 1899 by Paul Vieille, who published shock tube results in “Comptes Rendus de l’Académie des Sciences - Paris” [85]. The shock tube has the capability of compressing (and thereby heating) a gaseous sample of

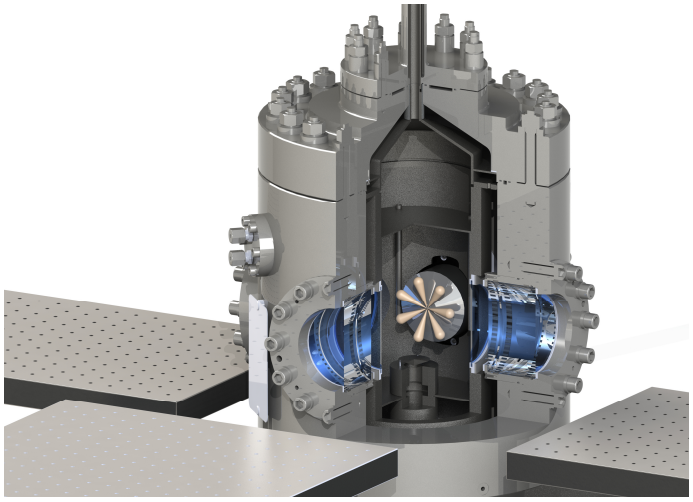

***Figure 2.14.*** *Picture of the constant flow test rig available at CMT - Motores Térmicos.*

an air-fuel homogeneous mixture virtually instantaneously, and it allows to follow the complex changes that take place until the oxidation reaction is complete and the final products, usually water and carbon dioxide, emerge [86]. Detonations and explosions are usually studied with these facilities [87]. However, shock tubes are described in this paragraph according to their capability to study autoignition. In order to trace the chemical kinetics of a homogeneous reactive mixture under constant conditions of pressure and temperature it is important to reach the desired conditions as fast as possible to avoid the fuel decomposition during the heating process, and this is guaranteed thanks to the characteristic compression times of a shock tube [88].

Fig. 2.15 shows the basic schematic of a shock tube, where the test sample and the driver gas are separated by a diaphragm. The operating principle of this facility is based on the expansion of the high-pressure driver gas upon the opening of the diaphragm, creating a shock wave. The test gas is compressed to ignition conditions by the incident and reflected shock waves and the experiments can be monitored between both shock fronts or after the reflected wave.

Several methods are commonly used to burst the diaphragm depending on the type of study being performed, including mechanically-driven plungers,

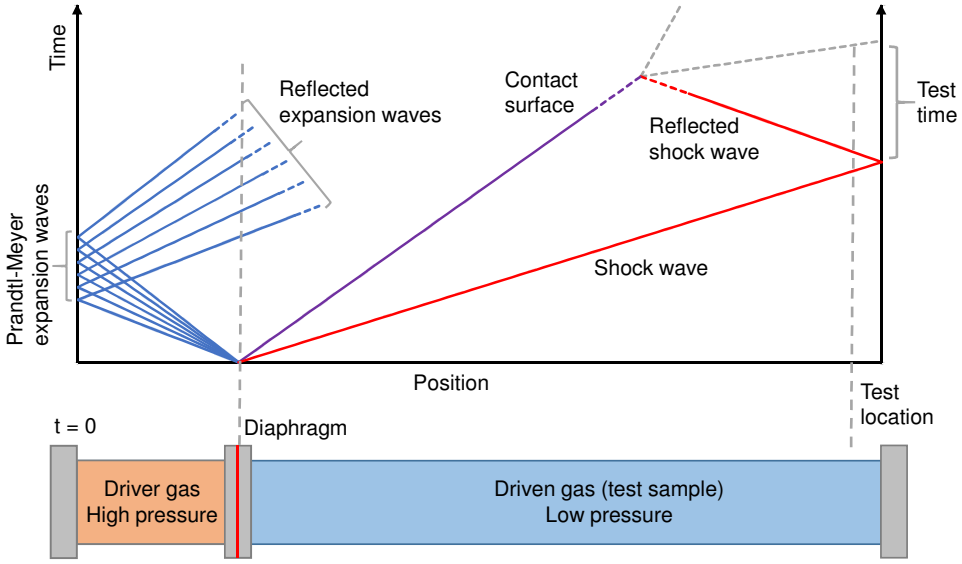


***Figure 2.15.*** *Schematic of a shock tube and its operating principle.*

explosive charges, mixtures of combustible gases designed to produce a detonation and the use of plastic or metal diaphragms that define a specific bursting pressure [89]. The diaphragm bursting produces a series of pressure waves, each of which increasing the speed of sound behind it. Thus, a shock front that is propagated through the test sample is originated. This shock front increases the temperature and pressure of the driven gas and induces a flow in its direction. However, such flow has lower velocity than the incident wave, so that driver and driven gases keep decoupled by a contact surface [90]. The thermodynamic conditions reached in the test sample depend on the intensity of the incident shock wave, the velocity of which can be calculated by using the Rankine-Hugoniot equations. In fact, Fig. 2.16 shows the thermodynamic conditions that can be reached in a shock tube compared to the conditions at TDC reached in engines without combustion. The driver gas is usually chosen to have a low molecular weight, (e.g., helium or hydrogen) and it is heated up to high initial temperature, since the lighter the driver gas and the higher its speed of sound, the higher the intensity of the wave [91]. Simultaneously, a rarefaction wave, named Prandtl-Meyer expansion wave, goes back to the driver gas, the conditions of which are also known.

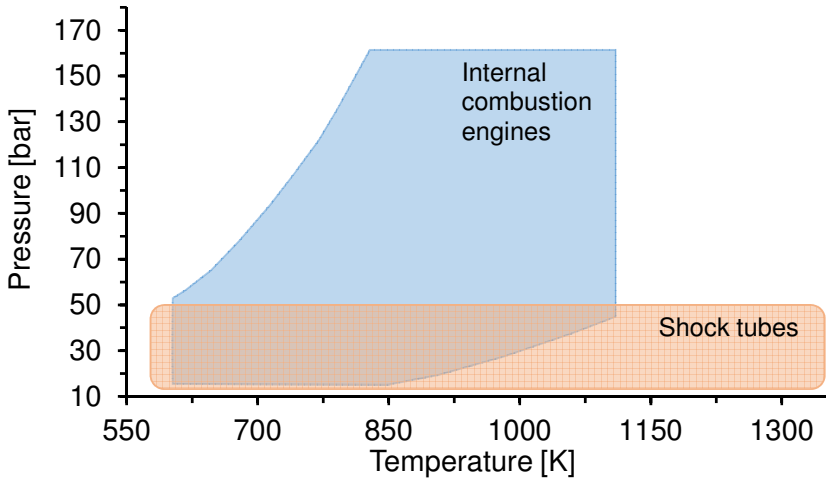


***Figure 2.16.*** *Thermodynamic conditions reached in shock tubes compared to the ones reached in engines under motoring conditions.*

Shock tubes are characterized by the existence of a testing time, which is defined by the interaction between the incident shock wave, the reflected shock wave and the contact surface. Observations can be made in the flow behind the incident front or, as usual, behind the reflected wave, since this last option shows advantages of longer testing times [92]. Despite the fact that the typical test time is around 1-3 $ms$, longer driver lengths and custom-made compositions of driver gases can optimize the interaction between the reflected shock wave and the contact surface, increasing the test time over 10 $ms$ (up to 35-45 $ms$) [93]. The reflected shock allows low-to-medium pressure conditions (up to 50 $bar$) and high temperature conditions (up to 1800 $K$). It should be noted that there is no overlap with the conditions achievable in rapid compression machines, in which the test time is around 10-150 $ms$ and where high pressure (up to 120 $bar$) and low-to-medium temperature (up to 1100 $K$) can be reached [94].

These facilities present some characteristics that provide a suitable environment to study autoignition, where the ignition delay is usually defined as the time between the crossing of the reflected shock wave and the onset of ignition (for measurements performed after the reflected shock) [95]. Despite the fact that fuel sprays can be also tested in shock tubes, homogeneous air-fuel mixtures are usually studied with them. Shock tubes can show a virtually constant positive pressure gradient after the reflected wave, which means a

constant rate of pressure rise as a function of time due to a non-ideal facility behavior. This effect causes that measured ignition delays are shorter than the ones obtained with an ideal facility such as a perfectly stirred reactor, and it should be taken into account when comparisons are made [90].

#### 2.3.1.3 Rapid Compression Machines

Rapid Compression Machines (RCM) have a long history in the study of the autoignition phenomenon. The first machine was built by George Falk at Columbia University (USA) in 1906 [96] and the original design has been improved during years in order to obtain facilities that provide the ideal conditions to study chemical kinetics and to measure ignition delays. An RCM is able to perform a single compression event in a few milliseconds, forming a constant volume combustion chamber under high thermodynamic conditions. RCMs allow the study of fuel-air mixtures autoignition under easily controlled and reproducible conditions in a cleaner environment than the traditional engine [97]. The analysis of the chemical and physical behavior of different fuels during the ignition process can be performed in these machines, including a wide range of equivalence ratios, gas or liquid fuels [98] or alternative fuels as hydrogen or bio-fuels [41].

The enclosed gases are rapidly compressed to high pressure and temperature conditions and the chemical reactions proceed in a constant volume and constant mass chamber in the RCM. In order to avoid significant heat losses and the occurrence of relevant chemical activity before reaching its end position, the piston is required to travel very fast. High velocities are reached thanks to a (usually) pneumatically driven piston, which is hydraulically decelerated by using a stopping ring and a groove mechanism [71]. Moreover, the compression process should be free from any significant mechanical vibration, especially to allow the use of optical techniques and to avoid undesirable effects in the acquired data caused by changes in the volume of the reaction chamber. There are two different structural constructions of RCMs, depending on how they perform the compression stroke: some RCMs use a single piston to compress the air-fuel mixture [99], while other machines use twin opposed pistons (which has shown to reduce vibrations and compression time) [100]. RCMs are very flexible facilities, in which the compression ratio (stroke and/or cylinder clearance), the initial pressure and the initial temperature can be changed in a wide range. Minimizing the final volume of the combustion chamber is important in order to ensure uniformity. The reaction chamber is equipped with static pressure sensors and thermocouples to control the initial and boundary conditions, dynamic

pressure sensors to measure the ignition delay, and usually with quartz windows for the application of optical techniques [101].

RCMs are usually home-made facilities, so that it is very hard to compare results from different laboratories [102]. Heat losses and fluid mechanics effects associated with these tools cause that even under the same experimental conditions data obtained from several RCMs can be quantitatively different. Because of the temperature heterogeneity in the combustion chamber (wall effects) and the lack of a heat losses characterization of the machine, the interpretation and comparison of RCM data from the literature can be extremely difficult [103]. From a chemical kinetics point of view, the accurate determination of temperature is extremely important due to the exponential dependence of the specific reaction rate on such parameter, so that a guaranteed adiabatic gas core or an accurate heat losses model are mandatory. The addition of a crevice to the piston edge has shown the capability of isolating the cold gases that form the thermal boundary layer and the gas core, simplifying the complicated fluid dynamics and resulting in a more homogeneous mixture [104]. However, the crevice design is very complex and should be optimized for a particular operating condition. On the one hand, the crevice volume should be large enough to contain the thermal boundary layer and the inlet area should be large enough to allow the boundary layer to flow into it. On the other hand, there is a critical dimension of the crevice inlet beyond which a back flow from the crevice to the combustion chamber appears, and since the gas in the crevice is cooler than the gas core due to its higher heat losses, this back flow breaks the homogeneity of the core [105]. Finally, the effectiveness of the cleft piston depends on the thermodynamic conditions and on the test gas, since different gases imply different thermal diffusivities, heat losses and, therefore, thermal boundary layer thicknesses.

In an RCM, both homogeneous and heterogeneous (direct injection) air-fuel mixtures can be tested. The dynamic in-cylinder pressure is recorded allowing the direct measurement of the ignition delay, which is usually defined as the time from the end of the compression stroke, when the peak of pressure caused by the compression is observed, to the rapid pressure rise caused by the high exothermic combustion [106]. RCMs are characterized by the existence of a testing time, the maximum value of whcih is limited by the heat losses in the combustion chamber and the minimum value of which is defined by the compression time, since any relevant chemical activity should be avoided during the compression stroke. The typical test time is around 10-150 $ms$, which implies that RCMs and shock tubes are complementary facilities [71]. High pressure (up to 120 $bar$) and low-to-medium temperature

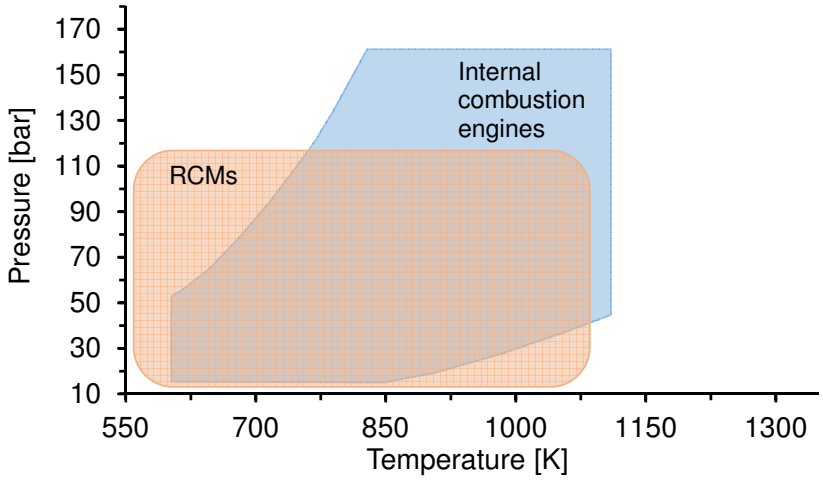


***Figure 2.17.*** *Thermodynamic conditions reached in RCMs compared to the ones reached in engines under motoring conditions.*

(up to 1100 $K$) conditions can be reached in RCMs prior to the autoignition event, complementing also the thermodynamic work range of shock tubes. In fact, Fig. 2.17 shows the thermodynamic conditions that can be reached in an RCM compared to the conditions at TDC reached in engines without combustion. As can be seen, ignition delays can be studied even under low reactivity conditions, including the low temperature combustion regime, cool flames (in case of having a two stage ignition pattern) and the NTC zone, which provides renewed relevance to RCMs.

It should be noted that the ignition delay is not measured at constant thermodynamic conditions due to the heat losses of the machine. The variation of such conditions during the ignition delay time depends on the physical properties of the air-fuel mixture. In fact, if the heat capacity of the mixture increases, the thermodynamic conditions become more stable. Therefore, inert gases with high heat capacity are usually chosen [106]. Furthermore, the compression process is not instantaneous and there is some chemical activity during the compression stroke, which results in a buildup of active radicals at the end of this stage. These two phenomena have opposite effects on the ignition delay. On the one hand, the radical buildup dominates for short ignition times and the measured ignition delay is shorter than the obtained with a theoretical constant-volume reactor that does not consider the compression stroke. On the other hand, for long ignition delays, the heat

loss effect can dominate over the radical buildup effect and the measured ignition delay is longer than the obtained with a theoretical constant-volume adiabatic reactor [107]. Curiously, this behavior is opposite to the one found for shock tubes (explained in the previous section), where measured ignition delays are shorter than the ones obtained with a perfect reactor due to the positive pressure rise that these facilities present. Therefore, the longer the ignition delay, the higher the differences between the measurements from RCMs and shock tubes. An uncorrected comparison of ignition delays from both facilities may conclude, mistakenly, that the results diverge and that the experiments are incompatible [9]. In summary, taking into account heat losses in RCMs and pressure gradients in shock tubes are critical to perform a proper comparison between both sources of experimental data.

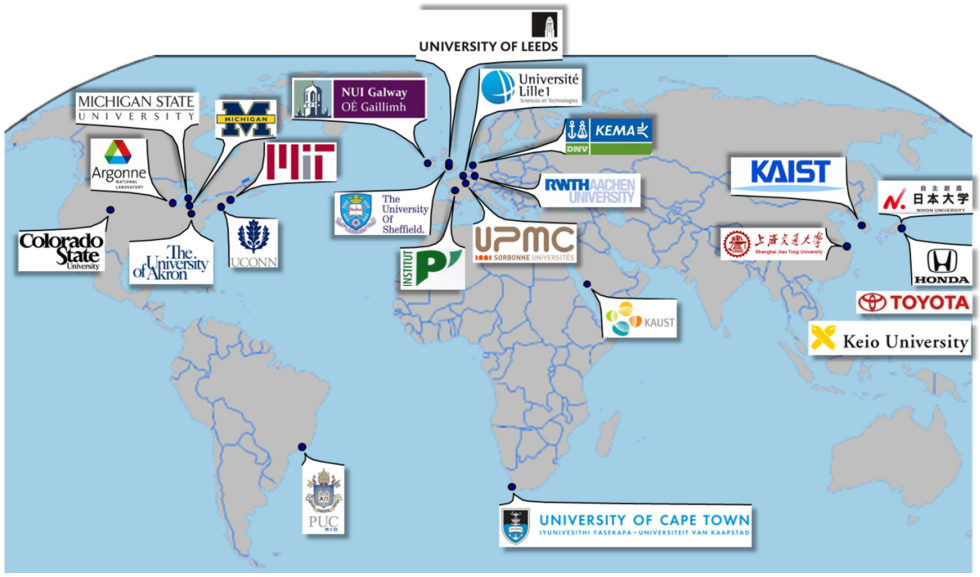


***Figure 2.18.*** *Location of RCMs in the world according to the* $2^{nd}$ *International RCM Workshop (*$1^{st}$ *August 2014, Berkeley, USA).*

Finally, it should be mentioned that there are only two dozen or so RCMs in the world. In fact, Fig. 2.18 shows the location of these machines according to the $2^{nd}$ *International RCM Workshop* ($1^{st}$ August 2014, Berkeley, USA). Such a facility is employed to perform advanced combustion research, which is inaccessible to most of the universities and research institutes.

#### 2.3.1.4 Rapid Compression-Expansion Machines

Rapid Compression-Expansion Machines (RCEMs) are a variant of the RCMs described in the previous section. There is considerable interest in having experimental facilities which can simulate the reacting environment generated in practical combustion devices. In that way, an RCEM allows a detailed analysis of a single cycle of an internal combustion engine, including not only the compression stroke, but also virtually all the expansion stroke. Therefore, RCEMs have the capability of replicating reasonably well the low-to-medium temperature, high pressure and fuel loading combustion conditions of reciprocating internal combustion engines, avoiding their associated complexities but keeping almost all the advantages of RCMs.

RCEMs usually have some important features that allow to perform various diagnostic studies under a wide range of experimental conditions. The ability to modify stroke and clearance to reach different compression ratios, the ability to provide optical accessibility and vibration-free compression to apply non-intrusive optical techniques and the ability to vary the compression velocity in order to simulate different engine speeds are essential [108]. Furthermore, the capability of extracting the reacting mixture for species analysis is also of interest. The hydraulic system to stop the piston at top dead center available in RCMs is avoided in an RCEM. Thus, the expansion stroke can be also analyzed and most of the engine parameters can be calculated under realistic fully-controlled initial and boundary conditions, such as the heat release rate or the combustion efficiency [109].

In these facilities both homogeneous and heterogeneous (direct injection) mixtures can be tested [110], as well as new combustion modes such as dual fuel technology [111] or the ones based on low temperature combustion conditions [112]. According to autoignition studies, RCEMs provide easily controlled and reproducible conditions in a cleaner environment than in a traditional engine, with the absence of residual gases and with full control over the pressure, temperature, volume, composition and mass trapped. Fig. 2.19 shows the thermodynamic conditions that can be reached in an RCEM compared to the conditions reached in shock tubes, RCMs and at TDC in engines without combustion. As it can be seen, an RCEM can be described as an optically-accessible engine with variable geometry that covers the same thermodynamic range than internal combustion engines.

RCEMs are usually based, similarly to RCMs, on the movement of one or several pistons pneumatically driven and hydraulically coupled, but obviously, the twin-opposed pistons configuration is avoided. It is possible to buy an RCEM since 2005 [113]. Therefore, various of the existing RCEMs are

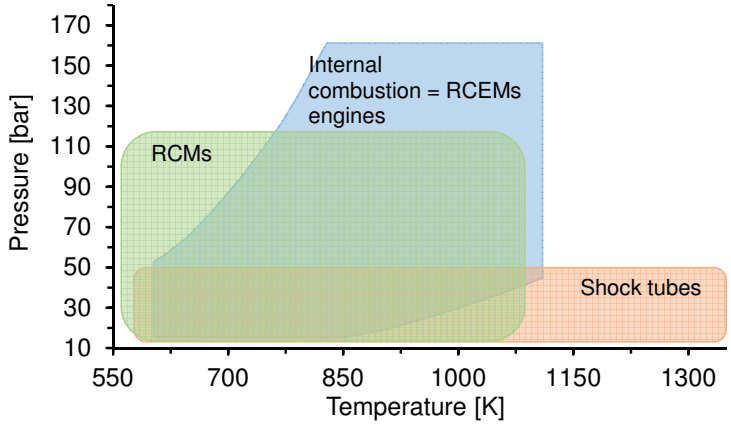


***Figure 2.19.*** *Thermodynamic conditions reached in RCEMs compared to the ones reached in shock tubes, RCMs and engines under motoring conditions.*

virtually the same, which means that it is much easier to compare results from different laboratories. Concretely, standard RCEMs can be found in the following research centers:

- Bayreuth Engine Research Center, University of Bayreuth, Germany [114].
- Aerothermic and Internal Combustion Engine Technological Research Centre (CERTAM), France [115].
- Institute of Thermodynamics, Technical University of Munich, Germany [116].
- Aerothermochemistry and Combustion Systems Laboratory, Swiss Federal Institute of Technology (ETH-Zurich), Switzerland [117].
- Department of Mechanical Engineering, Mississippi State University, USA [118].
- Department of Mechanical Engineering, PUC-Río Pontifical Catholic University of Rio de Janeiro, Brazil [98].
- CMT-Motores Térmicos, Polytechnic University of Valencia, Spain [119].
- Other private companies from the automotive industry.

The operating mode of this type of machine is widely described in Chapter 3, where the facility used in this Thesis is presented. A picture of the RCEM available at CMT - Motores Térmicos can be seen in Fig. 2.20.

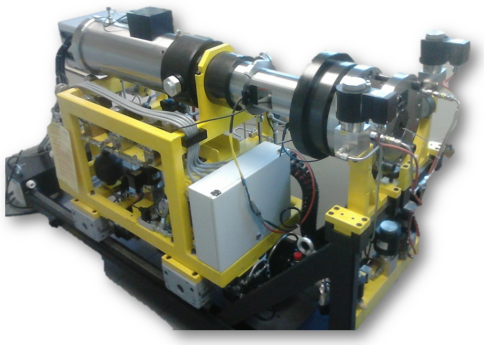

***Figure 2.20.*** *The Rapid Compression-Expansion Machine available at CMT - Motores Térmicos.*

Whereas in an RCM a constant volume reactor under virtually constant temperature and pressure conditions is generated when the piston reaches top dead center, in an RCEM the thermodynamic conditions change continuously as in an internal combustion engine. Therefore, whereas in an RCM the measured ignition delays are referred to constant thermodynamic conditions, $\tau$, the ignition delay measurements performed in an RCEM are referred to variable conditions, $t_i$, where the evolution of the pressure and temperature inside the combustion chamber is known. Thus, it should be noted that RCEMs are the next step after RCMs from basic combustion science to applied studies.

### 2.3.2 Current challenges in experimental autoignition studies

The main challenges of the different experimental methodologies adopted in the study of the autoignition phenomenon are presented in the following paragraphs. First, differences between the experimental facilities described in the previous sections will be analyzed, highlighting the advantages and disadvantages of each facility. Then, the main uncertainties according to the autoignition phenomenon will be described, including the calculation of the temperature evolution and the gas composition, as well as some optical techniques that are usually applied. Finally, different criteria to

define the start of ignition are presented, highlighting in their advantages and disadvantages.

#### 2.3.2.1 Advantages and disadvantages of the different facilities

The experimental facilities where the autoignition event can be performed, but that are not usually used to study the autoignition phenomenon under engine conditions, are the following:

- Flow reactors.
- Well-stirred reactors.
- Combustion vessels.
- Engines.

On the one hand, flow reactors offer the advantage of direct measurements of temperature and species concentration, but they work only under thermodynamic conditions that are unrealistic according to engines [120]. On the other hand, well-stirred reactors can operate at elevated pressure and temperature. However, rapid mixing of reactants in a well-stirred reactor becomes very complex at high temperature when the characteristic reaction time is comparable to the mixing time. Thus, it is not possible to use such a facility to measure ignition delays under engine conditions [121].

Despite the fact that combustion vessels are widely used for the study of sprays, including the ignition event, tracing the chemical kinetics of the phenomenon is extremely complex due to the existence of both a temperature and an equivalence ratio distribution along the spray [77]. Furthermore, combustion vessels can be used to study knocking or, in a similar way, the autoignition of a homogeneous mixture where a chemical analysis can be performed. However, the establishment of a flame front is mandatory to promote the autoignition of a certain area of the combustion chamber [58]. Thus, the interaction between the flame front and the unburned gases should be taken into account, resulting in a transient temperature distribution that makes much complex the analyses.

Finally, engines represent the direct application, but it is difficult to trace the chemical kinetics of the reactive mixture and to isolate the different chemical and physical effects due to the complex fluid dynamics and the existence of uncontrolled conditions [122].

Studies about autoignition are usually performed in the following facilities:

- Shock tubes.
- Rapid Compression Machines (RCM).
- Rapid Compression-Expansion Machines (RCEM).

Shock tubes are able to create a medium pressure and high temperature environment downstream of a reflected shock wave without complex fluid dynamics. The autoignition pressure and temperature can be accurately calculated. However, the thermodynamic conditions are available only for less than 10 $ms$, which is not enough to measure the ignition delay in many cases [93]. Moreover, the maximum ignition pressure available can be not enough to replicate engine conditions [94]. Time zero is usually defined as the instant at which the reflected wave pass through the piezoelectric pressure sensor in these facilities, and the ignition delay can be directly measured using the pressure signal.

RCMs also offer the advantage of a direct measurement of the ignition delay. Besides, high pressure and temperature conditions can be sustained for long time in an ambient without residual gases using these facilities. However, the thermodynamic conditions are not constant after the compression stroke due to heat losses and this variation should be taken into account to properly define the ignition delay [123]. Moreover, sampling of species is difficult and measurement of the temperature is indirect. Typically, time zero is defined as the peak of pressure caused by the compression event in RCM experiments, but vibrations at the end of the stroke can turn into uncertainties in setting this time reference and the corresponding thermodynamic conditions. Therefore, each experiment should be repeated several times to ensure repeatability and the coefficient of variation of each thermodynamic condition should be calculated and reported [124].

Finally, ignition delays under real engine conditions can be directly measured using RCEMs. Furthermore, an engine cycle can be reproduced in these facilities under controlled initial and boundary conditions [109]. However, transient thermodynamic conditions during the ignition delay imply a more complex analysis of both chemical and physical effects on the autoignition phenomenon. Moreover, tracing species is difficult and the analysis of pollutant emissions is harder than in an engine due to the absence of a quasi-continuous flow of exhaust gases [101].

#### 2.3.2.2 Uncertainties on the autoignition phenomenon

Even in the facilities usually used in autoignition studies (shock tubes, RCMs and RCEMs), the calculation of the temperature evolution and the preparation of the gas mixture are also uncertainty sources for a proper definition of the ignition delay.

The uncertainty in the calculation of the autoignition temperature depends on the uncertainties in the initial pressure and temperature, the evolution of the pressure measured, the mixture composition and the models used to characterize deformations, leaks and heat losses. If the pressure rise is fast enough, depending on the facility design, uncertainties in heat losses can be negligible [104]. Besides, in this case the largest contributor to the uncertainty in temperature is the value of the initial pressure, which is affected by the initial gas velocity, since the initial temperature and the in-cylinder pressure are more accurately measured. In the same way, the in-cylinder temperature is not very sensitive to the uncertainty in the mixture composition and, therefore, to the specific heat ratio and to the molecular weight of the gases [125].

Sequential autoignition is an intrinsic phenomenon to experimental autoignition measurements under realistic conditions. Specifically, the existence of small heterogeneties caused by wall effects and heat losses under theoretically homogeneous conditions (e.g., HCCI conditions) lead to a reactivity gradient and, therefore, to a sequential autoignition [126]. Several experimental and simulation works have been performed about the thermal stratification in autoignition studies [127], and not only under HCCI conditions, but also for the study of knocking in SI-engines [128] or for the study of noise [129].

Sjöberg et al. [130] studied the role of the natural thermal stratification on the combustion duration and on the pressure rise rate experimentally in an HCCI engine and by simulation solving a multi-zone model in CHEMKIN. The authors found that natural thermal stratification generated by heat losses can explain the progressive pressure rise that is typical of this combustion mode. Furthermore, Bradley et al. [131] showed that a critical temperature gradient from which the autoignition propagation reaches acoustic conditions can be estimated, which is a concept also studied by Gu et al. [132].

Moreover, Chen et al. [133] studied the effect of thermal stratification on $H_2$ autoignition by means of direct numerical simulations. The authors found that autoignition propagation seems to be inversely proportional to $\bigtriangledown T$ for medium-to-low temperature gradients, while diffusive effects become relevant when $\bigtriangledown T$ increases. Besides, the ignition delay seems to be governed by

the competition between accumulation of chain carriers and diffusion in the different zones of the combustion chamber.

Finally, Yoo et al. [134] studied the sequential autoignition of n-heptane by thermal stratification using direct numerical simulations (DNS). The authors showed that the ignition delay behavior with the temperature fluctuations changes depending on the mean temperature value and the NTC regime of the fuel. Thus, if fluctuations are increased, the ignition delay increases for a mean temperature lower than the NTC zone, while it decreased for a mean temperature higher than the NTC zone. For a mean temperature value within the NTC zone the ignition delay increases for small fluctuations but it decreased for large fluctuations. Furthermore, Yoo et al. also studied the effects of the turbulence timescale on the ignition. Thus, fast turbulence timescale homogenizes the mixture leading to a faster ignition propagation, while longer turbulence timescales are not able to homogenize the temperature and the ignition propagation occurs mainly by deflagration. However, the effect of the turbulence timescales on the ignition delay is almost negligible compared to that of thermal stratification. Similar DNS studies have been performed by Bansal and Im [135]. However, analyses under engine-like conditions have to be carried out in order to understand the autoignition propagation phenomenon in a real engine.

In an experiment, the ignition event is detected by an in-cylinder pressure rise, which is directly measured with a pressure transducer. But thanks to the great optical access that is usually available in these facilities, several optical techniques can be employed as a complementary diagnostic of the experiment. Direct visualization techniques, simple as Schlieren, shadowgraphy or diffuse backlight, or more complex as chemiluminescence and spectroscopy, can be used to study the combustion development or even radical concentrations in a qualitative way [136]. Furthermore, direct measurement of the in-cylinder temperature evolution is highly desirable. Laser Rayleigh scattering technique, two-color pyrometry, $H_2O$ laser absorption, as well as acetone or toluene LIF (Laser-Induced Fluorescence) and PLIF (Planar Laser-Induced Fluorescence), can be used to measure the core gas temperature and the temperature field [137]. However, the measurement accuracy can be not very good due to the high pressure conditions, noise and vibrations. Other optical techniques widely used in autoignition experiments include measurements of soot by applying LEI (Light Extinction Imaging), LII/PLII (Planar Laser Induced Incandescence) or DBIEI (Diffused Back-Illumination Extinction Imaging) [138].

PIV (Particle Image Velocimetry) can be employed to determine the flow characteristics inside the combustion chamber prior to ignition, as well as the sensitivity of the chemical kinetics to the turbulence generated during the compression of the test sample. A criterion based on the Damköhler number was proposed by Ihme [139] in order to characterize the sensitivity of the induction reactions to turbulence fluctuations. It was found that the effects of turbulence and mixture fluctuations should be taken into account for mixtures with Damköhler numbers below 50, since they show higher sensitivity to these phenomena.

OH* chemiluminescence and spectroscopy are non-intrusive optical techniques widely used in combustion diagnosis [140]. Such optical techniques are powerful tools to analyze not only the ignition of homogeneous mixtures, but also different parameters of the combustion event, including sprays and even exhaust emissions. In fact, natural luminosity analysis and spectroscopy have shown to be able to describe the different stages of the autoignition phenomenon and the combustion process of a homogeneous air-fuel mixture [141].

Mancaruso and Vaglieco [142] applied spectroscopic measurements to a transparent Diesel engine in order to study the low temperature combustion process. They saw that the OH* was widely distributed in the chamber during the whole combustion process, concluding that OH* was recognized as the most important radical that marked premixed combustions. In another study, Mancaruso and Vaglieco [143] performed chemiluminescence measurements in a transparent engine fueled with RME and Diesel commercial fuel. They found that OH* is responsible of the NO formation in the chamber and, therefore, of much of the $NO_x$ emissions. The OH* behavior in the chamber was strictly correlated to the formation of $NO_x$ and the oxidation of soot, demonstrating that OH* chemiluminescence can be used to study engine-out emissions.

Iijima and Shoji [144] also performed a spectroscopic analysis of HCCI combustion for n-heptane and iso-octane in a 2-stroke single cylinder engine. The authors found that the time of the peak of light emission intensity in a wavelength range of 300-500 $nm$ nearly coincides with the time of the peak of heat release rate, which could be used as a tracer of the high temperature ignition delay. However, no light emission spectrum attributable to cool flames was observed at high EGR rates. Moreover, a strong and long-lived light emission attributable to the OH* radical can be seen only under high equivalence ratios. Thus, care should be taken when OH* chemiluminescence wants to be applied under lean homogeneous conditions, since the OH* radiation can be outshined by other luminous reactions.

Kim et al. [145] compared the HCCI mode with PCCI and standard spark ignition (SI) using spectrum analysis, with a transparent engine. The authors found that the CO-O* emission dominates the spectra in the HCCI chemiluminescence emission, but that it was difficult to measure OH*, CH*, and C2* radicals. Moreover, the presence of OH* peaks in the spectra of very lean HCCI combustion could be an indication of non-homogeneous conditions. Finally, the authors concluded that chemiluminescence is a good method for analyzing the different stages of the combustion process.

Murase et al. [146] have studied the HCCI combustion with a Rapid Compression Machine by means of direct visualization and spectroscopy. They could see that during the main heat release duration the distinct OH* emission appeared, and it was superimposed on the carbon monoxide oxidation continuum. After the main heat release, the broad peak of the spectrum was shifted to the longer-wavelength side ($H_2O$ vibration-rotation bands at 580.7-966.9 $nm$).

Dubreuil et al. [14] studied the global effect of the EGR on the HCCI combustion of n-heptane in a transparent single-cylinder Diesel engine for two EGR rates at a constant equivalence ratio by means of OH* chemiluminescence. By observing cool and main flame emissions, the authors found that the EGR delays and degrades the combustion phenomenon. They also proved that the natural emissions of combustion are sufficiently sensitive to allow the combustion process analysis. Finally, the authors observed that the increase of the EGR rate decreases the OH* chemiluminescence, which is linked to the reduction of the global combustion reactivity.

Finally, Hwang et al. [136] studied the temporal phases of autoignition and combustion in a HCCI optical engine for several fuels by applying a spectroscopic and a chemical-kinetic analysis. The authors divide the combustion process in four different stages, which can be described by spectroscopy: low-temperature heat release phase or cool flames (only existing in two-stage ignition processes), intermediate-temperature heat release phase (which affects the fuel ignition quality), main high-temperature heat release phase and, finally, a burnout phase (with very weak uniform emission and near-zero heat release rate).

It can be deducted from the previous studies mentioned above that OH* is one of the main tracers of the combustion process. However, the presence of OH* radiation in the autoignition of homogeneous mixtures is not clear, since it can be outshined by other luminous reactions. Thus, it is necessary to define a criterion to know when OH* is really seen by means of chemiluminescence under HCCI conditions. Moreover, the chemical kinetics related with this

phenomenon should be analyzed in order to be able to describe the different stages of the combustion process even if the OH* radiation is superimposed by other light. Chemiluminescence is also a good tool to evaluate the generalization of the ignition event. There is a great interest in knowing how the propagation of the autoignition front occurs, since a perfect homogeneous mixture under perfect homogeneous thermodynamic conditions cannot be obtained experimentally. It should be noted that the velocity of propagation, as well as the area of ignition, can be studied by tracing the OH* radiation.

The uncertainty in the initial composition of the gas mixture is caused by several sources. Typically, synthetic gas mixtures are formed by a filling based on partial pressures, so that uncertainties in the measured partial pressure result in deviations between the desired and the real mixture composition. These deviations are mainly caused by three effects: the pressure fluctuations generated during the opening and closing of the valves, the existence of a dynamic pressure that is different than the static one because of the velocity of the gas during the filling, and the changes in temperature during the process because of the expansion of the gas through the pipes and the subsequent compression in the filling tank.

The synthetic gas mixture can be formed in an external tank or directly in the combustion chamber of the facility. While using an external tank implies less flexibility because of the big amount of mixture generated (i.e., more time is needed to prepare the mixture), employing the combustion chamber to perform the mixture is only possible if the sealing is enough to guarantee that leaks are negligible during all the filling and homogenization time. Furthermore, phenomena such as mass diffusion, absorption or adsorption of any species by the tank surface, can alter the initial composition. Luckily, the existence of any of these phenomena can be easily checked by monitoring the in-tank pressure once the absence of leaks is guaranteed. If there is a pressure drop over time, gas absorption occurs. When working with liquid species, such as some fuels and water, a heating system to ensure the vaporization of the liquid phase is needed. In case of preparing the mixture in an external tank not only this volume should be heated, but also the reaction chamber and the inlet pipes of the facility. Given the partial pressure of the liquid species, its boiling point and its volatility, the preheat temperature of the walls to ensure complete vaporization can be determined [147]. Another option is to perform the gas mixture in an external tank and add the liquid species directly in the chamber [148], but whatever the method employed, a methodology has to be carefully developed to ensure the vaporization of the liquids and the homogeneity of the mixture.

In addition, the possibility of chemical activity of the fuel when the mixture is being prepared should be avoided, otherwise, shorter ignition delays will be measured. This issue is critical when working with nonvolatile liquid fuels, such as bio-Diesel or very long chain hydrocarbons, because of the high temperature needed for their vaporization [149]. While the premature thermal decomposition of the fuel is the main challenge when performing the mixture in an external tank due to the long residence times, the homogeneity is guaranteed if a stirrer or mixer is used. Otherwise, if the mixture is performed directly in the combustion chamber, the inlet gases have to produce enough turbulence to ensure homogeneity not only in terms of species concentration, but also according to the initial temperature of the mixture.

Special attention should be taken when the effects of the EGR rate on the ignition delay is intended to be analyzed. New combustion modes based on autoignition use massive amounts of EGR to reduce the maximum temperature reached in the cycle. By applying this strategy, together with a lean air-fuel mixture, soot and $NO_x$ emissions can be highly reduced from an internal point of view (their formation is directly avoided during the combustion process). Thus, autoignition studies should be performed testing diluted environments with high EGR rates in order to replicate engine conditions. However, these studies are typically carried out in facilities where the lack of enough exhaust gas flux require working with synthetic EGR. So, it is necessary to define an optimal composition of such synthetic EGR to replicate the same conditions that can be found in a real engine and, by this way, to obtain results with realistic practical application.

Ladommatos et al. [150–153] performed a thorough study about the effect of EGR on Diesel combustion, including ignition delay and exhaust emissions. They classified the effects of EGR into three different types. First, the effect of decreasing the percentage of oxygen was evaluated. It reduces the $NO_x$ emissions at the expense of rising particulate matter and unburnt hydrocarbon emissions, and it proves to be the most relevant of all the effects. Then, the chemical and thermal effects of $CO_2$ were studied, concluding that both have only a small effect on ignition delay and emissions. Finally, the chemical and thermal effects of $H_2O$ were studied. $H_2O$ was added up to 3% in mass, resulting in a slight increase in the ignition delay due to its higher heat capacity.

Zhao et al. [154] studied, experimentally and by simulation, five effects of EGR on ignition delay, combustion duration and heat release rate (HRR): EGR increases the intake charge temperature since it is composed of hot burned gases, which implies shorter ignition delays, shorter combustion

durations and higher peaks of HRR. EGR has higher specific heat capacity than the fresh air and it reduces the oxygen concentration, which implies longer ignition delays, longer combustion durations and lower peaks of HRR. Chemical reactions involving the $CO_2$ and the $H_2O$ of EGR slightly reduce the combustion duration at high concentrations of burned gases. Finally, the stratification of the burned gases from the fuel/air mixture reduces the ignition delay due to the presence of higher temperature zones at the boundary between the hot burned gases and the unburnt charge. Dec [63] also performed a computational study of the EGR effects on the heat release rate using iso-octane, obtaining that the higher the EGR rate, the smoother the HRR curve.

Chen and Milovanovic [155] studied the effect of EGR by simulation, using internal combustion engine models from CHEMKIN fuelled with methane. They divided the effects of the EGR into three: the thermal factor (referred to the high temperature of the hot EGR), the dilution factor and the chemical factor. Their results agree with the results of Zhao et al. presented previously. Of course, the overall effect of the hot EGR depends on the temperature of the gases and the degree of dilution together with the chemical effects. The composition of the EGR used by Chen and Milovanovic was fixed and equal to 79% $N_2$, 15.5% $H_2O$, 5% $CO_2$ and 0.5% $O_2$, which provides quite realistic results. However, different fuels and different EGR compositions should be studied.

Sjöberg et al. [156] performed a similar study where autoignition results of PRF blends with different diluents were compared. The experiments were carried out using a single-cylinder engine and by simulation with CHEMKIN. They studied three EGR effects: thermodynamic cooling effect due to the increased specific-heat capacity of the mixture; $O_2$ reduction effect, which increase ignition delays; and chemical effects. Sjöberg et al. considered two chemical effects of EGR: the $H_2O$ chemical effect that enhances autoignition, and the effect of trace species, such as unburned or partially oxidized hydrocarbons, that enhance or suppress autoignition depending on the type of fuel. The study of Sjöberg et al. was completed afterwards with ethanol [157] obtaining similar results.

A complete CFD study about the thermodynamic effects of EGR was performed by Babajimopoulos et al. [158] using KIVA-3V. Both the influence of the EGR temperature on the heat losses and the degree of EGR stratification (temperature and composition heterogeneities) were analyzed in a natural gas engine for different variable valve actuation strategies. These EGR thermodynamic effects in natural gas engines were also studied by Fathi

et al. [159] concluding that the thermal losses decrease if the percentage of cold EGR increases because lower temperature is reached.

Cong and Dagaut [160] studied the effect of $CO_2$ on methane oxidation in a jet-stirred reactor at low pressure (1 to 10 *bar*) and medium-to-high temperature (900 to 1400 *K*). These authors found a slight increase of the ignition delay working with 20% of $CO_2$. Herzler and Naumann [161] employed a shock tube to study the effects of $NO_x$, $H_2O$ and $CO_2$ on the ignition delay of natural gas at 16 *bar* and high temperature (1000 to 1700 *K*). They found that even small amounts of $NO_x$ lead to significantly shorter ignition delays. No significant influence on the ignition delay with $H_2O$ volume fractions of 30 and 50% was found because the promoting chemical effect of $H_2O$ on ignition is balanced by its higher heat capacity. Moreover, an increase of the ignition delay is found with 30% of $CO_2$ due to its higher heat capacity (at low temperature) and due to relevant chemical effects (at high temperature). Finally, Di et al. [162] studied the effects of gas composition on low temperature ignition of iso-octane and n-heptane computationally and with a rapid compression machine, working with $N_2$, Ar and a blend of Ar and $CO_2$. Their results showed that thermal effects are very pronounced and are dominant at low temperature conditions, whereas at temperature higher than 850 *K*, the chemical effects of $CO_2$ became more important than the thermal ones.

From this literature survey, it can be seen that there are a lot of studies about the effects of the EGR components on the different parameters of the combustion process. However, it is necessary to analyze these effects with realistic species concentrations in order to define the relevance of each of them under engine conditions. In typical autoignition studies, the ignition delay is obtained in environments poor in oxygen, and the dilution is done by adding $N_2$, Ar or $CO_2$ indistinctly [35, 36, 68]. This way to control the percent of oxygen is very useful to obtain ignition delays at different temperature and pressure, and with different combustion temperature. However, a proper composition of the dilution gases is necessary if a more realistic study is intended to be performed. In order to obtain ignition delays under several engine conditions, the question is how to dilute the air in the simplest way, but without altering the reality.

#### 2.3.2.3 Criteria to define the start of ignition

There is not a general criterion to define the ignition delay. Therefore, especial attention should be paid when experimental results from different

researchers want to be compared. A clear definition of the ignition delay when ignition data are shown is mandatory. Whereas the time reference, $t = 0$, is majorly standard depending on the experimental facility used, there are lots of different criteria to define the start of combustion.

The more extended criteria to experimentally define the start of ignition are described in the following lines, highlighting their physical sense, the stage of the process at which they are referred and the relationships between them. Besides, the criteria are classified depending on the experimental data in which they are based on. Examples of the different criteria are shown in figures 2.21 to 2.24, which would be described in short. On the one hand, all four figures show the result from the same experiment performed in an RCEM fueled with a homogeneous n-heptane-air mixture under the following conditions: initial temperature and pressure $T_0$=358 $K$ and $P_0$=1.4 $bar$, oxygen molar fraction $X_{O_2}$=0.21, equivalence ratio $F_r$=0.4 and compression ratio CR=15. On the other hand, Fig. 2.25 shows Schlieren images from an experiment performed in an RCEM fueled with a homogeneous methane-air mixture under the same conditions than the previous case, but in which a direct injection of n-heptane is performed during the compression stroke.

- Criteria based on the pressure signal.
  - Relative maximum of the time derivative of the pressure signal (pressure rise rate): peaks in the pressure rise rate signal are related to inflection points in the pressure trace. By applying this criterion both pressure rises, the one caused by cool flames and the other one caused by the high-temperature ignition, can be distinguished [163]. Moreover, even the pressure rise caused by the compression stroke of the experimental facility (if it exists) can be identified. It should be noted that a pressure rise rate caused by the combustion can be directly related with the energy released during the process. Thus, a maximum pressure rise rate occurs when a peak of heat release rate is present. An example of this criterion is shown in Fig. 2.21 (top). The main advantage of this criterion is that it is based on a measured signal, which can be easily filtered and derived. Uncertainties appear when a high-intensity combustion occurs, where pressure waves propagate through the chamber and make much more complex the filtering of the average pressure. However, this is the main criterion adopted in experimental autoignition studies [36, 100, 164].
  - Crossing through zero of a secant line of the combustion pressure (pressure minus pressure under motoring conditions):

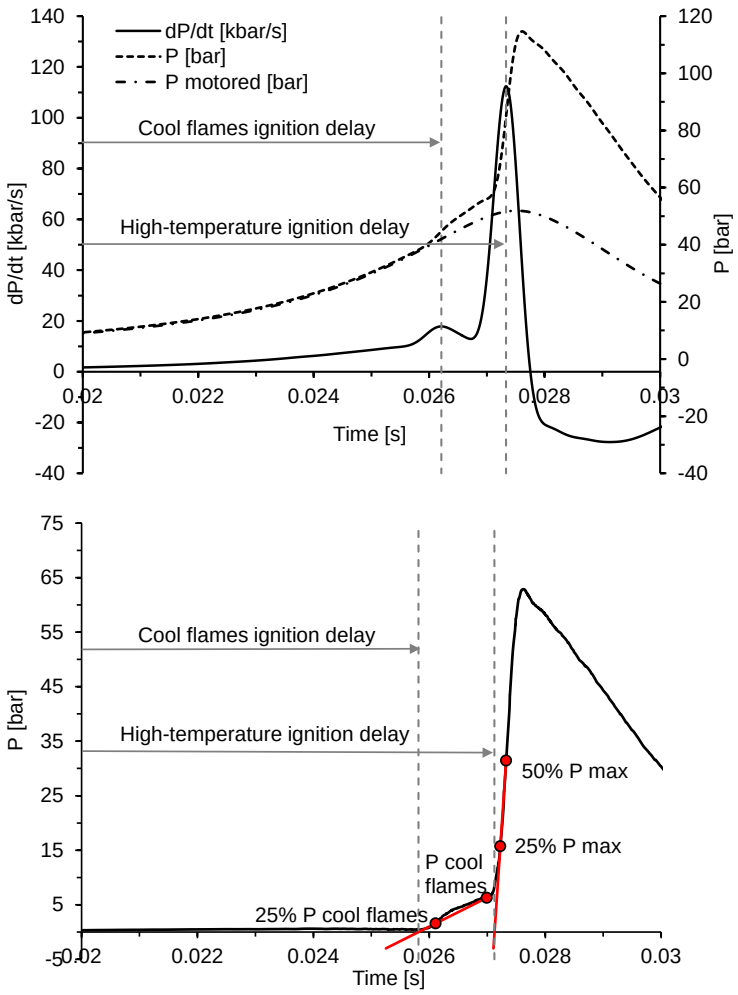


***Figure 2.21.*** *Criteria to define the start of ignition based on the pressure signal. Top.- Relative maximum of the pressure rise rate. Bottom.- Crossing through zero of the slope of the combustion pressure.*

the combustion pressure, $P_{comb} = P - P_{motored}$, represents the increment in pressure directly caused by the combustion event and, therefore, it is directly related with the energy released by the fuel. As it can be seen in Fig. 2.21 (bottom), if a two-stage ignition pattern occurs, both cool flames and the high-temperature stage of the process can be identified. The secant line of each

ignition event is obtained by selecting two arbitrary points of the signal. For instance, in Fig. 2.21 (bottom) cool flames are described using a 100% and a 25% of the combustion pressure related to this phase, while the high-temperature stage is defined by using the 50% and a 25% of the maximum combustion pressure. The main advantage of this method is that it intends to describe the ignition at its very beginning, just when the pressure path start to be different to the theoretical inert path. Moreover, criteria based on the crossing through zero of a secant line usually have higher repeatabilities. however, two different disadvantages can be found when this criterion wants to be applied. On the one hand, it is necessary to know the pressure path under motoring conditions of a homogeneous air-fuel mixture, which cannot be experimentally obtained. Thus, the experiment under motoring conditions has to be performed with an inert mixture with similar heat capacity than the test sample. The corresponding pressure under motoring conditions can be also obtained by modeling, but in this case, the uncertainties of the models appear in the definition of the ignition delay. On the other hand, the criterion depends a lot on the two points selected for the calculation of the secant line. Moreover, arbitrary points below the maximum combustion pressure of cool flames can lead to a wrong definition of the high-temperature ignition delay if cool flames and the high-temperature stage are not completely decoupled.

- Criteria based on the temperature signal.
  - Relative maximum of the temperature rise rate: by identifying the different relative maxima of the temperature rise rate signal, both cool flames and the high-temperature ignition delays can be defined [165]. It should be noted that this criterion is not completely consistent with the maximum pressure rise rate, since there is a gap between the temperature and the pressure traces because of the volume profile. However, as it can be seen in Fig. 2.22, this gap is negligible (in some cases it is even smaller than the time resolution) and the maximum temperature rise rate virtually occurs at the same time than the maximum pressure rise rate (and also at the same time than the maximum heat release rate). Thus, the maximum energy release rate of each stage can be identified by applying this criterion. The main disadvantages of this method are related with the signal used. The temperature evolution is not

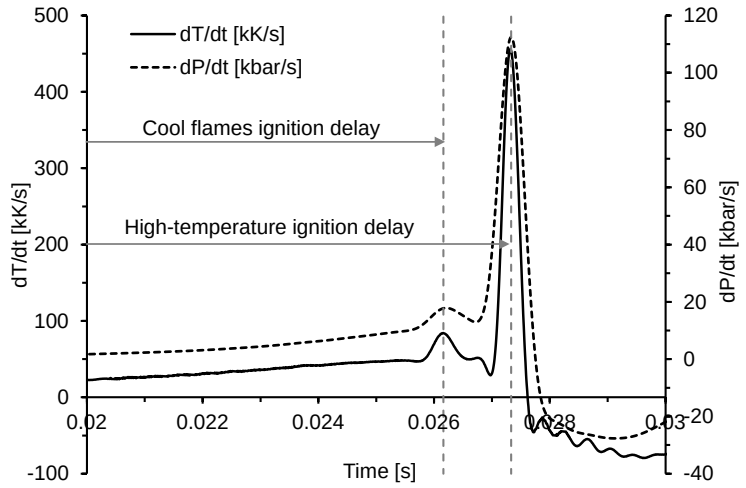


***Figure 2.22.*** *Criterion to define the start of ignition based on the relative maximum of the temperature rise rate.*

directly measured in the combustion chamber, so that it has to be indirectly obtained using the equation of state. Uncertainties on the mass trapped (leaks model), on the molecular weight (composition of the mixture) and on the volume profile (deformations model) affect to the temperature calculation. Fortunately, this criterion is based on the location of the maximum $dT/dt$, so that uncertainties on the temperature signal values are not relevant. Finally, since this criterion is based on the time derivative of the temperature signal, high-frequency noise is magnified when $dT/dt$ is obtained.

– Increment in temperature: this criterion is based on the definition of an ignition temperature or ignition $\Delta T$, which can take any arbitrary value. This criterion is widely used in autoignition modeling [166, 167], where the ignition time is usually defined as the time at which the temperature is 400 $K$ higher than the initial value. A $\Delta T = 400K$ criterion seems to be inappropriate, since the ignition delay is referenced to different phases of the combustion for different operating conditions. Therefore, its consistency with other criteria has to be checked. Samuelsen et al. [168] have checked that despite the fact that more accurate definitions for the ignition time can be adopted, comparison of results based on these different

definitions indicated that the $\Delta T = 400K$ definition provides representative results and it is actually similar to ignition delays determined from the maximum temperature rise rate. Regardless these comments, the $\Delta T = 400K$ definition is sufficient to show the trends of the autoignition characteristics of a certain fuel. However, clear disadvantages appear when this criterion is applied. First, the temperature evolution has to be known, which implies certain uncertainties derived from applying the state equation. Besides, the criterion is completely dependent on the chosen $\Delta T$ value, and the ignition delay can be referred to different stages of the autoignition process depending on the operating conditions and the combustion intensity. Moreover, it is even more complex to apply this criterion under transient thermodynamic conditions, since the $\Delta T$ has to be referred to the temperature path under motoring conditions instead of to the initial temperature. Thus, the temperature evolution under motoring conditions should be also known. Finally, the definition of two ignition delays, one referred to cool flames and the other one referred to the high-temperature stage, could be hard by using this criterion, since two different $\Delta T$ are needed. Depending on the operating conditions, wrong definitions of the ignition delay can be obtained if the $\Delta T$ values are not properly chosen.

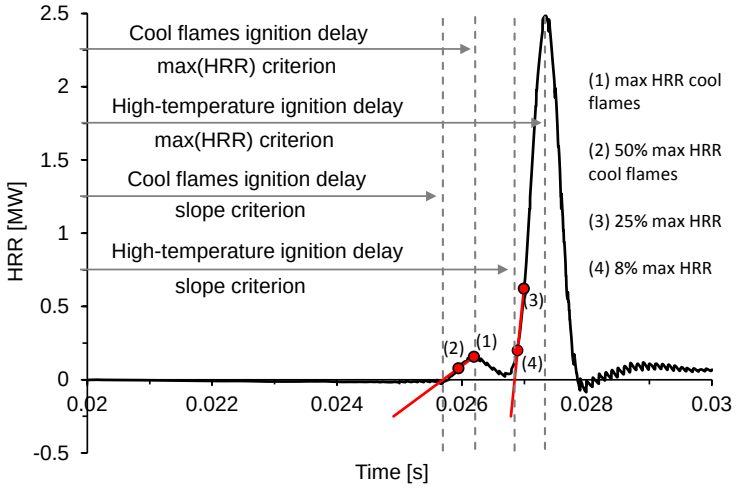


***Figure 2.23.*** *Criteria to define the start of ignition based on the heat release rate.*

- Criteria based on the heat release rate (HHR).
  - Relative maximum of the HRR signal: peaks in the HRR signal are related to inflection points in the accumulated energy released during the process. By applying this criterion both HRRs, the one caused by cool flames and the other one caused by the high-temperature ignition, can be distinguished. It should be noted that the energy released in the combustion event causes a pressure rise. Thus the criterion based on a maximum pressure rise rate and this criterion are virtually the same, as it can be seen by comparing Fig. 2.21 (top) and Fig. 2.23. This criterion has certain disadvantages related to the calculation of the HRR. Uncertainties in the pressure and volume signals (which have to be filtered and derived), in the evolution of the gas composition (the heat capacity of which should be known), and in the leaks, deformation and heat losses models result in uncertainties on the ignition delay. Therefore, this criterion is only recommended if the HRR has to be obtained for additional analyses.
  - Crossing through zero of a secant line of the HRR: this criterion is described in Fig. 2.23. As it can be seen, cool flames and the high-temperature stage of the process can be identified when a two-stage ignition pattern occurs. The secant line is usually obtained by selecting two arbitrary points of the signal. Mitakos et al. [147], for instance, take 100% and 50% of the maximum HRR of cool flames for the calculation of the secant line and the subsequent ignition delay referred to cool flames. In order to define the high-temperature ignition event, these authors propose the 25% and the 8% of the maximum HRR for the secant line calculation. This criterion intends to identify when the energy release starts, so that the defined ignition delay will be referred to the first stage of the combustion. The main disadvantages of the method include the calculation of the HRR, as it has been explained in the previous point. Moreover, the criterion also depends on the two points selected for the calculation of the secant line. Once again, arbitrary points below the maximum HRR of cool flames can lead to a wrong definition of the high-temperature ignition delay if cool flames and the high-temperature stage are not completely decoupled. A similar criterion based on the accumulated heat released can be adopted. In this case, not only the crossing through zero of a secant line of the heat release can be selected as the ignition time, but also an arbitrary value of energy can be taken as the criterion to define

the ignition [169]. The disadvantages of criteria based on the accumulated heat release include the complexities related to the HRR signal that, if the HRR is not properly calculated, cause drift in the accumulated heat release signal, which leads to deviations in the start of ignition point.

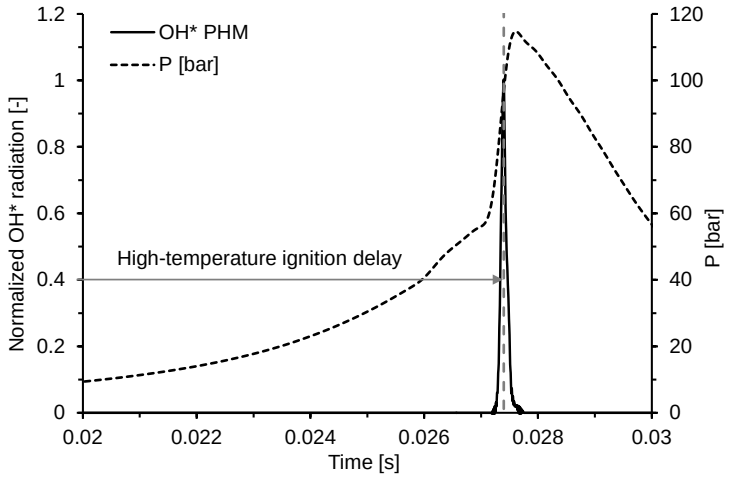


***Figure 2.24.*** *Criterion to define the start of ignition based on the maximum combustion radiation at 310 nm.*

- Criteria based on optical techniques.
  - Maximum combustion radiation at a certain wavelength: chemiluminescence of different radicals can be used to define the start of ignition. The radiation emitted by a certain active radical depends on the decay rate of its excited state species. Thus, different stages of the process can be described by means of chemiluminescence, including the ignition event, by tracing different excited species during the combustion. OH* emission at 310 *nm* can be used to define the instant at which the maximum decomposition rate of OH* to OH occurs, which corresponds to the maximum oxidation rate of CO to $CO_2$. Therefore, this instant defines the high-temperature stage of the process [170]. While the ignition delay referred to the high temperature stage of the process can be measured by applying this technique, the ignition delay referred to cool flames cannot be defined since the light radiation of cool

flames is usually too weak. Besides, in these cases in which the cool flames radiation can be recorded, the measurement range of the optical sensor is usually not enough to see the radiation of the high-temperature stage without any damaging effect. Finally, the main challenge to overcome in the application of this technique is that it is mandatory to have a full optical access available and an optical sensor with high temporal resolution, e.g. a photo-multiplier (PHM), which can be used to measure the integrated radiation with an acquisition frequency higher than 100 $kHz$. Fig. 2.24 shows the intensity of radiation at 310 $nm$ recorded by a PHM compared to the pressure path for a certain autoignition event. The ignition delay referred to the high-temperature stage that is defined by this criterion is also plotted in the figure and both pieces of information are fully consistent. However, no radiation related to cool flames can be distinguished from the experimental measurements.

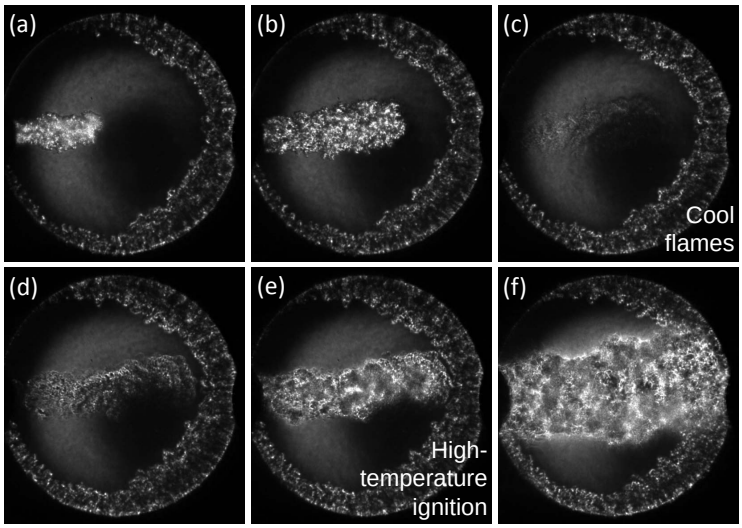


***Figure 2.25.*** *Schlieren measurements of the spray development of n-heptane in an environment composed by methane and air. Cool flames and the high-temperature ignition can be identified by this technique. Unpublished data obtained at ETH-Zurich.*

– Turbulence generated by combustion: turbulence can be recorded by means of Schlieren or shadowgraphy thanks to the differences in the refraction index that are caused by the gradients of density in the combustion chamber. These techniques are widely used to see a flame front propagation or a spray development. However, it

is also possible to define the start of combustion of homogeneous and heterogeneous mixtures by comparing the images with the ones from an experiment under motoring conditions [171]. As it can be seen in Fig. 2.25 (c), cool flames are described by a sudden decrease in the light intensity, since a lighter area means a lower density because of the expansion caused by the ignition. Moreover, the high-temperature ignition can be also defined because of the increase in turbulence caused by the combustion (Fig. 2.25 (e)). The main disadvantages of this method are two: on the one hand, full optical access to the chamber, as well as a high-speed camera are needed. Obviously, the accuracy of the method is limited by the camera temporal resolution (frames per second). On the other hand, it could be necessary to perform first an experiment under motoring conditions to compare with the images with combustion in order to distinguish the turbulence generated by the ignition from the one generated by the movement of the air into the facility, especially working under homogeneous mixtures.

### 2.3.3 Chemical kinetic mechanisms

A chemical kinetic mechanism is a set of reactions that describe the chemical paths followed by the fuel during its decomposition and oxidation. Each reaction is processed as a source term in the species conservation differential equations and the evolution of each species concentration, as well as the evolution of each reaction rate, can be obtained by applying numerical methods. Thus, chemical kinetic mechanisms can be linked with numerical solvers to model the chemical activity of a physical problem.

All the information needed to solve the species consevation equations is provided by the mechanism, which includes the values of different constants that parameterize the specific reaction rate and the thermodynamic and transport properties of each species. Thus, every chemical kinetic mechanism has to include three files: a chemical kinetics file, a thermodynamic data file and a transport properties file [172, 173]. A full description about the internal structure of all these files can be found in different reports from Sandia National Laboratories [172, 173].

Once a chemical kinetic mechanism has been validated versus experimental results under a certain range of conditions, it can be assumed that this set of reactions represent the real chemical paths. Thus, the phenomenon can be analyzed from a chemical kinetics point of view by tracing the different

reaction rates [32]. In this way, a sensitivity study can be performed to know the dominant reactions for a specific combustion parameter, such as the ignition delay, the combustion temperature or the pollutant emissions. The sensitivity of a certain reaction, $R$, to a certain combustion parameter, $\phi$, is defined as follows:

$$Se_R = \frac{\phi_{k_{f/b}\cdot 2} - \phi_{k_{f/b}}}{\phi_{k_{f/b}}} 100 \tag{2.11}$$

Therefore, sensitivity analyses are performed by multiplying the specific reaction rate of a particular reaction by a factor of two (both forward and backward rates) and then calculating the percent change in $\phi$ [24]. This type of analyses are usually employed to evaluate the effects of a set of reactions on the reactivity of the mixture. In these cases, the combustion parameter that appears in Eq. 4.10 is the ignition delay, $\phi = \tau$.

Chemical kinetic mechanisms are usually classified in two groups: detailed and reduced [18]. Whereas a detailed mechanism is formed by thousands of reactions, a reduced one has a much smaller number of equations and, therefore, the computational cost of solving it is also much lower. It should be noted that reduced mechanisms are so named because they are built by means of simplifying a more detailed one. According to reduced mechanisms, they are usually tuned to model a certain parameter of the combustion process, which is the selected specific simulation target of interest (flame speed, burning velocity, ignition delay, $NO_x$ or soot emissions, etc). The reduction of a chemical kinetic mechanism can be performed following different strategies [174], as e.g. principal component analysis [175], sensitivity analysis [176], Jacobian analysis [177], detailed reduction [178], directed relation graph (DRG) [179] or path flux analysis [180], among others. Besides, an evaluation of the skeletal mechanism accuracy relative to that of the original one has great interest as a method to analyze the mechanism reduction process.

The number of species and reactions determines the chemical computing time and the accuracy of the mechanism. Only reduced mechanisms can be linked to CFD codes to solve the thermo-fluid-dynamics of a reactive flow, since all the chemical equations of the mechanism have to be solved for each cell of the domain, resulting in an unacceptable computational cost for detailed mechanisms. Therefore, detailed mechanisms can be only used in 0-D or 1-D models due to time restrictions. It should be noted that the more complex the hydrocarbon, the higher the number of species and reactions needed to describe its oxidation. Thus, while 660 species and 2735 reactions describe the oxidation of n-heptane ($C_7H_{16}$) [24], 2885 species and 11754 reactions

are needed to describe the n-dodecane oxidation ($C_{12}H_{26}$) [181]. Finally, it is important to note that even detailed chemical kinetic mechanisms have to be validated by comparison to experimental results over a wide range of temperature, pressure and equivalence ratios.

As it has been said before, a chemical kinetic mechanism is a set of differential equations that represent the reaction rates of the chemical paths followed by the fuel during its oxidation. Any numerical solver can be used to solve such differential equations. However, there are some standard software products usually used to this aim.

CHEMKIN is a wide-spread numerical tool to perform chemical kinetic simulations [182]. This software, which was developed by Sandia National Laboratories and distributed by Reaction Design (ANSYS), is consolidated in the world of engineering investigations [183] and the chemical kinetic mechanisms of several hydrocarbons are perfectly defined to be used with it. CHEMKIN provides different models for specific applications, such as perfectly or partially stirred open or closed reactors, internal combustion engines, flow reactors, flame simulators, chemical vapor deposition reactors and shock tubes. Reactor networks can be used to model complex flow-fields, allowing the simulation of real combustion chambers, burners and chemical reactors. In fact, CHEMKIN models have been extensively validated versus experimental data [184]. According to combustion, ignition delays, burning velocities, chemical equilibrium or pollutant emissions can be modeled using CHEMKIN. An extinction model can be applied to perform the calculations of the extinction strain rate used to determine the combustion stability of a system. Moreover, particle inception, growth, aggregation and oxidation can be modeled. Fuel formulation and automated mechanism-reduction capabilities are included in CHEMKIN. In fact, a reaction path analyzer is included, which provides an overview of the dominant reaction paths. Moreover, different surrogate fuel blends can be created to match both the physical and chemical properties of a certain complex fuel. This software can be combined with different CFD codes, enabling the introduction of more accurate chemistry into reacting fluid-flow simulations. If the use of a chemical kinetic mechanism wants to be avoided, flamelet tables for input into CFD models can be created in CHEMKIN. Finally, a multi-zone reactor can be used for the analysis of combustion effects, including ignition, $NO_x$, CO, HC and soot emissions for internal combustion engines, being an intermediate step from 0-D models to complex CFD simulations.

Other software widely used to solve chemical kinetic mechanisms is Cantera, which is a free software for problems that involve chemical kinetics,

thermodynamics and transport processes [185]. Cantera is an object-oriented software where different objects represent phases of matter, interfaces between these phases, reaction managers, time-dependent reactor networks and steady 1-D reactive flows. It is currently used for applications including combustion, detonations, electrochemical energy conversion and storage, fuel cells, batteries, aqueous electrolyte solutions, plasma, and thin film deposition. This software can be used with Python and Matlab, or in applications written in C++ and Fortran 90.

While CHEMKIN is a commercial software that acts as a *black box* in which it is not possible to modify the code nor the numerical methods used to solve the differential equations from the mechanisms, Cantera is a fully open software, in which the user can adapt the code to a particular problem with the desired numerical discretization. This can be really useful for the development of new models or for the usage of particularly unstable mechanisms.

## 2.4 Research gaps present in the autoignition phenomenon

A brief summary of the literature survey that has been discussed in this Chapter is present in this section, highlighting the challenges to overcome in autoignition studies, as well as the uncertainties and the concepts that nowadays are not completely clear. As it is explained in Chapter 1, the increasingly restrictive regulations about pollutant emissions in internal combustion engines promote the research activity about this topic. There are two possible ways for the reduction of pollutant emissions: by means of after-treatment systems or by avoiding their formation during the combustion process. The last option shows clear advantages, such as avoiding additional complexities, lower cost and the possibility of improving the engine efficiency, among others. Thus, new combustion modes based on autoigniting an air-fuel mixture under LTC conditions, combined with well-known after-treatment techniques, are consolidated as a strategy to decrease the pollutant emissions by avoiding $NO_x$ and soot formation and by oxidizing UHC and CO in the exhaust.

Two main challenges appear in these advanced combustion modes. On the one hand, the engine control is much more complex due to the absence of an start event for the combustion process, since the ignition is controlled by the chemical kinetics of the mixture. On the other hand, autoignition causes high pressure rise rates that imply loud noise and high mechanical strains, so

that these modes are limited to low-to-medium loads. An accurate prediction of the ignition delay allows to control the engine settings for a proper heat release rate, improving the engine efficiency. However, the numerical method to predict the ignition characteristics of the fuel should have a computational cost low enough to be implemented in an ECU. Furthermore, a dual fuel strategy based on Diesel/gasoline blends is able to extend the operating range of LTC modes by using low octane fuels at low loads and high octane fuels at medium-to-high loads. Therefore, good predictions of the ignition event should be obtained not only for Diesel and gasoline surrogate fuels, but also for all the octane number reference scale.

The existing numerical methods simple enough to control the engine in real time can be summarized in the classic Livengood & Wu integral method [43]. As it can be read in detail in Section 2.2.3, the Livengood & Wu integral assumes that the oxidation process during the ignition delay can be described by a single zero-order global reaction, assumption under which it is impossible to describe the NTC behavior. Moreover, the autoignition is assumed to occur when a critical concentration of chain carriers is reached, being this critical concentration constant for a given air-fuel mixture. Therefore, the ignition data used in the numerical method, as well as the predicted ignition delay, should be referred to a critical concentration of chain carriers. It should be noted that the high-temperature stage of the autoignition occurs after any critical concentration of chain carriers, when these ones are completely consumed, so that, strictly, it is not possible to predict the high exothermic stage of the process.

Several authors [59] have called into question the validity of the Livengood & Wu integral when a two-stage ignition occurs (under very pronounced NTC behaviors). In this case, the ignition delay cannot be accurately predicted by the integral method, since it is based on a single global reaction mechanism that ignores the cool flames. Liang and Reitz [60] or Edenhofer et al. [61], among others, have declared that simple numerical methods (but more sophisticated than the Livengood & Wu integral while keeping the low computational cost) to characterize the autoignition at low temperature without using any chemical kinetic mechanism should be developed. However, most of the few alternatives to the Livengood & Wu integral that can be found in the literature are based on the integral itself or assume the same hypothesis.

Thus, three different research gaps can be identified:

i The validity of the hypotheses assumed in the Livengood & Wu integral method should be revised. Is it possible to describe the autoignition phenomenon by a zero-order global reaction? Is the critical concentration

of chain carriers constant for a given air-fuel mixture? The answer to these questions seems to depend on the existence of a two-stage or a single-stage ignition pattern. Thus, the limits of application of the integral method should be clearly defined.

ii Numerical expressions to predict the ignition delay based on more sophisticated autoignition mechanisms are needed in order to extend the range of validity of the existing methods. Moreover, both exothermic stages should be predicted in the case of fuels that show a two-stage ignition pattern: cool flames and the high-exothermic heat release.

iii In order to implement an alternative predictive method in an ECU, it should not only have low computational cost, but also be able to predict the ignition delay along all the octane number reference scale, since different octanes are needed under different loads in LTC modes.

Every model has to be validated by comparison to experimental data. Thus, the research gaps previously mentioned have to be solved with the support of experimental measurements. Autoignition studies are usually carried out in experimental facilities such as RCMs or shock tubes. However, since the ignition delay under transient thermodynamic conditions is intended to be predicted, an RCEM is the appropriate facility for the generation of a wide database for the validation of the numerical methods. Moreover, there is great interest in comparing the predictive capability of such numerical procedures to the accuracy of detailed chemical kinetic mechanisms. For this reason, the used mechanisms have to be also validated in the working range.

LTC modes use massive amounts of EGR to reduce the maximum temperature reached in the cycle. Thus, autoignition studies should be performed by testing diluted environments with high EGR rates in order to replicate engine conditions. However, the lack of enough exhaust gas flux in RCEMs requires working with synthetic EGR. So, it is necessary to define an optimal composition of such synthetic EGR to replicate the same conditions that can be found in a real engine and, by this way, to obtain results with realistic practical application. As it can be seen in Section 2.3.2, the effects of the EGR components on the different parameters of the combustion process have been widely studied. However, these effects should be analyzed with realistic proportions of the species under different temperature regimes in order to define the relevance of each of them under engine conditions. In typical autoignition studies, the ignition delay is obtained in environments diluted by adding $N_2$, Ar or $CO_2$ indistinctly [35, 36, 68]. This way to control the percent of oxygen is very useful to obtain ignition delays at different temperature

and pressure, and with different combustion temperature. However, a more proper composition of the dilution gases is necessary if a more realistic study is intended to be performed.

Thus, another research gap is clearly identified:

iv In order to obtain experimental ignition delays under engine conditions, the question is how to dilute the air in the simplest way, but without altering the reality. I.e., a criterion to define the composition of the synthetic EGR used in autoignition studies should be developed.

Despite the fact that the ignition event can be characterized by two different ignition delays, one referred to cool flames and another one referred to the high-temperature stage, there is great interest in knowing how the combustion is developed in realistic applications. The energy released is directly related to the establishment and propagation of an autoignition front, since even *homogeneous* mixtures have a certain degree of heterogeneity in real applications because of the existence of turbulence, temperature gradients and wall effects. Thus the generalization and propagation of the ignition and the combustion development should be studied.

OH* chemiluminescence and spectroscopy are non-intrusive optical techniques widely used in combustion diagnosis [140]. Such techniques are powerful tools to analyze the autoignition event, as well as different parameters of the combustion process. In fact, natural luminosity analysis and spectroscopy have shown to be able to describe the different stages of the autoignition phenomenon and the combustion process of a homogeneous air-fuel mixture [141].

As it is discussed in detail in Section 2.3.2, OH* is one of the main tracers of the combustion process. However, the presence of OH* radiation in the autoignition of homogeneous mixtures is not clear, since it can be outshined by other luminous reactions such as the CO continuum. The dominant luminosity under different temperature regimes should be analyzed from a chemical kinetics point of view, since the combustion diagnosis will be different depending on the source of radiation. Chemiluminescence can be also used to evaluate the generalization of the ignition event, since the velocity of propagation, as well as the area of ignition, can be studied by tracing the OH* radiation.

Thus, two more research gaps can be identified:

v It is necessary to analyze the actual establishment and propagation of the ignition event by studying the generalization of the autoignition and the

existence of an autoignition front, since the heat release rate is directly related to the characteristics of these phenomena. OH* has proved to be a good tracer of the ignition event, so that the evolution of the autoignition can be studied by tracing the spatial distribution of the OH* radiation in the combustion chamber.

v It is necessary to analyze the actual source of radiation when OH* chemiluminescence under LTC conditions is intended to be applied. Moreover, the chemical kinetics related with this phenomenon should be analyzed in order to be able to describe the different stages of the combustion process even if the OH* radiation is masked by other light.

The research gaps previously discussed will be intended to be solved in this Thesis, which results in a contribution to the scientific community by improving the knowledge about the autoignition phenomenon.

# References


[1] Challen Bernard, Baranescu Rodica and others. *Diesel Engine Reference Book*. Digital Designs.

[2] Doménech Llopis Vicente. *Estudio de nuevas estrategias para el control de la combustion en modos parcialmente premezclados en motores de encendido por compresión*. Doctoral Thesis, 2013.

[3] Asad Usman, Tjong Jimi and Zheng Ming. "Exhaust gas recirculation - Zero dimensional modelling and characterization for transient diesel combustion control". *Energy Conversion and Management*, Vol. 86, pp. 309–324, 2014.

[4] Li T., Wu D. and Xu M. "Thermodynamic analysis of EGR effects on the first and second law efficiencies of a boosted spark-ignited direct-injection gasoline engine". *Energy Conversion and Management*, Vol. 70, pp. 130–138, 2013.

[5] Zheng Zunqing, Yue Lang, Liu Haifeng, Zhu Yuxuan, Zhong Xiaofan and Yao Mingfa. "Effect of two-stage injection on combustion and emissions under high EGR rate on a diesel engine by fueling blends of diesel/gasoline, diesel/n-butanol, diesel/gasoline/n-butanol and pure diesel". *Energy Conversion and Management*, Vol. 90, pp. 1–11, 2015.

[6] Bahlouli Keyvan, Atikol Ugur, Khoshbakhti Saray R. and Mohammadi Vahid. "A reduced mechanism for predicting the ignition timing of a fuel blend of natural-gas and n-heptane in HCCI engine". *Energy Conversion and Management*, Vol. 79, pp. 85–96, 2014.

[7] Kuhl A. L., editor. *Dynamics of reactive systems*. Progress in astronautics and aeronautics. American Institute of Aeronautics and Astronautics, Washington, DC, 1988.

[8] Peters N. *Turbulent Combustion*. Cambridge University Press, 2000.

[9] Westbrook Charles K. "Chemical kinetics of hydrocarbon ignition in practical combustion systems". *Proceedings of the Combustion Institute*, Vol. 28, pp. 1563–1577, 2000.

[10] Weber Bryan William. *Autoigniton of n-butanol at low to intermediate temperature and elevated pressure*. Doctoral Thesis, University of Connecticut, 2010.

[11] Glassman Irvin. *Combustion*. Academic Press, Orlando [Fla.], 2nd ed edition, 1987.

[12] Onishi S., Jo S. H., Shoda K., Jo P. D. and Kato S. "Active thermo-atmosphere combustion (ATAC) - A new combustion process for internal combustion engines". *SAE Technical Papers 790501*, 1979.

[13] Mastorakos Epaminondas. "Ignition of turbulent non-premixed flames". *Progress in Energy and Combustion Science*, Vol. 35, pp. 57–97, 2009.

[14] Dubreuil A., Foucher F. and Mounam-Rousselle C. "Analysis of flame and OH natural emissions of n-heptane combustion in a Homogeneous Charge Compression Ignition (HCCI) engine: Effect of burnt gas dilution". *Energy and Fuels*, Vol. 23, pp. 1406–1411, 2009.

[15] Turns S. R. *An Introduction to Combustion*. McGraw-Hill.

[16] Lü Xing-Cai, Chen Wei and Huang Zhen. "A fundamental study on the control of the HCCI combustion and emissions by fuel design concept combined with controllable EGR. Part 1. The basic characteristics of HCCI combustion". *Fuel*, Vol. 84, pp. 1074–1083, 2005.

[17] Kumar Kamal, Mittal Gaurav and Sung Chih-Jen. "Autoignition of n-decane under elevated pressure and low-to-intermediate temperature conditions". *Combustion and Flame*, Vol. 156, pp. 1278–1288, 2009.

[18] Several Authors. "Lawrence Livermore National Laboratories Chemical Kinetic Mechanisms". *http://combustion.llnl.gov/mechanisms*, 2016.

[19] Pei Y., Mehl M., Liu W., Lu T., Pitz W. J. and Som S. "A multicomponent blend as a Diesel fuel surrogate for compression ignition engine applications". *Journal of Engineering for Gas Turbines and Power*, Vol. 137, pp. 111502–111502, 2015.

[20] Simmie John M. "Detailed chemical kinetic models for the combustion of hydrocarbon fuels". *Progress in Energy and Combustion Science*, Vol. 29, pp. 599–634, 2003.

[21] Curran H. J., Gaffuri P., Pitz W. J. and Westbrook C. K. "A comprehensive modeling study of iso-octane oxidation". *Combustion and Flame*, Vol. 129, pp. 253–280, 2002.

[22] Müller U. C., Peters N. and Liñán A. "Global kinetics for n-heptane ignition at high pressures". *Twenty-Fourth Symposium (International) on Combustion-The Combustion Institute*, pp. 777–784, 1992.

[23] Herbinet Olivier, Husson Benoit, Serinyel Zeynep, Cord Maximilien, Warth Valérie, Fournet René, Glaude Pierre-Alexandre, Sirjean Baptiste, Battin-Leclerc Frédérique, Wang Zhandong, Xie Mingfeng, Cheng Zhanjun and Qi Fei. "Experimental and modeling investigation of the low-temperature oxidation of n-heptane". *Combustion and Flame*, Vol. 159, pp. 3455–3471, 2012.

[24] Curran H. J., Gaffuri P., Pitz W. J. and Westbrook C. K. "A comprehensive modeling study of n-heptane oxidation". *Combustion and Flame*, Vol. 114, pp. 149–177, 1998.

[25] Westbrook Charles K., Pitz William J., Herbinet Olivier, Curran Henry J. and Silke Emma J. "A comprehensive detailed chemical kinetic reaction mechanism for combustion of n-alkane hydrocarbons from n-octane to n-hexadecane". *Combustion and Flame*, Vol. 156, pp. 181–199, 2009.

[26] Baeuerle B., Warnatz J. and Behrendt F. "Time-resolved investigation of hot spots in the end gas of an S.I. engine by means of 2-D double-pulse LIF of formaldehyde". *Symposium (International) on Combustion*, Vol. 2, pp. 2619–2626, 1996.

[27] Koert David N., Pit William J., Boelli Joseph W. and Cernansky Nicholas P. "Chemical kinetic modeling of high-pressure propane oxidation and comparison to experimental results". *Symposium (International) on Combustion*, Vol. 26, pp. 633–640, 1996.

[28] Gibson C., Gray P., Griffiths J. F. and Hasko S. M. "Spontaneous ignition of hydrocarbon and related fuels: A fundamental study of thermokinetic interactions". *Symposium (International) on Combustion*, Vol. 20, pp. 101–109, 1985.

[29] Dagaut Philippe, Reuillon Marcelline and Cathonnet Michel. "Experimental study of the oxidation of n-heptane in a jet stirred reactor from low to high temperature and pressures up to 40 atm". *Combustion and Flame*, Vol. 101, pp. 132–140, 1995.

[30] Zheng Z and Yao M. "Numerical study on the chemical reaction kinetics of n-heptane for HCCI combustion process". *Fuel*, Vol. 85, pp. 2605–2615, 2006.

[31] Pastor J. V., García-Oliver J. M., García A., Micó C. and Durrett R. "A spectroscopy study of gasoline partially premixed compression ignition spark assisted combustion". *Applied Energy*, Vol. 104, pp. 568–575, 2013.

[32] Mehl Marco, Pitz William J., Westbrook Charles K. and Curran Henry J. "Kinetic modeling of gasoline surrogate components and mixtures under engine conditions". *Proceedings of the Combustion Institute*, Vol. 33, pp. 193–200, 2011.

[33] Curran Henry, Simmie John M., Dagaut Philippe, Voisin David and Cathonnet Michel. "The ignition and oxidation of allene and propyne: Experiments and kinetic modeling". *Symposium (International) on Combustion*, Vol. 26, pp. 613–620, 1996.

[34] Kukkadapu Goutham, Kumar Kamal, Sung Chih-Jen, Mehl Marco and Pitz William J. "Experimental and surrogate modeling study of gasoline ignition in a Rapid Compression Machine". *Combustion and Flame*, Vol. 159, pp. 3066–3078, 2012.

[35] Weber Bryan W., Kumar Kamal, Zhang Yu and Sung Chih-Jen. "Autoignition of n-butanol at elevated pressure and low-to-intermediate temperature". *Combustion and Flame*, Vol. 158, pp. 809–819, 2011.

[36] Mittal Gaurav, Chaos Marcos, Sung Chih-Jen and Dryer Frederick L. "Dimethyl ether autoignition in a Rapid Compression Machine: Experiments and chemical kinetic modeling". *Fuel Processing Technology*, Vol. 89, pp. 1244–1254, 2008.

[37] Petrucci R. H., Harwood W. S. and Herring F. G. *General Chemistry*. Prentice Hall, 2001.

[38] Kumar Kamal and Sung Chih-Jen. "An experimental study of the autoignition characteristics of conventional jet fuel-oxidizer mixtures: Jet-A and JP-8". *Combustion and Flame*, Vol. 157, pp. 676–685, 2010.

[39] Blin-Simiand N., Rigny R., Viossat V., Circan S. and Sahetchian K. "Autoignition of hydrocarbon/air mixtures in a CFR engine: Experimental and modeling study". *Combustion Science and Technology*, Vol. 88, pp. 329–348, 1993.

[40] Gray Jeffrey A. and Westbrook Charles K. "High-temperature ignition of propane with MTBE as an additive: Shock tube experiments and modeling". *International Journal of Chemical Kinetics*, Vol. 26, pp. 757–770, 1994.

[41] Darcy D., Nakamura H., Tobin C.J., Mehl M., Metcalfe W.K., Pitz W.J., Westbrook C.K. and Curran H.J. "A high-pressure Rapid Compression Machine study of n-propylbenzene ignition". *Combustion and Flame*, Vol. 161, pp. 65–74, 2014.

[42] Vandersickel A., Hartmann M., Vogel K., Wright Y.M., Fikri M., Starke R., Schulz C. and Boulouchos K. "The autoignition of practical fuels at HCCI conditions: High-pressure shock tube experiments and phenomenological modeling". *Fuel*, Vol. 93, pp. 492–501, 2012.

[43] Livengood J. C. and Wu P. C. "Correlation of autoignition phenomena in internal combustion engines and rapid compression machines". *Symposium (International) on Combustion*, Vol. 5, pp. 347–356, 1955.

[44] Chen L., Li T., Yin T. and Zheng B. "A predictive model for knock onset in spark-ignition engines with cooled EGR". *Energy Conversion and Management*, Vol. 87, pp. 946–955, 2014.

[45] Swan K., Shahbakhti M. and Koch C.R. "Predicting start of combustion using a modified knock integral method for an HCCI engine". *SAE Technical Papers 2006-01-1086*, 2006.

[46] Hoepke Bjoern, Jannsen Stefan, Kasseris Emmanuel and Cheng Wai K. "EGR effects on boosted SI engine operation and knock integral correlation". *SAE Technical Papers 2012-01-0707*, 2012.

[47] Hernández J. J., Sanz-Argent J., Carot J. M. and Jabaloyes J. M. "Ignition delay time correlations for a diesel fuel with application to engine combustion modelling". *International Journal of Engine Research*, Vol. 11, pp. 199–206, 2010.

[48] Weisser German Andreas. *Modelling of combustion and nitric oxide formation for medium-speed DI diesel engines*. Doctoral Thesis, Diss., Technische Wissenschaften ETH Zürich, Nr. 14465, 2002, 2001.

[49] Blomberg Christopher, Mitakos Dimitrios, Bardi Michele, Boulouchos Konstantinos, Wright Yuri M. and Vandersickel Annelies. "Extension of the phenomenological 3-Arrhenius auto-ignition model for six surrogate automotive fuels". *SAE Technical Papers 2016-01-0755*, 2016.

[50] Imamori Y., Endo H., Sakaguchi K. and Yanagi J. "Development of combustion system in low speed two-stroke diesel engine using CFD". *International Council on Combustion Engines*, 2004.

[51] Li G., Bo T., Chen C. and Johns R.J.R. "CFD Simulation of HCCI Combustion in a 2-Stroke DI Gasoline Engine". *SAE Technical Papers 2003-01-1855*, 2003.

[52] Ohyama Y. "Engine control using a combustion model". *Seoul 2000 FISITA World Automotive Congress*, 2000.

[53] Rausen D. J., Stefanopoulou A. G., Kang J.-M., Eng J. A. and Kuo T.-W. "A mean-value model for control of Homogeneous Charge Compression Ignition (HCCI) engines". *Journal of Dynamic Systems, Measurement, and Control*, Vol. 127, pp. 355, 2005.

[54] Choi Y. and Chen J.-Y. "Fast prediction of start-of-combustion in HCCI with combined artificial neural networks and ignition delay model". *Proceedings of the Combustion Institute*, Vol. 30, pp. 2711–2718, 2005.

[55] Hillion M., Chauvin J. and Petit N. "Control of highly diluted combustion in Diesel engines". *Control Engineering Practice*, Vol. 19, pp. 1274–1286, 2011.

[56] Bradley D. and Kalghatgi G.T. "Influence of autoignition delay time characteristics of different fuels on pressure waves and knock in reciprocating engines". *Combustion and Flame*, Vol. 156, pp. 2307–2318, 2009.

[57] Bradley Derek and Head R.A. "Engine autoignition: The relationship between octane numbers and autoignition delay times". *Combustion and Flame*, Vol. 147, pp. 171–184, 2006.

[58] Reyes M., Tinaut F.V., Andrés C. and Pérez A. "A method to determine ignition delay times for Diesel surrogate fuels from combustion in a constant volume bomb: Inverse Livengood-Wu method". *Fuel*, Vol. 102, pp. 289–298, 2012.

[59] Yates Andy D. B., Swarts André and Viljoen Carl L. "Correlating auto-ignition delays and knock-limited spark-advance data for different types of fuel". *SAE Technical Papers 2005-01-2083*, 2005.

[60] Liang Long and Reitz Rolf D. "Spark ignition engine combustion modeling using a level set method with detailed chemistry". *SAE Technical Papers 2006-01-0243*, pág. 0243, 2006.

[61] Edenhofer R., Lucka K. and Kohne H. "Low temperature oxidation of diesel-air mixtures at atmospheric pressure". *Proceedings of the Combustion Institute*, Vol. 31, pp. 2947–2954, 2007.

[62] Hernandéz J. J., Lapuerta M. and Sanz-Argent J. "Autoignition prediction capability of the Livengood-Wu correlation applied to fuels of commercial interest". *International Journal of Engine Research*, Vol. 15, pp. 817–829, 2014.

[63] Dec John E. "A computational study of the effects of low fuel loading and EGR on heat release rates and combustion limits in HCCI engines". *SAE Technical Papers 2002-01-1309*, 2002.

[64] Kobashi Y., Tanaka D., Maruko T. and Kato S. "Effects of mixedness and ignition timings on PCCI combustion with a dual fuel operation". *SAE Technical Papers 2011-01-1768*, 2011.

[65] Munsin Ronnachart, Laoonual Yossapong, Jugjai Sumrerng, Matsuki Masataka and Kosaka Hidenori. "Investigation of effects of ignition improvers on ignition delay time of ethanol combustion with Rapid Compression and Expansion Machine". *SAE Technical Papers 2012-01-0854*, 2012.

[66] Siebers Dennis L., Higgins Brian and Pickett Lyle. "Flame lift-off on direct-injection diesel fuel jets: oxygen concentration effects". *SAE Technical Papers 2002-01-0890*, 2002.

[67] Cho Gyubaek, Jeong Dongsoo, Moon Gunfeel and Bae Choongsik. "Controlled auto-ignition characteristics of methane-air mixture in a Rapid Intake Compression and Expansion Machine". *Energy*, Vol. 35, pp. 4184–4191, 2010.

[68] Kukkadapu Goutham, Kumar Kamal, Sung Chih-Jen, Mehl Marco and Pitz William J. "Autoignition of gasoline and its surrogates in a Rapid Compression Machine". *Proceedings of the Combustion Institute*, Vol. 34, pp. 345–352, 2013.

[69] Cheng Yu, Hu Erjiang, Deng Fuquan, Yang Feiyu, Zhang Yingjia, Tang Chenglong and Huang Zuohua. "Experimental and kinetic comparative study on ignition characteristics of 1-pentene and n-pentane". *Fuel*, Vol. 172, pp. 263–272, 2016.

[70] Pickett Lyle M., Siebers Dennis L. and Idicheria Cherian A. "Relationship between ignition processes and the lift-off length of diesel fuel jets". *SAE Technical Papers 2005-01-3843*, 2005.

[71] Sung Chih-Jen and Curran Henry J. "Using Rapid Compression Machines for chemical kinetics studies". *Progress in Energy and Combustion Science*, Vol. 44, pp. 1–18, 2014.

[72] Payri Raul, Gimeno Jaime, Viera Juan P. and Plazas Alejandro H. "Needle lift profile influence on the vapor phase penetration for a prototype diesel direct acting piezoelectric injector". *Fuel*, Vol. 113, pp. 257–265, 2013.

[73] Ghojel Jamil I. and Tran Xuan-Thien. "Ignition Characteristics of Diesel-Water Emulsion Sprays in a Constant-Volume Vessel: Effect of Injection Pressure and Water Content". *Energy & Fuels*, Vol. 24, pp. 3860–3866, 2010.

[74] Dreizler A., Lindenmaier S., Maas U., Hult J., Aldén M. and Kaminski C. F. "Characterisation of a spark ignition system by planar laser-induced fluorescence of OH at high repetition rates and comparison with chemical kinetic calculations". *Applied Physics B*, Vol. 70, pp. 287–294, 2000.

[75] Gu X. J., Haq M. Z., Lawes M. and Woolley R. "Laminar burning velocity and Markstein lengths of methane-air mixtures". *Combustion and Flame*, Vol. 121, pp. 41–58, 2000.

[76] Pickett Lyle M. and Siebers Dennis L. "Soot in diesel fuel jets: effects of ambient temperature, ambient density, and injection pressure". *Combustion and Flame*, Vol. 138, pp. 114–135, 2004.

[77] Meijer Maarten, Somers Bart, Johnson Jaclyn, Naber Jeffrey, Lee Seong-Young, Malbec Louis Marie, Bruneaux Gilles, Pickett Lyle M., Bardi Michele, Payri Raul and Bazyn Tim. "Engine Combustion Network (ECN): Characterization and comparison of boundary conditions for different combustion vessels". *Atomization and Sprays*, Vol. 22, pp. 777–806, 2012.

[78] Lapuerta Magín, Sanz-Argent Josep and Raine Robert R. "Ignition Characteristics of Diesel Fuel in a Constant Volume Bomb under Diesel-Like Conditions. Effect of the Operation Parameters". *Energy & Fuels*, Vol. 28, pp. 5445–5454, 2014.

[79] Lapuerta Magín, Sanz-Argent Josep and Raine Robert. "Heat release determination in a constant volume combustion chamber from the instantaneous cylinder pressure". *Applied Thermal Engineering*, Vol. 63, pp. 520–527, 2014.

[80] Higgins Brian, Siebers Dennis L. and Aradi Allen. "Diesel-spray ignition and premixed-burn behavior". *SAE Technical Papers 2000-01-0940*, 2000.

[81] Siebers D. "Ignition delay characteristics of alternative Diesel fuels: Implications on cetane number". *SAE Technical Papers 852102*, 1985.

[82] Bardi Michele, Payri Raul, Malbec Louis Marie, Bruneaux Gilles, Pickett Lyle M., Manin Julien, Bazyn Tim and Genzale Caroline L. "Engine combustion network: comparison of spray development, vaporization, and combustion in different combustion vessels". *Atomization and Sprays*, Vol. 22, 2012.

[83] Baert R. S. G., Frijters P. J. M., Somers B., Luijten C. C. M. and de Boer W. "Design and operation of a high pressure, high temperature cell for HD Diesel spray diagnostics: Guidelines and results". *SAE Technical Papers 2009-01-0649*, 2009.

[84] Payri Raul, García-Oliver Jose M., Bardi Michele and Manin Julien. "Fuel temperature influence on diesel sprays in inert and reacting conditions". *Applied Thermal Engineering*, Vol. 35, pp. 185–195, 2012.

[85] Krehl Peter O. K. *History of Shock Waves, Explosions and Impact: A Chronological and Biographical Reference*. Springer Science & Business Media, 2008.

[86] Davidson D. F. and Hanson R. K. "Interpreting shock tube ignition data". *International Journal of Chemical Kinetics*, Vol. 36, pp. 510–523, 2004.

[87] Strehlow Roger A. and Cohen Arthur. "Initiation of detonation". *Physics of Fluids (1958-1988)*, Vol. 5, pp. 97–101, 1962.

[88] Davidson D. F., Gauthier B. M. and Hanson R. K. "Shock tube ignition measurements of iso-octane/air and toluene/air at high pressures". *Proceedings of the Combustion Institute*, Vol. 30, pp. 1175–1182, 2005.

[89] Soloukhin Rem Ivanovich. *Shock waves and detonations in gases*. Mono Book Corp., Baltimore, 1966.

[90] Hanson R.K. "Quantitative laser diagnostics for combustion chemistry and propulsion: Shock tube techniques and applications". *Princeton, New Jersey, USA*, 2015.

[91] Gaydon Alfred Gordon and Hurle Ian Roy. *The shock tube in high-temperature chemical physics*. Chapman and Hall, 1963.

[92] Bradley J. *Shock Waves in Chemistry and Physics*. Chapman and Hall, London, 1962.

[93] Nakamura Hisashi, Darcy Daniel, Mehl Marco, Tobin Colin J., Metcalfe Wayne K., Pitz William J., Westbrook Charles K. and Curran Henry J. "An experimental and modeling study of shock tube and rapid compression machine ignition of n-butylbenzene/air mixtures". *Combustion and Flame*, Vol. 161, pp. 49–64, 2014.

[94] Nicolas Ghassan and Metghalchi Hameed. "Comparison between RCCE and shock tube ignition delay times at low temperatures". *Journal of Energy Resources Technology*, Vol. 137, pp. 062203–062203, 2015.

[95] Burke Ultan, Metcalfe Wayne K., Burke Sinead M., Heufer K. Alexander, Dagaut Philippe and Curran Henry J. "A detailed chemical kinetic modeling, ignition delay time and jet-stirred reactor study of methanol oxidation". *Combustion and Flame*, Vol. 165, pp. 125–136, 2016.

[96] Falk K. George. "The ignition temperatures of hydrogen-oxygen mixtures". *Journal of the American Chemical Society*, Vol. 28, pp. 1517 – 1534, 1906.

[97] Neuman John. *Development of a Rapid Compression Controlled-Expansion Machine for chemical ignition studies.* Doctoral Thesis, University of Wisconsin, 2015.

[98] Egusquiza J. C. Cuisano, Braga S. Leal, Braga C. V. Maciel, Villela A. C. Scardini and Moura N. Reis de. "Experimental investigation of the natural gas / Diesel dual-fuel combustion using a Rapid Compression Machine". *SAE Technical Papers 2011-36-0360*, 2011.

[99] Liu Hao, Zhang Hongguang, Shi Zhicheng, Lu Haitao, Zhao Guangyao and Yao Baofeng. "Performance characterization and auto-ignition performance of a Rapid Compression Machine". *Energies*, Vol. 7, pp. 6083–6104, 2014.

[100] Heufer K. A., Bugler J. and Curran H. J. "A comparison of longer alkane and alcohol ignition including new experimental results for n-pentanol and n-hexanol". *Proceedings of the Combustion Institute*, Vol. 34, pp. 511–518, 2013.

[101] Lezanski T., Seczyk J. and Wolanski P. "Design of the rapid compression machines for combustion researches in spark ignition engines". *Journal of KONES*, Vol. 19, pp. 379–391, 2012.

[102] Gupta Sreenath and Singh Gurpreet. "Rapid Compression Machine - A key experimental device to dffectively collaborate with basic energy sciences". *ACE 2011 Program Review, Washington D.C., USA*, 2011.

[103] Mittal Gaurav and Chomier Mickael. "Interpretation of experimental data from Rapid Compression Machines without creviced pistons". *Combustion and Flame*, Vol. 161, pp. 75–83, 2014.

[104] Mittal Gaurav and Chomier Mickael. "Effect of crevice mass transfer in a Rapid Compression Machine". *Combustion and Flame*, Vol. 161, pp. 398–404, 2014.

[105] Lee Daeyup and Hochgreb Simone. "Rapid Compression Machines: Heat transfer and suppression of corner vortex". *Combustion and Flame*, Vol. 114, pp. 531–545, 1998.

[106] Lee Changyoul, Vranckx Stijn, Heufer Karl A., Khomik Sergey V., Uygun Yasar, Olivier Herbert and Fernandez Ravi X. "On the chemical kinetics of ethanol oxidation: Shock tube, Rapid Compression Machine and detailed modeling study". *Zeitschrift für Physikalische Chemie*, Vol. 226, pp. 1–28, 2012.

[107] Bradley D., Lawes M. and Materego M. "Interpretation of auto-ignition delay times measured in different Rapid Compression Machines". *25th International Colloquium on the Dynamics of Explosions and Reactive systems*, 2015.

[108] Pöschl M. and Sattelmayer T. "Influence of temperature inhomogeneities on knocking combustion". *Combustion and Flame*, Vol. 153, pp. 562–573, 2008.

[109] Villela A. C. Scardini, Braga S. Leal, Egusquiza J. C. Cuisano and Machado G. Bastos. "Rapid Compression Machine tests for brazilian Otto cycle fuels". *SAE Technical Papers 2011-36-0349*, 2011.

[110] Schlatter Stephanie, Schneider Bruno, Wright Yuri M. and Boulouchos Konstantinos. "Comparative study of ignition systems for lean burn gas engines in an optically accessible Rapid Compression Expansion Machine". *SAE Technical Papers 2013-24-0112*, 2013.

[111] Schlatter Stephanie, Schneider Bruno, Wright Yuri and Boulouchos Konstantinos. "Experimental study of ignition and combustion characteristics of a Diesel pilot spray in a lean premixed methane/air charge using a Rapid Compression Expansion Machine". *SAE Technical Papers 2012-01-0825*, 2012.

[112] Barroso G., Escher A. and Boulouchos K. "Experimental and numerical investigations on HCCI-combustion". *SAE Technical Papers 2005-24-038*, 2005.

[113] Several Authors. "TESTEM GMBH". *http://www.testem.de/26/Einhubtriebwerk/*, 2016.

[114] Manasra Salih and Brueggemann Dieter. "Effect of injection pressure and timing on the in-cylinder soot formation characteristics of low CR neat GTL-fueled DI Diesel engine". *SAE Technical Papers 2011-01-2464*, 2011.

[115] Salaun Erwan, Apeloig Julien, Grisch Frédéric, Yvonnet Charles-Edouard, Nicolas Baptiste and Dionnet Frederic. "Optical Investigation of Ignition Timing and Equivalence Ratio in Dual-Fuel CNG/Diesel Combustion". *SAE Technical Papers 2016-01-0772*, 2016.

[116] Steinhilber T. and Sattelmayer T. "The effect of water addition on HCCI Diesel combustion". *SAE Technical Papers 2006-01-3321*, 2006.

[117] Mitakos Dimitrios Angelos, Blomberg Christopher, Wright Yuri M., Obrecht Peter, Schneider Bruno and Boulouchos Konstantinos. "Integration of a cool-flame heat release rate model into a 3-stage ignition model for HCCI applications and different fuels". *SAE Technical Papers 2014-01-1268*, 2014.

[118] Krishnan Sundar Rajan, Srinivasan Kalyan Kumar and Stegmeir Matthew. "Characterization of Diesel and Gasoline Compression Ignition Combustion in a Rapid Compression-Expansion Machine using OH* Chemiluminescence Imaging". *Bulletin of the American Physical Society*, Vol. 60, 2015.

[119] Several Authors. "CMT - Motores Termicos RCEM". *cmt.upv.es*, 2016.

[120] Vermeersch M.L., Held T.J., Stein Y. and Dryer F.L. "Auto-ignition chemistry studies of n-butane in a variable pressure flow reactor". *SAE Technical Papers 912316*, 1991.

[121] Dagaut P., Reuillon M. and Cathonnet M. "Experimental study of the oxidation of n-heptane in a jet stirred reactor from low to high temperature and pressures up to 40 atm". *Combustion and Flame*, Vol. 101, pp. 132–140, 1995.

[122] Li G., Bo T., Chen C. and Johns R. "CFD simulation of HCCI combustion in a 2-stroke DI gasoline engine". *SAE Technical Papers 2003-01-1855*, 2003.

[123] Mittal Gaurav, Davies Varun Anthony and Parajuli Bikash. "Autoignition of ethanol in a Rapid Compression Machine". *8th U.S. National Combustion Meeting - Western States Section of the Combustion Institute*, Vol. Paper 070RK-0222, 2013.

[124] Mittal Gaurav and Sung Chih-Jen. "A Rapid Compression Machine for chemical kinetics studies at elevated pressures and temperatures". *Combustion Science and Technology*, Vol. 179, pp. 497–530, 2007.

[125] Allen Casey, Valco Daniel, Toulson Elisa, Yoo Ji Hyung and Lee Tonghun. "JP-5 and HRJ-5 Autoignition Characteristics and Surrogate Modeling". *Energy & Fuels*, Vol. 27, pp. 7790–7799, 2013.

[126] Liu Y., Li L., Ye J., Deng J. and Wu Z. "Ion current signal and characteristics of ethanol/gasoline dual fuel HCCI combustion". *Fuel*, Vol. 166, pp. 42–50, 2016.

[127] Zhou L. and Wei H. "Chemistry acceleration with tabulated dynamic adaptive chemistry in a realistic engine with a primary reference fuel". *Fuel*, Vol. 171, pp. 186–194, 2016.

[128] Terashima H. and Koshi M. "Mechanisms of strong pressure wave generation in end-gas autoignition during knocking combustion". *Combustion and Flame*, Vol. 162, pp. 1944–1956, 2015.

[129] Dernotte J., Dec J. and Ji C. "Investigation of the Sources of Combustion Noise in HCCI Engines". *SAE Technical Paper 2014-01-1272*, 2014.

[130] Sjoberg M., Dec J.E. and Cernansky N.P. "Potential of thermal stratification and combustion retard for reducing pressure-rise rates in HCCI engines, based on multi-zone modeling and experiments". *SAE Technical Paper 2005-01-0113*, 2005.

[131] Bradley D., Morley C., Gu X.J. and Emerson D.R. "Amplified Pressure Waves During Autoignition: Relevance to CAI Engines". *SAE Technical Paper 2002-01-2868*, 2002.

[132] Gu X.J., Emerson D.R. and Bradley D. "Modes of reaction front propagation from hot spots". *Combustion and Flame*, Vol. 133, pp. 63–74, 2003.

[133] Chen J.H., Hawkes E.R., Sankaran R., Mason S.D. and Im H.G. "Direct numerical simulation of ignition front propagation in a constant volume with temperature inhomogeneities I. Fundamental analysis and diagnostics". *Combustion and Flame*, Vol. 145, pp. 128–144, 2006.

[134] Yoo C.S., Lu T., Chen J.H. and Law C.K. "Direct numerical simulations of ignition of a lean n-heptane/air mixture with temperature inhomogeneities at constant volume: Parametric study". *Combustion and Flame*, Vol. 158, pp. 1727–1741, 2011.

[135] Bansal G. and Im H.G. "Autoignition and front propagation in low temperature combustion engine environments". *Combustion and Flame*, Vol. 158, pp. 2105–2112, 2011.

[136] Hwang W., Dec J. and Sjöberg M. "Spectroscopic and chemical-kinetic analysis of the phases of HCCI autoignition and combustion for single- and two-stage ignition fuels". *Combustion and Flame*, Vol. 154, pp. 387–409, 2008.

[137] Clarkson J., Griffiths J. F., MacNamara J. P. and Whitaker B. J. "Temperature fields during the development of combustion in a Rapid Compression Machine". *Combustion and Flame*, Vol. 125, pp. 1162–1175, 2001.

[138] Skeen Scott A., Manin Julien, Pickett Lyle M., Cenker Emre, Bruneaux Gilles, Kondo Katsufumi, Aizawa Tets, Westlye Fredrik, Dalen Kristine, Ivarsson Anders, Xuan Tiemin, Garcia-Oliver Jose M, Pei Yuanjiang, Som Sibendu, Hu Wang, Reitz Rolf D., Lucchini Tommaso, D'Errico Gianluca, Farrace Daniele, Pandurangi Sushant S., Wright Yuri M., Chishty Muhammad Aqib, Bolla Michele and Hawkes Evatt. "A progress review on soot experiments and modeling in the Engine Combustion Network (ECN)". *SAE Technical Papers 2016-01-0734*, 2016.

[139] Ihme Matthias. "Reconcile discrepancies of current syngas kinetics models by considering turbulence effects on ignition delay at gas-turbine relevant operating conditions". *49th AIAA Aerospace Sciences Meeting including the New Horizons Forum and Aerospace Exposition*, 2011.

[140] Augusta R., Foster D. E., Ghandhi J. B., Eng J. and Najt P. M. "Chemiluminescence measurements of homogeneous charge compression ignition (HCCI) combustion". *SAE Technical Papers 2006-01-1520*, 2006.

[141] Liu H. F., Yao M. F., Jin C., Zhang P., Li Z. M. and Zheng Z.Q. "Chemiluminescence spectroscopic analysis of homogeneous charge compression ignition combustion processes". *Spectroscopy and Spectral Analysis*, Vol. 30, pp. 2611–2615, 2010.

[142] Mancaruso E. and Vaglieco B. M. "Spectroscopic measurements of premixed combustion in diesel engine". *Fuel*, Vol. 90, pp. 511–520, 2011.

[143] Mancaruso E. and Vaglieco B. M. "Optical investigation of the combustion behaviour inside the engine operating in HCCI mode and using alternative diesel fuel". *Experimental Thermal and Fluid Science*, Vol. 34, pp. 346–351, 2010.

[144] Iijima A. and Shoji H. "A spectroscopic analysis of combustion in Homogeneous Charge Compression Ignition engine". *ASME-JSME Thermal Engineering Summer Heat Transfer Conference*, Vol. HT2007-32552, 2007.

[145] Kim B., Kaneko M., Ikeda Y. and Nakajima T. "Detailed spectral analysis of the process of HCCI combustion". *Proceedings of the Combustion Institute*, Vol. 29, pp. 671–677, 2002.

[146] Murase E., Hanada K., Miyaura T. and Ikeda J. "Photographic observation and emission spectral analysis of Homogeneous Charge Compression Ignition combustion". *Combustion Science and Technology*, Vol. 177, pp. 1699–1723, 2005.

[147] Mitakos D., Blomberg C., Vandersickel A., Wright Y., Schneider B. and Boulouchos K. "Ignition delays of different homogeneous fuel-air mixtures in a Rapid Compression Expansion Machine and comparison with a 3-stage-ignition model parametrized on shock tube data". *SAE Technical Papers 2013-01-2625*, 2013.

[148] Goldsborough S. Scott. "A crevice blow-by model for a Rapid Compression Expansion Machine used for chemical kinetic (HCCI) studies". *SAE Technical Papers 2007-01-1052*, 2007.

[149] Allen Casey, Toulson Elisa, Edwards Tim and Lee Tonghun. "Application of a novel charge preparation approach to testing the autoignition characteristics of JP-8 and camelina hydroprocessed renewable jet fuel in a rapid compression machine". *Combustion and Flame*, Vol. 159, pp. 2780–2788, 2012.

[150] Ladommatos N., Abdelhalim S., Zhao H. and Hu Z. "The dilution, chemical, and thermal effects of Exhaust Gas Recirculation on Diesel engine emissions - Part 1: Effect of reducing inlet charge oxygen". *SAE Technical Papers 961165*, 1996.

[151] Ladommatos N., Abdelhalim S., Zhao H. and Hu Z. "The dilution, chemical, and thermal effects of Exhaust Gas Recirculation on Diesel engine emissions - Part 2: Effects of carbon dioxide". *SAE Technical Papers 961167*, 1996.

[152] Ladommatos N., Abdelhalim S., Zhao H. and Hu Z. "The dilution, chemical, and thermalt effects of Exhaust Gas Recirculation on Diesel engine emissions - Part 3: Effects of water vapour". *SAE Technical Papers 971659*, 1997.

[153] Ladommatos N., Abdelhalim S., Zhao H. and Hu Z. "The dilution, chemical, and thermal effects of Exhaust Gas Recirculation on Disesel engine emissions - Part 4: Effects of carbon dioxide and water vapour". *SAE Technical Papers 971660*, 1997.

[154] Zhao H., Peng Z., Williams J. and Ladommatos N. "Understanding the effects of recycled burnt gases on the Controlled Autoignition (CAI) combustion in four-stroke gasoline engines". *SAE Technical Papers 2001-01-3607*, 2001.

[155] Chen R. and Milovanovic N. "A computational study into the effect of exhaust gas recycling on homogeneous charge compression ignition combustion in internal combustion engines fuelled with methane". *International Journal of Thermal Sciences*, Vol. 41, pp. 805–813, 2002.

[156] Sjöberg Magnus, Dec John E. and Hwang Wontae. "Thermodynamic and chemical effects of EGR and its constituents on HCCI autoignition". *SAE Technical Papers 2007-01-0207*, 2007.

[157] Sjöberg Magnus and Dec John E. "Effects of EGR and its constituents on HCCI autoignition of ethanol". *Proceedings of the Combustion Institute*, Vol. 33, pp. 3031–3038, 2011.

[158] Babajimopoulos A., Lavoie G. A. and Assanis D. N. "Modeling HCCI combustion with high levels of residual gas fraction. A comparison of two VVA strategies". *SAE Technical Papers 2003-01-3220*, 2003.

[159] Fathi Morteza, Saray R. Khoshbakhti and Checkel M. David. "The influence of Exhaust Gas Recirculation (EGR) on combustion and emissions of n-heptane/natural gas fueled Homogeneous Charge Compression Ignition (HCCI) engines". *Applied Energy*, Vol. 88, pp. 4719–4724, 2011.

[160] Le Cong T. and Dagaut P. "Experimental and detailed kinetic modeling of the oxidation of natural gas, natural gas/syngas mixtures, and effect of burnt gas recirculation". *Proceedings of the European Combustion Meeting, July 23-27, 2007, Poitiers, France.*

[161] Herzler J. and Naumann C. "Shock tube study of the influence of NOx on the ignition delay times of natural gas at high pressure". *Combustion Science and Technology*, Vol. 184, pp. 1635–1650, 2012.

[162] Di Haisheng, He Xin, Zhang Peng, Wang Zhi, Wooldridge Margaret S., Law Chung K., Wang Cuiping, Shuai Shijin and Wang Jianxin. "Effects of buffer gas composition on low temperature ignition of iso-octane and n-heptane". *Combustion and Flame*, Vol. 161, pp. 2531–2538, 2014.

[163] Tanaka Shigeyuki, Ayala Ferran, Keck James C. and Heywood John B. "Two-stage ignition in HCCI combustion and HCCI control by fuels and additives". *Combustion and Flame*, Vol. 132, pp. 219–239, 2003.

[164] Han Dong, Guang Huanyu, Yang Zheng, Lu Xingcai and Huang Zhen. "Premixed ignition characteristics of blends of gasoline and diesel-like fuels on a Rapid Compression Machine". *Thermal Science*, Vol. 17, pp. 1–10, 2013.

[165] Colin Olivier, Pires da Cruz Antonio and Jay Stephane. "Detailed chemistry-based auto-ignition model including low temperature phenomena applied to 3-D engine calculations". *Proceedings of the Combustion Institute*, Vol. 30, pp. 2649–2656, 2005.

[166] Lopez J.J., Novella R., Garcia A. and Winklinger J.F. "Investigation of the ignition and combustion processes of a dual-fuel spray under diesel-like conditions using computational fluid dynamics (CFD) modeling". *Mathematical and Computer Modelling*, Vol. 57, pp. 1897–1906, 2013.

[167] Novella R., Garcia A., Pastor J. M. and Domenech V. "The role of detailed chemical kinetics on CFD diesel spray ignition and combustion modelling". *Mathematical and Computer Modelling*, Vol. 54, pp. 1706–1719, 2011.

[168] Samuelsen S., McDonell V., Greene M. and Beerer D. "Correlation of ignition delay with natural gas and IGCC type fuels". *University of California*, Vol. DOE Award Number: DE-FC26-02NT41431 UTSR Project Number: 03-01-SR112, 2006.

[169] Dec John E. and Sjöberg Magnus. "Isolating the effects of fuel chemistry on combustion phasing in an HCCI engine and the potential of fuel stratification for ignition control". *SAE Technical Papers 2004-01-0557*, 2004.

[170] Gauthier B.M., Davidson D.F. and Hanson R.K. "Shock tube determination of ignition delay times in full-blend and surrogate fuel mixtures". *Combustion and Flame*, Vol. 139, pp. 300–311, 2004.

[171] Payri Raul, Viera Juan Pablo, Pei Yuanjiang and Som Sibendu. "Experimental and numerical study of lift-off length and ignition delay of a two-component diesel surrogate". *Fuel*, Vol. 158, pp. 957–967, 2015.

[172] Kee Robert J., Rupley Fran M., Meeks Ellen and Miller James A. "CHEMKIN-III: A FORTRAN chemical kinetics package for the analysis of gas phase chemical and plasma kinetics". *Sandia National Laboratories Report*, Vol. UC-405 SAND96-8216, 1996.

[173] Kee Robert J., Dixon-Lewis Graham, Warnatz Jurgen, Coltrin Michael E., Miller James A. and Moffat Harry K. "A FORTRAN computer code package for the evaluation of gas-phase, multicomponent transport properties". *Sandia National Laboratories Report*, Vol. SAND86-8246B, 1998.

[174] Pepiot Perrine and Pitsch Heinz. "Systematic reduction of large chemical mechanisms". *4th Joint Meeting of the U.S. Sections of the Combustion Institute*, 2005.

[175] Vajda S., Valko P. and Turányi T. "Principal component analysis of kinetic models". *International Journal of Chemical Kinetics*, Vol. 17, pp. 55–81, 1985.

[176] Turányi T. "Sensitivity analysis of complex kinetic systems. Tools and applications". *Journal of Mathematical Chemistry*, Vol. 5, pp. 203–248, 1990.

[177] Turányi T. "Reduction of large reaction mechanisms". *New Journal of Chemistry*, Vol. 14, pp. 795–803, 1990.

[178] Wang H. and Frenklach M. "Detailed reduction of reaction mechanisms for flame modeling". *Combustion and Flame*, Vol. 87, pp. 365–370, 1991.

[179] Lu T. and Law C.K. "Linear time reduction of large kinetic mechanisms with directed relation graph: n-neptane and iso-octane". *Combustion and Flame*, Vol. 144, pp. 24–36, 2006.

[180] W. Sun and Z. Chen, Gou X. and Ju Y. "A path flux analysis method for the reduction of detailed chemical kinetic mechanisms". *Combustion and Flame*, Vol. 157, pp. 1298–1307, 2010.

[181] Sarathy S.M., Westbrook C.K., Mehl M., Pitz W.J., Togbe C., Dagaut P., Wang H., Oehlschlaeger M.A., Niemann U., Seshadri K., Veloo P.S., Ji C., Egolfopoulos F.N. and Lu T. "Comprehensive chemical kinetic modeling of the oxidation of 2-methylalkanes from C7 to C20". *Combustion and Flame*, Vol. 158, pp. 2338–2357, 2011.

[182] Several Authors. "CHEMKIN-PRO description". *http://reactiondesign.com/products/chemkin/chemkin-pro*, 2016.

[183] Syed I., Mukherjee A. and Naber J. "Numerical Simulation of Autoignition of Gasoline-Ethanol/Air Mixtures under Different Conditions of Pressure, Temperature, Dilution, and Equivalence Ratio". *SAE Technical Paper 2011-01-0341*, 2011.

[184] Reitz Rolf D. "CFD combustion models for IC engines". *Engine Research Center Symposium*, 2007.

[185] Several Authors. "CANTERA description". *http://cantera.org*, 2016.

# Chapter 3

# Experiments and methods

## Contents

The experimental facilities and tools used in this Thesis, as well as their setups and arrangements, are described in this chapter. Moreover, the methodological approach followed during the development of this investigation is also presented, including the experimental methods and the models involved in the simulation work. The parametric study performed is also shown for all the tested fuels. This investigation has been performed in the Instituto Univeritario de Investigación CMT - Motores Térmicos from the Universitat Politècnica de València, and it is the first work carried out in the RCEM available at this institution. Thus, a full description of this facility is critical to justify the validity of the results. Therefore, the developed post-processing tools and models are reported, highlighting the advantages and disadvantages of the methods and the challenges overcome.

It should be noted that this Thesis has been partially performed in the Aerothermochemistry and Combustion Systems Laboratory (LAV) from the Swiss Federal Institute of Technology in Zurich (ETH - Zurich). Thus, despite the fact that the RCEM is the main experimental facility involved in this work, two different RCEMs have been used. However, the methodological approach, models and post-processing routines are the same independently of where the experiments have been carried out. Therefore, all the explanations that can be read in this chapter will be referred to both experimental facilities.

First, the two RCEMs used in this work, one available at CMT - Motores Térmicos and the other one available at ETH - Zurich, are described in detail. Then, the optical techniques implemented in the RCEM are explained from a point of view of setup, hardware and tools. Afterwards, the aforementioned parametric study performed is presented. Next, the methodological approach followed to perform an experiment is described, starting from the preparation of the facility and ending with the post-processing of both pressure-based and optical experiments. Moreover, the methods involved in the simulation work are also described. The different models and mechanisms used are presented and the replication of the RCEM by simulation, as well as the post-procesing of simulated results, are explained. Finally, the validation of the experimental facility available at CMT - Motores Térmicos is shown in the appendix, including the repeatability analysis, a comparison to the RCEM available at ETH - Zurich and the congruence in the experimental trends of the measured ignition delays. Besides, the post-processing tools and models

developed as part of this Thesis are also presented in an appendix, emphasizing the hypotheses that have been taken into account.

## 3.1 Experimental facilities

### 3.1.1 RCEM

An RCEM is an experimental facility widely used in autoignition studies due to its capability to reproduce engine conditions [1]. It allows a detailed analysis of a single engine cycle of an internal combustion engine, including not only the compression stroke, but also part of the expansion stroke [2]. Thus, RCEMs have the capability of replicating reasonably well the combustion process of reciprocating engines with fully controlled initial and boundary conditions, and avoiding the complexities associated to engines [3].

#### 3.1.1.1 The RCEM available at CMT - Motores Térmicos

The RCEM available at CMT - Motores Térmicos is a quasi-standard experimental facility purchased by this laboratory, the results of which can be compared directly to those from other RCEMs produced by the same company. The RCEM has some important features to perform several diagnostic studies under a wide range of experimental conditions: different compression ratios can be reached by varying the stroke and the clearance volume, axial and lateral optical accesses are available [4, 5] and the compression velocity can be varied in order to simulate different engine speeds. In an RCEM the expansion stroke of the piston can be also analyzed and most of the engine parameters can be calculated under real conditions, such as the heat release rate or the combustion efficiency. In this facility both homogeneous and heterogeneous (direct injection) mixtures can be tested, as well as new combustion modes such as the dual fuel technology [6, 7] or LTC [8]. Of course, the RCEM allows the study of autoignition of fuel-air mixtures under easily controlled and reproducible conditions in a cleaner environment than in a traditional engine, without residual gases and with full control over the initial pressure and temperature, the volume and the trapped mass.

A schematic of the RCEM is shown in Fig. 3.1. The RCEM is pneumatically driven and its pistons are hydraulically coupled. As it can be seen, it can be divided in two different zones: the experimentation zone and the driving zone. The experimentation zone is composed by the combustion chamber. The driving zone is composed by four different pistons. Piston

1, which is called pushing piston, is pneumatically driven and hydraulically coupled to piston 2, which is called driver piston and is directly connected to the combustion chamber. Piston 3 is hydraulically driven and can be adjusted to select the compression stroke. Finally, piston 4 contains the compressed air that drives the machine.

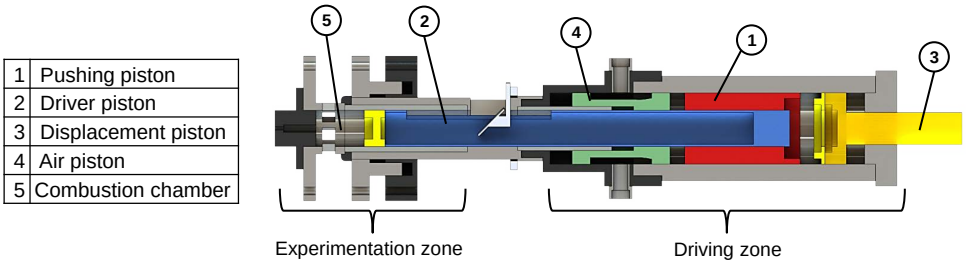


***Figure 3.1.*** *Rapid Compression Expansion Machine schematic.*

First, the oil is pressurized by the driving gas, which is composed by compressed air. The driver piston does not move because it is perfectly coupled to piston 3, avoiding contact between the pushing oil and the piston base. Then, pressure is established behind the driver piston by a bypass valve and it starts to advance at low velocity in a slow compression process. It should be noted that when the driver piston advances, the pushing piston must advance also in the opposite direction, keeping constant the volume of oil. In fact, both pistons are inertially balanced, leading to a process free of vibrations.

When the driver piston leaves piston 3, it is suddenly accelerated and the rapid compression stroke starts. The driving air suffers an expansion process whereby its pressure and, consequently, the pushing oil pressure, are reduced. The piston stops when the pressure in the combustion chamber is high enough to compensate the pushing force and the inertia, defining TDC. Thereby, TDC is highly dependent on the operation conditions of the RCEM, which is completely different for engines. Moreover, there is a certain maximum driving pressure for each operating condition to avoid collision of the piston with the cylinder head, since in the RCEM there is not any mechanism as the rod-crank mechanism that fixes the maximum position of the piston. Once the piston reaches TDC, the pressure in the combustion chamber is higher than the pushing oil pressure and the expansion stroke starts. More details on the operation principle of the RCEM can be found in [9].

| | | |
|---|---|---|
| Bore | 84 | mm |
| Stroke | 120 - 249 | mm |
| Compression ratio | 5 - 30 | - |
| Maximum cylinder pressure | 200 | bar |
| Initial pressure | 1 - 5 | bar |
| Maximum heating temperature | 473 | K |

***Table 3.1.*** *Technical characteristics of the RCEM.*

The main technical characteristics of the RCEM can be seen in Table 3.1. The pushing piston and the driver piston are instrumented with two AMO LMK102 incremental position sensors (0.01 $mm$ of resolution), which allow knowing the absolute position of each piston and, therefore, the combustion chamber volume. The combustion chamber is composed by three elements: the experimentation piston (mechanically connected to the driver piston), the liner and the cylinder head. The experimentation piston consists on a steel-made piston with 84 $mm$ of bore and a quartz-made bowl with cylindrical shape, 46 $mm$ of bore and 17 $mm$ of depth, which allow the axial optical access. As the bowl is flat, the chamber can be recorded without any image distortion. Moreover, an alternative liner with three quartz-made windows with rectangular shape to allow lateral optical access is available.

The experimentation piston is provided with an electrical 80 $W$ heater that allows varying the temperature of the bowl, and the liner has two more spire-shape electrical heaters of 600 $W$ each, which are responsible for heating the cylinder walls. The wall temperature is measured by three thermocouples located in the liner, in the piston and in the bowl. The intake and exhaust pipes are located in the liner of the combustion chamber. These ducts are designed to induce swirl motion to the gases admitted by the machine. The turbulence generated during the filling is enough to guarantee a homogeneous temperature in the chamber equal to the wall temperature, as demonstrated by some CFD calculations that can be seen in Appendix 7.1 (Chapter 7). The cylinder head is instrumented with a Kistler 6045A uncooled piezoelectric pressure sensor with a sensitivity of -45 $pC/bar$, which is coupled to a Kistler 5018 charge amplifier, and whereby the in-cylinder pressure is measured. Three Wika piezoresistive pressure sensors are available to control the filling of the driving gas and of the combustion chamber with a resolution of 0.01 $bar$.

The injection system is a common rail system, including a BOSCH solenoid-commanded injector with a 7-hole nozzle, which is centered in the cylinder head, and controlled by a EFS IPod power driving module. This injection system has been characterized as explained in [10].

The acquisition system is a Yokogawa DL850V composed by one 10 $MHz$-12 bits module and five more 1 $MHz$-16 bits modules with two channels each. The acquisition frequency is fixed to 10 $MHz$, which is necessary to capture the pulses of the incremental position sensor. However, the in-cylinder pressure and the injection pressure are recorded at 1 $MHz$.

The RCEM is filled from an external tank that can be heated up to 520 $K$ thanks to three electrical heaters of 1200 $W$ each. The synthetic air is produced in the tank by a filling based on partial pressures where $N_2$, $CO_2$ and $O_2$ can be used. Besides, a syringe pump is available to allow the use of $H_2O$. A vacuum pump is used to ensure no contamination of the mixture composition in this tank, nor in the RCEM charge. Finally, the synthetic air is analyzed by gas chromathography in a Rapid Refinery Gas Analyser from Bruker (450-GC) in order to know the exact composition and ensure the correct reproduction of the experiments in CHEMKIN.

#### 3.1.1.2 The RCEM available at ETH - Zurich

The RCEM available at ETH - Zurich is a quasi-standard experimental facility very similar to the one available at CMT - Motores Térmicos, so that the results of both can be directly compared. In fact, the working principle of both machines is exactly the same. Therefore, only the differences between machines are described in the following paragraphs, being the explanation that is shown in the previous section consistent with the RCEM from ETH - Zurich.

The technical characteristics of the RCEM can be seen in Table 3.1, which are the same than the technical characteristics of the RCEM available at CMT - Motores Térmicos. The pushing piston and the driver piston are instrumented with two incremental position sensors (AMO LMK102) with a resolution of 0.01 $mm$, which allow knowing the absolute position of each piston and, therefore, the combustion chamber volume. The experimentation piston consists on a steel-made piston with 84 $mm$ of bore and a quartz-made bowl with cylindrical shape, 50 $mm$ of bore and 2.2 $mm$ of depth, which allows the axial optical access. As the bowl is flat, the chamber images can be recorded without any image distortion. It should be noted that the bowl dimensions are not exactly the same in both machines. Thus, the dead volume

is not the same and the reached compression ratio for a certain configuration (driver gas and test mixture initial pressure) will be different.

The cylinder head and the cylinder liner have different heating elements arranged in six separately controlled zones, which are responsible for heating the cylinder walls and the experimentation piston. The wall temperature is measured by a total of six type K thermocouples, two located in the cylinder head and four in the liner. Very good temperature homogeneity has been observed [11], with a standard deviation of the gas temperature in the order of 3 $K$. It was found that the temperature distribution is barely affected by the gas in-flow due to its slow speed. An initial gas temperature equal to the wall temperature is achieved due to the long duration of the intake process.

The cylinder head is instrumented with a Kistler 7061B cooled piezoelectric pressure sensor (-80 $pC/bar$ of sensitivity), which is coupled to a Kistler 5011 charge amplifier, and whereby the in-cylinder pressure is measured. Different piezo-resistive pressure sensors are available to control the filling of the driving gas and of the combustion chamber (0.01 $bar$ of resolution). The injection system is composed by a Siemens hollow cone piezo-injector with a cone angle of 90°, which is centered in the cylinder head. Its fuel delivery rate has been previously measured with an IAV injection rate analyzer. The transient signals have been recorder at 100 $kHz$ with a PC-based transient measurement recorder. The RCEM is filled from an external tank that can be heated up to 373 $K$. The synthetic air is produced in the tank by a filling based on partial pressures where $N_2$, $CO_2$ and $O_2$ can be used. The mixture is analyzed in a Horiba PG-250 portable gas analyzer in order to know the exact composition and ensure the correct reproduction of the experiments in CHEMKIN.

### 3.1.2 Optical setups

The optical techniques presented in this Thesis have been applied in the RCEM available at ETH - Zurich.

#### 3.1.2.1 Chemiluminescence

The evolution of the autoignition process and the luminous intensity were recorded by OH* chemiluminescence imaging. This technique records radiation at 310 $nm$, which is controlled by the OH* radical, a marker of the high temperature combustion [12].

A schematic of the optical arrangement is shown in Fig. 3.2. The camera has been pointed directly at the mirror inside the machine, which due to its

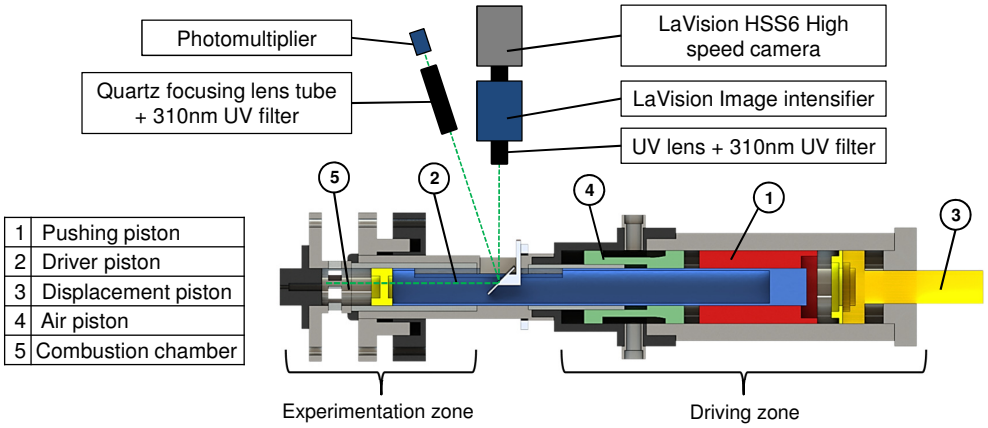


***Figure 3.2.*** *Schematic of the optical arrangement for OH* chemiluminescence.*

45° tilt gives a direct view of the combustion chamber through the piston window. A 12-bit LaVision HighSpeedStar 6 camera coupled to a LaVision HighSpeed IRO intensifier equipped with a 100 $mm$ focal length $f = 2$ UV objective (by Bernhard Halle Nachfolger GmbH) were used for image acquisition. Additionally, a 310 $nm$ interference filter (FWHM = 10 $nm$) was used to eliminate any additional radiation outside the OH* radical wavelength. Because of the transient nature of the combustion, an acquisition frequency of 30 $kHz$ has been chosen in order to capture the evolution of the radical inside the combustion chamber. An exposure time of 33 $\mu$s and a rectangular image of 384x448 pixels allowed to see the whole effective window diameter of 50 $mm$ while obtaining a pixel/mm ratio of 6.89. The maximum exposure time has been selected in order to use lower gain values and therefore reducing image noise.

Additionally, a Hamamatsu H5784-03 photo-multiplier (PHM), spectrally filtered at 310 $nm$, captured the spatially integrated light emission through the piston window. It was placed at an angle due to the lack of space (Fig. 3.2). The information from the photo-multiplier is complementary to the one obtained by the camera, as its higher dynamic range allows to see peaks in OH* luminosity when the camera might be saturating. However, while the camera shows the distribution of the radical in a 2-dimensional image, the photo-multiplier only returns an integrated value for the whole area. The transient signal from the photo-multiplier along with the control and

synchronization signals (i.e. camera triggers) have been recorded at 100 $kHz$ with a PC-based transient measurement recorder.

#### 3.1.2.2 Spectroscopy

A schematic of the optical arrangement is shown in Fig. 3.3. Passive spectroscopy measurements were performed with an Acton SpectraPro150 spectroscope (grating: 150 $g/mm$, blaze wavelength: 500 $nm$) coupled with a 12-bit LaVision HighSpeedStar 6 camera and a LaVision HighSpeed IRO intensifier. The spectroscope has been pointed directly at the mirror inside the machine, which due to its 45° tilt gives a direct view of the combustion chamber through the piston window. Because of the transient nature of the combustion, an acquisition frequency of 67.5 $kHz$ has been chosen in order to capture the evolution of the spectra inside the combustion chamber. An exposure time of 14.5 $\mu$s and a rectangular image of 1024x80 pixels were selected. The whole system was calibrated by the use of an Acton MS-416 mercury lamp. The transient control and synchronization signals (i.e. camera triggers) have been recorded at 100 $kHz$ with a PC-based transient measurement recorder.

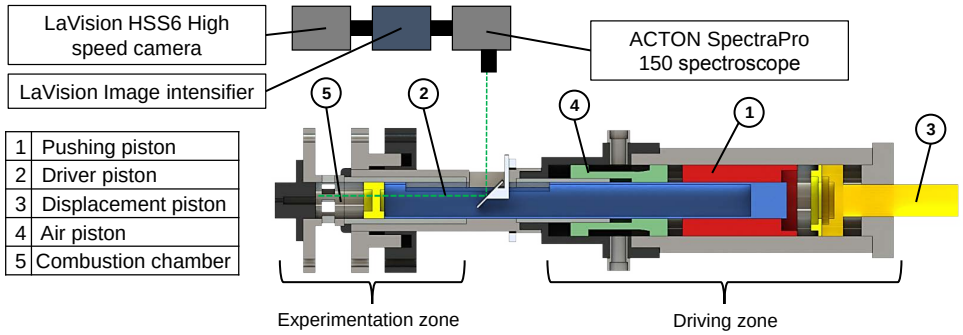


***Figure 3.3.*** *Schematic of the optical arrangement for spectroscopy.*

## 3.2 Parametric study performed

The parametric study performed has been decoupled in three different blocks. First, the study performed with pure n-heptane and iso-octane, which

has been carried out at ETH - Zurich, is described. Moreover, an additional parametric study has been also performed with these two fuels in the software of chemical simulation CHEMKIN in order to describe the effects of the different species that compose the synthetic EGR on the ignition delay and, based on these results, to design a criteria to define the proper composition of the mixture to replicate engine conditions. Then, the experimental study performed with PRF mixtures (n-heptane/iso-octane blends) is separately shown, since these fuels have been tested at CMT - Motores Térmcios. Finally, the parametric study performed with n-dodecane is also independently explained, since the boiling temperature of such fuel requires a different range of initial temperatures than for PRF mixtures.

### 3.2.1 N-heptane and iso-octane

These fuels have been tested in the RCEM available at ETH - Zurich. Besides, the experimental measurements of n-heptane have been used for the validation of the RCEM available at CMT - Motores Térmicos, as it can be seen in Appendix 3.A. The performed experimental study was as follows:

- Fuel: n-heptane and iso-octane.
- Initial temperature ($T_0$): 358 $K$ (only for n-heptane), 383 $K$, 408 $K$, 433 $K$ and 458 $K$.
- Initial pressure ($P_0$): 1.4 $bar$ and 1.7 $bar$.
- Compression stroke: 249 $mm$.
- Compression ratio ($CR$): 15 and 17 to 1.
- Oxygen molar fraction ($X_{O_2}$): 0.21, 0.147, 0.126 and 0.105.
- Equivalence ratio ($F_r$): 0.3 to 0.8 depending on the fuel and on the oxygen mass fraction.

The expected pressure and temperature at TDC under motoring conditions (without fuel) for these initial operating points are summarized in Table 3.2. It should be noted that in an experiment with fuel, the heat capacity of the mixture will be higher and, therefore, the temperature and pressure reached at TDC will be lower. Moreover, the thermodynamic conditions at TDC does not have to be representative conditions of the ignition, since the mixture can ignite during the compression stroke (before TDC).

| **CR 15:1** | | **CR 17:1** | |
|---|---|---|---|
| $T_0$ $[K]$ | $T_{TDC}$ $[K]$ | $T_0$ $[K]$ | $T_{TDC}$ $[K]$ |
| 358 | 874 | 358 | 911 |
| 383 | 936 | 383 | 975 |
| 408 | 997 | 408 | 1039 |
| 433 | 1058 | 433 | 1102 |
| 458 | 1119 | 458 | 1166 |
| $P_0$ $[bar]$ | $P_{TDC}$ $[bar]$ | $P_0$ $[bar]$ | $P_{TDC}$ $[bar]$ |
| 1.4 | 51.3 | 1.4 | 60.6 |
| 1.7 | 62.3 | 1.7 | 73.6 |

***Table 3.2.*** *Pressure and temperature conditions at TDC under motoring conditions for the initial operating points.*

| | | $\mathbf{X}_{O_2}$ [-] | | | |
|---|---|---|---|---|---|
| | | **0.21** | **0.147** | **0.126** | **0.105** |
| $\mathbf{T}_0$ $[K]$ | **358** | *0.4* | *0.4* | *0.3, 0.4, 0.5, 0.6* | *0.4* |
| | **383** | | | 0.4, 0.5 | 0.4 |
| | **408** | 0.3, 0.4 | 0.3, 0.4 | 0.3, 0.4, 0.5, 0.6, **0.7**, **0.8** | 0.3, 0.4, 0.5, 0.6, **0.7**, **0.8** |
| | **433** | | | 0.4, 0.5 | 0.4 |
| | **458** | **0.4** | **0.4** | **0.3**, 0.4, 0.5, **0.6** | 0.4 |

***Table 3.3.*** *Parametric study performed for pure n-heptane and iso-octane. Equivalence ratio for different initial temperature and oxygen molar fractions. Italic.- exclusively for n-heptane.* ***Bold****.- exclusively for iso-octane.*

The maximum equivalence ratio is limited by the working oxygen mass fraction in order to avoid extremely violent combustions. The equivalence ratio of 0.4 has been chosen as the base point in order to have the possibility to try leaner and richer mixtures without damaging the facility. The performed parametric study can be seen in Table 3.3. Finally, the temperature of the combustion chamber is always above the boiling point of the fuel, therefore ensuring that the fuel is in vapor phase before the beginning of the cycle.

The performed parametric study to analyze the effects of the EGR species on the ignition, which is a work of simulation and modeling in CHEMKIN, was as follows:

- Fuel: n-heptane and iso-octane.
- Initial temperature ($T_0$): from 600 $K$ to 1100 $K$, at steps of 50 $K$.
- Initial pressure ($P_0$): from 50 $bar$ to 150 $bar$, at steps of 25 $bar$.
- Oxygen molar fraction ($X_{O_2}$): from 0.21 (ambient air, without EGR) to 0.07, at steps of 0.02.
- Equivalence ratio ($F_r$): from 0.25 to 2.5, at steps of 0.25.

Most of the operating range of internal combustion engines is covered with this parametric study. Although equivalence ratios of 2.5 can seem uninteresting for practical applications, it must be taken into account that autoignition occurs under rich local equivalence ratios in direct-injection diesel engines [13]. This concept is known as *most reactive mixture fraction* and it arises due to the balance of reactivities between the fuel-air ratio distribution and the temperature distribution. Depending on the working conditions, local equivalence ratios on the order of 2 can be the most reactive ones. Furthermore, high pressure, such as 150 $bar$, have been studied in order to explore very smooth NTC regimes, which helps to understand how the NTC behavior affects to the effects of the different species on the ignition delay.

In this study, EGR was considered as the products of a complete combustion reaction between the fuel and dry air in which the amount of oxygen is chosen by the user. Thus, the EGR is composed by $N_2$, $O_2$, $CO_2$ and $H_2O$ as explained in Chapter 4.

### 3.2.2 PRF25, PRF50 and PRF75

These fuels have been tested in the RCEM available at CMT - Motores Térmicos. The performed experimental study was as follows:

- Fuel: PRF25, PRF50 and PRF75.
- Initial temperature ($T_0$): 363 $K$, 383 $K$, 403 $K$ and 423 $K$.
- Initial pressure ($P_0$): 1.5 $bar$.
- Compression stroke: 180 $mm$.
- Compression ratio ($CR$): 14 and 19 to 1.
- Oxygen molar fraction ($X_{O_2}$): 0.21, 0.18 and 0.16.

- Equivalence ratio ($F_r$): from 0.4 to 0.8 depending on the fuel and on the oxygen molar fraction.

The expected pressure and temperature at TDC under motoring conditions (without fuel) for these initial operating points are summarized in Table 3.4. It should be noted that in an experiment with fuel, the heat capacity of the mixture will be higher and, therefore, the temperature and pressure reached at TDC will be lower. Moreover, the thermodynamic conditions at TDC does not have to be representative conditions of the ignition, since the mixture can ignite during the compression stroke (before TDC).

| **CR 14:1** | | **CR 19:1** | |
|---|---|---|---|
| $T_0$ $[K]$ | $T_{TDC}$ $[K]$ | $T_0$ $[K]$ | $T_{TDC}$ $[K]$ |
| 363 | 860 | 363 | 872 |
| 383 | 892 | 383 | 929 |
| 403 | 941 | 403 | 967 |
| 423 | 969 | 423 | 1019 |
| $P_0$ $[bar]$ | $P_{TDC}$ $[bar]$ | $P_0$ $[bar]$ | $P_{TDC}$ $[bar]$ |
| 1.5 | 50.6 | 1.5 | 60.3 |

***Table 3.4.*** *Pressure and temperature conditions at TDC under motoring conditions for the initial operating points.*

The maximum equivalence ratio is limited by the working oxygen molar fraction in order to avoid extremely violent combustions. The performed parametric study can be seen in Table 3.5. Finally, the temperature of the combustion chamber is always above the boiling point of the fuel, therefore ensuring that the fuel is in vapor phase before the beginning of the cycle.

### 3.2.3 N-dodecane

These fuels have been tested in the RCEM available at CMT - Motores Térmicos. The performed experimental study was as follows:

- Fuel: n-dodecane.
- Initial temperature ($T_0$): 403 $K$, 423 $K$, 443 $K$ and 463 $K$.

| | | $\mathbf{X}_{O_2}$ [-] | | |
|---|---|---|---|---|
| | | **0.21** | **0.18** | **0.16** |
| $\mathbf{T}_0$ $[K]$ | **363** | 0.4, 0.5, 0.6 | *0.4*, 0.5, 0.6, **0.7** | |
| | **383** | 0.4, 0.5, 0.6 | *0.4*, 0.5, 0.6, **0.7** | 0.5, 0.6, 0.7, <u>0.8</u> |
| | **403** | 0.4, 0.5, 0.6 | *0.4*, 0.5, 0.6, **0.7** | |
| | **423** | 0.4, 0.5, 0.6 | *0.4*, 0.5, 0.6, **0.7** | 0.5, 0.6, 0.7, <u>0.8</u> |

***Table 3.5.*** *Parametric study performed. Equivalence ratio for different initial temperature and oxygen molar fractions. Italic.- exclusively for CR 19.* ***Bold.-*** *exclusively for CR 14.* <u>*Underlined*</u>*.- exclusively for PRF75.*

- Initial pressure ($P_0$): 1.5 $bar$.
- Compression stroke: 180 $mm$.
- Compression ratio ($CR$): 14 and 19 to 1.
- Oxygen molar fraction ($X_{O_2}$): 0.21, 0.18 and 0.16.
- Equivalence ratio ($F_r$): from 0.4 to 0.7 depending on the oxygen molar fraction.

The expected pressure and temperature at TDC under motoring conditions (without fuel) for these initial operating points are summarized in Table 3.6. It should be noted that in an experiment with fuel, the heat capacity of the mixture will be higher and, therefore, the temperature and pressure reached at TDC will be lower. Moreover, the thermodynamic conditions at TDC does not have to be representative conditions of the ignition, since the mixture can ignite during the compression stroke (before TDC).

The maximum equivalence ratio is limited by the working oxygen molar fraction in order to avoid extremely violent combustions. The performed parametric study can be seen in Table 3.7. Finally, it should be noticed that the temperature of the combustion chamber is lower than the boiling point of the fuel (489 $K$ at 1 $bar$). However, as explained in Appendix 7.2 (Chapter 7), the filling time is long enough to ensure that the fuel is in vapor phase before the beginning of the cycle.

| **CR 14:1** | | **CR 19:1** | |
|---|---|---|---|
| $T_0$ $[K]$ | $T_{TDC}$ $[K]$ | $T_0$ $[K]$ | $T_{TDC}$ $[K]$ |
| 403 | 941 | 403 | 967 |
| 423 | 969 | 423 | 1019 |
| 443 | 1021 | 443 | 1106 |
| 463 | 1068 | 463 | 1146 |
| $P_0$ $[bar]$ | $P_{TDC}$ $[bar]$ | $P_0$ $[bar]$ | $P_{TDC}$ $[bar]$ |
| 1.5 | 50.6 | 1.5 | 60.3 |

***Table 3.6.*** *Pressure and temperature conditions at TDC under motoring conditions for the initial operating points.*

| | | $\mathbf{X}_{O_2}$ [-] | | |
|---|---|---|---|---|
| | | **0.21** | **0.18** | **0.16** |
| $\mathbf{T}_0$ $[K]$ | **363** | 0.4, 0.5, 0.6 | 0.4, 0.5, 0.6 | |
| | **383** | 0.4, 0.5, 0.6 | 0.4, 0.5, 0.6 | 0.5, 0.6, 0.7 |
| | **403** | 0.4, 0.5, 0.6 | 0.4, 0.5, 0.6 | |
| | **423** | 0.4, 0.5, 0.6 | 0.4, 0.5, 0.6 | 0.5, 0.6, 0.7 |

***Table 3.7.*** *Parametric study performed. Equivalence ratio for different initial temperature and oxygen molar fractions.*

## 3.3 Methodological approach

The methodological approach followed in this Thesis is presented in this section. The methodology followed for the preparation, performance and post-processing of an experiment is described, including the cases in which an optical technique is applied. Besides, the simulation software, including the models, the chemical kinetic mechanisms used and the criteria taken to define the different ignition delays are presented.

### 3.3.1 RCEM

The desired stroke of the machine is selected and the RCEM is heated up to the desired temperature. Two hours are needed in order to ensure a homogeneous wall temperature.

In this study, EGR was considered as the products of a complete combustion reaction between the fuel and dry air in which the amount of oxygen is the one chosen by the user. The influence of minor components of the EGR on the ignition delay has been checked in previous studies [14–17]. These minor components (UHC, CO, formaldehyde and NO) have been obviated in this study due to the great difficulty implied by adding them to a synthetic EGR mixture. Although NO, for instance, has a significant effect on the ignition delay, trying to use it in a synthetic EGR mixture involves complex issues. On the one hand, the difficulty lies in the impossibility to know the amount to be added for each particular case, as the proportion of this component cannot be easily determined. On the other hand, if that amount is known, this species is found at a rate of a few parts per million, so that obtaining a synthetic mixture with such a precise amount would be extremely complex. The species that are taken into account for the EGR composition follow the criterion explained in Chapter 4, Section 4.1, in order to ensure that the results are representative of a real engine.

In order to ensure a clean environment into the cylinder, vacuum is created in the combustion chamber before the filling in the RCEM available at CMT - Motores Térmicos. Due to the absence of vacuum pump at ETH - Zurich, the combustion chamber is scavenged several times before the filling in such RCEM. This way, the residual gases are enough diluted to avoid any effect on the ignition characteristics.

The fuel is injected into the combustion chamber at the start of the intake process to avoid problems of stratification or other inhomogeneities. The turbulence generated during the filling, as well as the long duration of the process (aproximately 40 $s$), are enough to guarantee a homogeneous environment in the chamber when the compression stroke starts, as demonstrated by CFD calculations in Appendix 7.1 (Chapter 7).

In order to ensure a representative ignition delay time measurement, the number of repetitions of each point has been selected so that the semi-amplitude of the confidence interval within a level of confidence of 95% is smaller than 1% of the mean ignition delay value. I.e., the number $N$ of repetitions of each point have to satisfy:

$$\mu = \frac{\sigma t_{1-\alpha/2,N-1}}{\sqrt{N}} \leqslant \frac{\bar{t_i}}{100} \tag{3.1}$$

where $\bar{t_i}$ represents the mean value of the measured ignition delays, $\sigma$ is the standard deviation and $t_{1-\alpha/2,N-1}$ is the Student's t-distribution, in which $\alpha = 0.05$ for a level of confidence of 95% and $N-1$ represents the degrees of freedom. Furthermore, the minimum number of repetitions has been fixed in $N = 5$ to ensure a representative standard deviation.

In this work the autoignition of the mixture is considered to be produced when the time derivative of the pressure signal (which will be referred as pressure rise rate further on) reaches a maximum. Thus, the ignition delay in the experimental facility is defined as the time between the start of the rapid compression process (piston position equal to 29 $mm$), which is a constant reference due to constructive aspects of the machine, and the instant in which the maximum pressure rise is obtained, as can be seen in Fig. 3.4. This way, cool flames and high temperature ignition delay can be easily distinguished in case of having a two-stage ignition pattern.

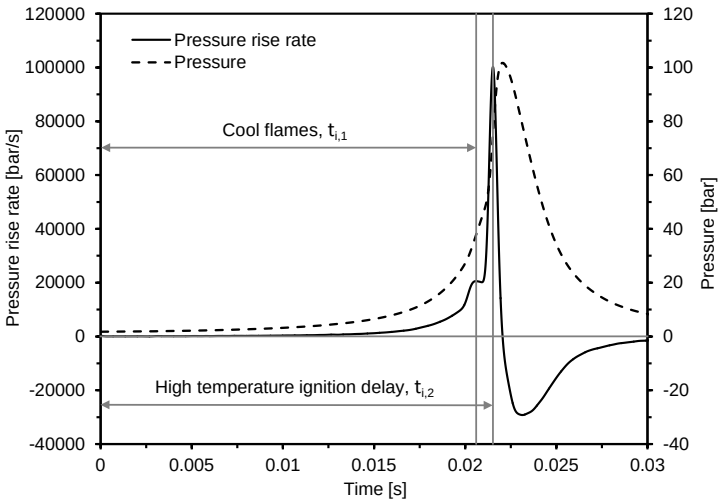


***Figure 3.4.*** *Ignition delay definition. The autoignition of the mixture is considered to be produced when the maximum pressure rise occurs.*

Moreover, the selected acquisition frequency (100 $kHz$ at ETH - Zurich and 1 $MHz$ at CMT - Motores Térmicos) is large enough to yield negligible error on measured ignition delay times. In fact, uncertainties on the ignition

delay equal to 10 $\mu s$ and to 1 $\mu s$ are caused by the acquisition frequency for the RCEM available at ETH - Zurich and for the RCEM available at CMT - Motores Térmicos, respectively. Taking into account the lowest acquisition frequency, as well as a characteristic value of the ignition delay ($2/3 \cdot t_{compression} \approx 0.020\ s$), the uncertainty caused by the acquisition frequency is the following:

$$uncertainty = \frac{\Delta t}{t_i} 100 \simeq \frac{10^{-5}}{0.020} 100 = 0.05\% \tag{3.2}$$

which is a negligible value.

Finally, the temperature profile is calculated for each experiment by applying the equation of state, since the pressure profile and the piston position are known. The heat losses are characterized by a model based on the Woschni correlation [18], the parameters of which are fitted for each experimental condition. Besides, the diagnosis of the combustion is performed by calculating the heat release rate and the combustion efficiency by applying the energy equation. These calculations include two additional models for deformations and leakages [19, 20], the parameters of which are also fitted for each experimental condition. A detailed description about the post-processing of the experimental data, including a description of the models involved in the combustion diagnosis, as well as the parameters fitting, can be read in Appendix 7.3 (Chapter 7).

### 3.3.2 Optical techniques

#### 3.3.2.1 Chemiluminescence

The images have been processed by an in-house developed routine in MATLAB. The processing algorithm starts by calculating the maximum pixel intensity of each frame in order to determine the useful dynamic range of the image sequence. Then, a background noise level, $I_{back}$, is calculated by averaging 100 images where there is no presence of OH* luminosity, determining the average and standard deviation values of the noise. Besides, the maximum pixel intensity among all the images is also determined. With this two values, the cut-off intensity is calculated using the probable error in order to select which frames will be processed. I.e., if the dynamic range of the image is higher than four times the probable error of the noise level, the image is selected as *useful*. It should be noted that the probable error is defined as 0.6745 times the standard deviation of the noise, assuming that the

noise follows a normal distribution. An example of the evolution of the pixel intensity, the background level and the selected points are shown in Fig. 3.5.

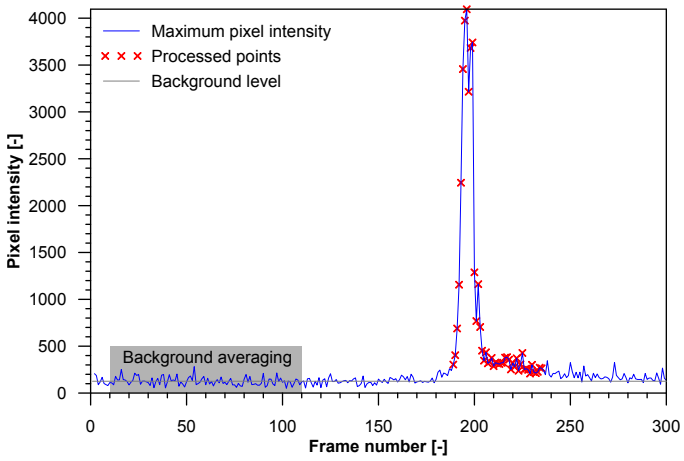


***Figure 3.5.*** *Evolution of the maximum pixel intensity for a frame sequence.*

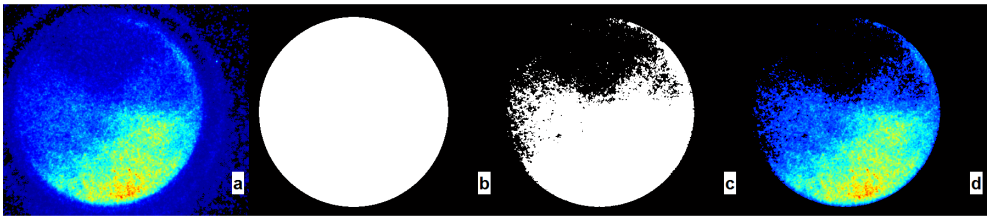


***Figure 3.6.*** *Processing sequence: raw image (a), geometrical mask (b), intensity mask (c) and final image (d).*

Once the images where the OH* radiation is present are selected, the area of the chemiluminescence is determined by using two different masks: one based on the window geometry and another one based on the luminosity. Fig. 3.6-a shows a raw image directly from the camera. As it can be seen, there is a wide range of intensity values inside the chamber as well as reflections outside the window. In order to discriminate the light reflected by the piston and cylinder walls, a geometrical mask with the diameter of the effective window is applied to all the images, leaving only the light that passes directly

through the window to be processed. A sample of that mask is shown in Fig. 3.6-b. Afterwards, a second mask based on the pixel intensity is applied. This mask, which is different for each image, is determined using the values of the maximum pixel intensity for a certain image, $I_{max}$, and the background noise level, $I_{back}$, previously calculated. A threshold is calculated as $I_{back} + p(I_{max} - I_{back})$, where $p$ is a percentage. Therefore, all the values that fall below this threshold are considered to be part of the background, and the values above are accounted as OH* chemiluminescence. A sample of such mask is shown in Fig. 3.6-c. Finally, the true intensity image excludes all the background light and the reflected light, as shown in Fig. 3.6-d. Once the final image is obtained, the accumulated light intensity is calculated, as well as the OH* area as a percentage of the full window. Furthermore, since the images are time-resolved the instant at which the largest area and peak of intensity take place are also determined.

An important factor to keep in mind while applying two-dimensional imaging on a 3-D phenomenon is the following: since the light detected is an integrated value of the whole volume and not a single first plane acquisition, the maximum local intensity per volume may not be accurately detected by the optical techniques applied. The intensity gradients could have had an effect on the threshold of the images to obtain the combustion area, so a high-intensity single point could have been ignored. Nevertheless, since the combustion of homogeneous mixtures is being studied, the existence of high-intensity single points is very unlikely. Furthermore, for the calculation of the total combustion area this single non-detected point should represent a very small deviation.

The integrated radiation from the combustion chamber is recorded (with the same time resolution than the in-cylinder pressure) by a photo-multiplier. Thus, the ignition delay referred to a maximum intensity of radiation can be measured and compared directly to the pressure rise rate.

The velocity of propagation of the autoignition front is also calculated from the images. The position of the reaction front can be determined by the radiation filtered at 310 $nm$, either if OH* or CO-to-$CO_2$ are the radiation source, since both are good tracers of the high temperature combustion [12].

The propagation velocity is obtained by averaging the perimeter increment between two consecutive images. The sequential autoignition is promoted by the temperature distribution in the combustion chamber, since the cooled piezo-electric pressure sensor available in the RCEM from ETH - Zurich leads to a cold spot at the bottom of the cylinder head, resulting in a hot spot at the top, which originates the ignition. Thus, the autoignition propagation

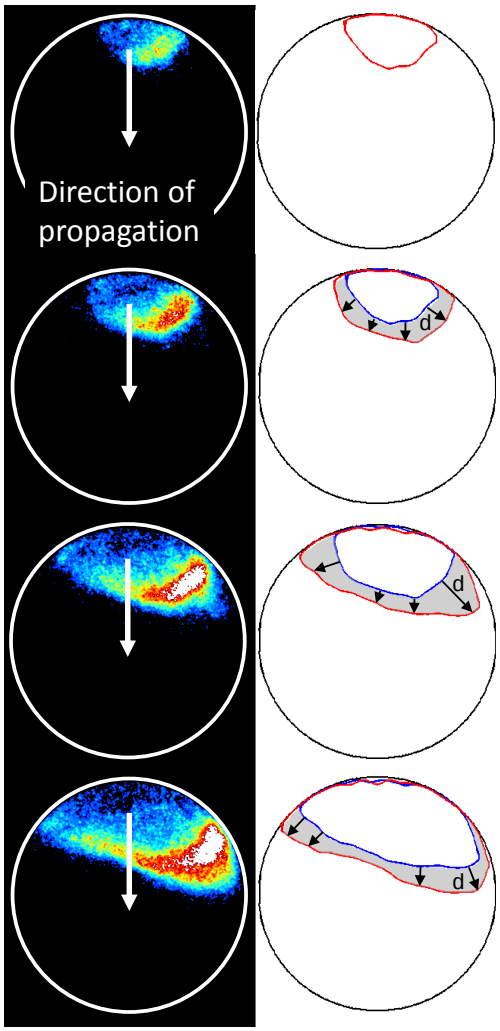


***Figure 3.7.*** *Sequential autoignition caused by the cooled piezo-electric pressure sensor located at the bottom of the cylinder head of the RCEM available at ETH - Zurich.*

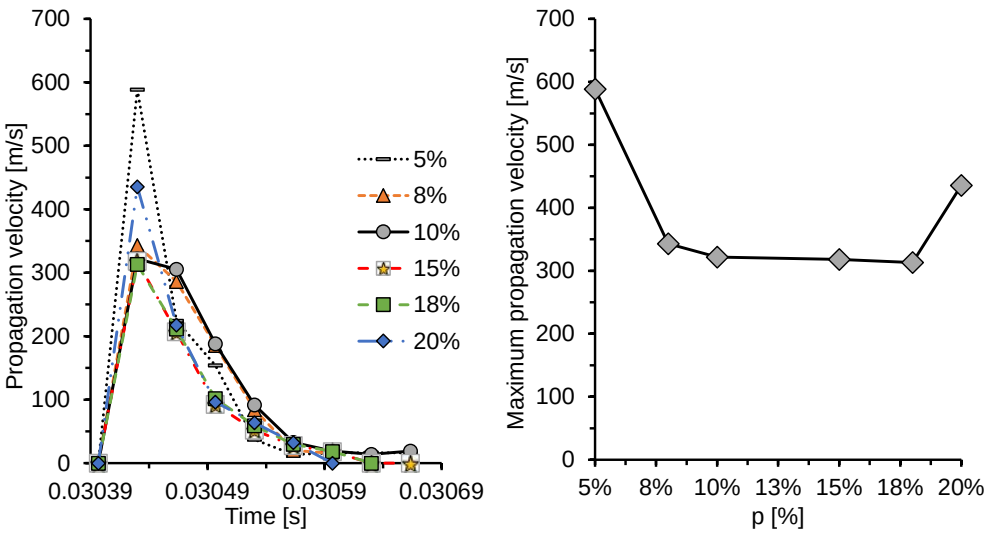


***Figure 3.8.*** *Propagation velocity for $T_0$=408K, $P_0$=1.4bar, CR=15, $X_{O_2}$=0.126, $F_r$=0.5 and six different values of p. Left.- Propagation velocity evolution. Right.- Maximum propagation velocity.*

always occurs from the top to the bottom side of the combustion chamber, as shown in Fig. 3.7 to the left. For a given image, the reaction front, which is obtained avoiding isolated pixels, is filtered in order to easily obtain the normal distance between fronts for two consecutive images, as shown in Fig. 3.7 to the right. Thus, the velocity of propagation is calculated as $u_{prop} = \bar{d}/\Delta t$, where $\bar{d}$ represents the averaged normal distance between two consecutive fronts.

Finally, a sensitivity analysis about how the propagation velocity is affected by the filtering of the images has been performed by varying the percentage, $p$, that defines the filtering threshold. Fig. 3.8 to the left shows the propagation velocity evolution during the sequential autoignition process for $T_0$=408$K$, $P_0$=1.4$bar$, $CR$=15, $X_{O_2}$=0.126 and $F_r$=0.5, for six different values of $p$. It can be seen that the maximum propagation velocity can significantly change depending on the selected value of $p$. In fact, Fig. 3.8 to the right shows the maximum propagation velocity for the six $p$ values. It can be deducted from the figure that $p$ should be properly selected to avoid unsuccessful results. Values of $p$ between 8% and 18% lead to approximately the same values of the propagation velocity. Specifically, $p$ = 10% has been chosen in this study.

#### 3.3.2.2 Spectroscopy

The spectral information has been obtained by processing the images captured with the intensifier-camera group coupled to the spectroscope. An in-house routine developed in MATLAB has been used to calculate the temporal evolution of the spectrum. The fluctuations and noise are smoothed by averaging 80 vertical pixels of each image. In this way, the 2-D image is reduced to a 1-D vector with the intensity per each wavelength.

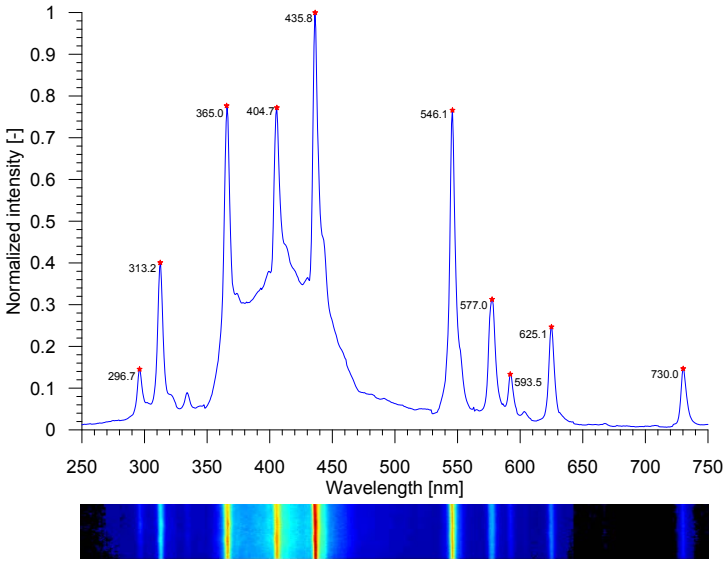


***Figure 3.9.*** *Spectral information of a sample image.*

Fig. 3.9 shows the result of the processing routine. It can be seen that, for a certain image, the spectral information is resolved in the horizontal axis and that the vertical one is used as a filter for noise and oscillations. Finally, what is represented in the figure is the calibration of the spectroscope with a mercury lamp from which the linear relationship between pixel and wavelength is deducted with a $R^2$ coefficient of approximately 1.

### 3.3.3 CHEMKIN

CHEMKIN-PRO is the software used to solve the chemical kinetics of the air-fuel mixture, obtaining the different ignition delays and critical concentrations, and tracing the relevant chemical paths. Two different

chemical kinetic mechanisms have been used in this work: On the one hand, the Curran's mechanism is used for n-heptane/iso-octane blends [21, 22]. This mechanism consists of 1034 species and 4238 reactions, and includes the detailed chemical kinetics of the two pure hydrocarbons that form the PRF scale. Thus, the oxidation of any PRF mixture can be described by means of this mechanism. Besides, its validity has been checked in several studies [23, 24] by comparison to experimental results. On the other hand, the reduced chemical kinetic mechanism for n-dodecane from the Lawrence Livermore National Laboratory [25] is used to describe the oxidation paths of such fuel. This mechanism consists of 163 species and 887 reactions. Despite the fact that more detailed mechanisms for n-dodecane can be found in the literature [26], this reduced mechanism is used for computing-time reasons. The detailed chemical kinetic mechanism from which the mechanism is obtained is composed by 2885 species and 11754 reactions [27], which results in unacceptable computing time when the ignition characteristics under constant thermodynamic conditions want to be obtained for their use in the predictive methods (which implies thousands of simulations). Moreover, the reduced mechanism for n-dodecane used in this Thesis has been successfully applied in other simulation works [28].

Additionally, the Curran's chemical mechanism for PRF blends has been modified to incorporate an OH* sub-mechanism in order to be able to compare the chemiluminescence results in an easy way [29]. Furthermore, since the Curran's chemical kinetics mechanism does not distinguish between OH (ground estate) and OH* (excited estate), the main generation reactions of excited OH have been located and modified in order to take into account the coexistence of both species [30]. The reduced mechanism for n-dodecane does not have to be modified since the chemiluminescence measurements have been carried out only with n-heptane and iso-octane. The complete OH* sub-model is described in Appendix 3.B.

Different ignition delays are defined in the simulations:

- $\tau_1$ is the ignition delay under constant thermodynamic conditions referred to the maximum pressure rise caused by cool flames.
- $\tau_2$ is the ignition delay under constant thermodynamic conditions referred to the maximum pressure rise caused by the high-temperature stage of the combustion process.
- $\tau_{CC}$ is the ignition delay under constant thermodynamic conditions referred to the critical concentration of chain carriers. As will be explained in Chapter 4, different species are proposed as chain carrier

depending on the stage of the ignition to be predicted: $CC$=$HO_2$ for cool flames and $CC$=$CH_2O$ for the high-temperature stage of the process. However, any active radical with chain behavior can be taken as chain carrier, e. g. $H_2O_2$.

- $t_{i,1}$ is the ignition delay under transient thermodynamic conditions referred to the maximum pressure rise caused by cool flames. This ignition delay is also experimentally obtained.
- $t_{i,2}$ is the ignition delay under transient thermodynamic conditions referred to the maximum pressure rise caused by the high-temperature stage of the combustion process. This ignition delay is also experimentally obtained.
- $t_{i,OH}$ is the ignition delay under transient thermodynamic conditions referred to the maximum OH* decay rate, which coincides with the maximum intensity of radiation at 310 $nm$. This ignition delay is also experimentally obtained.
- $t_{i,CO}$ is the ignition delay under transient thermodynamic conditions referred to the maximum oxidation rate of CO to $CO_2$, which coincides with the maximum intensity of radiation of the CO continuum. This ignition delay is also experimentally obtained.
- $t_{i,CC}$ is the ignition delay under transient thermodynamic conditions referred to the critical concentration of chain carriers. This time cannot be determined experimentally and it is used to evaluate the hypotheses of the Livengood & Wu integral method.

The model used to obtain ignition delays under constant conditions ($\tau_1$, $\tau_2$ and $\tau_{CC}$) and critical concentrations of chain carriers is a homogeneous closed reactor (perfectly stirred reactor, PSR), which works with constant pressure and uses the energy equation to solve the temperature temporal evolution. This model is the most appropriate to obtain ignition delays at constant pressure and temperature conditions [31]. Besides, working with constant pressure corrects, somehow, the over-prediction of the pressure that is typical of this kind of reactor [32].

The model used to obtain ignition delays under transient conditions ($t_{i,1}$, $t_{i,2}$, $t_{i,OH}$, $t_{i,CO}$ and $t_{i,CC}$) is a reciprocating internal combustion engine operating with homogeneous charge (IC-engine, closed 0-D reactors from CHEMKIN). The volume profile as well as the heat losses profile are imposed in order to reproduce the RCEM conditions. The piston starts at Bottom Dead

Center (BDC) and a complete cycle of the RCEM is simulated. Moreover, the $OH^*$, CO and $CO_2$ concentration profiles are obtained and an analysis of their reaction rates has been performed in order to compare the simulations with the results obtained from the photo-multiplier, from the high speed camera and from the spectroscope.

In order to be able to apply the different methods to predict ignition delays, the ignition characteristics under constant thermodynamic conditions for each state (T, P) of the experimental temperature and pressure paths have to be obtained in a PSR (see Chapter 4). The ignition delays and the critical concentrations are obtained for each thermodynamic state with a $\Delta t$ of $10^{-5}s$, which is the minimum experimental resolution of the pressure signal (experiments that have been carried out at ETH - Zurich). This value of the time step also represents an equilibrium between appropriate prediction accuracy and reasonable calculation time. Besides, the maximum waiting time for the autoignition of the mixture has been set to 30 $s$.

Finally, a wide analysis of the effects of the different species that compose the synthetic EGR on the ignition delay has been performed for n-heptane and iso-octane in a PSR, in order to establish a criterion for the definition of the proper EGR composition for autoignition studies (see Chapter 4). In this work the auto-ignition of the mixture is considered to be produced when the temperature in the reactor increases 400 $K$ over the initial temperature ($\Delta T$ criterion). The time corresponding to this instant will be considered as the ignition delay, $\tau$. Although the criterion chosen could seem inappropriate, since the ignition delay seems to be referenced to different phases of the combustion for different simulations, it is widely recognized by the scientific community [32, 33] and its consistency with other criteria has been checked for both fuels and various equivalence ratios ($F_r \in \{0.5, 1, 2\}$ ), initial pressures ($P_0 \in \{50, 100, 150\}$ $bar$), initial temperatures ($T_0 \in \{700, 800, 900, 1000\}$ $K$) and oxygen molar fractions ($X_{O_2} \in \{0.21, 0.15\}$). For each case, the ignition delay is obtained from the $\Delta T$ criterion and from the criterion of using the time at which the maximum temperature rise rate occurs ($dT/dt$ criterion) in a PSR.

The resulting ignition delays are represented in Fig. 3.10, those obtained from the $\Delta T$ criterion in the ordinate axis and those obtained from the $dT/dt$ criterion in the abscissas axis. The graph to the left shows the results obtained for iso-octane whereas the graph to the right shows the results obtained for n-heptane. The line $y = x$, which represents a perfect match between both criteria, is plotted in all graphics. Both figures show an excellent agreement between both criteria. In fact, the coefficients of determination, $R^2$, have been

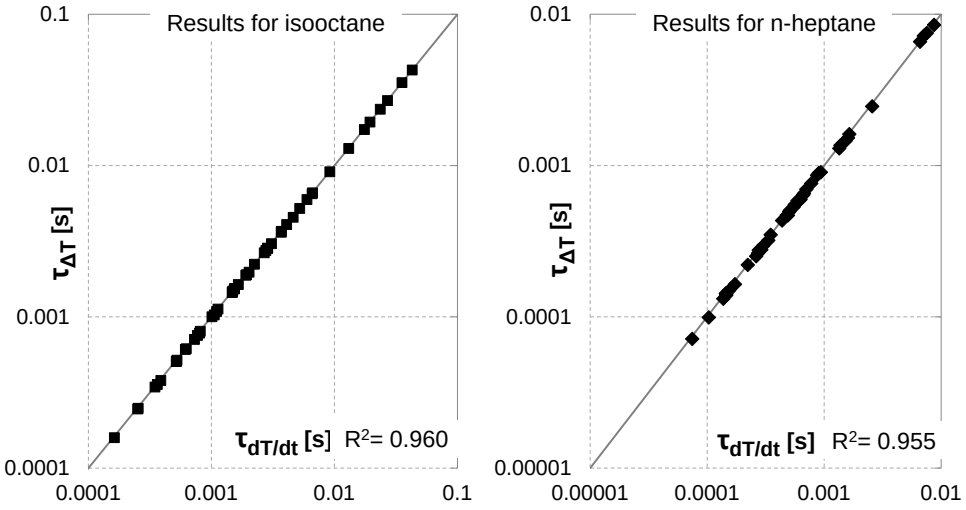


***Figure 3.10.*** *Ignition delays obtained from the $\Delta T$ criterion versus ignition delays obtained from the $dT/dt$ criterion. All cases in which autoignition occurs are represented. Left.- Isooctane. Right.- N-heptane.*

calculated for each fuel and each method and their values can be seen in the corresponding figure.

Ignition delays are always slightly underpredicted by using the $\Delta T$ criterion instead of using the $dT/dt$ criterion. However, this underprediction is lower than 5% in case of using n-heptane and lower than 2.5% in case of using iso-octane. Moreover, the difference between both criteria has always the same trend, which guarantees the correct interpretation of the results. The $\Delta T$ criterion is chosen in this study because of its higher stability, while the maximum waiting time for the auto-ignition of the mixture has been set to 30 $ms$. This value has been chosen because higher ignition delays would be equivalent to combustions after TDC in an engine operating at 1000 $rpm$ or higher. Therefore, mixtures with ignition delays longer than 30 $ms$ have no interest in the context of automotive engines.

The experimental validation of the chemical kinetic mechanisms used in this Thesis (a detailed one for PRF mixtures and a reduced one for n-dodecane) is shown in this section. However, the validation of the OH* sub-mechanism will be presented in Chapter 5, since it is necessary a full analysis of the optical results to be able to properly compare simulations and experiments.

In order to be able to directly compare the experimentally measured ignition delay with the simulated one, the ignition delay is defined as the time between the start of the compression process and the instant in which the maximum pressure rise rate occurs. Moreover, in this way it is possible to identify both ignition delays, the one referred to cool flames ($t_{i,1}$) and the one referred to the high-temperature stage ($t_{i,2}$), in case of having a two-stage ignition pattern.

The relative deviation in ignition delay, $\epsilon$, has been calculated in order to more easily compare experimental and simulation results. This deviation is defined as follows:

$$\epsilon = \frac{t_{i,ICE} - t_{i,RCEM}}{t_{compression}} 100 \tag{3.3}$$

where $t_i$ represents the time of ignition (ignition delay under transient conditions) that can be referred either to cool flames ($t_{i,1}$) or to the high-temperature stage ($t_{i,2}$). The subscript $ICE$ represents a data obtained from a chemical simulation with CHEMKIN using a closed 0-D IC-engine reactor. Finally, the subscript $RCEM$ represents a data obtained experimentally from the RCEM. It should be noted that the previous definition for the deviation compares a difference between chemical times, $t_{i,ICE} - t_{i,RCEM}$, with the physical time of the process, $t_{compression}$. Therefore, $\epsilon$ represents the difference of the inverse of the Damköhler number of both, simulation and experiment ($\epsilon = 1/Da_{ICE} - 1/Da_{RCEM}$).

The compression time has been chosen as the way to normalize the ignition delay deviations, since ignition delays under engine conditions have been obtained in this investigation. Thus, a relative deviation in CAD is much more interesting than a relative deviation respect to the measured ignition delay, and it can be easily obtained if the deviation is normalized by means of the compression time. In fact, the ignition delay deviation in CAD can be simply calculated as $\Delta\theta\ [CAD] = 1.80\epsilon$, where $\epsilon$ represents the ignition delay deviation in percent ([%]) normalized by means of the compression time. Thus, the consequences of the deviations between experiments and simulations on the engine can be more easily interpreted. Furthermore, normalizing by means of the compression time allows to compare results under different compression velocities, which can be modified, for instance, by varying the stroke, the compression ratio or the driving gas pressure.

#### 3.3.3.1 Validation of the detailed chemical kinetic mechanism for PRF mixtures

The Curran's detailed chemical kinetic mechanism for PRF mixtures has been validated versus experimental data in the working range. As said before, this mechanism includes the detailed chemical kinetics of the two pure hydrocarbons that form the PRF scale, i.e., n-heptane and iso-octane. This validation has been decoupled in two different blocks: evaluation of the sub-mechanisms for n-heptane and iso-octane and evaluation of the complete mechanism for PRF blends. In this way, it is possible to identify deficiencies in the description of the chemical paths of any of both pure fuels.

- Validation of both sub-mechanisms for pure n-heptane and pure iso-octane.

Ignition delays obtained solving the n-heptane and iso-octane detailed chemical kinetic mechanisms are compared to the experimental results as a method to validate the mechanism in the desired range.

Cool flames is a phenomenon only present in the cases performed with n-heptane. The ignition delay deviations between the chemical kinetic simulations and the experimental results are shown in Fig. 3.11 for all cases that show a two-stage ignition pattern. The average of the deviations in absolute value, $|\bar{\epsilon}| = \sum \mid \epsilon \mid /N$, has been calculated and its value can be seen in the figure.

The results show that simulations are able to reproduce the experimental ignition delays with quite a good accuracy. In fact, the confidence interval for the mean absolute deviation, $|\bar{\epsilon}|$, with a confidence level of 95% is equal to $[1.202, 4.169]$ %. Ignition delay deviations are caused partly by the chemical kinetic mechanism used and partly by the experimental uncertainties mainly associated to the calculation of the effective volume and the heat losses in the RCEM. It can be seen that the ignition delay referred to cool flames is underestimated by the mechanism. As Fig. 3.12 shows, this is mainly caused because of the higher pressure rise rate calculated by CHEMKIN. Despite the fact that cool flames start in both cases approximately at the same instant, the maximum pressure rise rate is reached much faster in the simulations, which leads to a certain deviation between these cases and the experiments. The absence of wall effects and heterogeneities in CHEMKIN causes a faster pressure rise, especially in the case of cool flames. This effect can be mitigated by modifying the ignition delay criterion, as will be explained in Section 3.3.3.2. If ignition is defined by a criterion based on the beginning

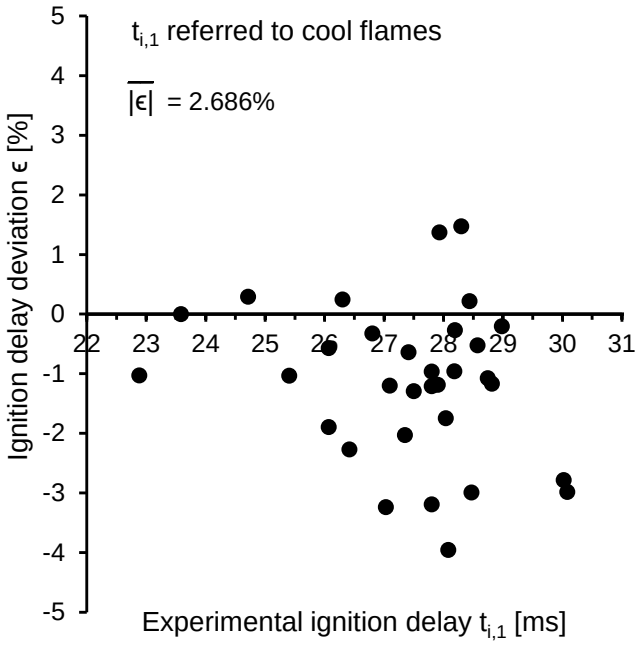


***Figure 3.11.*** *Percentage deviation in ignition delay referred to cool flames, $t_{i,1}$. The mean absolute deviation, $|\bar{\epsilon}|$, shows good agreement between both experimental and simulated results.*

of the combustion event (on the initial part of the heat release), the trend to underpredict the cool flames can be corrected.

The ignition delay deviation referred to the high-temperature stage is shown in Fig. 3.13 for all cases and both fuels. The average of the deviations in absolute value, $|\bar{\epsilon}| = \sum \mid \epsilon \mid /N$, has been calculated for each fuel and its value can be seen in the figure.

The results show that simulations are able to reproduce the experimental ignition delays with quite a good accuracy. In fact, the confidence interval for the mean absolute deviation, $|\bar{\epsilon}|$, with a confidence level of 95% is equal to $[1.202, 2.207]$ % for n-heptane and equal to $[1.188, 1.822]$ % for iso-octane. As before, ignition delay deviations are caused partly by the chemical kinetic mechanism used and partly by the experimental uncertainties mainly associated to the calculation of the effective volume and the heat losses in the RCEM.

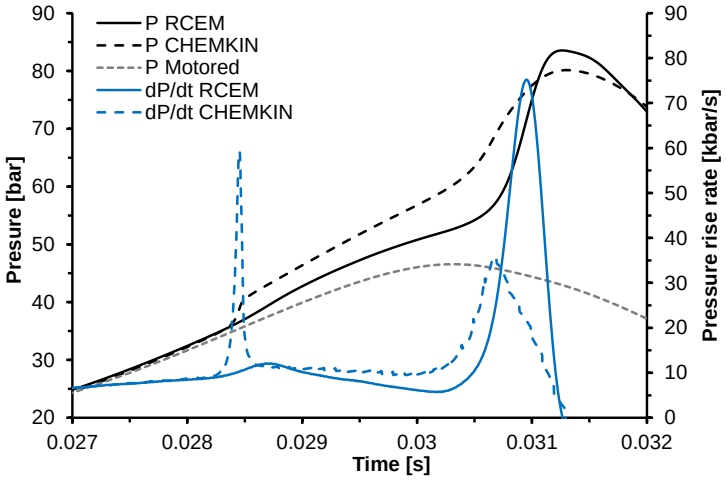


***Figure 3.12.*** *Pressure signal and pressure rise rate obtained experimentally and by simulation.* $T_0$*=358 K,* $P_0$*=1.4 bar, CR=15,* $X_{O_2}$*=0.126,* $F_r$*=0.4, n-heptane.*

It can be seen that the ignition delay referred to a maximum pressure rise rate is underestimated for n-heptane but overestimated for iso-octane (Fig. 3.13). This fact is independent of the physical models used to characterize the heat losses and the deformations, since they are the same for both fuels. Moreover, the temperature is always high enough to keep the fuel in vapor phase, therefore these discrepancies are not due to a physical evaporation time. The chemical mechanism that has been used in this investigation has been designed from the detailed chemical kinetics of n-heptane [21] and iso-octane [22]. Moreover, the iso-octane mechanism is based on that of n-heptane, where the rates of alkyl-peroxyl radical isomerization and peroxy-alkylhydroperoxyl radical isomerization have been decreased by a factor of three (relative to the n-heptane) in order to reproduce the very low reactivity observed experimentally at low temperature (600-770 $K$). The reason why the isomerization rates of iso-octane are slower than those of n-heptane is not clear (other pathways could occur at low temperature). To the author's opinion, this reduction of isomerization rates is the cause why the mechanism over-predicts the ignition delays for iso-octane.

- Validation of the detailed chemical kinetic mechanism for PRF mixtures.

Three different PRF mixtures have been tested: PRF25, PRF50 and PRF75, which are defined by 25%, 50% and 75% of iso-octane, and that

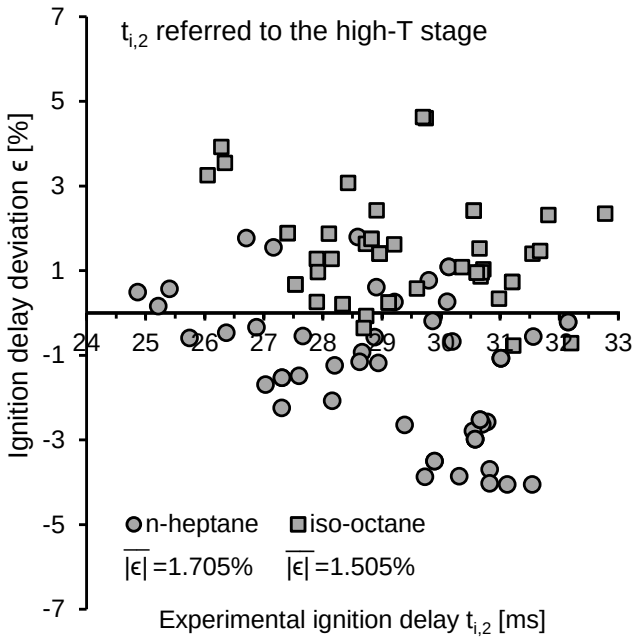


***Figure 3.13.*** *Percentage deviation in ignition delay referred to the high-temperature stage, $t_{i,2}$. The average of the deviations in absolute value, $|\bar{\epsilon}|$, shows good agreement between both experimental and simulated results.*

correspond to 25, 50 and 75 of octane number, respectively. Cool flames is a phenomenon only present in the cases performed with PRF25 and PRF50. The high octane number and the percentage of iso-octane of PRF75 cause that cool flames cannot be clearly identified.

The ignition delay deviations, $\epsilon$, between the chemical kinetic simulations and the experimental results are shown in Fig. 3.14 for all cases that show a two-stage ignition pattern. The mean absolute deviation, $|\bar{\epsilon}|$, has been calculated and its value can be seen in the figure.

The results show that simulations are able to reproduce the experimental ignition delays with quite a good accuracy. In fact, the confidence intervals for the mean absolute deviation, $|\bar{\epsilon}|$, with a confidence level of 95% are equal to $[1.633, 2.362]$ % for PRF25 and to $[1.344, 1.984]$ % for PRF50. The predicted ignition delays also show quite a good agreement with the experimental results. As it can be seen, simulated ignition delays follow a random distribution around the line $y = 0$, which means that ignition delay deviations are caused

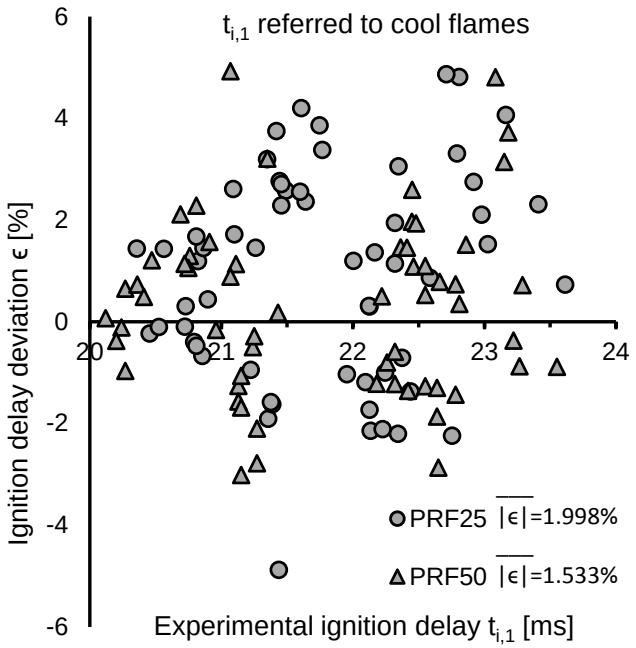


***Figure 3.14.*** *Percentage deviation in ignition delay referred to cool flames, $t_{i,1}$, for PRF25 and PRF50. The mean absolute deviation, $|\bar{\epsilon}|$, shows good agreement between both experimental and simulated results.*

partly by the chemical kinetic mechanism used and partly by the experimental uncertainties mainly associated to the calculation of the effective volume and the heat losses in the RCEM.

The ignition delay deviations, $\epsilon$, referred to the high-temperature stage between the chemical kinetic simulations and the experimental results are shown in Fig. 3.21 for all cases. The mean absolute deviation, $|\bar{\epsilon}|$, has been calculated and its value can be seen in the figure.

The results show that simulations are able to reproduce the experimental ignition delays with quite a good accuracy. In fact, the confidence interval for the mean absolute deviation, $|\bar{\epsilon}|$, with a confidence level of 95% is equal to $[1.344, 1.984]$ % for PRF25, equal to $[1.809, 2.648]$ % for PRF50 and equal to $[2.463, 3.765]$ % for PRF75. It can be seen that the higher the octane number, the worse the simulation capability of the mechanism, which means that the accuracy of the n-heptane sub-mechanism is higher than the accuracy of the iso-octane sub-mechanism when PRF blends are tested (when both sub-

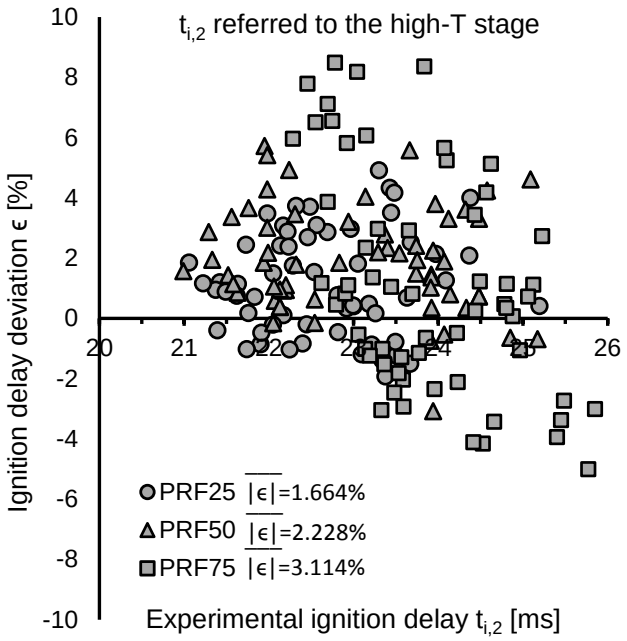


***Figure 3.15.*** *Percentage deviation in ignition delay referred to the high-temperature stage, $t_{i,2}$. The mean absolute deviation, $\overline{|\epsilon|}$, shows good agreement between both experimental and simulated results.*

mechanisms are involved). This result is caused mainly by two effects. On the one hand, this fact is probably because the rates of alkyl-peroxyl radical isomerization and peroxy-alkylhydroperoxyl radical isomerization have been decreased by a factor of three compared to n-heptane in the case of the iso-octane sub-mechanism. Thus, higher percentage of iso-octane implies more overestimated ignition delays. On the other hand, the lower the reactivity of the mixture, the more relevant the wall effects on the ignition. The maximum pressure rise rate is reached much faster in the simulations (without wall effects) than in the experiments, which leads to a certain negative deviation between simulations and experiments.

The confidence intervals for $\overline{|\epsilon|}$ with a confidence level of 95% are summarized in Table 3.8 for all the simulations with n-heptane/iso-octane blends. These values of $\overline{|\epsilon|}$ are very similar to each other, meaning that both ignition delays of all fuels can be obtained by using the Curran's detailed chemical kinetic mechanism.

| | Cool flames | | High-T stage | |
|---|---|---|---|---|
| | $\bar{\lvert\epsilon\rvert}$ [%] | **CI 95%** [%] | $\bar{\lvert\epsilon\rvert}$ [%] | **CI 95%** [%] |
| **PRF0 (n-heptane)** | 2.686 | [1.202, 4.169] | 1.705 | [1.202, 2.207] |
| **PRF25** | 1.998 | [1.633, 2.362] | 1.664 | [1.344, 1.984] |
| **PRF50** | 1.533 | [1.344, 1.984] | 2.228 | [1.809, 2.648] |
| **PRF75** | - | - | 3.114 | [2.463, 3.765] |
| **PRF100 (iso-octane)** | - | - | 1.505 | [1.188, 1.822] |

***Table 3.8.*** *Confidence intervals for both mean absolute deviations, $\bar{\lvert\epsilon\rvert}$, referred to cool flames and referred to the high-temperature stage with a confidence level of 95% for the chemical kinetic simulations.*

#### 3.3.3.2 Validation of the reduced chemical kinetic mechanism for n-dodecane

First, the reduced chemical kinetic mechanism for n-dodecane from Lawrence Livermore National Laboratory is compared to the detailed one. To do so, a parametric study has been carried out in CHEMKIN by simulating the ignition characteristics of a homogeneous n-dodecane - air mixture in a closed PSR in which the pressure is kept constant and the temperature evolution is obtained by solving the energy equation. The consistency between mechanisms has been checked for various equivalence ratios ($F_r \in\{0.5,\ 1,\ 2\}$ ), initial pressure ($P_0 \in\{50,\ 100,\ 150\}\ bar$), initial temperature ($T_0 \in\{700,\ 800,\ 900,\ 1000\}\ K$) and oxygen molar fractions ($X_{O_2} \in\{0.21,\ 0.15\}$). Fig. 3.16 shows the ignition delay referred to cool flames (left) and the ignition delay referred to the high-temperature stage (right) obtained by the reduced mechanism versus the corresponding ignition delay obtained by the detailed mechanism. The line $y = x$, which represents a perfect match between both mechanisms, is plotted in all graphics. Both figures show good agreement between both mechanisms. In fact, the coefficients of determination, $R^2$, have been calculated for each fuel and each method and their values can be seen in the corresponding figure.

It can be checked that the reduced mechanism tends to under-predict the ignition delay at high temperature ($\approx$ 1000 $K$), while it over-predicts the ignition delay at low temperature ($\approx$ 700 $K$). This is probably because the mechanism is optimized to replicate the ignition delays of the

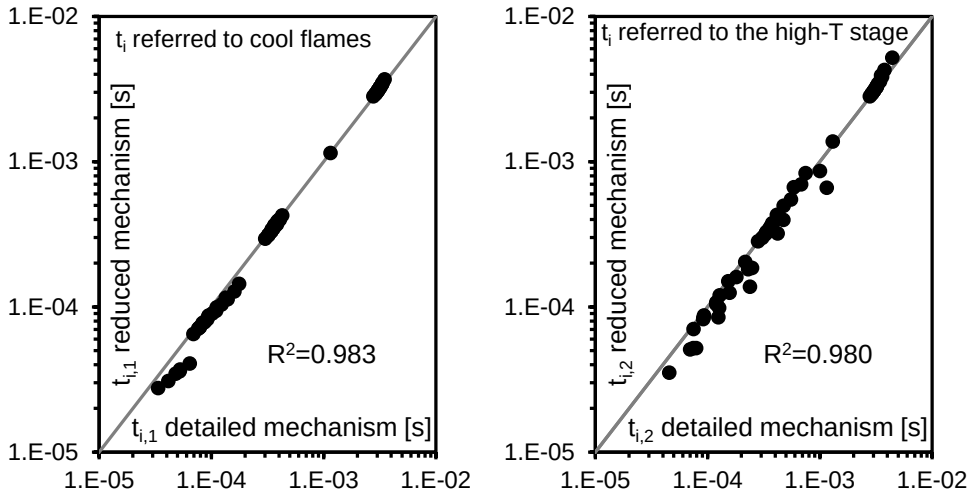


***Figure 3.16.*** *Ignition delays for n-dodecane obtained by the reduced mechanism versus ignition delays obtained by the detailed mechanism. All cases in which autoignition occurs are represented. Left.- Cool flames. Right.- High-temperature stage.*

detailed mechanism at medium temperature (usual working range in engines). However, as shown in Fig 3.16, both mechanisms are consistent with each other.

Then, the reduced chemical kinetic mechanism has been validated versus experimental data in the working range. Cool flames can be identified for n-dodecane under the operating conditions that have been tested. The ignition delay deviations, $\epsilon$, referred to cool flames between the chemical kinetic simulations and the experimental results are shown in Fig. 3.17 for all cases. The mean absolute deviation, $|\bar{\epsilon}|$, has been calculated and its value can be seen in the figure.

The results show that simulations are able to reproduce the experimental ignition delays with quite a good accuracy, but in a worse way than the detailed chemical kinetic mechanisms for PRFs. In fact, the confidence interval for the mean absolute deviation, $|\bar{\epsilon}|$, with a confidence level of 95% is equal to $[2.383, 3.329]$ %.

The ignition delay deviations, $\epsilon$, referred to the high-temperature stage between the chemical kinetic simulations and the experimental results are

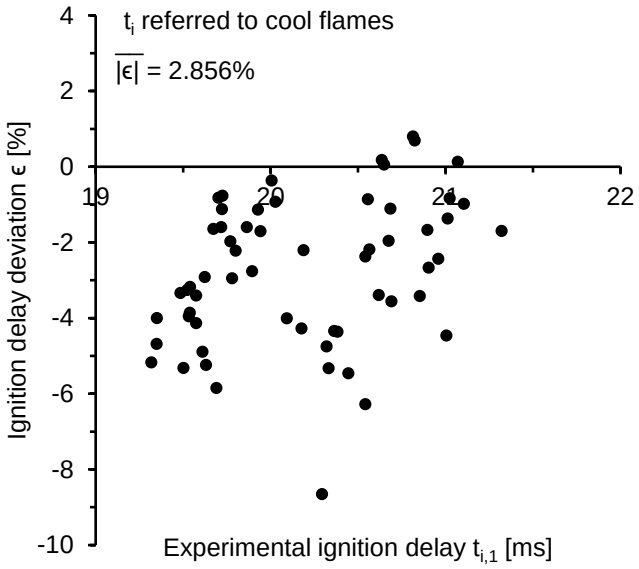


***Figure 3.17.*** *Percentage deviation in ignition delay referred to cool flames, $t_{i,1}$, for n-dodecane. The mean absolute deviation, $|\bar{\epsilon}|$, shows good agreement between both experimental and simulated results.*

shown in Fig. 3.18 for all cases. The mean absolute deviation, $|\bar{\epsilon}|$, has been calculated and its value can be seen in the figure.

The results show that simulations are able to reproduce the experimental ignition delays with quite a good accuracy, but in a worse way than the detailed chemical kinetic mechanisms for PRFs. In fact, the confidence interval for the mean absolute deviation, $|\bar{\epsilon}|$, with a confidence level of 95% is equal to $[3.169, 3.750]$ %.

It can be seen that both ignition delays, the one referred to cool flames and the one referred to the high-temperature stage, are underestimated by the simulations. As Fig. 3.19 shows, this is mainly because of the higher pressure rise rate calculated by CHEMKIN, which is one order of magnitude higher than the experimental $dP/dt$. Despite the fact that cool flames start in both cases approximately at the same instant, the maximum pressure rise rate is reached much faster in the simulations, which leads to a certain deviation between these cases and the experiments. Besides, this effect is even higher for the high-temperature stage, in which the pressure is suddenly increased and the duration of the combustion is negligible.

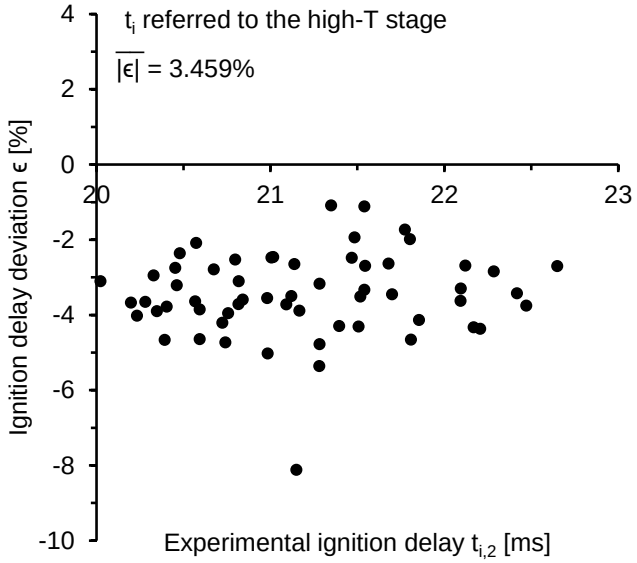


***Figure 3.18.*** *Percentage deviation in ignition delay referred to the high-temperature stage, $t_{i,2}$, for n-dodecane. The mean absolute deviation, $|\bar{\epsilon}|$, shows good agreement between both experimental and simulated results.*

On the one hand, the absence of wall effects and heterogeneities in CHEMKIN causes a faster pressure rise, especially in the case of cool flames. Moreover, since the ignition of n-dodecane occurs at low temperature and pressure (during the compression stroke because of its short ignition delay), the propagation of the ignition near to the walls is slower than for autoignitions that occur at TDC. Thus, the wall effects become even more important for n-dodecane than for other fuels. On the other hand, since the reduced chemical kinetic mechanism consists of a lower number of reactions than the detailed one, which means a lower number of steps during the combustion process, the combustion event is not as accurately replicated as in a detailed description of the chemistry. However, as Fig. 3.19 shows, this trend can be also seen by using the detailed chemical kinetic mechanism (even to a greater extent). Therefore, the reaction rates of the exothermic reactions seem to be too fast under lean low-temperature conditions, and the description of the oxidation of such a long-chain hydrocarbon as n-dodecane needs to be improved at least under these conditions. I.e., the maximum pressure rise rate is reached too fast in the simulations, which leads to a certain negative deviation between simulations and experiments (the ignition delay is underestimated).

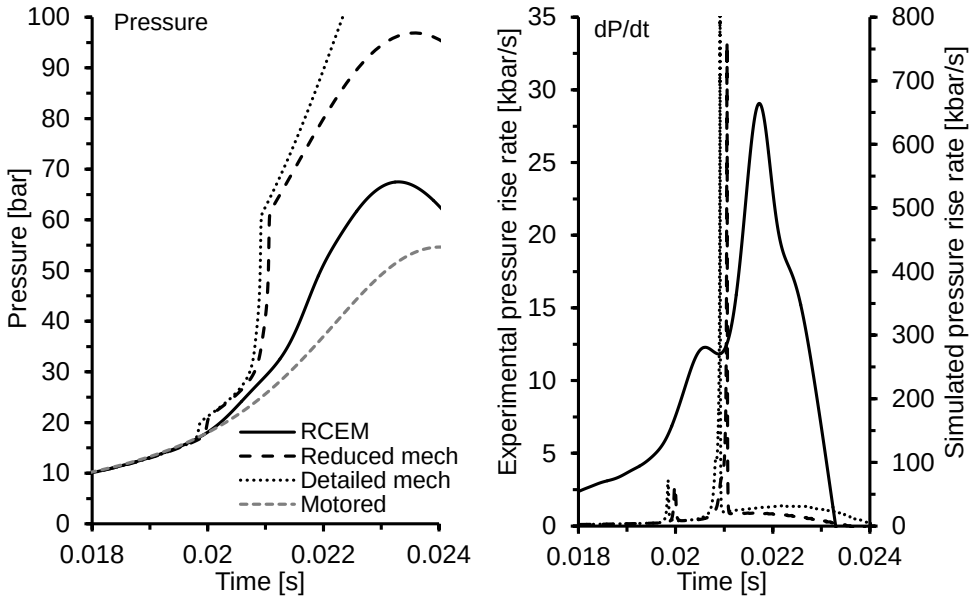


***Figure 3.19.*** *Pressure signal (left) and pressure rise rate (right) obtained experimentally and by simulation.* $T_0$*=443 K,* $P_0$*=1.5 bar, CR=14,* $X_{O_2}$*=0.21,* $F_r$*=0.4, n-dodecane.*

In order to solve the problematic presented above that is related to the definition of the ignition delay, the autoignition of the mixture is considered to be produced when the first signs of combustion are visible. Besides, the location of the combustion initiation can be seen more easily in the HRR profile, rather than in the pressure rise rate. More specifically, ignition is defined as the crossing through zero of a secant line of the HRR as described in Fig. 3.20. As it can be seen, both cool flames and the high-temperature stage of the process can be identified when a two-stage ignition pattern occurs. The points at 75% and 25% of the maximum HRR referred to each ignition stage are selected for the calculation of the secant line and the subsequent ignition time. 25% of the maximum HRR has been selected in order to avoid wrong calculations of the secant line when cool flames and the high-temperature stage are coupled. Besides, 75% of the maximum HRR has been selected in order to avoid undesirable effects of the rounded peak of the HRR on the slope of the secant line. Thus, the ignition delay ($t_{i,1}$ or $t_{i,2}$ for cool flames and high-temperature, respectively) in the experimental facility is defined as the time

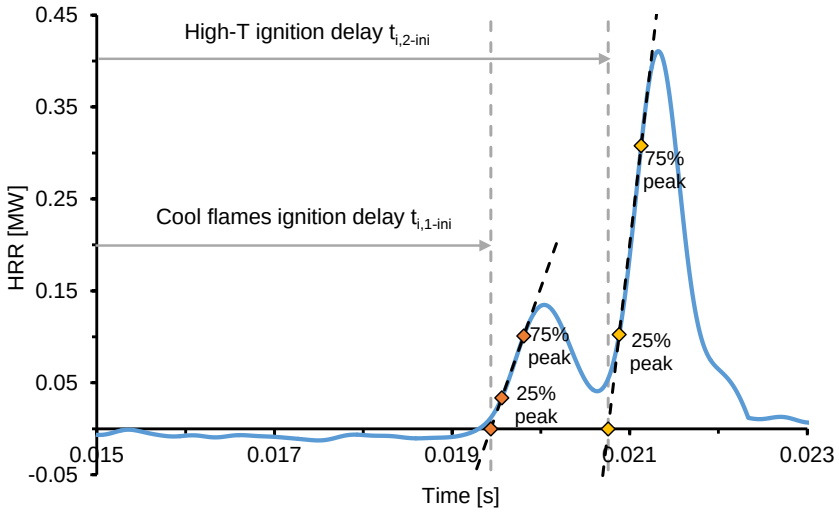


***Figure 3.20.*** *Ignition delay definition based on the heat release rate. The autoignition of the mixture is considered to be produced when the crossing through zero of a secant line of the HRR occurs.*

between the start of the rapid compression process and the calculated (from the start of the HRR) ignition time.

The ignition delay deviations between the simulations and the measurements are shown in Fig. 3.21 for all cases and both ignition stages. The ignition delay based on the initial part of the HRR has been considered for the comparison, avoiding deviations promoted by the existence of gradual autoignition event in the combustion chamber. Fig. 3.21 to the left shows that the ignition delay deviation referred to cool flames seems to be more positive if the ignition delay is increased, i.e., if the reactivity of the mixture is decreased. The lower the reactivity the nearer the ignition to TDC. Besides, wall effects are more relevant near TDC because of the higher area-to-volume ratio of the combustion chamber. Thus, if the ignition occurs near TDC, the in-cylinder temperature gradients will be higher, leading to higher differences between the maximum local temperature and the mean temperature of the homogeneous gas bulk. Taking into account that cool flames are highly dependent on temperature and that the temperature in CHEMKIN corresponds to the mean temperature of the homogeneous gas core, the lower the reactivity the higher the differences between the experimental ignition delay referred to cool flames (defined by the maximum local temperature) and the simulated ignition delay

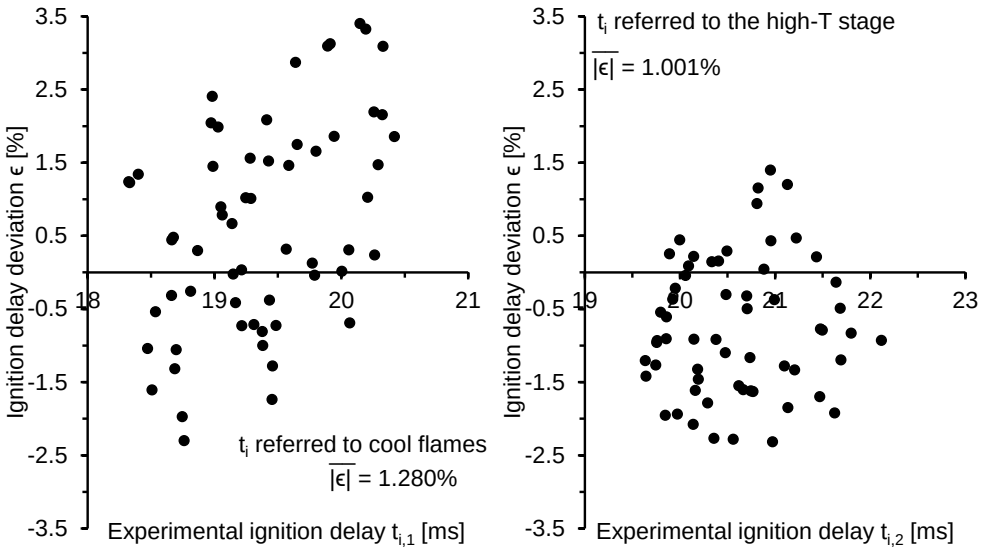


***Figure 3.21.*** *Ignition delay deviation for n-dodecane using an ignition delay criteria based on the HRR. Left.- Deviations referred to cool flames. Right.- Deviations referred to the high-temperature stage of the process.*

referred to cool flames (defined by the mean temperature of the homogeneous gas bulk). Therefore, the lower the reactivity the more positive the ignition delay deviation according to Eq. 5.2, since shorter ignition delays will be obtained in the RCEM.

Fig. 3.21 to the right shows a random distribution of the ignition delay deviations referred to the high-temperature stage of the process. The confidence intervals for the mean absolute deviation, $|\overline{\epsilon}| = \sum |\epsilon|/N$, with a confidence level of 95% are equal to $[1.046, 1.515]$ % for cool flames and equal to $[0.834, 1.169]$ % for the high-temperature stage. Despite the fact that $t_{i,2-ini}$ is more accurately modeled than the ignition delay referred to cool flames, both ignition delays seems to be simulated with quite a good accuracy.

The criterion based on the initial part of the HRR can be used also to improve the comparison between simulations and experiments for the cool flames of n-heptane (Section 3.3.3.1). Thus, deviations shown in Fig. 3.11 will be decreased if the ignition delay criterion is modified. However, the ignition criterion is only changed for n-dodecane because deviations caused by the pressure rise rate criterion are only critical for this fuel, being less relevant in case of testing PRF mixtures.

## 3.A Appendix: Validation of the experimental facility

The RCEM available at CMT-Motores Térmicos is a new facility that had not been used in any previous studies. Therefore, a wide validation of such experimental facility is mandatory to ensure the accuracy of the results. First, the repeatability of the machine is analyzed under motoring conditions and also with combustion. Besides, the accuracy of the machine is tested by comparing directly the experimental results with other results from a similar facility working under the same conditions.

### 3.A.1 Repeatability of the RCEM

The repeatability of the RCEM has been evaluated in two different ways: under motoring conditions and with combustion by working with homogeneous air-fuel mixtures. To do so, ten repetitions of an experiment under the same initial and boundary conditions have been carried out in order to obtain representative results. Later on, a statistical analysis of the other combustion characteristics is performed. The maximum pressure is taken as target for the confidence interval under motoring conditions, while this role is assumed by the ignition delay in combustion studies.

- Repeatability of the RCEM under motoring conditions.

Fig. 3.22 shows the pressure (left) and position (right) paths near TDC for ten different experiments under motoring conditions. Specifically, the initial temperature, which coincides with the wall temperature, and pressure are equal to 383 $K$ and 1.4 $bar$, respectively, while the driving gas pressure that impulses the RCEM is equal to 30 $bar$ and the stroke is fixed to 249 $mm$. The instant at which the rapid compression stroke starts is taken as time reference, which coincides to a piston position equal to 29 $mm$ due to constructive aspects of the machine. It can be seen that good repeatability is reached not only in terms of maximum pressure and piston position, but also according to the instant at which the maximum values occur. Furthermore, the deviation in maximum pressure is caused by the differences in the compression ratio reached in the different experiments. The maximum piston position is determined by a force balance between in-cylinder pressure, driving gas pressure and piston inertia, since there is not any mechanism to stop the piston, as the rod-to-crank mechanism in an engine. Thus, small fluctuations in the initial pressure

values lead to small differences in compression ratio, which imply a variation of the maximum pressure reached in the cycle. In fact, Fig. 3.23 shows that pressure variations in Fig. 3.22 to the left correspond to position fluctuations in Fig. 3.22 to the right, since a clear relation can be found between the maximum in-cylinder pressure and the maximum piston position.

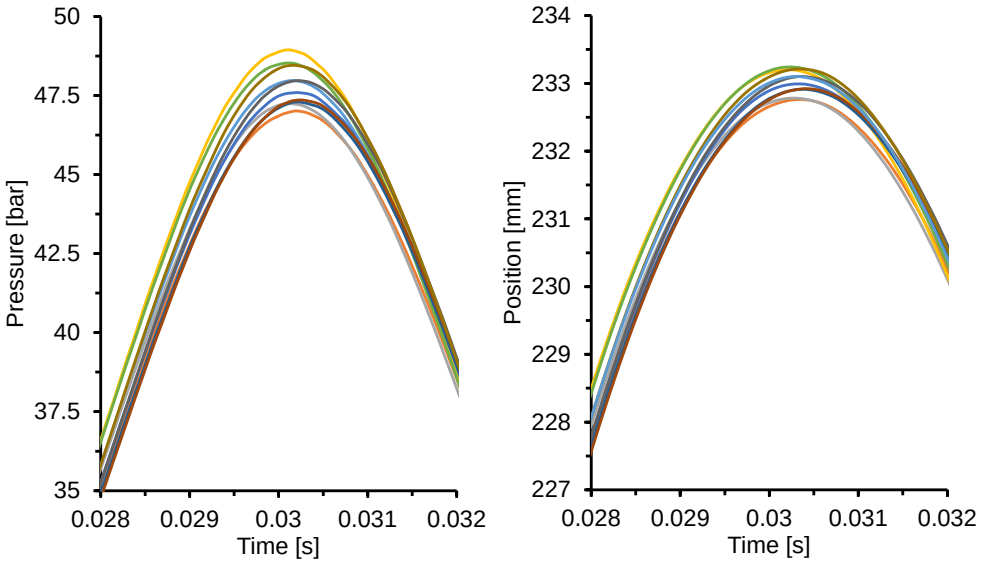


***Figure 3.22.*** *In-cylinder pressure and piston position near TDC for ten different repetitions under the same conditions. Left.- Pressure. Right.- Piston position.*

A complete statistical analysis of the relevant characteristics of the process is presented in Table 3.9, in which the average ($\bar{x}$), standard deviation ($\sigma$), coefficient of variation ($CV$) and semi-amplitude of the confidence interval with a 95% of level of confidence ($\mu$) are shown. Moreover, the repeatability is evaluated for a certain parameter as the $\mu/\bar{x}$ ratio in percentage, assuming a good repeatability if such value is below 1%. Specifically, the maximum piston position ($X_{max}$), the instant at which it occurs ($t_{X_{max}}$), the maximum in-cylinder pressure ($P_{max}$), the instant at which it occurs ($t_{P_{max}}$) and the effective compression ratio ($CR$) are analyzed. It can be seen in the table that the $\mu/\bar{x}$ ratio is lower than 1% for all the analyzed parameters, which means that the RCEM shows very good repeatability under motoring conditions.

- Repeatability of the RCEM with combustion.

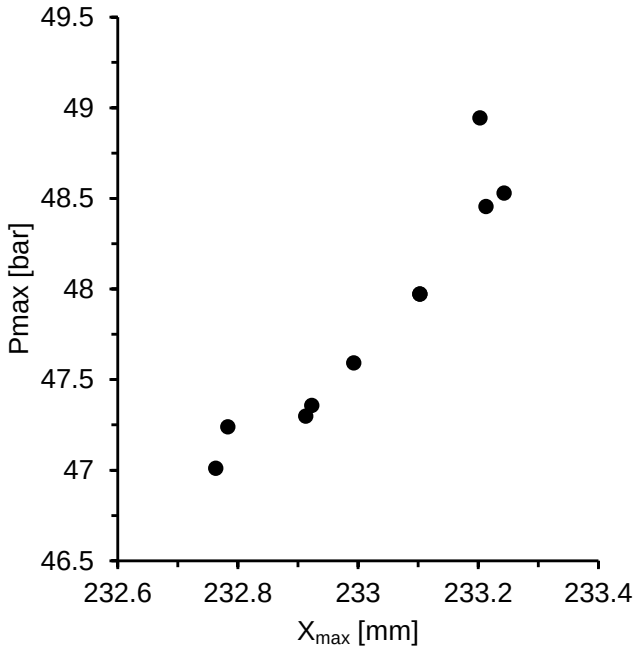


***Figure 3.23.*** *Maximum in-cylinder pressure versus maximum piston position for the ten repetitions shown in Fig. 3.22.*

The repeatability of the RCEM working under a direct injection combustion mode (stratified fuel-air mixture) has been evaluated for n-heptane under three different equivalence ratios, which correspond to low, medium and high load. Specifically, the fuel injection is performed at the beginning of the rapid compression stroke (piston position equal to 29 $mm$) using 1750 $bar$ as injection pressure, which results in a stratified mixture, since the mixing time is around 20 $ms$. It is worthy to note that despite the fact that homogeneous mixtures have been tested in this Thesis, the repeatability under reactive conditions has been analyzed with stratified mixtures in order to evaluate also that of the injection time. The specified stroke and driving gas pressure are 140 $mm$ and 35 $bar$, respectively, while the initial temperature (i.e., wall temperature) and pressure are 353 $K$ and 2.5 $bar$, respectively. Finally, dry air is used as oxidizer and the working equivalence ratio is equal to 0.3, 0.4 and 0.5 depending on the load.

Fig 3.24 shows the piston position path and the injection electrical pulse for ten experiments under the same initial and boundary conditions (medium

| | $X_{max}$ $[mm]$ | $t_{X_{max}}$ $[s]$ | $P_{max}$ $[bar]$ | $t_{P_{max}}$ $[s]$ | $CR$ $[-]$ |
|---|---|---|---|---|---|
| $\bar{x}$ | 232.987 | 0.03033 | 47.931 | 0.03017 | 14.720 |
| $\sigma$ | 0.185 | 0.00006 | 0.648 | 0.00004 | 0.160 |
| $CV$ [%] | 0.079 | 0.198 | 1.353 | 0.131 | 1.089 |
| $\mu$ | 0.132 | 0.00004 | 0.464 | 0.00003 | 0.115 |
| $\mu/\bar{x}$ [%] | 0.057 | 0.142 | 0.968 | 0.093 | 0.779 |

***Table 3.9.*** *Statistical analysis of different characteristic parameters from ten experiments under motoring conditions with the same initial and boundary conditions.*

load, $F_r = 0.4$). As it can be seen in the adjusted-scale images (right), the repeatability of the position path is really good during the compression stroke, being only affected in the expansion by the dispersion of the combustion pressure. Moreover, the repeatability of the electrical pulse that command the injector is almost perfect.

Furthermore, Fig 3.25 shows the raw in-cylinder pressure for the same ten experiments under medium load ($F_r = 0.4$) using an adjusted scale around TDC. Even by plotting the raw signals, a very good repeatability in the pressure reached in the combustion process can be seen, and not only according to the high-temperature stage, but also to cool flames.

In this context, the ignition delay is defined as the time between the beginning of the injection process and the instant at which the maximum pressure rise rate occurs. Thus, a complete statistical analysis, the results of which are presented in Tables 3.10, 3.11 and 3.12, has been done for the characteristic parameters of the combustion process, including the ignition delay ($t_i$), the compression ratio ($CR$) and the maximum pressure and piston position ($P_{max}$ and $X_{max}$). It can be seen in the tables that the $\mu/\bar{x}$ ratio is lower than 1.7% for all the analyzed parameters, specially for the ignition delay, where the $\mu/\bar{t_i}$ ratio is lower than 0.3% for the three tested equivalence ratios. Thus, the RCEM shows a very good repeatability, which is even better in terms of ignition delay (which is the target parameter to measure in this Thesis).

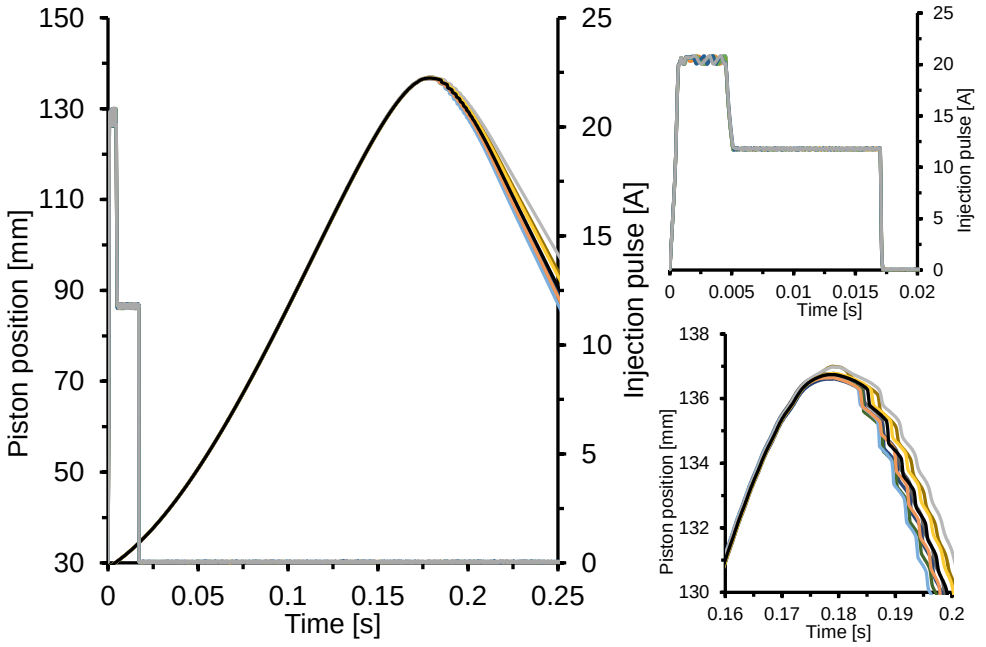


***Figure 3.24.*** *Injection pulse and piston position for ten different repetitions under the same conditions (medium load, $F_r = 0.4$). Left.- Original image. Right, top.- Zoom on the piston position. Right, bottom.- Zoom on the electrical pulse.*

### 3.A.2 Comparison versus other similar facilities

This RCEM has been validated by comparison with the machine available at ETH-Zurich, using the results shown in [5]. In that study, Mitakos et al. studied the ignition delays referred to cool flames and referred to the high temperature heat release of different fuels under several conditions of temperature, equivalence ratio and EGR rate. The operating points of n-heptane have been reproduced with the RCEM available at CMT-Motores Térmicos, and the results have been compared with the published ones.

The corresponding operating points can be seen in Table 3.13, with an initial temperature, pressure and stroke of 383 $K$, 1.34 $bar$ and 249 $mm$, respectively, and using a driving gas pressure equal to 30 $bar$.

In that case, the criterion to define the start of ignition delay is the time at which the piston is at 200 mm. Besides, the start of ignition is considered as the time at which the secant line that includes 8% and 25% of the maximum

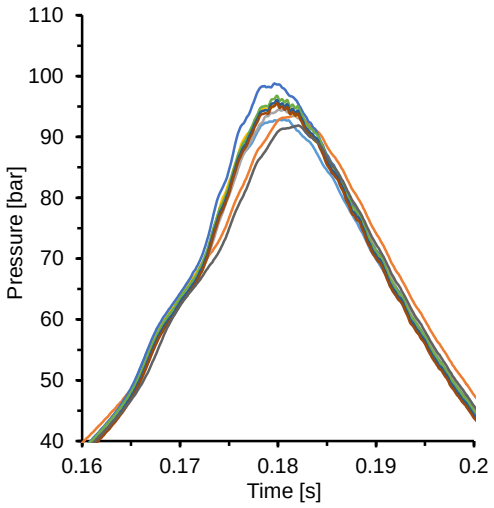


***Figure 3.25.*** *In-cylinder pressure for ten different repetitions under the same conditions (medium load, $F_r$ = 0.4).*

| | **Low load ($F_r$=0.3)** | | | |
|---|---|---|---|---|
| | $P_{max}$ $[bar]$ | $X_{max}$ $[mm]$ | $CR$ $[-]$ | $t_i$ $[ms]$ |
| $\bar{x}$ | 89.665 | 136.945 | 15.907 | 17.872 |
| $\sigma$ | 0.610 | 0.051 | 0.104 | 0.064 |
| $CV$ [%] | 0.680 | 0.037 | 0.654 | 0.358 |
| $\mu$ | 0.436 | 0.036 | 0.074 | 0.046 |
| $\mu/\bar{x}$ [%] | 0.486 | 0.027 | 0.468 | 0.256 |

***Table 3.10.*** *Statistical analysis of different characteristic parameters from ten experiments under autoignition combustion conditions imposing the same initial and boundary conditions. Low load ($F_r$=0.3).*

heat release rate crosses through zero. Finally, the start of ignition referred to the cool flames is considered as the time at which the secant line that includes the peak and 50% of the maximum heat release rate of cool flames crosses through zero. This criterion, which can is graphically described in Fig. 3.26, is the one used by Mitakos et al. in their experiments.

| | **Medium load ($F_r$=0.4)** | | | |
|---|---|---|---|---|
| | $P_{max}$ $[bar]$ | $X_{max}$ $[mm]$ | $CR$ $[-]$ | $t_i$ $[ms]$ |
| $\bar{x}$ | 94.943 | 136.766 | 15.600 | 17.747 |
| $\sigma$ | 2.199 | 0.139 | 0.234 | 0.070 |
| $CV$ [%] | 2.316 | 0.101 | 1.498 | 0.396 |
| $\mu$ | 1.573 | 0.099 | 0.167 | 0.050 |
| $\mu/\bar{x}$ [%] | 1.657 | 0.072 | 1.072 | 0.283 |

***Table 3.11.*** *Statistical analysis of different characteristic parameters from ten experiments under autoignition combustion conditions imposing the same initial and boundary conditions. Medium load ($F_r$=0.4).*

| | **High load ($F_r$=0.5)** | | | |
|---|---|---|---|---|
| | $P_{max}$ $[bar]$ | $X_{max}$ $[mm]$ | $CR$ $[-]$ | $t_i$ $[ms]$ |
| $\bar{x}$ | 116.575 | 136.703 | 15.493 | 17.701 |
| $\sigma$ | 0.913 | 0.061 | 0.112 | 0.068 |
| $CV$ [%] | 0.783 | 0.045 | 0.720 | 0.382 |
| $\mu$ | 0.653 | 0.044 | 0.080 | 0.048 |
| $\mu/\bar{x}$ [%] | 0.560 | 0.032 | 0.515 | 0.273 |

***Table 3.12.*** *Statistical analysis of different characteristic parameters from ten experiments under autoignition combustion conditions imposing the same initial and boundary conditions. High load ($F_r$=0.5).*

| $Y_{O_2}$ | 0.23 | | 0.17 | | 0.11 | |
|---|---|---|---|---|---|---|
| $F_r$ | 0.42 | 0.3 | 0.56 | 0.4 | 0.86 | 0.6 |

***Table 3.13.*** *Operating points of Mitakos et al. reproduced in the RCEM of CMT-Motores Térmicos.*

It should be taken into account that the RCEM available at ETH is the most similar to the one available at CMT. However, there are some constructive differences between machines that cause a difference in the combustion chamber volume and in some boundary conditions. The main

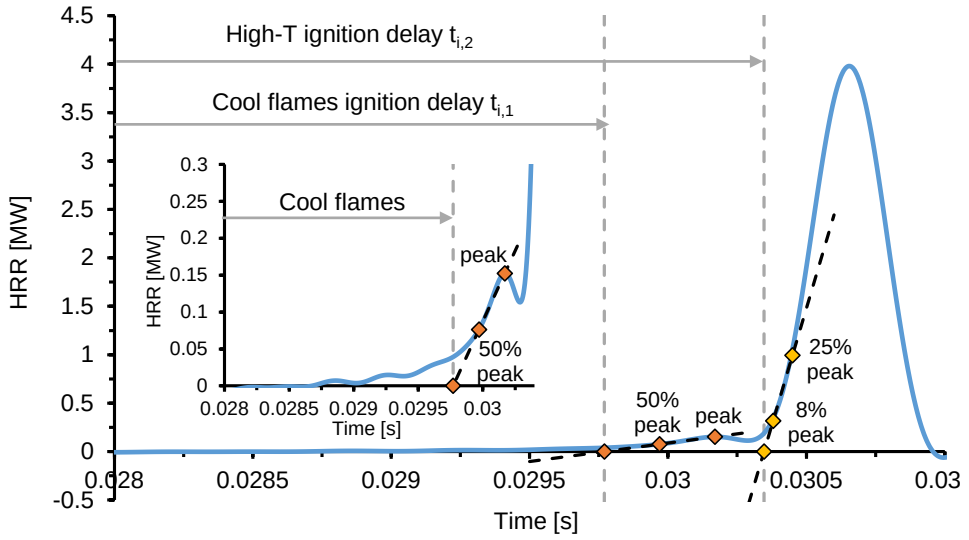


***Figure 3.26.*** *Ignition delay definition. The autoignition of the mixture is considered to be produced when the crossing through zero of a secant line of the HRR occurs.*

differences include the dead volume of the machine (which is higher in the RCEM available at CMT - Motores Térmicos), the heat losses (since the machines are equipped with different heating systems) and the friction forces (which seems to be higher in the RCEM available at CMT - Motores Térmicos, since it is a much newer facility). Therefore, it is not possible to ensure the same pressure and temperature evolutions by reproducing the same initial conditions and command settings.

In Fig. 3.27 the correlation between both RCEMs can be analyzed. The ignition delays obtained with the RCEM of CMT are plotted versus the ignition delays obtained at ETH. The line y = x, which represents a perfect match between values, has been also plotted in the figure. Finally, the coefficient of correlation $R^2$ has been calculated between both machines and it is equal to 0.9069. As can be seen, the trends are perfectly reproduced at CMT. However, there is an offset between both results that is mainly caused by the difference in friction forces between machines. Friction seems to be higher in the RCEM available at CMT - Motores Térmicos because it is equipped with much newer sealing rings. Thus, lower pressure (and, subsequently, lower temperature) is needed to stop the piston during an experiment, defining TDC. Therefore, the in-cylinder temperature and pressure evolution reaches lower

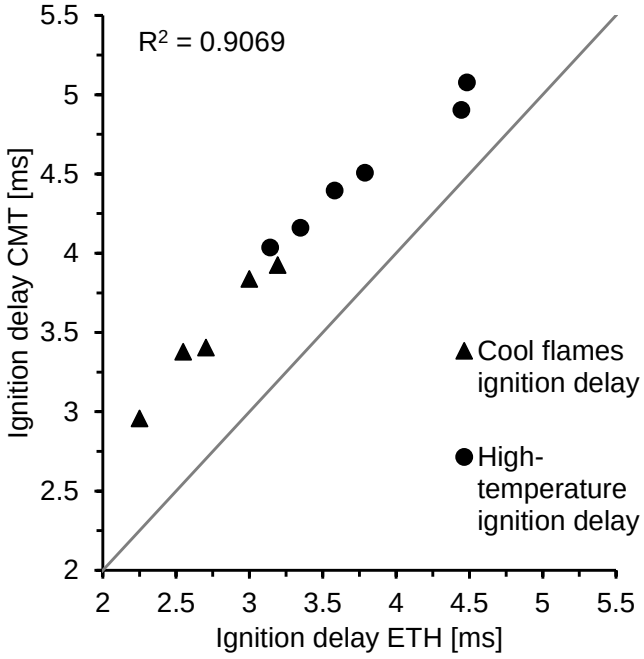


***Figure 3.27.*** *Ignition delays obtained at CMT versus the corresponding values obtained at ETH. The coefficient of correlation between both machines has been calculated and its value is represented in the figure.*

values during the compression, leading to longer compression times and longer ignition delays. However, since friction is almost constant for a given piston velocity, the differences in the temperature evolution are also almost constant, leading to a certain offset in the ignition delay, which is the behavior seen in Fig. 3.27. The machine available at CMT-Motores Térmicos is validated, since the differences in ignition delay are constant for all the experiments and it can be explained by constructive differences between RCEMs.

## 3.B Appendix: Excited OH* sub-model

The excited $OH^*$ sub-model is composed by two blocks of reactions. On the one hand, some reactions of the Curran chemical kinetics mechanism have been modified in order to distinguish the ground state $OH$ from the excited state one ($OH^*$) keeping the specific reaction rates of the original mechanism [21, 22]. On the other hand, the Hall and Petersen sub-model for the $OH^*$

has been taken into account. The specific reaction rate of each reaction can be found in the corresponding reference [29]. All 22 reactions where the $OH^*$ is involved are shown below.

| | Reaction | Reference |
|---|---|---|
| 1 | $CH + O_2 \Leftrightarrow CO + OH^*$ | [29] |
| 2 | $H + O + M \Leftrightarrow OH^* + M$ | [29] |
| 3 | $H + 2OH \Leftrightarrow OH^* + H_2O$ | [29] |
| 4 | $OH^* + Ar \Leftrightarrow OH + Ar$ | [29] |
| 5 | $OH^* + H_2O \Leftrightarrow OH + H_2O$ | [29] |
| 6 | $OH^* + CO_2 \Leftrightarrow OH + CO_2$ | [29] |
| 7 | $OH^* + CO \Leftrightarrow OH + CO$ | [29] |
| 8 | $OH^* + H \Leftrightarrow OH + H$ | [29] |
| 9 | $OH^* + H_2 \Leftrightarrow OH + H_2$ | [29] |
| 10 | $OH^* + O_2 \Leftrightarrow OH + O_2$ | [29] |
| 11 | $OH^* + O \Leftrightarrow OH + O$ | [29] |
| 12 | $OH^* + OH \Leftrightarrow OH + OH$ | [29] |
| 13 | $OH^* + CH_4 \Leftrightarrow OH + CH_4$ | [29] |
| 14 | $OH^* + N_2 \Leftrightarrow OH + N_2$ | [29] |
| 15 | $OH^* \Leftrightarrow OH + hv$ | [29] |
| 16 | $CH_4 + O \Leftrightarrow CH_3 + OH^*$ | [30] |
| 17 | $O + H_2 \Leftrightarrow H + OH^*$ | [30] |
| 18 | $O + H_2O \Leftrightarrow OH + OH^*$ | [30] |
| 19 | $CH_3OH + M \Leftrightarrow CH_3 + OH^* + M$ | [30] |
| 20 | $NH_3 + O \Leftrightarrow NH_2 + OH^*$ | [30] |
| 21 | $HO_2 + O \Leftrightarrow OH^* + O_2$ | [34] |
| 22 | $HO_2 + H \Leftrightarrow OH + OH^*$ | [34] |

# References

[1] Mitakos Dimitrios Angelos, Blomberg Christopher, Wright Yuri M., Obrecht Peter, Schneider Bruno and Boulouchos Konstantinos. "Integration of a cool-flame heat release rate model into a 3-stage ignition model for HCCI applications and different fuels". *SAE Technical Papers 2014-01-1268*, 2014.

[2] Barroso G., Escher A. and Boulouchos K. "Experimental and numerical investigations on HCCI-combustion". *SAE Technical Papers 2005-24-038*, 2005.

[3] Villela A. C. Scardini, Braga S. Leal, Egusquiza J. C. Cuisano and Machado G. Bastos. "Rapid Compression Machine tests for brazilian Otto cycle fuels". *SAE Technical Papers 2011-36-0349*, 2011.

[4] Manasra Salih and Brueggemann Dieter. "Effect of injection pressure and timing on the in-cylinder soot formation characteristics of low CR neat GTL-fueled DI Diesel engine". *SAE Technical Papers 2011-01-2464*, 2011.

[5] Mitakos D., Blomberg C., Vandersickel A., Wright Y., Schneider B. and Boulouchos K. "Ignition delays of different homogeneous fuel-air mixtures in a Rapid Compression Expansion Machine and comparison with a 3-stage-ignition model parametrized on shock tube data". *SAE Technical Papers 2013-01-2625*, 2013.

[6] Egusquiza J. C. Cuisano, Braga S. Leal, Braga C. V. Maciel, Villela A. C. Scardini and Moura N. Reis de. "Experimental investigation of the natural gas / Diesel dual-fuel combustion using a Rapid Compression Machine". *SAE Technical Papers 2011-36-0360*, 2011.

[7] Schlatter Stephanie, Schneider Bruno, Wright Yuri M. and Boulouchos Konstantinos. "Comparative study of ignition systems for lean burn gas engines in an optically accessible Rapid Compression Expansion Machine". *SAE Technical Papers 2013-24-0112*, 2013.

[8] Steinhilber T. and Sattelmayer T. "The effect of water addition on HCCI Diesel combustion". *SAE Technical Papers 2006-01-3321*, 2006.

[9] Pöschl M. and Sattelmayer T. "Influence of temperature inhomogeneities on knocking combustion". *Combustion and Flame*, Vol. 153, pp. 562–573, 2008.

[10] Payri R., Salvador F.J., Gimeno J. and Bracho G. "A new methodology for correcting the signal cumulative phenomenon on injection rate measurements". *Experimental Techniques*, Vol. 32, pp. 46–49, 2008.

[11] Schlatter Stephanie, Schneider Bruno, Wright Yuri and Boulouchos Konstantinos. "Experimental study of ignition and combustion characteristics of a Diesel pilot spray in a lean premixed methane/air charge using a Rapid Compression Expansion Machine". *SAE Technical Papers 2012-01-0825*, 2012.

[12] Gaydon A. G. *The Spectroscopy of Flames*. Chapman and Hall, 1974.

[13] Mastorakos Epaminondas. "Ignition of turbulent non-premixed flames". *Progress in Energy and Combustion Science*, Vol. 35, pp. 57–97, 2009.

[14] Anderlohr J.M., Piperel A., Pires da Cruz A., Bounaceur R., Battin-Leclerc F., Dagaut P. and Montagne X. "Influence of EGR compounds on the oxidation of an HCCI-diesel surrogate". *Proceedings of the Combustion Institute*, Vol. 32, pp. 2851–2859, 2009.

[15] Machrafi Hatim. "Experimental validation of a kinetic multi-component mechanism in a wide HCCI engine operating range for mixtures of n-heptane, iso-octane and toluene: Influence of EGR parameters". *Energy Conversion and Management*, Vol. 49, pp. 2956–2965, 2008.

[16] Frassoldati A, Faravelli T and Ranzi E. "Kinetic modeling of the interactions between NO and hydrocarbons at high temperature". *Combustion and Flame*, Vol. 135, pp. 97–112, 2003.

[17] Herzler J. and Naumann C. "Shock tube study of the influence of NOx on the ignition delay times of natural gas at high pressure". *Combustion Science and Technology*, Vol. 184, pp. 1635–1650, 2012.

[18] Woschni G. "A universally applicable equation for the instantaneous heat transfer coefficient in the internal combustion engine". *SAE Technical Papers 670931*, 1967.

[19] Payri F., Molina S., Martín J. and Armas O. "Influence of measurement errors and estimated parameters on combustion diagnosis". *Applied Thermal Engineering*, Vol. 26, pp. 226–236, 2006.

[20] Benajes J., Olmeda P., Martín J. and Carreño R. "A new methodology for uncertainties characterization in combustion diagnosis and thermodynamic modelling". *Applied Thermal Engineering*, Vol. 71, pp. 389–399, 2014.

[21] Curran H. J., Gaffuri P., Pitz W. J. and Westbrook C. K. "A comprehensive modeling study of n-heptane oxidation". *Combustion and Flame*, Vol. 114, pp. 149–177, 1998.

[22] Curran H. J., Gaffuri P., Pitz W. J. and Westbrook C. K. "A comprehensive modeling study of iso-octane oxidation". *Combustion and Flame*, Vol. 129, pp. 253–280, 2002.

[23] Sjöberg Magnus and Dec John E. "An investigation into lowest acceptable combustion temperatures for hydrocarbon fuels in HCCI engines". *Proceedings of the Combustion Institute*, Vol. 30, pp. 2719–2726, 2005.

[24] Curran H.J., Pitz W.J., Westbrook C.K., Callahan C.V. and Dryer F.L. "Oxidation of automotive primary reference fuels at elevated pressures". *Symposium (International) on Combustion*, Vol. 37, pp. 379–389, 1999.

[25] Sarathy S.M., Westbrook C.K., Mehl M., Pitz W.J., Togbe C., Dagaut P., Wang H., Oehlschlaeger M.A., Niemann U., Seshadri K., Veloo P.S., Ji C., Egolfopoulos F.N. and Lu T. "Comprehensive chemical kinetic modeling of the oxidation of 2-methylalkanes from C7 to C20". *Combustion and Flame*, Vol. 158, pp. 2338–2357, 2011.

[26] Narayanaswamy K., Pepiot P. and Pitsch H. "A chemical mechanism for low to high temperature oxidation of n-dodecane as a component of transportation fuel surrogates". *Combustion and Flame*, Vol. 161, pp. 866–884, 2014.

[27] Pei Y., Mehl M., Liu W., Lu T., Pitz W. J. and Som S. "A multicomponent blend as a Diesel fuel surrogate for compression ignition engine applications". *Journal of Engineering for Gas Turbines and Power*, Vol. 137, pp. 111502–111502, 2015.

[28] Pei Y., Mehl M., Liu W., Lu T.F., Pitz W.J. and Som S. "A multi-component blend as a diesel fuel surrogate for compression ignition engine applications". *Proceedings of the ASME 2014 Internal Combustion Engine Division Fall Technical Conference*, Vol. ICEF2014, 2014.

[29] Hall J. M. and Petersen E. L. "An optimized kinetics model for OH chemiluminescence at high temperatures and atmospheric pressures". *International Journal of Chemical Kinetics*, Vol. 38, pp. 714–724, 2006.

[30] Bamford C. H., Compton R. G. and Tipper C. F. H. *The Formation and Decay of Excited Species*. Elsevier Science, 1st edition, 1969.

[31] Payri F., Margot X., Patouna S., Ravet F. and Funk M. "Use of a single-zone thermodynamic model with detailed chemestry to study a natural gas fueled Homogeneous Charge Compression Ignition engine". *Energy Conversion and Management*, Vol. 53, pp. 298–304, 2012.

[32] Redón P. *Modelling of the nitogen oxides formation process applicable to several diesel combustion modes*. Doctoral Thesis, Universitat Politècnica de València, Valencia (Spain), 2013.

[33] Jerzembeck S., Petersa N., Pepiot-Desjardins P. and Pitsch H. "Laminar burning velocities at high pressure for primary reference fuels and gasoline: Experimental and numerical investigation". *Combustion and flame*, Vol. 156, pp. 292–301, 2009.

[34] Lunt S. T., Marston G. and Wayne R. P. "Formation of $O_2(a^1\Delta_g)$ and vibrational excited OH in the reaction between O atoms and $HO_x$ species". *Journal of the Chemical Society, Faraday Transactions 2: Molecular and Chemical Physics*, Vol. 84(7), pp. 899–912, 1988.

# Chapter 4

# Theoretical and modeling results

## Contents

Theoretical and modeling results derived from this Thesis are shown in this chapter. First, the effects of the different species that can compose the synthetic EGR on the ignition delay are analyzed, including both thermodynamic and chemical effects. Thus, the key species to properly replicate the EGR effects under engine conditions are identified, defining the composition of the synthetic EGR used in this investigation. Afterwards, the theoretical developments of different predictive methods for the ignition delay are described, highlighting the hypotheses and limits of application of each method. Different methods are proposed for the prediction of the ignition delay, since the ignition delay can be referred to different stages of the autoignition process depending on its definition. Predictive methods that cannot be compared to experimental results are validated versus results from chemical kinetic simulations. Finally, the conclusions about the theoretical results are shown.

## 4.1 Design of synthetic EGR for autoignition studies

A method to create synthetic mixtures that simulate the EGR of an internal combustion engine, using $O_2$, $N_2$, $CO_2$, $H_2O$ and Ar, has been designed. Different simplifications of this synthetic EGR have been validated in order to reproduce the ignition delay of the complete mixture. To do so, a parametric study has been carried out in CHEMKIN solving a detailed chemical kinetic mechanism in perfectly stirred reactors, in which the ignition delay of each simplified mixture and the ignition delay of the complete mixture have been simulated for different initial pressures, temperatures, equivalence ratios, oxygen mass fractions and for two different fuels: iso-octane and n-heptane. The results obtained with each simplification have been compared to the results obtained with the complete EGR, and based on this comparison the ignition delay deviations have been calculated. Furthermore, the behavior of the ignition delay deviations with the variation of the different simulation

settings has been analyzed, defining a proper simplified EGR composition to replicate the ignition delay under certain conditions.

The methodology employed in this study was presented in Section 3.3.3, while the parametric study performed was described in Section 3.2.1 (Chapter 3). First, the synthetic EGR is defined, as well as the equations employed to calculate its composition. Then, the simplifications of the complete synthetic EGR considered are shown and justified. Finally, each simplification is compared to the complete mixture and the differences are analyzed. Furthermore, all the information related to the investigation discussed in this section has been published in [1].

### 4.1.1 Definition of the synthetic EGR

As it has been mentioned above, the in-cylinder composition when EGR is present in an engine is intended to be simulated using $O_2$, $N_2$, $CO_2$, $H_2O$ and Ar, which implies that minor compounds as UHC, CO and $NO_x$, are neglected. The influence of such minor components on the ignition delay has been checked in previous studies [2–5]. Despite the fact that UHC, CO, formaldehyde or NO can have a significant effect on the ignition delay, these species have been obviated in this study due to the difficulty implied by adding them to a synthetic EGR mixture. On the one hand, the amount to be added cannot be hardly known for each particular case, since the proportion of these components in the exhaust gases cannot be easily determined. On the other hand, if that amount was known, these species are found at a rate of a few parts per million, so that obtaining a synthetic mixture with such a precise amount would be extremely complex. Thus, the synthetic mixture considered as *real EGR* in the present investigation consists of the products of a complete combustion of a mixture between fuel and dry air with such a proportion of each component so as to achieve the final oxygen mass fraction desired by the user. If the minor compounds of air are neglected (those with volume fractions lower than 0.04%), dry air may be assumed as formed by 20.954% oxygen, 78.112% nitrogen and 0.934% argon (all figures given in molar fractions). For any hydrocarbon with the form $C_nH_mO_p$ the complete combustion reaction with dry air can be written as:

$$C_nH_mO_p + \frac{a_{st}}{\phi} \cdot (O_2 + \frac{0.78112}{0.20954} \cdot N_2 + \frac{0.00934}{0.20954} \cdot Ar) \rightarrow nCO_2 + \\ + \frac{m}{2}H_2O + (\frac{a_{st}}{\phi} - n - \frac{m}{4} + \frac{p}{2})O_2 + \frac{0.78112}{0.20954} \cdot \frac{a_{st}}{\phi}N_2 + \frac{0.00934}{0.20954} \cdot \frac{a_{st}}{\phi}Ar \quad (4.1)$$

where $a_{st} = n + m/4 - p/2$ and $\phi$ represents an auxiliary equivalence ratio, which is used to determine the EGR composition and that is not related to the working equivalence ratio, $F_r$. Obviously, the factor $a_{st}/\phi - n - m/4 + p/2$ is higher than or equal to zero if the auxiliary equivalence ratio is less than or equal to 1, which means that this combustion reaction is only valid for lean mixtures. If it is intended to work with a given molar fraction of oxygen, $X_{O_2}$, the composition of synthetic EGR providing it must satisfy the following equation:

$$X_{O_2} = \frac{\frac{a_{st}}{\phi} - n - \frac{m}{4} + \frac{p}{2}}{4.77236\frac{a_{st}}{\phi} + \frac{m}{4} + \frac{p}{2}} \tag{4.2}$$

where all the terms are known except the necessary auxiliary equivalence ratio, $\phi$. In fact, as it has been mentioned above, $\phi$ is only used to determine the composition of the synthetic EGR and it is by no means related to the working equivalence ratio, $F_r$, that later on will have the fuel + EGR mixture, as described further below. Once this auxiliary equivalence ratio is known, the determination of the composition of the synthetic EGR providing a mixture with the desired oxygen content is quite obvious.

$$X_{CO_2} = \frac{n}{4.77236\frac{a_{st}}{\phi} + \frac{m}{4} + \frac{p}{2}} \tag{4.3}$$

$$X_{H_2O} = \frac{\frac{m}{2}}{4.77236\frac{a_{st}}{\phi} + \frac{m}{4} + \frac{p}{2}} \tag{4.4}$$

$$X_{N_2} = \frac{3.72778\frac{a_{st}}{\phi}}{4.77236\frac{a_{st}}{\phi} + \frac{m}{4} + \frac{p}{2}} \tag{4.5}$$

$$X_{Ar} = \frac{0.04457\frac{a_{st}}{\phi}}{4.77236\frac{a_{st}}{\phi} + \frac{m}{4} + \frac{p}{2}} \tag{4.6}$$

This method to design synthetic EGR is based on obtaining a mixture that satisfies an objective in oxygen molar fraction. When studying the auto-ignition at low temperature conditions (with deficit of $O_2$) it makes much more sense to talk about oxygen molar fractions rather than EGR rates. The same EGR rate, depending on the working equivalence ratio, leads to different amounts of oxygen in the intake and, therefore, to different values of combustion temperature. However, the conditions of the study are perfectly determined if the molar fraction of $O_2$ and the working equivalence ratio are used. Furthermore, since the fuel is not mixed with pure air, but with a blend of air and exhaust gases with a given oxygen molar fraction, it is

necessary to define how to compute the fuel-air ratio. For this purpose, a fuel-to-oxygen ratio defined as $F = m_f/m_{O_2}$ was used. This concept is very useful to study the autoignition process in environments with deficit of oxygen, since it maintains the meaning of the equivalence ratio and, at the same time, it defines, unambiguously, the working amount of fuel. The equivalence ratio is defined in this work as $F_r = F/F_{st}$, where $st$ refers to stoichiometric conditions. Thus, for a certain required equivalence ratio, $F_r$, the amount of fuel is given by:

$$X_f = \frac{X_{O_2} F_r}{a_{st} + X_{O_2} F_r} \tag{4.7}$$

where $X_{O_2}$ is the oxygen molar fraction in the synthetic EGR.

The methodology used to obtain the composition of the fuel-EGR mixture can be summarized as follows: an auxiliary equivalence ratio, $\phi$, is calculated for a desired oxygen molar fraction by using Eq. 4.2. The EGR composition is defined with this auxiliary equivalence ratio and Eqs. 4.3, 4.4, 4.5 and 4.6. The molar fraction of fuel, $X_f$, is calculated for a desired working equivalence ratio, $F_r$, by using Eq. 4.7. Finally, the composition of the fuel-EGR mixture is calculated by $X_{i\ \ mixture} = X_i(1 - X_f)$.

It should be noted that this methodology allows working with very low amounts of oxygen even if very lean mixtures are being studied, which can be non realistic. To check the realism, the EGR rate that corresponds to a certain oxygen molar fraction, $X_{O_2}$, and to a working equivalence ratio, $F_r$, can be estimated by using Eq. (4.8), which should give values below 100%.

$$\%EGR = \frac{X_{O_2\ \ atm} - X_{O_2}}{F_r} \cdot 100 \tag{4.8}$$

Five different types of synthetic EGR have been evaluated: one formed by all the species that compose the products in reaction 4.1 and four simplified mixtures. More specifically, the following mixtures have been tested:

- Mixture formed by $O_2$, $N_2$, $CO_2$, $H_2O$ and Ar: it is called *real EGR* and it is formed by all the species except the minor compounds (NO, CO, UHC and formaldehyde), which have complex reproducibility, as already mentioned before.
- Mixture formed by $O_2$, $N_2$, $CO_2$ and $H_2O$: argon has been obviated because it is, typically, the minor compound of the *real EGR* mixture.

- Mixture formed by $O_2$, $N_2$ and $CO_2$: water has been obviated due to the difficulty in adding it to the mixture. Water is the only species in use that is liquid at ambient conditions, and since its dosage in vapor phase is complex, it is preferable to work with it in liquid phase. This implies that a system is needed for $H_2O$ injection and also for its evaporation. In case of working with a synthetic EGR without water, it would be possible to prepare the mixture more easily with a filling based on partial pressures, since all the components will be in gas phase.

- Mixture formed by $O_2$, $N_2$ and $H_2O$: carbon dioxide has been obviated due to the difficulty in adding it to the mixture when the oxygen content is similar to the atmospheric one. The higher the molar fraction of oxygen, the smaller the amount of $CO_2$ to be added and, therefore, the lower the partial pressure of $CO_2$ in the mixture. Thus, if a filling based on partial pressures is done, it is necessary to have an initial vacuum pressure much lower than the lowest partial pressure of the mixture to avoid unacceptable deviations between the obtained and the desired compositions. Moreover, a high enough resolution in the pressure sensor used to control the filling is needed. Finally, the lower the partial pressure of the minor species, the more relevant the uncertainties associated to a filling based on partial pressures (pressure fluctuations, measurement of dynamic pressure instead of static pressure, transient temperature during the filling, etc). For all these reasons, using $CO_2$ under certain conditions can be really difficult.

- Mixture formed by $O_2$ and $N_2$: it is the simplest form of diluting the amount of oxygen, by using nitrogen, the major component both in the ambient air and in the exhaust gases of an engine.

For each of the four types of mixtures in which some of the species are obviated, the value of the molar fraction of each of these species is added into the molar fraction of nitrogen. Thus, the oxygen ratio desired by the user is conserved.

The validity of each of these mixtures has been checked by comparing their ignition delays with the ignition delays for the *real EGR* mixture, all of them obtained by simulation with CHEMKIN. This comparison has been carried out at different equivalence ratios, oxygen mass fractions, temperatures and pressures, and it has been done with iso-octane and n-heptane.

An ignition delay deviation has been obtained for each case. For each synthetic mixture $i$ at some given conditions of pressure, temperature, equivalence ratio and molar fraction of oxygen, this deviation is calculated

as follows:

$$\xi_i = \frac{\tau_i - \tau_{realEGR}}{\tau_{realEGR}} 100 \tag{4.9}$$

where $realEGR$ corresponds to the mixture formed by $O_2$, $N_2$, $CO_2$, $H_2O$ and Ar.

The behavior of this deviation as a function of different parameters will be analyzed in the following sections. First, how the deviation varies with the initial temperature is studied, as well as the causes of this variation. Then, how it varies with the equivalence ratio and with the oxygen molar fraction of the synthetic mixture will be analyzed.

### 4.1.2 Effect of the initial temperature on the ignition delay deviation

The effect of the initial temperature on the ignition delay deviation is shown in Figs. 4.1 and 4.2. The ignition delay deviation increases when the initial temperature is increased, up to a maximum. The behavior of the deviation with the temperature variation is justified by two effects, a thermodynamic effect and a chemical effect. As will be explained below, both effects cause an opposite behavior on the ignition delay deviation. Thus, a maximum in the ignition delay deviation (a change of trend in the evolution of the error) implies a change in the relevance of the effects. The location of this maximum is affected by the following trends, all of them shown in the figures:

- The higher the equivalence ratio, the higher the initial temperature where this maximum deviation is located. In fact, in some cases this maximum cannot be seen in the explored range.
- The maximum deviation in ignition delay is also displaced to higher initial temperatures when either the pressure (Fig. 4.2) or the oxygen content are increased.
- The initial temperature at which the maximum ignition delay deviation occurs is, for the same conditions, higher for n-heptane than for iso-octane.

Furthermore, these trends can be seen for both fuels and for all types of EGR.

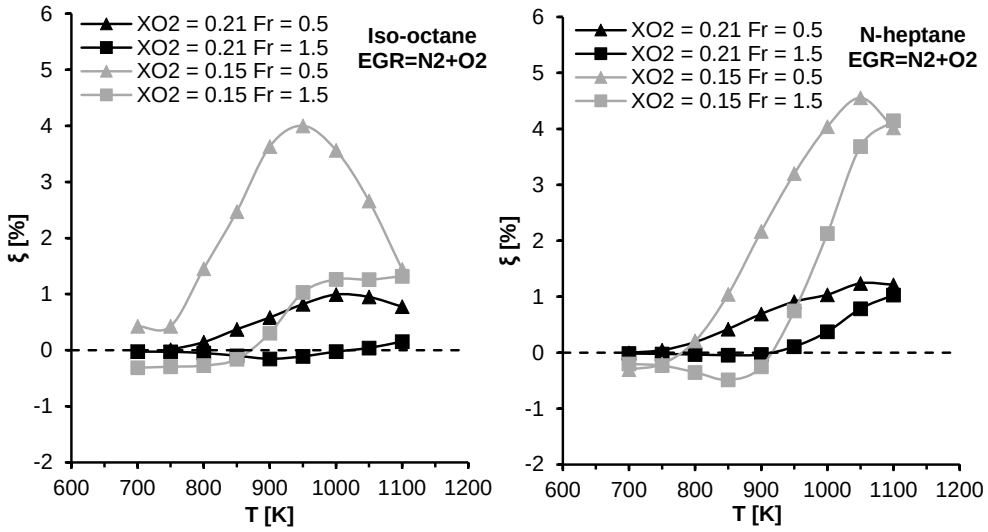


***Figure 4.1.*** *Ignition delay deviation versus temperature at 100 bar, different equivalence ratios and oxygen mass fractions, which have been obtained with an EGR formed by $O_2$ and $N_2$. Left.- Iso-octane. Right.- N-heptane.*

#### 4.1.2.1 Thermodynamic effect

The thermodynamic effect is caused by the heat capacity of the mixture, which is different for each synthetic EGR. A different composition implies different heat capacities, which imply different temperature evolutions during the ignition process. Since a lower heat capacity means less heat sink effect, the mixture with a lower heat capacity also undergoes, obviating chemical aspects, a faster temperature rise. Taking into account the different heat capacities of the different species, Thermodynamics predicts lower ignition delays in those mixtures where $H_2O$ and $CO_2$ are obviated (since both species have higher heat capacity than $N_2$) and longer ignition delays in the mixture where Ar is obviated (since Ar has lower heat capacity than $N_2$). Thus, the ignition delay deviation, $\xi$, will be negative in those mixtures in which $H_2O$ and $CO_2$ are obviated, while it will be positive in the mixture in which Ar is obviated.

On the one hand, the higher the initial temperature, the higher the differences in heat capacities, which causes higher differences in the temperature evolution and, therefore, a higher ignition delay deviation. On the other hand, for a fixed temperature deviation, the higher the initial temperature, the higher the differences in specific reaction rates (due to the

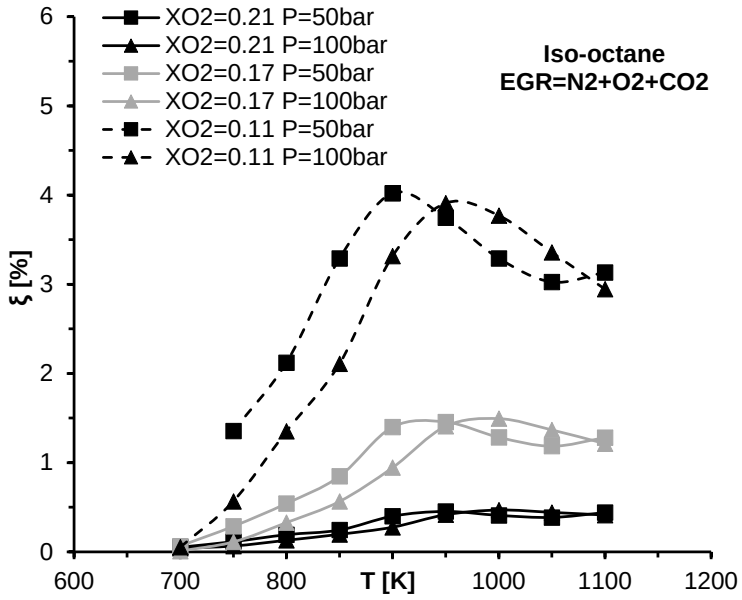


***Figure 4.2.*** *Ignition delay deviation versus temperature for iso-octane at $F_r$=1, different oxygen mass fractions and pressures, which were obtained with an EGR formed by $O_2$+$N_2$+$CO_2$.*

exponential dependency of the specific reaction rate on temperature). Finally, deviations in specific reaction rates can be directly extrapolated to ignition delay deviations. These two behaviors imply that the absolute value of the ignition delay deviation increases with the initial temperature.

Besides, the ignition delay deviation caused by thermodynamic effects is also affected by the duration of the combustion. If the exothermic stage (and, consequently, the temperature rise) occurs in a shorter time interval, the differences in heat capacities become less relevant for the ignition delay.

The consequences of all the thermodynamic effects can be seen in Fig. 4.3, where only Ar is obviated and, therefore, only thermodynamic effects are present. During the low-temperature regime, deviations become more positive as the temperature increases. This is an expected result, since Ar has lower heat capacity than $N_2$ and the differences in heat capacity increase and become more relevant as the temperature increases. Besides, the longer the exothermic stage (when a two-stage ignition pattern occurs or during the NTC regime) the higher the ignition delay deviation. However, once the NTC behavior ends (above a certain temperature), the deviation decreases because the duration of

the combustion is highly reduced, causing a maximum of deviation. Finally, it becomes increasing again, as expected because of the differences in heat capacity already indicated. This behavior is much less pronounced in case of using iso-octane, since this fuel does not present a two-stage ignition pattern (smoother NTC regime). In fact, the maximum of deviation cannot be seen in Fig. 4.3 for iso-octane and an equivalence ratio equal to 1.5.

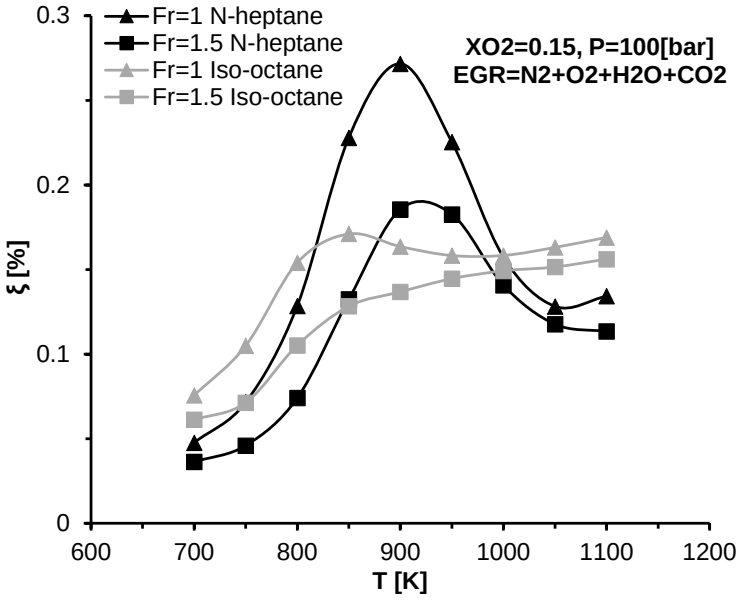


***Figure 4.3.*** *Ignition delay deviation versus temperature at P=100 bar and $X_{O_2}$=0.15 for different fuels and equivalence ratios, which were obtained with an EGR formed by $O_2$+$N_2$+$CO_2$+$H_2O$.*

In summary, regarding the definition of the ignition delay deviation (Eq. 4.9), the impact of the thermodynamic effect on it is very clear:

- If Ar is obviated the deviation becomes more positive as the initial temperature is increased, up to a maximum. Then, the deviation decreases due to the end of the two-stage ignition behavior or the end of the NTC regime. Finally, it increases again, as expected.

- If $H_2O$ or $CO_2$ are obviated, the deviation becomes more negative as the initial temperature is increased, up to a minimum. Then, the deviation becomes less negative due to the end of the two-stage ignition or the

end of the NTC regime. Finally, it becomes more negative again, as expected.

Despite the fact that the thermodynamic behavior is observed in all the range of initial temperatures when only Ar is obviated (Fig. 4.3), since Ar is chemically inert, this behavior is observed only at very low and high temperature when $H_2O$ or $CO_2$ are obviated (Fig. 4.1 and 4.2). To explain the behavior of the ignition delay deviation at medium temperature in these cases, the chemical effect should be also analyzed.

#### 4.1.2.2 Chemical effect

The chemical effect is caused by the differences in the initial concentration of the species when any of the synthetic EGR mixtures are used. A different initial concentration of any species affects the reaction rates and, as a consequence, the relevance of the reactions. All this leads to deviations in the ignition delay.

Only two of the three species that can be obviated in the synthetic EGR are chemically reactive ($CO_2$ and $H_2O$). The effects of each of these species on the ignition delay will be explained from a chemical point of view below. Sensitivity analyses of the most relevant reactions in which the two species mentioned above are involved in have been performed, the results of which are shown in Fig. 4.4. Such reactions have been identified using the Curran's detailed chemical kinetic mechanism for PRF mixtures [6]. A sensitivity analysis of a reaction consists in multiplying the rate constants of this particular reaction by a factor of two (both forward and reverse rates) and then calculating the percent change in ignition delay, as defined by the following equation:

$$Se_R = \frac{\tau_{k_{f/b}\cdot 2} - \tau_{k_{f/b}}}{\tau_{k_{f/b}}} 100 \tag{4.10}$$

where $\tau_{k_{f/b}\cdot 2}$ represents the ignition delay when the specific reaction rates are modified and $\tau_{k_{f/b}}$ represents the original ignition delay. Thus, those reactions affecting the ignition delay more significantly are found between the most relevant reactions that involve $CO_2$ and $H_2O$.

The most relevant reaction for the ignition delay in which $CO_2$ and $H_2O$ are involved in is:

$$H_2O_2 + M \leftrightarrow OH + OH + M \tag{4.11}$$

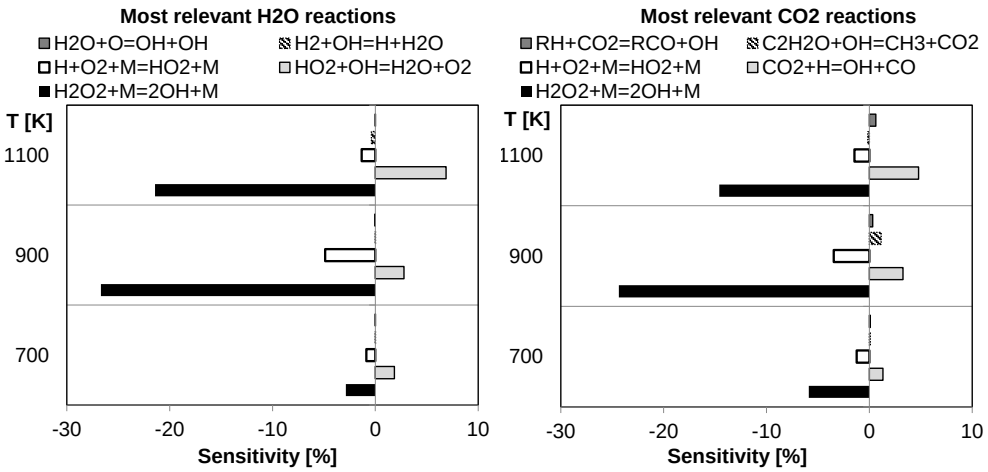


***Figure 4.4.*** *Sensitivity analyses for the most relevant reactions in which $H_2O$ and $CO_2$ are involved in. Simulations have been performed with iso-octane for the real EGR mixture at P=50 bar, $X_{O_2}$=0.15, $F_r$=1 and different initial temperature.*

which is a third body reaction where $M$ can be any non-reactive compound required to stabilize the excited products by colliding with them. The role of $M$ ($H_2$, $H_2O$, CO or $CO_2$, among others) is to remove the excess of energy from the radicals involved in the reaction and, eventually, dissipate it as heat. The reaction rate of a third body reaction can be different depending on the species that acts as $M$. In fact, in case of reaction 4.11 the collision efficiency associated to $H_2O$ is equal to 12 while the corresponding value for $CO_2$ is equal to 3.8. Finally, it should be noted that $H_2O_2$ is one of the key species in the autoignition process, since its decomposition generates the OH radicals that control the start of the high exothermic stage of the combustion.

$CO_2$ and $H_2O$ are, therefore, OH radical generators. This means that while adding $CO_2$ or $H_2O$ increases the heat capacity of the mixture, which would increase the ignition delay, it also generates free radicals, thus reducing this delay. Regarding the definition of the ignition delay deviation (Eq. 4.9), the impact of the chemical effect on it is very clear: the deviation increases (becomes more positive) as the mixture is more simplified. Thereby, the chemical and the thermodynamic effects are opposite when $CO_2$ or $H_2O$ are obviated and the behavior of the ignition delay deviation will depend on the evolution of the relevance of each one.

Reaction 4.11 is not very significant at low temperature due to its lower specific reaction rate (strongly dependent on temperature), while its reaction rate increases at intermediate initial temperature and it becomes less relevant at high initial temperature. This trend of the chemical effect, if combined with the thermodynamic effect, leads to the existence of a maximum in the ignition delay error at high initial temperature (e.g. Fig. 4.2).

The relevance of reaction 4.11 at intermediate initial temperature is caused by two factors. First, the specific reaction rate increases due to the temperature increment with respect to the low temperature range. Secondly, the $H_2O_2$ concentration increases at intermediate temperature due to the appearance of the NTC regime. The NTC regime appears when the formation of carbonylhydroperoxide radicals and their decomposition into active radicals competes with the formation of olefines from the alkyl and alkylhydroperoxide radicals [7]. Such competence causes a reactivity decrease and an increase in the accumulated concentration of $H_2O_2$, promoting the relevance of reaction 4.11. In fact, the global reaction rate of the ignition process at the end of the NTC region is controlled by reaction 4.11 [8].

At high initial temperature the reaction rate of 4.11 is found to decrease. This is solely due to the lower concentration of $H_2O_2$, since the concentrations of $CO_2$ and $H_2O$ before auto-ignition are approximately the same regardless of the initial temperature. Lower concentration of $H_2O_2$ is reached at high initial temperature for two reasons:

- $H_2O_2$ dissociation. Dissociation of hydrogen peroxide occurs at temperature of the order of the auto-ignition temperature but with a much shorter characteristic time than the ignition delay, thus being an important mechanism of $H_2O_2$ destruction. This dissociation generates also active radicals, and consequently the ignition delay is shortened approximately to the same extent as with reaction 4.11. However, if the hydrogen peroxide dissociates, its reaction with $CO_2$ and $H_2O$ becomes less relevant and the effect of both species is not so important at high initial temperature.

- Lower $H_2O_2$ generation. Hydrogen peroxide is generated by $HO_2$, mainly by the following reaction:

$$HO_2 + HO_2 \leftrightarrow H_2O_2 + O_2 \tag{4.12}$$

  At high temperature, the fuel not only suffers dehydrogenation by means of active radicals ($O_2$, $HO_2$ or OH), but it also disappears by unimolecular decomposition in alkyl radicals ($C_nH_{2n+1}$) and other

hydrocarbon chains of lower molecular weight (thermal cracking) [8]. Thereby, $CH_3$ concentration increases at high initial temperature, promoting the relevance of reaction 4.13:

$$CH_3 + HO_2 \leftrightarrow CH_3O + OH \tag{4.13}$$

The $CH_3$ affinity for $HO_2$ causes a lower formation rate of $H_2O_2$, and its reaction with $CO_2$ and $H_2O$ becomes less relevant.

For these reasons, obviating $CO_2$ or $H_2O$ has a very important effect on the medium-temperature range, but a lower one at high temperature.

The sensitivity analyses presented in Fig. 4.4 show that the following third body reaction has also an influence on the ignition delay (although much less than reaction 4.11) .

$$H + O_2 + M \leftrightarrow HO_2 + M \tag{4.14}$$

where $M$ has enhanced collision efficiencies for $H_2O$ (equal to 12) and $CO_2$ (equal to 3.8), among others. Hydrogen from the fuel dehydrogenation process and molecular oxygen react with $CO_2$ and $H_2O$ to form the active radical $HO_2$. An increment in the concentration of $HO_2$ leads to a faster decomposition of the fuel and, therefore, to a shorter ignition delay. Therefore, if $CO_2$ or $H_2O$ are obviated, longer ignition delays are obtained. This means that the effect of reaction 4.14 is the same as the effect of reaction 4.11. In fact, both lose their relevance at high initial temperature due to the thermal cracking of the fuel. The higher the thermal cracking, the lower the relevance of the low-temperature chain branching mechanism, in which reaction 4.14 is involved.

The chemical effects of $H_2O$ do not only come from reactions 4.11 and 4.14. $H_2O$ is able to generate OH radicals by means of the following reaction:

$$HO_2 + OH \leftrightarrow H_2O + O_2 \tag{4.15}$$

which is important in the forward direction, i.e., acting as a sink of OH radicals and, therefore, leading to longer ignition delays if its specific reaction rate is enhanced, as shown in Fig. 4.4. If $H_2O$ is obviated, the forward reaction rate of reaction 4.15 is enhanced and longer ignition delays are obtained, leading to more positive deviations (same effect as reaction 4.11). However, the sensitivity analysis shows that reaction 4.15 has not an impact on ignition delay as relevant as reaction 4.11.

The chemical effects of $CO_2$ do not only come from reactions 4.11 and 4.14. $CO_2$ destruction can be seen at temperatures where $CO_2$ dissociation is not relevant. This is caused by reactions as:

$$C_nH_{2n+1} + CO_2 \leftrightarrow C_nH_{2n}CO + OH \tag{4.16}$$

and

$$CO_2 + H \leftrightarrow OH + CO \tag{4.17}$$

On the one hand, the sensitivity analysis shows that reaction 4.16 has not a relevant impact on ignition delay. On the other hand, reaction 4.17, which is a well known CO oxidation path, affects the ignition delay by competing with the h-abstraction of the fuel [2, 5, 9, 10] and, therefore, leading to longer ignition delays if its specific reaction rate is enhanced. Thus, if $CO_2$ is obviated, reaction 4.17 becomes less relevant, leading to shorter ignition delays and more negative deviations, which is the opposite trend than the showed by reaction 4.11. Therefore, the effect of obviating $H_2O$ is more relevant than the effect of obviating $CO_2$, since more enhanced collision efficiency is considered for $H_2O$ in reactions 4.11 and 4.14. Besides, reaction 4.17 shows an opposite effect on the ignition delay deviation than reactions 4.11 and 4.14, thus reducing the $CO_2$ relevance.

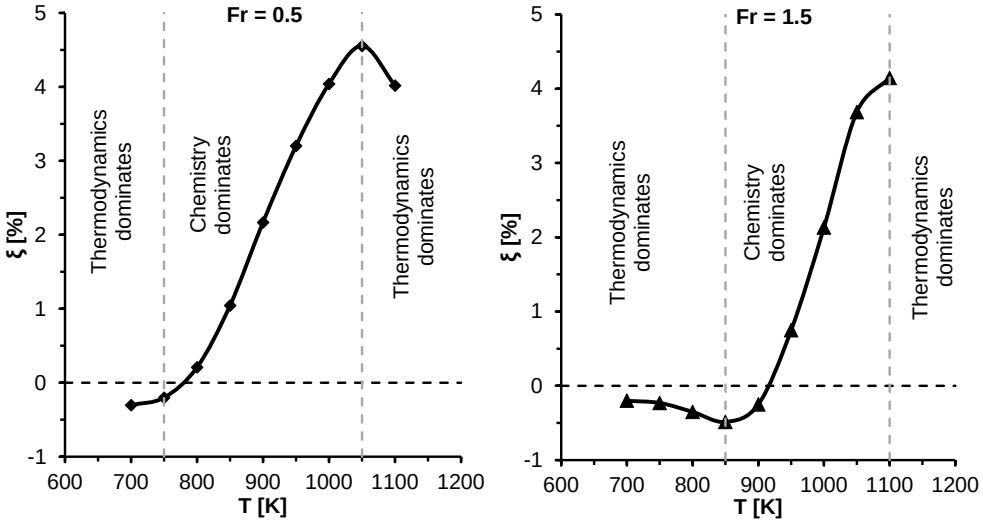


***Figure 4.5.*** *Ignition delay deviation versus temperature for n-heptane at 100 bar and $X_{O_2}$=0.1, which have been obtained with an EGR formed by $O_2$ and $N_2$. Left.- $F_r$=0.5. Right.- $F_r$=1.5.*

A summary of the combination of both the thermodynamic and the chemical effects can be seen in Fig. 4.5, where the different behaviors of the ignition delay deviation, caused by obviating both $CO_2$ and $H_2O$, are reflected for the EGR mixture composed by $N_2$+$O_2$. At low temperature, the figure shows that the effect of the heat capacity is the dominant one.

Consequently, the ignition delay of the simplified mixture is shorter than the ignition delay of the *real EGR* and, therefore, ignition delay deviations are negative. Furthermore, the higher the initial temperature, the higher this thermodynamic effect and the more negative the deviations (Fig. 4.5 to the right). A change of trend in the ignition delay deviation can be seen at a certain temperature. This is caused by the higher relevance of the chemical effects in the medium-temperature range. Now, reactions in which $H_2O$ and $CO_2$ are involved shorten the auto-ignition time. Consequently, the ignition delay of the simplified mixture is longer and the deviation becomes positive and increases with the initial temperature. However, a new change of trend in the error can be seen at high temperature. This change is caused by the gradual loss in importance of the chemistry of $H_2O$ and $CO_2$ (especially of the former), caused by a lower formation of $H_2O_2$ in favor of the reaction of $HO_2$ with $CH_3$, and by a higher $H_2O_2$ dissociation. Thus, thermodynamic effects become dominant again and the ignition delay deviations start going to negative values (Fig. 4.5 to the left), leading to a maximum in the deviation versus temperature plots. These thermodynamic and chemical effects are coherent with those exposed by Fathi et al. [11], Di et al. [12], Sjöberg and Dec [13] and Wooldridge et al. [14].

As can be seen in Fig. 4.1, the maximum ignition delay deviations are slightly higher for n-heptane than for iso-octane. A more pronounced NTC zone implies a higher accumulated concentration of $H_2O_2$ under the same initial conditions, which promotes the relevance of the chemical effect and leads to higher ignition delay deviations. Therefore, obviating $H_2O$ or $CO_2$ has a bigger impact on the autoignition process in the case of n-heptane than in the case of iso-octane.

There is not any relevant chemical interaction between $H_2O$ and $CO_2$. However, the prediction accuracy is substantially improved when both species are added. This is caused by the thermodynamic effect of the EGR on the ignition delay. Due to the absence of relevant chemical interactions between both species, the chemical improvement obtained when both species are added is equal to the sum of the improvements. However, due to the exponential dependency of the specific reaction rate on temperature, the thermodynamic improvement obtained when both species are added is higher than the sum of the improvements. Thus, a synergistic effect appears when $H_2O$ and $CO_2$ are both taken into account.

### 4.1.3 Effect of the equivalence ratio and the oxygen molar fraction on the ignition delay deviation

The ignition delay deviation becomes more negative when the equivalence ratio is increased, crossing the zero value. The crossing through zero is caused by a balance between chemical and thermodynamic effects, for these specific conditions. As it can been seen in Fig. 4.6, the location of the zero crossing exhibits the following trends:

- The equivalence ratio at which the crossing by zero occurs increases if the initial temperature is increased.
- The equivalence ratio at which the crossing by zero occurs increases if the pressure is decreased.
- The equivalence ratio at which the crossing by zero occurs increases if the oxygen content is decreased.

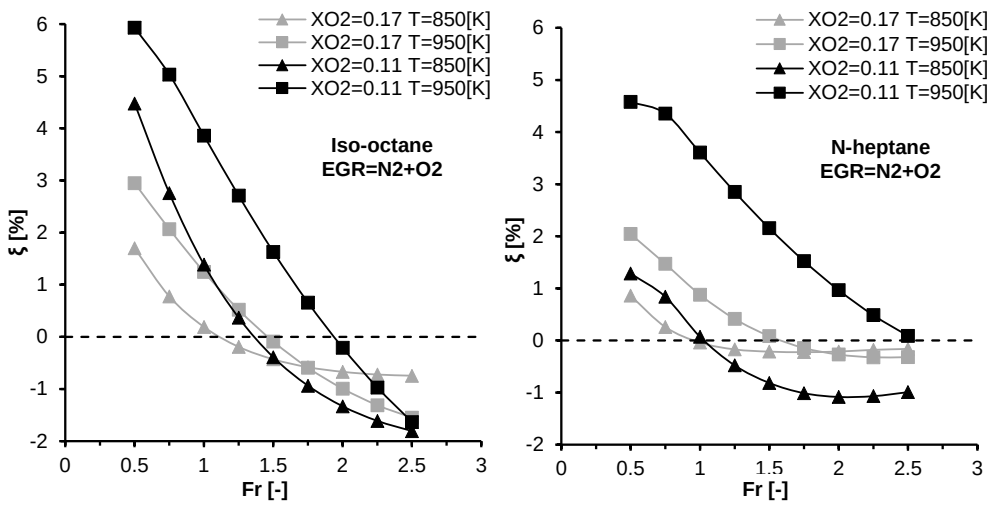


***Figure 4.6.*** *Ignition delay deviation versus equivalence ratio at 100 bar, different initial temperatures and oxygen molar fractions. The EGR is formed by $O_2$ + $N_2$. Left.- Iso-octane. Right.- N-heptane.*

Fig. 4.6 also shows that the chemical effect is dominant for lean mixtures, while the richer the equivalence ratio, the more relevant the thermodynamic effect. In the explored range, the chain branching is dependent on radical

species formed directly from the fuel, which causes rich mixtures to be more reactive [8]. Thus, the NTC zone becomes less pronounced if the equivalence ratio is increased and a smoother NTC regime implies lower accumulated concentration of $H_2O_2$ and, therefore, lower relevance of the chemical effects.

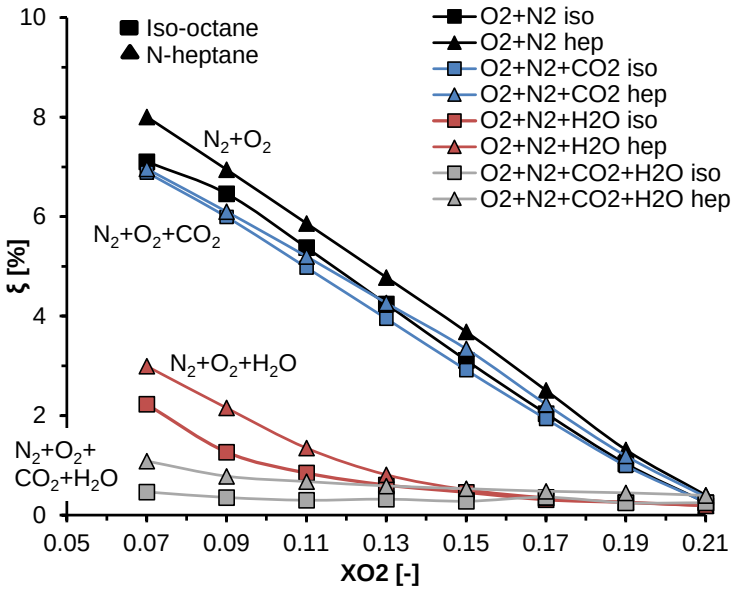


***Figure 4.7.*** *Maximum ignition delay deviation versus oxygen molar fraction. This is represented for the four simplified mixtures and for both fuels.*

The ignition delay deviation increases when the oxygen ratio is decreased, as seen in Fig. 4.7. Obviously, the more diluted the mixture, the higher the differences between the mole fractions of the different species between one or another type of synthetic EGR. And the more simplified the EGR composition, the higher the ignition delay deviation.

Fig. 4.7 also shows that the prediction accuracy is substantially improved when $CO_2$ and $H_2O$ are added. Moreover, while the effects of $CO_2$ are insignificant, it can be clearly seen that $H_2O$ is the key species to reproduce the *real EGR* and its effects are the most important ones.

### 4.1.4 Criterion to select the EGR composition

Based on Fig. 4.7, the ranges of use of one or another type of synthetic EGR, depending on the desired oxygen mole fraction, can be defined.

Establishing that an ignition delay deviation higher than 1% is not admissible, the following global intervals were obtained for the two fuels tested:

- Mixture formed by $N_2 + O_2$: it is valid for oxygen molar fractions higher than or equal to 0.205.
- Mixture formed by $N_2 + O_2 + CO_2$: it is valid for oxygen molar fractions higher than or equal to 0.20.
- Mixture formed by $N_2 + O_2 + H_2O$: it is valid for oxygen molar fractions higher than or equal to 0.12 if the fuel used is n-heptane and higher than or equal to 0.10 if the fuel used is iso-octane.
- Mixture formed by $N_2 + O_2 + CO_2 + H_2O$: in case of using iso-octane, it is valid for all the oxygen molar fractions simulated. In case of using n-heptane, it is valid for oxygen molar fractions higher than or equal to 0.07.

The criterion adopted here ($\xi \leqslant 1\%$) to give validity to each of the studied simplifications is completely arbitrary. This is a relatively strict criterion, but serves as a reference to select one synthetic mixture or another, ensuring that reality is accurately reproduced. In fact, setting any other deviation limit, the new ranges of use can be obtained from Fig. 4.7.

As expected, the smallest deviation is obtained in the EGR formed by $O_2 + N_2 + CO_2 + H_2O$, and it increases as additional species are obviated. As a consequence the highest deviation is found in the mixture formed by $O_2$+$N_2$. In fact, argon can be obviated if the oxygen molar fractions is less than or equal to 0.07 without exceeding 1% in the ignition delay deviation.

## 4.2 Theoretical development of an alternative procedure to predict ignition delays

The theoretical aspects related to the development of alternative methods to predict the ignition delay under transient thermodynamic conditions are described in this section. It should be noted that different definitions of the ignition event lead to ignition delays referred to different stages of the process. Therefore, the validity of the hypotheses assumed by a certain predictive method can change when the criterion for ignition is modified, which causes that several methods should be developed depending on the ignition delay definition.

Specifically, three different ignition times under transient conditions want to be predicted in this investigation: referred to a critical concentration of chain carriers, $t_{i,CC}$, referred to cool flames, $t_{i,1}$, and referred to the high-temperature exothermic stage of the combustion process, $t_{i,2}$, the two later referred to a maximum pressure rise rate. To do so, several ignition delays have been used in the theoretical developments, the definitions of which are the following:

- $\tau_{CC}$ is the ignition delay under constant thermodynamic conditions referred to the critical concentration of chain carriers.
- $\tau_1$ is the ignition delay under constant thermodynamic conditions referred to the maximum pressure rise caused by cool flames.
- $\tau_2$ is the ignition delay under constant thermodynamic conditions referred to the maximum pressure rise caused by the high-temperature stage of the combustion process.

Moreover, expressions to characterize the temporal evolution of the concentration of chain carriers, as well as the critical concentration of active radicals and the ignition delay under constant thermodynamic conditions, will be obtained. Finally, the alternative predictive procedures will be linked to the classic Livengood & Wu integral [15], highlighting the hypotheses assumed to obtain each expression. Furthermore, the information related to the investigation discussed in this section has been already published in [16–18].

### 4.2.1 Prediction of an ignition delay referred to a critical concentration of chain carriers

New expressions to predict ignition delays referred to a critical concentration of chain carriers have been developed starting from the Glassman's model for autoignition [19].

The Glassman's model is a simple model to characterize the autoignition phenomenon by a chain reactions mechanism. It is composed by the five following reactions:

$$R \xrightarrow{k_1} CC \tag{R1}$$

$$R + CC \xrightarrow{k_2} \alpha CC + R' \tag{R2}$$

$$R + CC \xrightarrow{k_3} CC + P \tag{R3}$$

$$R + CC \xrightarrow{k_4} P' \tag{R4}$$

$$CC \xrightarrow{k_5} P'' \tag{R5}$$

where R and R' represent the reactants, CC represents the chain carriers, P and P' represent the main products of the combustion process and P" represents the partially oxidized products such as those formed by wall effects. In this model, reaction R1 corresponds to the initiation reaction, R2 is the chain reaction that promotes the progression of the autoignition process by the generation of chain carriers, R3 is the propagation reaction and, finally, R4 and R5 correspond to the termination reactions: whereas in R4 the other main product of the combustion is generated, in reaction R5 partially oxidized products are formed due to an incomplete combustion because of lack of oxygen or quenching caused by wall effects.

Assuming the autoignition of a homogeneous mixture, the generation rate of the main products P and P' must stretch to infinity when the combustion starts. Under these conditions, the generation rate of the chain carriers CC must stretch to minus infinity (it has to be a disappearance rate). Since during the ignition delay there is a generation rate of chain carriers, which becomes a disappearance rate when combustion starts, ignition must happen when a maximum of concentration of chain carriers occurs. This maximum is known as critical concentration. With this concept, the autoignition delay phenomenon can be described as the accumulation of active radicals thanks to chain reactions, until a critical concentration is reached, instant at which the ignition occurs.

The generation rate of chain carriers has the following expression according to the Glassman's model:

$$\frac{d[CC]}{dt} = k_1[R] + (k_2(\alpha - 1) - k_4)[R][CC] - k_5[CC] \tag{4.18}$$

The chemical kinetic mechanism will be a chain reactions mechanism if reaction R2 introduces a multiplier effect on the generation of chain carriers. This means that the global generation rate of chain carriers must be higher than the generation rate corresponding to the initiation reaction. Imposing this condition on equation 4.18, there is a critical value of $\alpha$ from which reaction R2 is characterized as a chain reaction.

$$\alpha_{crit} = 1 + \frac{k_4[R] + k_5}{k_2[R]} \tag{4.19}$$

If $\alpha$ is written as $\alpha = \alpha_{crit} + \Delta\alpha$, then, equation 4.18 can be rewritten as follows:

$$\frac{d[CC]}{dt} = k_1[R] + \Delta\alpha k_2[R][CC] \tag{4.20}$$

Assuming that the concentration of chain carriers is always much smaller than the initial concentration of reactants, $[CC] \ll [R]$, $[R]$ can be considered as a constant during the ignition delay period. Considering an air-fuel mixture under constant conditions of temperature and pressure, the previous differential equation can be integrated with the initial condition $t = 0 \rightarrow [CC] = 0$ as follows:

$$exp\left(tk_2\Delta\alpha[R]\right) = 1 + [CC]\frac{k_2}{k_1}\Delta\alpha \tag{4.21}$$

where $\frac{1}{k_2\Delta\alpha[R]}$ is a characteristic time of the process and, therefore, it may be an estimator of the ignition delay referred to a critical concentration of chain carriers. Thus:

$$\tau_{CC} = \frac{1}{k_2\Delta\alpha[R]} \tag{4.22}$$

According to the above definition, Eq. 4.21 can be rewritten as follows:

$$exp\left(\frac{t}{\tau_{CC}}\right) = 1 + \frac{[CC]}{k_1[R]\tau_{CC}} \tag{4.23}$$

Thereby, when $t = \tau_{CC}$ the start of combustion occurs and the concentration of chain carriers is equal to the critical concentration. In this way, the critical concentration of active radicals can be defined by the following expression obtained from Eq. 4.23:

$$[CC]_{crit} = (e-1)k_1[R]\tau_{CC} = (e-1)\frac{k_1}{k_2\Delta\alpha} \tag{4.24}$$

Eq. 4.24 can be combined with Eq. 4.23 in order to obtain an expression for the temporal evolution of the concentration of chain carriers that depends only on the ignition delay and the critical concentration:

$$exp\left(\frac{t}{\tau_{CC}}\right) = 1 + \frac{[CC]}{[CC]_{crit}}(e-1) \tag{4.25}$$

or:

$$[CC] = \frac{[CC]_{crit}}{(e-1)} \left( exp\left(\frac{t}{\tau_{CC}}\right) - 1 \right) \tag{4.26}$$

Equation that is only valid under constant conditions of pressure and temperature.

It should be noted that ignition represents a discontinuity in the model. In fact, the expression deduced for the generation rate of chain carriers loses its validity when ignition occurs: this reaction rate suffers a discontinuity and the fast decomposition of the fuel by the consumption of active radicals starts. Thus, although ignition happens when a maximum concentration of chain carriers occurs (the critical concentration), the generation rate of chain carriers predicted by the model at this instant is not equal to zero.

The ignition delay, $\tau_{CC}$, and the critical concentration of chain carriers, $[CC]_{crit}$, can be correlated by Eq. 4.22 and Eq. 4.24, respectively. All the specific reaction rates and the value of $\Delta\alpha$ have to be adjusted for each fuel. Thus, the effect of pressure and temperature will be taken into account by the characterization of each specific reaction rate. The effect of the equivalence ratio will be taken into account with the concentration of fuel, $[R]$. Finally, the effect of the EGR rate cannot be directly taken into account since the Glassman's model does not consider the oxygen concentration. However, the EGR rate can be reflected in $\alpha$ since the multiplier effect of the chain carriers depends, in some way, on the concentration of oxygen.

#### 4.2.1.1 Method based on the Relative Concentration of Chain Carriers (RCCC)

As it is explained in the first theoretical development, Eq. 4.26 represents an expression for the time evolution of the concentration of chain carriers obtained from the Glassman's model. But it should be taken into account that this expression is only valid during the ignition delay and under constant temperature and pressure conditions. However, a process under transient thermodynamic conditions can be discretized as a series of thermodynamic states that remain constant for a time $\Delta t$. Thus, the working air-fuel mixture that has a concentration of chain carriers $[CC]_j$ at instant $j$ would reach the same concentration of active radicals by staying at constant pressure $P_j$ and constant temperature $T_j$ during a time $t_{P_j,T_j}$ obtained from Eq. 4.26:

$$t_{P_j,T_j} = \tau_{CC,j} ln\left(1 + \frac{[CC]_j}{[CC]_{crit,j}}(e-1)\right) \tag{4.27}$$

Therefore, if the working air-fuel mixture stay under constant conditions $P_j$, $T_j$ for a time $\Delta t$, the concentration of chain carriers will be the amount of active radicals accumulated at time $j$ plus the amount of active radicals generated from time $t_{P_j,T_j}$ to time $t_{P_j,T_j} + \Delta t$ following Eq. 4.26. Thus, the concentration of chain carriers at time $j+1$ can be obtained from the data at time $j$ by the following equation:

$$[CC]_{j+1} = \left(\frac{[CC]_{crit,j}}{e-1}\left(exp\left(\frac{t_{P_j,T_j} + \Delta t}{\tau_{CC,j}}\right) - 1\right)\right) \tag{4.28}$$

which results in the following equation regarding the expression $t_{P_j,T_j}$ (Eq. 4.27):

$$[CC]_{j+1} = \left(\frac{[CC]_{crit,j}}{e-1} + [CC]_j\right) exp\left(\frac{\Delta t}{\tau_{CC,j}}\right) - \frac{[CC]_{crit,j}}{e-1} \tag{4.29}$$

If $RCCC_j$ is defined as the ratio between the concentration of chain carriers and the critical concentration (Relative Concentration of Chain Carriers) at instant $j$ ($RCCC_j = [CC]_j/[CC]_{crit,j}$), the autoignition will occur when $RCCC_j = 1$ and Eq. 4.29 can be rewritten as follows by dividing the equality by $[CC]_{crit,j}$:

$$RCCC_{j+1} = \frac{[CC]_{crit,j}}{[CC]_{crit,j+1}}\left(\left(\frac{1}{e-1} + RCCC_j\right) exp\left(\frac{\Delta t}{\tau_{CC,j}}\right) - \frac{1}{e-1}\right) \tag{4.30}$$

This new method to obtain ignition delays under variable conditions is defined as follows: if the evolution of pressure and temperature is known, the evolution of the ignition delay, $\tau_{CC}$, and the evolution of the critical concentration, $[CC]_{crit}$, under constant conditions for each thermodynamic state can be obtained. With them, the evolution of the parameter $RCCC$ can be calculated. Finally, when $RCCC_j = 1$, this instant $j$ will correspond to the ignition time and the ignition delay referred to a critical concentration of chain carriers will be found.

It should be noted that a wide database of critical concentrations and ignition delays under constant conditions is easily obtainable with a detailed

chemical kinetic mechanism, which is impossible to be used in complex CFD calculations. This database linked to Eq. 4.30 allows obtaining ignition delays under variable conditions without spending too much computing time in solving complex chemical kinetics mechanisms.

#### 4.2.1.2 Simplification to a global zero-order reaction

In order to simplify the accumulation rate of chain carriers to a zero-order reaction, the exponential term in Eq. 4.23 can be approximated by a Taylor series expansion. The series can be truncated in the second term, since $\frac{t}{\tau_{CC}} < 1$ during the ignition delay, and Eq. 4.23 can be rewritten as follows:

$$[CC] = k_1[R]t \tag{4.31}$$

Eq. 4.31 implies that, under constant thermodynamic conditions, $d[CC]/dt = k_1[R] = constant$, i.e., the accumulation rate of chain carriers corresponds to a zero-order reaction. When $t = \tau_{CC}$ the concentration of chain carriers is equal to the critical concentration and the previous equation can be rewritten as follows:

$$[CC] = [CC]_{crit}\frac{t}{\tau_{CC}} \tag{4.32}$$

equation that is only valid under constant conditions of pressure and temperature.

Finally, it should be mentioned that analogous expressions to Eq. 4.32 can be obtained by performing the same theoretical development in other autoignition schemes. For instance, Eq. 4.32 can be similarly obtained starting from the Müller, Peters and Liñán's model [20], as explained in Appendix 4.A.

If a process under transient conditions of pressure and temperature is discretized as a series of thermodynamic states that remain constant during a time $dt$, Eq. 4.32 can be also discretized to obtain the evolution of the chain carriers concentration during such time interval $dt$:

$$d[CC] = \frac{[CC]_{crit}}{\tau_{CC}}dt \tag{4.33}$$

And Eq. 4.33 can be integrated during the process from the initial point ($[CC] = 0$, $t = 0$) up to the ignition time ($[CC] = [CC]_{crit}$, $t = t_{i,CC}$) as follows:

$$\int_0^{[CC]_{crit,t_{i,CC}}} d[CC] = \int_0^{t_{i,CC}} \frac{[CC]_{crit}}{\tau_{CC}} dt$$
$$1 = \frac{1}{[CC]_{crit,t_{i,CC}}} \int_0^{t_{i,CC}} \frac{[CC]_{crit}}{\tau_{CC}} dt \tag{4.34}$$

where $t_{i,CC}$ is the ignition delay of the process referred to a critical concentration of chain carriers, and $\tau_{CC}$ and $[CC]_{crit}$ are the ignition delay and the critical concentration of chain carriers under constant conditions of pressure and temperature for the successive thermodynamic states, respectively. Thus, the ignition delay can be obtained by calculating the upper limit of integration that satisfy Eq. 4.34. It should be noted that if the critical concentration of chain carriers is considered as a constant, Eq. 4.34 results in the Livengood & Wu integral [15].

Whereas the Livengood & Wu integral method assumes that the critical concentration of chain carriers is constant and the production rate of active radicals can be assumed as a zero-order reaction, the new integral proposed in this Thesis does not consider the critical concentration to be constant anymore, but still assumes a zero-order reaction for the chain carriers. Finally, the RCCC-method discards both hypotheses, which might lead to more accurate predictions but with a more complex numerical method.

### 4.2.2 Prediction of cool flames

A predictive method for ignition delays under transient conditions referred to cool flames is proposed in this section. This method is based on the accumulation of chain carriers up to reach a maximum of concentration, which should occur at the same time than cool flames. As explained in detail above, assuming that during the ignition delay the termination reactions are not very important and that $[R] >> [CC]$ (where $R$ represents the fuel and $CC$ represents the chain carriers), Eq. 4.34 can be obtained for the prediction of an ignition delay referred to a critical concentration of chain carriers, $t_{i,CC}$.

Despite the fact that Eq. 4.34 represents a method to predict ignition delays, only times of ignition referred to a critical concentration of chain carriers can be obtained. Therefore, the high exothermic stage of the process cannot be predicted, since the maximum heat release rate occurs after reaching the critical concentration of chain carriers. However, as can be seen in Fig. 4.8, a maximum in concentration of $HO_2$ is reached at the same time where the maximum pressure rise rate of cool flames occurs. Therefore, the cool

flames time can be predicted by taking into account $HO_2$ as chain carrier ($CC = HO_2$), since it seems to be a good tracer of such phenomenon.

Finally, a schematic of Eq. 4.34 can be also seen in Fig. 4.8. The accumulation behavior of $HO_2$ is modeled by the accumulated area of Eq. 4.34, by using the $\tau_{CC}$ and $[CC]_{crit}$ functions related to this species. Once the value of 1 is reached, the time at which the maximum concentration of $HO_2$ occurs is predicted and, therefore, the ignition delay referred to cool flames is obtained. It should be noted that the critical concentration of chain carriers is one order of magnitude lower than the initial amount of fuel, which is one of the hypotheses assumed in order to integrate Eq. 4.20. Besides, Fig. 4.8 B also shows that the $\tau_{HO_2}$ function increases from $t \approx 0.022\ s$ up to $t \approx 0.023\ s$, where it decreases again. This behavior is related to the transition from a two-stage ignition pattern to a single-stage ignition. In this case, the absence of cool flames leads to longer ignition delays referred to a critical concentration of $HO_2$, since the $HO_2$ peak related to cool flames does not exist.

### 4.2.3 Prediction of the high-temperature stage

A new procedure that intends to predict the ignition delay referred to the high-temperature exothermic stage of the autoignition process is developed in this section. Models based on a critical concentration of chain carriers are not able to accurately predict exothermic stages, since the critical concentration of chain carriers is reached before the sudden heat release rate. Thus, alternative procedures should be proposed, since exothermic stages are the ones with practical interest and also the only ones that can be easily measured in experiments.

Ignition delays referred to a maximum pressure rise occur once all chain carriers have disappeared. Besides, the accumulative behavior of the chain carriers and the time at which the critical concentration is reached can be predicted for a certain evolution of pressure and temperature by Eq. 4.34. Therefore, it is possible to study the decomposition of chain carriers from $t_{i,CC}$ and, thus, to obtain the ignition delay under transient thermodynamic conditions referred to the maximum pressure rise rate, $t_{i,2}$.

Starting from the Glassman's model for autoignition [19], the global disappearance rate of chain carriers, $[CC]$, can be written as:

$$\frac{d[CC]}{dt} = k_1[R] + ((k_2(\alpha - 1) - k_4)[R] - k_5)[CC] \tag{4.35}$$

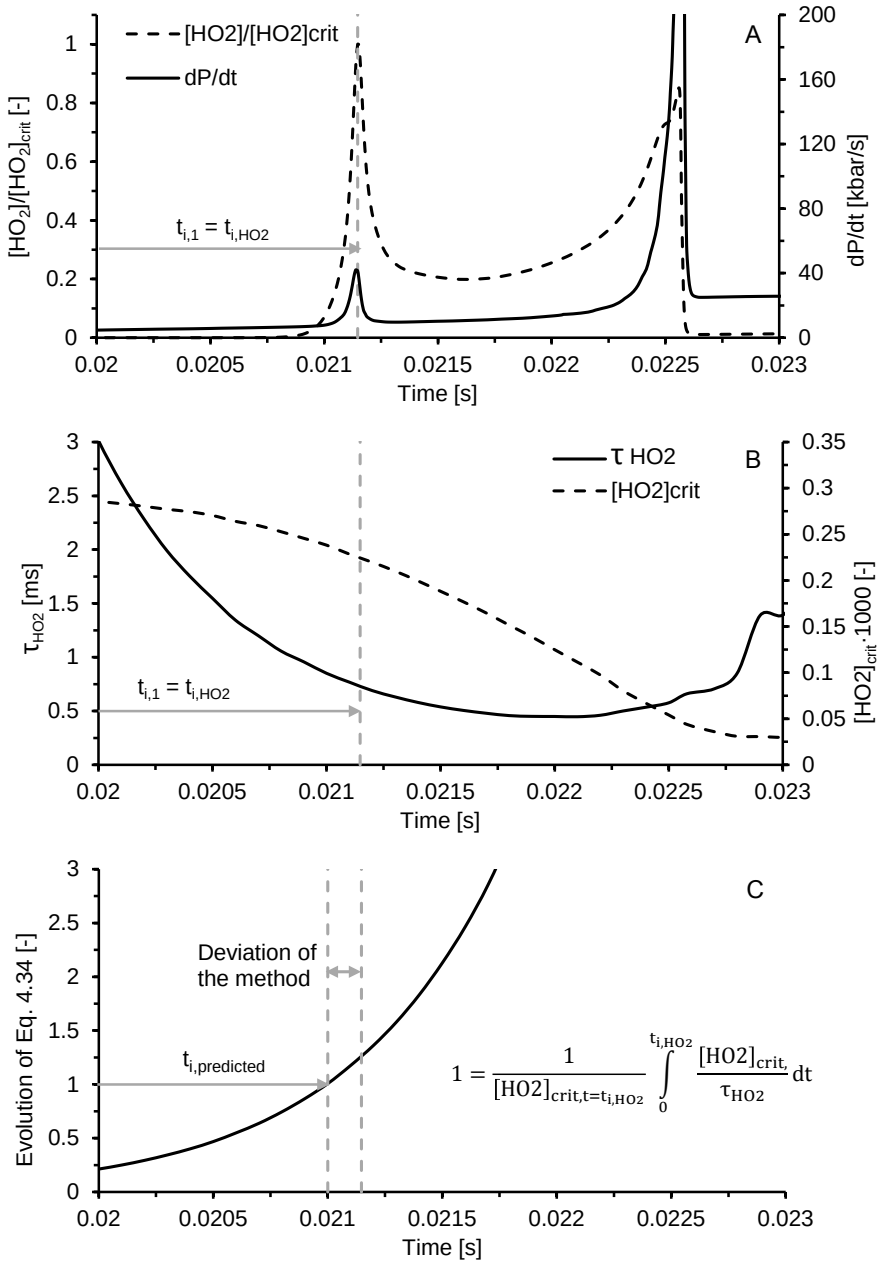


***Figure 4.8.*** *Results from CHEMKIN for $T_0$=408 K, $P_0$=1.4 bar, CR=15, $X_{O_2}$=0.147, $F_r$=0.5, n-heptane. A.- Normalized $HO_2$ concentration and pressure rise rate evolution. B.- Critical concentration function and $\tau_{HO2}$ function. C.- Accumulated area of Eq. 4.34.*

where $[R]$ represents the fuel, $\alpha$ is a multiplicative factor that represents the chain behavior of $[CC]$ and $k_1$, $k_2$, $k_4$ and $k_5$ represent the specific reaction rates of the initiation reaction, the chain reaction, the main termination reaction and the termination reaction by wall effects, respectively.

Taking into account that the termination reactions are dominant after reaching the critical concentration of chain carriers, the previous equation can be written as:

$$\frac{d[CC]}{dt} = -\left(k_4[R] + k_5\right)[CC] \tag{4.36}$$

From a theoretical point of view, the heat release in the autoignition of an homogeneous mixture can be assumed as a sudden event. Therefore, assuming a process under constant conditions of pressure and temperature during the ignition delay, and assuming that $[R] \gg [CC]$, Eq. 4.36 can be integrated with the condition $[CC] = [CC]_{crit}$ when $t = \tau_{CC}$ (ignition delay under constant thermodynamic conditions referred to a critical concentration) as follows:

$$\frac{[CC]}{[CC]_{crit}} = exp\left(\left(k_4[R] + k_5\right)\left(\tau_{CC} - t\right)\right) \tag{4.37}$$

The exponential term in Eq. 4.37 can be approximated by a Taylor series expansion that can be truncated in the second term, resulting in the following expression:

$$\frac{[CC]}{[CC]_{crit}} = 1 + \left(k_4[R] + k_5\right)\left(\tau_{CC} - t\right) \tag{4.38}$$

taking into account the condition $[CC] = 0$ when $t = \tau_2$ (ignition delay under constant thermodynamic conditions referred to a maximum pressure rise), the following expression can be finally obtained for the evolution of chain carriers:

$$\frac{[CC]}{[CC]_{crit}} = \frac{\tau_2 - t}{\tau_2 - \tau_{CC}} \tag{4.39}$$

equation that is only valid under constant conditions of pressure and temperature, since otherwise Eq. 4.36 cannot be integrated.

If a process under transient thermodynamic conditions is discretized as a series of thermodynamic states that remain constant for a time $dt$, the ignition time can be obtained by discretizing Eq. 4.39 as follows:

$$\frac{d[CC]}{[CC]_{crit}} = -\frac{dt}{\tau_2 - \tau_{CC}} \tag{4.40}$$

and integrating it during the period of time between the critical concentration of chain carriers and the maximum heat release rate:

$$\int_{[CC]_{crit,t_{i,CC}}}^{0} d[CC] = -\int_{t_{i,CC}}^{t_{i,2}} \frac{[CC]_{crit}}{\tau_2 - \tau_{CC}} dt$$
$$1 = \frac{1}{[CC]_{crit,t_{i,CC}}} \int_{t_{i,CC}}^{t_{i,2}} \frac{[CC]_{crit}}{\tau_2 - \tau_{CC}} dt \tag{4.41}$$

where $t_{i,2}$ is the ignition delay of the process referred to a maximum heat release rate, and $\tau_{CC}$, $\tau_2$ and $[CC]_{crit}$ are the ignition delay referred to a maximum of chain carriers, the ignition delay referred to the high exothermic stage and the critical concentration of chain carriers under constant conditions of pressure and temperature for the successive thermodynamic states, respectively. It should be noted that Eq. 4.41 can be combined with Eq. 4.34 to predict both ignition delays referred to a critical concentration and, starting from it, the one referred to a maximum pressure rise rate.

Any species that has an accumulative behavior during the ignition delay up to reach a maximum of concentration (the critical concentration) and that is consumed when the high-temperature ignition stage occurs can be assumed as chain carrier. It is known that the $H_2O_2$ decomposition triggers the high-temperature ignition process [8]. In fact, the $H_2O_2$ decomposition generates the OH radicals needed to oxidize the $CH_2O$ to CO, which is also a characteristic phenomenon of the transition to the high-exothermic stage of the process. Thus, both $H_2O_2$ or $CH_2O$ can take the role of chain carrier in this case.

A schematic of this new procedure is shown in Fig. 4.9. $CH_2O$ is selected as chain carrier, since formaldehyde is widely recognized as an autoignition tracer [21]. The time at which the maximum concentration of $CH_2O$ is reached can be predicted by using Eq. 4.34, the accumulated area of which represents the accumulation behavior of this chain carrier. Then, the consumption of $CH_2O$ is modeled by the accumulated area of Eq. 4.41, by using the $\tau_{CC}$ and $[CC]_{crit}$ functions related to this species. It should be noted that the decomposition of chain carriers starts once the value of 1 is reached in Eq. 4.34 (once the maximum concentration of chain carriers is reached). When the accumulated area of Eq. 4.41 is equal to 1, the time at which all $CH_2O$ is consumed is predicted and, therefore, the ignition delay referred to the high-temperature

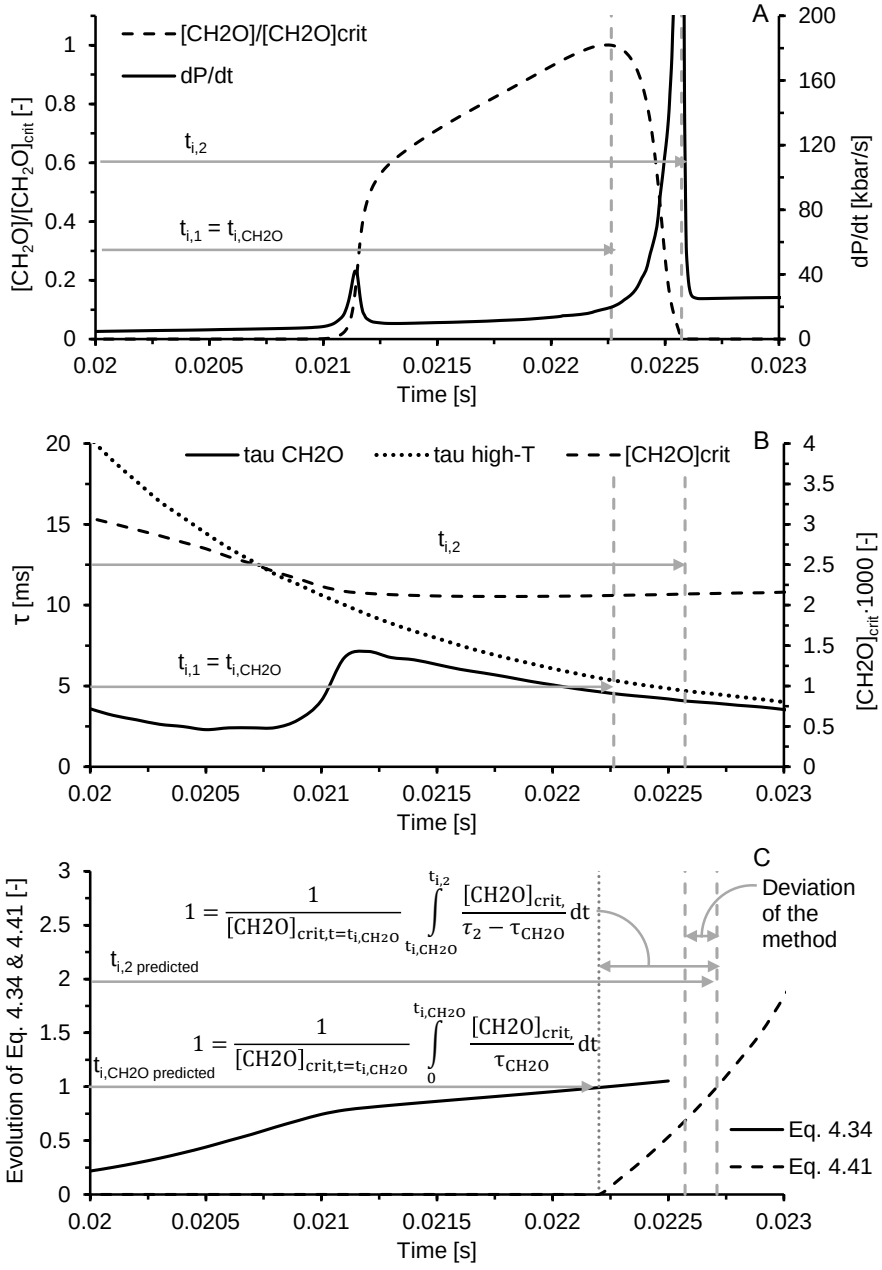


***Figure 4.9.*** *Results from CHEMKIN for $T_0$=408 K, $P_0$=1.4 bar, CR=15, $X_{O_2}$=0.147, $F_r$=0.5, n-heptane. A.- Normalized $CH_2O$ concentration and pressure rise rate evolution. B.- Critical concentration function and $\tau_{CH_2O}$ function. C.- Accumulated area of Eq. 4.34 and Eq. 4.41 for $CH_2O$ as chain carrier.*

stage is obtained. Besides, Fig. 4.9 B also shows that the $\tau_{CH_2O}$ function suddenly increases, as well as the critical concentration of $CH_2O$ shows a change of slope, at $t \approx 0.021\ s$. This behavior is related to the starting point of the NTC zone, defined by the in-cylinder thermodynamic conditions at $t \approx 0.021\ s$.

The combination of Eq. 4.34 and Eq. 4.41 allows the prediction of the time of ignition referred to a maximum heat release rate (or pressure rise rate) under variable thermodynamic conditions, which is a parameter easily measurable in experimental facilities. It should be noted that if the fuel does not present a two-stage ignition, $\tau_{CC}$ and $\tau_2$ are virtually the same, and the ignition delays predicted for both integrals, $t_{i,CC}$ and $t_{i,2}$, are also virtually the same.

### 4.2.4 Conclusions

In this investigation new alternative methods to predict ignition delays under variable conditions from those obtained under constant conditions are developed. These methods are theoretically deduced from the Glassman's model for autoignition and they allow to predict ignition delays referred to a critical concentration of chain carriers, to cool flames or to the high-temperature stage of the process.

It should be noted that predictive methods based on the premise that autoignition occurs when the critical concentration of chain carriers is reached lead to predicted ignition delays referred to this criterion. Moreover, the information used to obtain the predictions may be also referred to this criterion. Therefore, care should be taken in comparing the predictions obtained from these methods with experimental results, since both ignition delays could be referred to different stages of the combustion process.

Predictive methods based on the accumulation of chain carriers up to reach the critical concentration (which includes the classical Livengood & Wu correlation) are, in principle, difficult to validate versus experimental ignition delays. Predictive procedures based on a maximum pressure rise rate are more convenient, since the pressure trace can be easily measured in almost all experimental facilities. The predictive procedure for ignition delays referred to a maximum pressure rise rate proposed in this Thesis is composed by two different consecutive integrals:

$$1 = \frac{1}{[CC]_{crit,t_{i,CC}}} \int_0^{t_{i,CC}} \frac{[CC]_{crit}}{\tau_{CC}} dt \tag{4.42}$$

$$1 = \frac{1}{[CC]_{crit,t_{i,CC}}} \int_{t_{i,CC}}^{t_{i,2}} \frac{[CC]_{crit}}{\tau_2 - \tau_{CC}} dt \tag{4.43}$$

where $t_{i,CC}$ is the ignition delay of the process referred to a maximum concentration of chain carriers and $t_{i,2}$ is the ignition delay referred to the high-temperature stage of combustion. Besides, $\tau_2$, $\tau_{CC}$ and $[CC]_{crit}$ are the ignition delay referred to the high exothermic stage, the ignition delay referred to a maximum of chain carriers and the critical concentration of chain carriers, respectively, under constant conditions of pressure and temperature for the successive thermodynamic states.

The method is decoupled in two steps depending on the stage of the ignition to predict. On the one hand, a predictive method for cool flames is based on the accumulation of chain carriers up to reach the critical concentration. $HO_2$ is selected as chain carrier since it seems to be a good tracer of such phenomenon ($CC$=$HO_2$). The accumulation of $HO_2$ is modeled by Eq. 4.42, in which $\tau_{CC}$ and $[CC]_{crit}$ are related to this species. The upper limit of the integral represents the instant at which the maximum concentration of $HO_2$ occurs, which corresponds to the ignition delay referred to cool flames.

On the other hand, a predictive method for the high-temperature stage of the combustion process is based on the accumulation of chain carriers up to the critical concentration (Eq. 4.42), and the subsequent consumption from this maximum of concentration (Eq. 4.43). Thus, two different consecutive integrals have to be solved in this method. $CH_2O$ is selected as chain carrier ($CC$=$CH_2O$), since formaldehyde is widely recognized as an autoignition tracer and the maximum heat release rate occurs when this species is almost consumed. The instant at which the maximum concentration of $CH_2O$ is reached is obtained by solving Eq. 4.42, whereas the consumption of $CH_2O$ is modeled by Eq. 4.43. Obviously, $\tau_{CC}$ and $[CC]_{crit}$ have to be related to this species. The upper limit of the integral in Eq. 4.43 represents the time at which all formaldehyde is consumed, which corresponds to the ignition delay referred to the high-temperature stage.

## 4.3 Validity of the Livengood & Wu integral and other alternative predictive methods based on a critical concentration of chain carriers

In this section, the validity of the integral method proposed by Livengood & Wu [15], as well as the alternative predictive methods proposed in Section 4.2.1, are checked and explained. These procedures are based on ignition

delays defined as the instant at which the critical concentration of chain carriers is reached. Therefore, from a theoretical point of view, the $\tau$ function that has to be used to solve the methods should be referred to a critical concentration of chain carriers, and only ignition delays under transient conditions referred to a critical concentration of chain carriers, $t_{i,CC}$, can be predicted. This makes very complex the comparison between the methods and experimental results without including intrinsic deviation caused by comparing times referred to different ignition stages. Thus, these predictive methods are evaluated by comparison to chemical simulations solving chemical kinetic mechanisms.

Three different predictive methods are considered in this section:

- The Livengood & Wu integral method, defined by Eq. 2.6.
- The RCCC method, defined by Eq. 4.30.
- The integral method defined by Eq. 4.34 (referred as the Int-method further on).

First, the hypotheses assumed by each method are summarized now, to allow later fast and easy references in the upcoming paragraphs.

- Hypotheses of the Livengood & Wu integral method:
  - H1-LW: the oxidation process during the ignition delay can be described by a global 0-order chemical reaction.
  - H2-LW: the critical concentration of chain carriers at which the autoignition occurs does not depend on temperature and pressure.
  - H3-LW: the concentration of chain carriers increases linearly with time under certain given thermodynamic conditions of pressure and temperature.
  - H4-LW: the fuel molar fraction is approximately constant during the ignition delay.
  - H5-LW: there is not any exothermic activity during the ignition delay.
- Hypotheses avoided by the RCCC method:
  - The accumulation of chain carriers is modeled by a first-order reaction, which results in an exponential behavior of the chain carriers concentration with time, avoiding H1-LW and H3-LW.

  - The dependence of the critical concentration of chain carriers on the thermodynamic conditions is taken into account, avoiding H2-LW.

- Hypotheses avoided by the Int-method:
  - The dependence of the critical concentration of chain carriers on the thermodynamic conditions is taken into account, avoiding H2-LW.

The accuracy of the different methods are analyzed following this methodology: for a certain case, the evolution of both the in-cylinder temperature and pressure are obtained by simulation under motoring conditions (without solving the chemistry). Then, the ignition delay, $\tau_{CC}$, and the critical concentration, $[CC]_{crit}$, are obtained for each thermodynamic state by simulation in a perfectly stirred reactor. The ignition delay under transient conditions, $t_{i,CC}$, is then predicted by using the procedures involved in this section, and it is also calculated by simulating it in an internal combustion engine reactor (direct chemical simulation) solving the corresponding chemical kinetic mechanism. Finally, the predicted ignition delays are compared directly to the values obtained from the direct chemical simulations.

The parametric study performed and a detailed description of the methodological approach can be found in Chapter 3, Sections 3.2 and 3.3.3. Furthermore, the information related to the investigation discussed in this section has been already published in [16, 17].

### 4.3.1 Analysis of the Livengood & Wu hypotheses

Fig. 4.10 shows the simulated and predicted ignition delays referred to a critical concentration of $CH_2O$ under different operating conditions for PRF50, the octane number of which is centered in the octane number scale. $CH_2O$ has been chosen as chain carrier in order to take into account the effects of the NTC behavior, since the critical concentration of such species is controlled by the $H_2O_2$ decomposition, which also controls the end of the NTC zone. The ignition delay obtained by solving the detailed chemical kinetic mechanism for PRF mixtures in an ICE reactor, *Chemkin*, has shown to be shorter than the predicted ignition delays, whatever the predictive method used (the Livengood & Wu integral method, *LW*, the RCCC-method, *RCCC*, or the new integral method proposed in this Thesis, *Int*). This is mainly caused by the exothermic activity that occurs before reaching the critical concentration of $CH_2O$, which is assumed to be negligible by all the predictive methods. The critical concentration of $CH_2O$ is reached after cool flames, which means that H5-LW is not really accurate. Thus, if exothermic reactions are neglected,

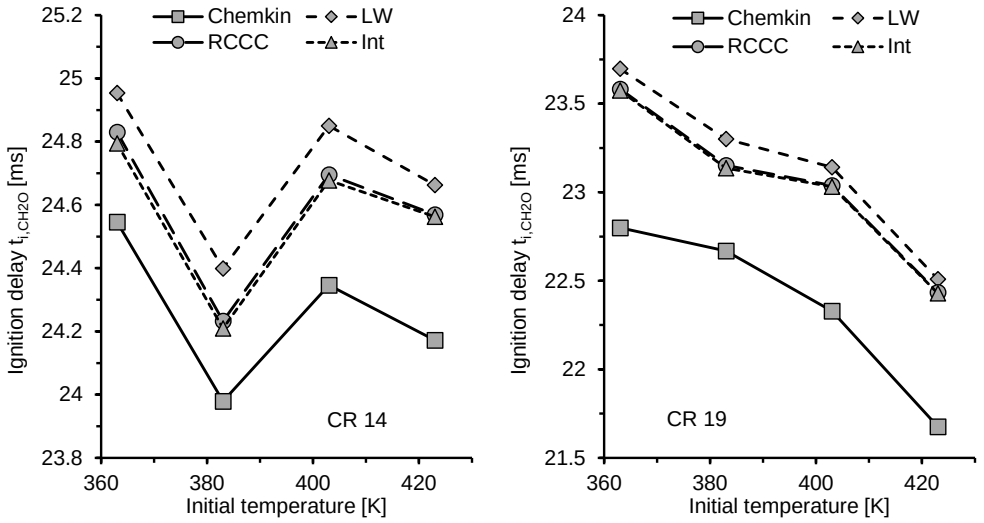


***Figure 4.10.*** *Simulated and predicted ignition delays referred to a critical concentration of $CH_2O$ versus initial temperature for PRF50, $F_r = 0.4$ and $X_{O_2} = 0.21$. Left.- $CR = 14$. Right.- $CR = 19$.*

the associated temperature rise is also neglected and longer ignition delays are predicted. Besides, the more dominant the NTC behavior the stronger this trend, since more heat is released during cool flames. In fact, it will be seen below that the ignition delay referred to a critical concentration of $CH_2O$ is slightly under-predicted for iso-octane (no cool flames), while it is usually over-predicted for n-heptane (strong NTC behavior).

Fig. 4.11 to the left shows the simulated and predicted ignition delays referred to $[CH_2O]_{crit}$ versus equivalence ratio under different operating conditions for PRF50, while Fig. 4.11 to the right shows analogous data versus oxygen molar fraction. It can be seen that the lower the fuel reactivity (the lower the equivalence ratio or the lower the oxygen molar fraction) the more over-predicted the ignition delay. The NTC behavior is more relevant if the equivalence ratio or the oxygen molar fraction is decreased, leading to worse predictions.

Furthermore, it can be seen that the accumulation of chain carriers during the ignition delay can be described by a zero-order reaction, since similar predictions are obtained with both the RCCC-method and the new integral method proposed. In Eq. 4.26, taking into account the Taylor's

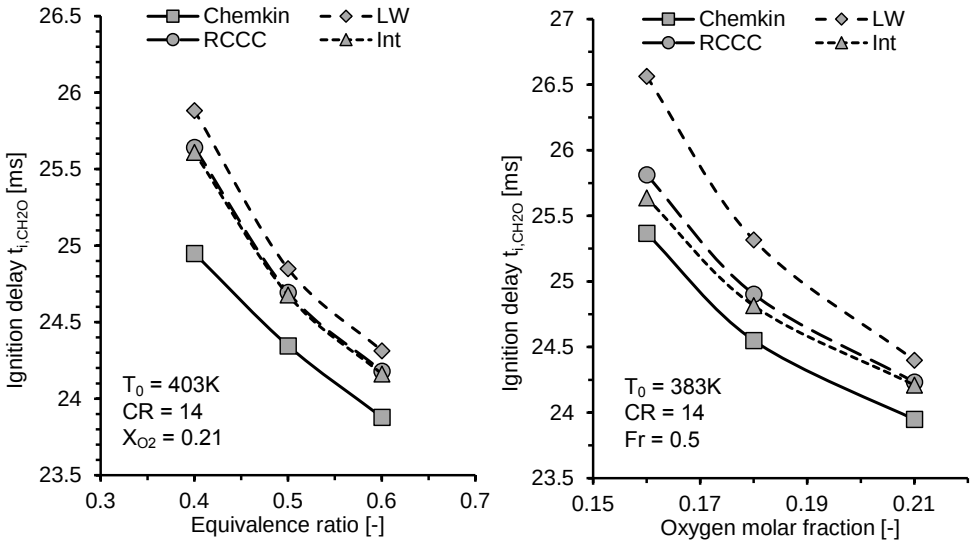


***Figure 4.11.*** *Simulated and predicted ignition delays referred to a critical concentration of $CH_2O$ for PRF50. Left.- versus equivalence ratio for $T_w$ = 403 K, $X_{O_2}$ = 0.21 and $CR$ = 14. Right.- versus oxygen molar fraction for $T_w$ = 383 K, $F_r$ = 0.5 and $CR$ = 14.*

series expansion of $exp(t/\tau)$, the lower the $t/\tau$ ratio the more accurate the linearization of the exponential term (the more accurate is H3-LW). Thus, a zero-order reaction (H1-LW, H3-LW) can be assumed when $t/\tau < 1$ (during the ignition delay). In conclusion, it is not worthy to implement a more complex predictive method such as the RCCC-method since similar results can be obtained with Eq. 4.34. That is the reason why the RCCC-method will not be evaluated versus the experimental measurements in the following chapter.

Finally, H2-LW can be evaluated by comparing predictions from the Livengood & Wu integral method and from the new integral proposed. Specifically, the ignition delay is over-predicted by the Livengood & Wu integral if the critical concentration of chain carriers decreases during the transient process, since Eq. 4.34 accelerates when a negative critical concentration rise rate occurs. In general, $[CH_2O]_{crit}$ increases linearly with the equivalence ratio and with the oxygen molar fraction, while it decreases with temperature (except in the NTC zone), which is consistent with Eq. 4.24.

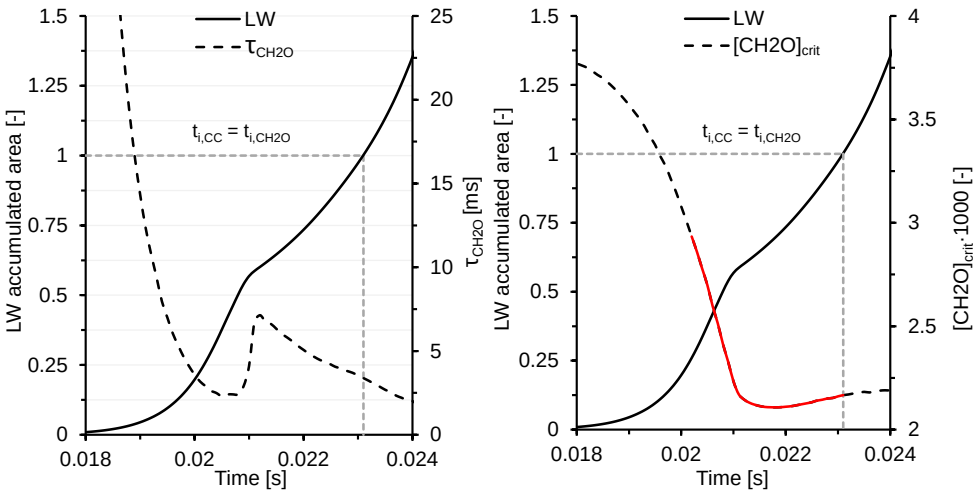


***Figure 4.12.*** *Results from CHEMKIN for $T_0$=408 K, $P_0$=1.4 bar, CR=15, $X_{O_2}$=0.147, $F_r$=0.5, n-heptane. Left.- $\tau_{CH2O}$ function. Right.- $[CH_2O]_{crit}$ function. The accumulated area of the Livengood & Wu integral method is shown in both plots.*

Predictions are significantly different when the critical concentration of chain carriers is assumed to be constant, which indicates the relevance of H2-LW.

The $\tau$ and $[CC]_{crit}$ functions are presented in Fig. 4.12 for $CH_2O$. As it can be seen, the critical concentration of chain carriers is not constant with pressure and temperature, as assumed by the Livengood & Wu method (hypothesis H2-LW). Furthermore, the NTC zone, which is usually crossed during the compression stroke, can cause a change of slope in $\tau$ and $[CC]_{crit}$. Despite the fact that the calculations were carried out with a detailed chemical kinetic mechanism for PRF mixtures, the transition between the low temperature regime and the NTC zone, as well as the transition between the NTC zone and the high temperature regime, can result in discontinuities in the $\tau$ function and non-derivable points in the $[CC]_{crit}$ function. Moreover, if the autoignition occurs just after the change of slope, the major contribution to the integral is made with data affected by the NTC behavior, which can lead to unexpected predictions. Therefore, depending on the working conditions, the NTC behavior can be more or less pronounced and can be located earlier or later, affecting more or less to the prediction deviation.

The temperature and pressure evolution typically present in an internal combustion engine causes that the largest contribution to the integral method is made in a relatively narrow range. Thus, if the variation of critical

concentration corresponding to the last 75% of the accumulated area of the integral method is plotted (red length of the dashed line in Fig. 4.12 to the right), it is found that this variation is not too large. Moreover, it can be checked that the critical concentration of chain carriers decreases with temperature whereas it increases with pressure. The relationship between pressure and temperature in an engine (simultaneous increase or decrease of both) causes that the net variation of the critical concentration is soft enough to validate the method. However, it should be noted that, while the Livengood & Wu integral is able to predict with high accuracy the ignition delay referred to the critical concentration of a species that occurs before the NTC zone (such as $HO_2$), worse predictions can be obtained if this method is used for species the critical concentration of which occurs during the NTC zone (such as $CH_2O$).

Finally, it is interesting to analyze what happens when the mixture does not autoignite. In Fig. 4.13, the accumulated area of the two integral methods evaluated in this section (the Livengood & Wu integral, $LW$, and the new integral proposed, $Int$), as well as the RCCC parameter of the RCCC-method, can be seen assuming $CH_2O$ as chain carrier. It should be noted that the transient behavior of the critical concentration in the RCCC-method and in the new integral proposed can cause not only an increment, but also a reduction of the accumulated value in the method. Moreover, since a negative critical concentration rise rate occurs, the $Int$ method is faster than the classic Livengood & Wu integral method during the compression stroke. As the accumulated area, nor the RCCC parameter, does not reach the value of 1, autoignition does not occur.

### 4.3.2 Comparison between the Livengood & Wu integral and the new proposed methods

The relative ignition delay deviation with relation to detailed chemistry simulations (or prediction deviation), $\epsilon$, was calculated in order to easily compare the prediction capability of the different predictive methods. This deviation is defined as follows:

$$\epsilon = \frac{t_{i,CC,x} - t_{i,CC,Chemkin}}{t_{i,CC,Chemkin}} 100 \tag{4.44}$$

where $t_{i,CC}$ represents the ignition delay under transient conditions referred to a critical concentration of chain carriers, $CC$. The subscript $Chemkin$ represents data obtained from a chemical simulation with CHEMKIN using a

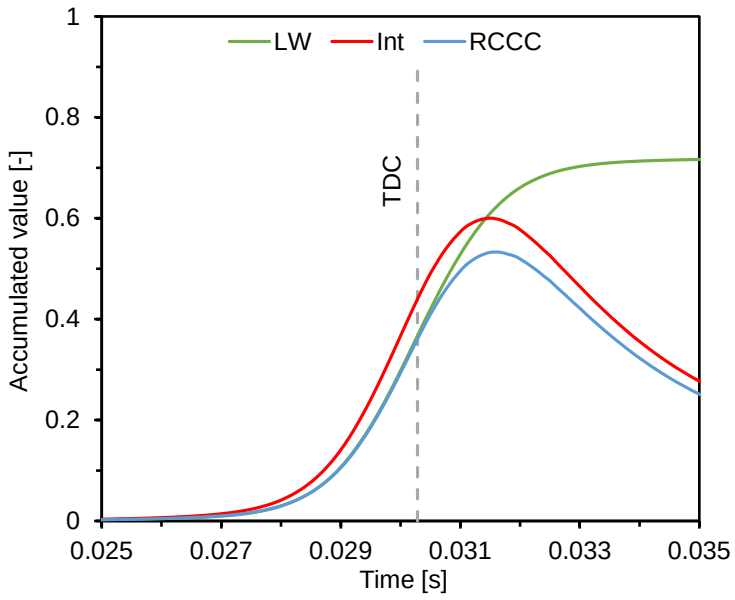


***Figure 4.13.*** *Evolution of the Livengod & Wu integral, LW, the new integral proposed, Int, and the RCCC-method, RCCC, for $T_0$=383 K, $P_0$=1.4 bar, CR=15, $X_{O_2}$=0.105, $F_r$=0.3, iso-octane. Misfire occurs under these conditions.*

closed 0-D IC-engine reactor that replicates the RCEM conditions. Finally, the subscript $x$ can represent data obtained from the Livengood & Wu integral method, $LW$, the new integral proposed, $Int$, or the RCCC-method, $RCCC$.

On the one hand, Figs. 4.14, 4.15, 4.16, 4.17, 4.18 and 4.19 to the left show the comparison between the different predictive methods and the corresponding chemical kinetic simulation for the six fuels tested in this investigation: n-dodecane, n-heptane, PRF25, PRF50, PRF75 and iso-octane, respectively, for all cases from the parametric study shown in Chapter 3, Section 3.2. Ignition delays under transient conditions referred to a critical concentration of $CH_2O$ are represented: those obtained from the predictive methods ($LW$, $Int$ or $RCCC$) in the ordinates axis and those obtained from chemical kinetic simulations ($Chemkin$) in the abscissas axis. The line $y = x$, which represents a perfect match between the numerical method and the chemical kinetic simulation, is plotted in all graphs. Finally, the Pearson's coefficients of determination, $R^2$, have been calculated for each procedure and each fuel, and their values can be seen in the corresponding figure.

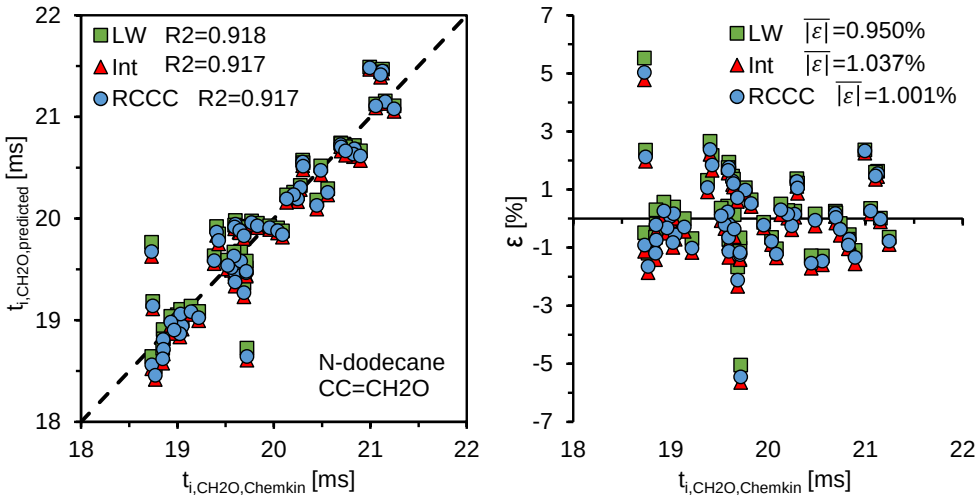


***Figure 4.14.*** *Left.- Predicted versus simulated ignition delay referred to $CH_2O$. Right.- Ignition delay deviation referred to $CH_2O$ for each predictive procedure.* ***The fuel used is n-dodecane****. All the operating conditions are plotted.*

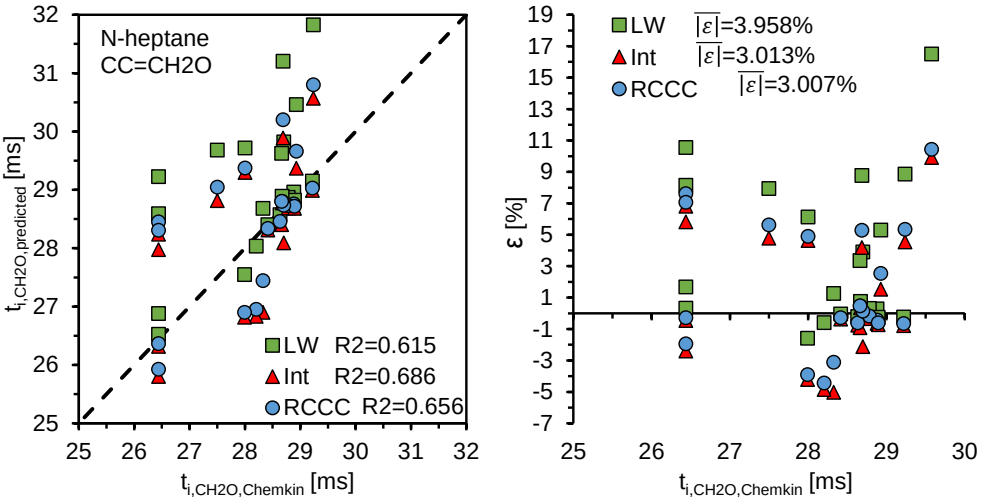


***Figure 4.15.*** *Left.- Predicted versus simulated ignition delay referred to $CH_2O$. Right.- Ignition delay deviation referred to $CH_2O$ for each predictive procedure.* ***The fuel used is n-heptane****. All the operating conditions are plotted.*

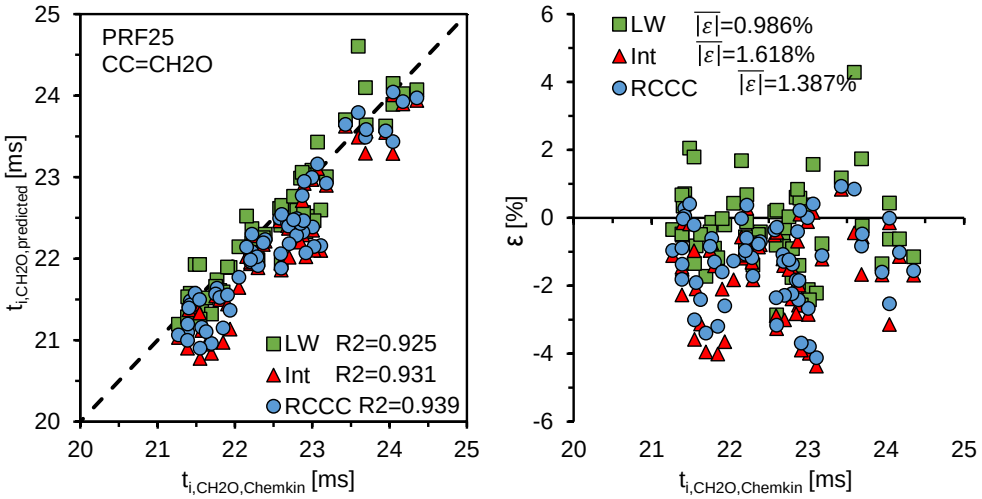


***Figure 4.16.*** *Left.- Predicted versus simulated ignition delay referred to $CH_2O$. Right.- Ignition delay deviation referred to $CH_2O$ for each predictive procedure.* ***The fuel used is PRF25****. All the operating conditions are plotted.*

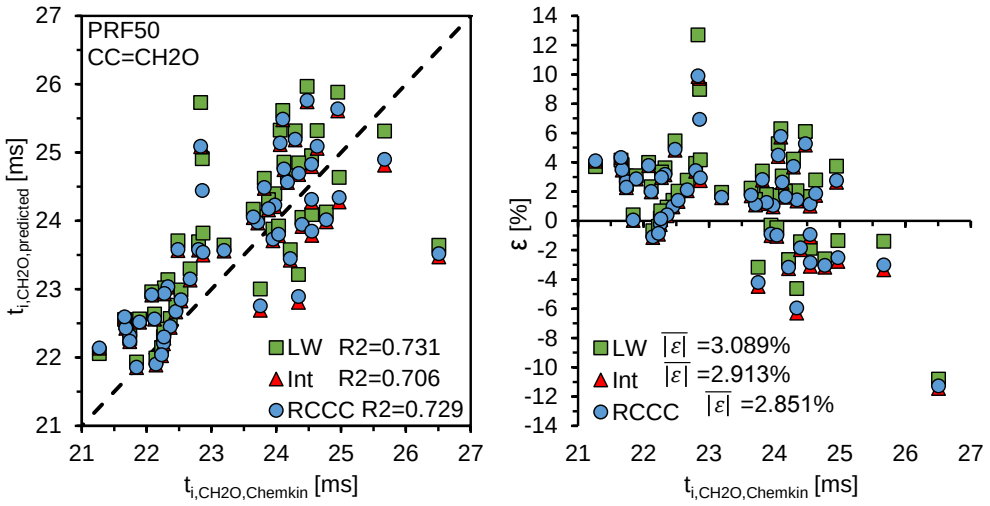


***Figure 4.17.*** *Left.- Predicted versus simulated ignition delay referred to $CH_2O$. Right.- Ignition delay deviation referred to $CH_2O$ for each predictive procedure.* ***The fuel used is PRF50****. All the operating conditions are plotted.*

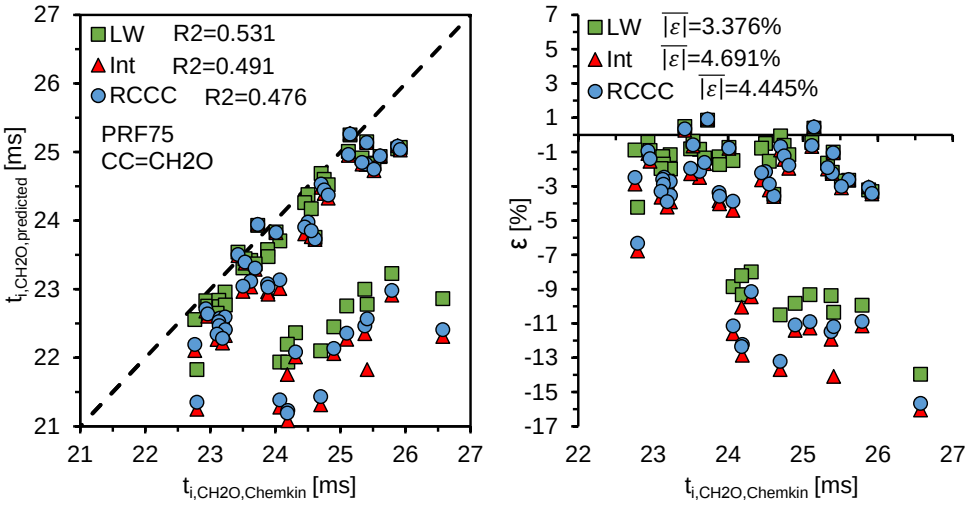


***Figure 4.18.*** *Left.- Predicted versus simulated ignition delay referred to $CH_2O$. Right.- Ignition delay deviation referred to $CH_2O$ for each predictive procedure.* ***The fuel used is PRF75****. All the operating conditions are plotted.*

On the other hand, the same figures to the right show the ignition delay deviations for the different predictive methods versus the ignition delay from the chemical kinetic simulations for the six fuels tested in this investigation. Once again, ignition delay deviations are referred to a critical concentration of $CH_2O$. The mean absolute deviations, $|\bar{\epsilon}| = \sum|\epsilon|/N$, have been obtained for each procedure and each fuel, and their values can be seen in the corresponding figure. Furthermore, the confidence intervals of $|\bar{\epsilon}|$ with a confidence level of 95% have been calculated, and they are summarized in Table 4.1.

Regarding the parametric study performed for pure iso-octane and pure n-heptane, the coefficients of determination for n-heptane are much worse than the $R^2$ for iso-octane. N-heptane presents a high NTC zone and this effect cannot be appropriately described by a global chemical reaction, as assumed in the predictive methods, which causes erroneous predictions in some cases. Moreover, the ignition delay deviation is higher for n-heptane than for iso-octane because iso-octane has a much smoother NTC zone. Besides, the NTC zone appears at lower temperature and pressure for iso-octane, so it affects much less to the numerical method.

Regarding the parametric study performed for PRF mixtures, the higher the amount of iso-octane (i.e., the higher the octane number) the worse the

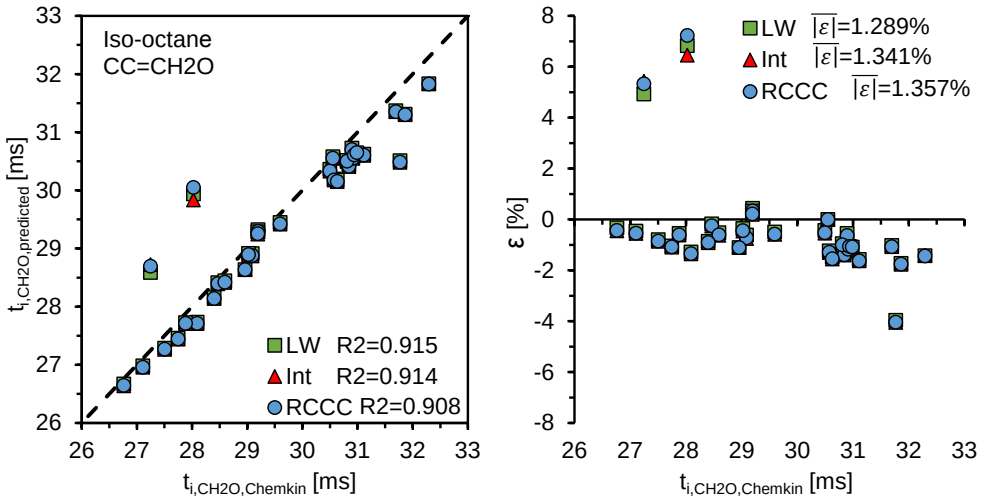


***Figure 4.19.*** *Left.- Predicted versus simulated ignition delay referred to $CH_2O$. Right.- Ignition delay deviation referred to $CH_2O$ for each predictive procedure.* ***The fuel used is iso-octane****. All the operating conditions are plotted.*

| | *LW* | | *Int* | | *RCCC* | |
|---|---|---|---|---|---|---|
| | $\overline{\lvert\epsilon\rvert}$ [%] | **CI 95%** [%] | $\overline{\lvert\epsilon\rvert}$ [%] | **CI 95%** [%] | $\overline{\lvert\epsilon\rvert}$ [%] | **CI 95%** [%] |
| **N-dodecane** | 0.950 | [0.679 - 1.222] | 1.037 | [0.777 - 1.297] | 1.001 | [0.738 - 1.264] |
| **N-heptane** | 3.958 | [1.962 - 5.954] | 3.013 | [1.692 - 4.334] | 3.007 | [1.841 - 4.173] |
| **PRF25** | 0.986 | [0.776 - 1.196] | 1.618 | [1.320 - 1.436] | 1.387 | [1.114 - 1.660] |
| **PRF50** | 3.089 | [2.403 - 3.776] | 2.913 | [2.255 - 3.572] | 2.851 | [2.235 - 3.467] |
| **PRF75** | 3.376 | [2.299 - 4.453] | 4.691 | [3.425 - 5.956] | 4.445 | [3.213 - 5.677] |
| **Iso-octane** | 1.289 | [0.764 - 1.813] | 1.341 | [0.820 - 1.862] | 1.357 | [0.804 - 1.910] |

***Table 4.1.*** *Mean absolute deviations, $\overline{\lvert\epsilon\rvert}$, and confidence interval of $\overline{\lvert\epsilon\rvert}$ with a confidence level of 95% for all fuels and the three predictive methods evaluated in this section.*

predictions. In this case the effects of the NTC behavior are similar for the three fuels, since the NTC zone can be clearly seen with similar intensity even for PRF75. Besides, it should be mentioned that PFR75 is near to misfire in some cases under the operating conditions tested in this investigation, which explains the very bad predictions that can be seen in Fig. 4.18 for long ignition delays.

Finally, it can be seen in Table 4.1 that the predictive methods based on a critical concentration of chain carriers lead, in general, to similar results than chemical kinetic simulations, but substantially decreasing the computation time. The main advantage of the new proposed procedures is discarding the hypotheses of constant critical concentration of chain carriers, which is assumed by the Livengood & Wu integral. However, when autoignition occurs in the NTC regime, better predictions can be obtained from the Livengood & Wu integral method due to, to some extent, a compensation of errors. On the one hand, the ignition delay from the chemical simulation tends to be longer than the predicted ignition delay during the NTC zone, since the NTC behavior reduces the reactivity of the mixture. On the other hand, the ignition delay predicted by the Livengood & Wu integral is longer than the other predictive methods assuming $CH_2O$ as chain carrier. Therefore, the combination of both effects can lead to better predictions for the Livengood & Wu methods if the ignition occurs in the NTC zone. Another important aspect to underline is that, since all methods work with integrated equations there are not problems of calculation instabilities.

### 4.3.3 Conclusions

The following conclusions can be deduced from this study:

- The predictive methods presented in this section are based on the premise that autoignition occurs when the critical concentration of chain carriers is reached. Therefore, the predicted ignition delays will be referred to this criterion and the information used to obtain the predictions may be also referred to this criterion. Thus, the predicted ignition delays cannot be compared to experimental results, since the measured ignition delays are referred to different stages of the combustion process.

- The Livengood & Wu integral is valid despite the hypothesis of constant critical concentration for an engine-like temperature and pressure evolution. The largest contribution to the integral method is made in a narrow time interval in which the assumption of constant critical concentration is not catastrophic.

- Since all methods are deduced from models that cannot reproduce the NTC zone, the more pronounced the NTC regime, the higher the prediction deviations.

- When autoignition occurs in the NTC regime, better predictions can be obtained from the Livengood & Wu integral method due to, to some extent, a compensation of errors.

## 4.A Appendix: Prediction of an ignition delay referred to a critical concentration of chain carriers by means of the Müller, Peters and Liñán's model for autoignition

New expressions to predict ignition delays referred to a critical concentration of chain carriers have been developed starting from the Müller, Peters and Liñán's model for autoignition [20] following an analogous way to the theoretical development shown in Section 4.2.1 for the Glassman's model [19].

The Müller, Peters and Liñán's model is a simple model to characterize the autoignition phenomenon of n-heptane by a chain reactions mechanism. It is composed by four reactions, which can be extended to any hydrocarbon $C_nH_mO_p$ as follows:

$$R \xrightarrow{k_1} Q \tag{R1}$$

$$Q + a_{st}O_2 \xrightarrow{k_2} P \tag{R2}$$

$$R + 2O_2 \underset{k_{3b}}{\overset{k_{3f}}{\longleftrightarrow}} CC \tag{R3}$$

$$CC + (a_{st} - 2)\, O_2 \xrightarrow{k_4} P \tag{R4}$$

where $a_{st}$ represents the oxygen-to-fuel molar ratio under stoichiometric conditions, which is equal to $n + m/4 - p/2$. Besides, R represents the fuel, Q represents the typical intermediates of the high-temperature fuel decomposition, CC represents the typical intermediates of the low-temperature fuel decomposition, and P represents the main products of the combustion.

In this model, reactions R1 and R2 correspond to the high-temperature reaction branch, where R1 represents the high-temperature dehydrogenation and the thermal cracking of the fuel. Reactions R3 and R4 correspond to the low-temperature chain branching mechanism. R3 is the chain reaction that promotes the progression of the autoignition process by the generation of chain carriers. Finally, R2 and R4 correspond to the termination reactions. The NTC behavior can be modeled by introducing a backward reaction in R3.

The low-temperature chain branching mechanism is the dominant one in internal combustion engines [7], since the evolution of the in-cylinder temperature covers a wide range below 1000 $K$ during the ignition delay. Thus, if ignition delays under engine-like conditions want to be predicted,

reactions R1 and R2 can be obviated. Under these hypotheses the species conservation equations can be written as follows:

$$\frac{d[R]}{dt} = -k_{3f}[R][O_2] + k_{3b}[CC] \tag{4.45}$$

$$\frac{d[CC]}{dt} = k_{3f}[R][O_2] - k_{3b}[CC] - k_4[CC][O_2] \tag{4.46}$$

$$\frac{d[O_2]}{dt} = a_{st}\frac{d[R]}{dt} + (a_{st} - 2)\frac{d[CC]}{dt} \tag{4.47}$$

where $[X]$ represents the concentration of the species $X$.

Moreover, assuming that during the ignition delay the consumption of oxygen is negligible, since the termination reactions are not very important, and as $[O_2] >> [R]$ and $[O_2] >> [CC]$, a constant oxygen concentration can be assumed. Therefore, the previous conservation equations can be simplified as follows (Eq. 4.48 is derived from Eq. 4.47, and Eq. 4.49 from 4.46 and 4.48):

$$[R] = [R]_0 - \frac{a_{st} - 2}{a_{st}}[CC] \tag{4.48}$$

$$\frac{d[CC]}{dt} = k_{3f}[O_2][R]_0 - \left(k_{3f}\frac{a_{st} - 2}{a_{st}}[O_2] + k_{3b} + k_4[O_2]\right)[CC] \tag{4.49}$$

where $[R]_0$ is the initial fuel concentration.

Considering an air-fuel mixture under constant conditions of temperature and pressure, the differential equation 4.49 can be integrated with the initial condition $t = 0 \rightarrow [CC] = 0$ as follows:

$$1 - \frac{k_{3f}\frac{a_{st}-2}{a_{st}}[O_2] + k_{3b} + k_4[O_2]}{k_{3f}[O_2][R]_0}[CC] = \\ = exp(-t(k_{3f}\frac{a_{st} - 2}{a_{st}}[O_2] + k_{3b} + k_4[O_2])) \tag{4.50}$$

where $\frac{1}{k_{3f}\frac{a_{st}-2}{a_{st}}[O_2]+k_{3b}+k_4[O_2]}$ is a characteristic time of the process and, therefore, it may be an ignition delay estimator. Thus:

$$\tau_{CC} = \frac{1}{k_{3f}\frac{a_{st}-2}{a_{st}}[O_2] + k_{3b} + k_4[O_2]} \tag{4.51}$$

According to the above definition, Eq. 4.50 can be rewritten as follows:

$$exp\left(-\frac{t}{\tau_{CC}}\right) = 1 - \frac{[CC]}{k_{3f}[O_2][R]_0\tau_{CC}} \tag{4.52}$$

Thereby, when $t = \tau_{CC}$ the start of combustion occurs and the concentration of chain carriers is equal to the critical concentration. In this way, the critical concentration of chain carriers can be defined by the following expression obtained from Eq. 4.52:

$$[CC]_{crit} = \left(1 - \frac{1}{e}\right) k_{3f}[O_2][R]_0\tau_{CC} \tag{4.53}$$

Eq. 4.53 can be combined with Eq. 4.52 in order to obtain an expression for the temporal evolution of the concentration of chain carriers that depends only on the ignition delay and the critical concentration:

$$exp\left(-\frac{t}{\tau_{CC}}\right) = 1 - \frac{[CC]}{[CC]_{crit}}\left(1 - \frac{1}{e}\right) \tag{4.54}$$

or:

$$[CC] = \frac{[CC]_{crit}}{e - 1/e}\left(1 - exp\left(-\frac{t}{\tau_{CC}}\right)\right) \tag{4.55}$$

Equation that is only valid under constant conditions of pressure and temperature.

- Simplification to a global zero-order reaction

In order to simplify the expressions, the exponential term in Eq. 4.52 can be approximated by a Taylor series expansion. The series can be truncated in the second term, since $\frac{t}{\tau_{CC}} < 1$ during the ignition delay, and Eq. 4.52 can be rewritten as follows:

$$[CC] = k_{3f}[O_2][R]_0 t \tag{4.56}$$

Eq. 4.56 implies that $d[CC]/dt = k_{3f}[O_2][R]_0$, i.e., the accumulation rate of chain carriers corresponds to a zero-order reaction. When $t = \tau_{CC}$ the concentration of chain carriers is equal to the critical concentration and the previous equation can be rewritten as follows:

$$[CC] = [CC]_{crit}\frac{t}{\tau_{CC}} \tag{4.57}$$

equation that is only valid under constant conditions of pressure and temperature and that is analogous to Eq. 4.32 obtained from the Glassman's model.

It should be noted that ignition represents a discontinuity in the model, since some hypotheses, as constant oxygen concentration, are no longer valid. In fact, the expression deduced for the generation rate of chain carriers loses its validity at ignition. Thus, although ignition happens when a maximum concentration of chain carriers occurs (the critical concentration), the generation rate of chain carriers predicted by the model at this instant is not equal to zero.

## References

[1] Desantes José M., López J. Javier, Molina Santiago and López-Pintor Darío. "Design of synthetic EGR and simulation study of the effect of simplified formulations on the ignition delay of isooctane and n-heptane". *Energy Conversion and Management*, Vol. 96, pp. 521–531, 2015.

[2] Anderlohr J.M., Piperel A., Pires da Cruz A., Bounaceur R., Battin-Leclerc F., Dagaut P. and Montagne X. "Influence of EGR compounds on the oxidation of an HCCI-diesel surrogate". *Proceedings of the Combustion Institute*, Vol. 32, pp. 2851–2859, 2009.

[3] Machrafi Hatim. "Experimental validation of a kinetic multi-component mechanism in a wide HCCI engine operating range for mixtures of n-heptane, iso-octane and toluene: Influence of EGR parameters". *Energy Conversion and Management*, Vol. 49, pp. 2956–2965, 2008.

[4] Frassoldati A, Faravelli T and Ranzi E. "Kinetic modeling of the interactions between NO and hydrocarbons at high temperature". *Combustion and Flame*, Vol. 135, pp. 97–112, 2003.

[5] Herzler J. and Naumann C. "Shock tube study of the influence of NOx on the ignition delay times of natural gas at high pressure". *Combustion Science and Technology*, Vol. 184, pp. 1635–1650, 2012.

[6] Curran H.J., Pitz W.J., Westbrook C.K., Callahan C.V. and Dryer F.L. "Oxidation of automotive primary reference fuels at elevated pressures". *Symposium (International) on Combustion*, Vol. 37, pp. 379–389, 1999.

[7] Lü Xing-Cai, Chen Wei and Huang Zhen. "A fundamental study on the control of the HCCI combustion and emissions by fuel design concept combined with controllable EGR. Part 2. Effect of operating conditions and EGR on HCCI combustion". *Fuel*, Vol. 84, pp. 1084–1092, 2005.

[8] Curran H. J., Gaffuri P., Pitz W. J. and Westbrook C. K. "A comprehensive modeling study of n-heptane oxidation". *Combustion and Flame*, Vol. 114, pp. 149–177, 1998.

[9] Le Cong T. and Dagaut P. "Experimental and detailed kinetic modeling of the oxidation of natural gas, natural gas/syngas mixtures, and effect of burnt gas recirculation". *Proceedings of the European Combustion Meeting, July 23-27, 2007, Poitiers, France.*

[10] Glarborg P. and Bentzen L. L. B. "Chemical effects of high CO2 concentration in oxy-fuel combustion of methane". *Energy and Fuels*, Vol. 22, pp. 291–296, 2008.

[11] Fathi Morteza, Saray R. Khoshbakhti and Checkel M. David. "The influence of Exhaust Gas Recirculation (EGR) on combustion and emissions of n-heptane/natural gas fueled Homogeneous Charge Compression Ignition (HCCI) engines". *Applied Energy*, Vol. 88, pp. 4719–4724, 2011.

[12] Di Haisheng, He Xin, Zhang Peng, Wang Zhi, Wooldridge Margaret S., Law Chung K., Wang Cuiping, Shuai Shijin and Wang Jianxin. "Effects of buffer gas composition on low temperature ignition of iso-octane and n-heptane". *Combustion and Flame*, Vol. 161, pp. 2531–2538, 2014.

[13] Sjöberg Magnus and Dec John E. "Effects of EGR and its constituents on HCCI autoignition of ethanol". *Proceedings of the Combustion Institute*, Vol. 33, pp. 3031–3038, 2011.

[14] Wagnon Scott W. and Wooldridge Margaret S. "Effects of buffer gas composition on autoignition". *Combustion and Flame*, Vol. 161, pp. 898–907, 2014.

[15] Livengood J. C. and Wu P. C. "Correlation of autoignition phenomena in internal combustion engines and rapid compression machines". *Symposium (International) on Combustion*, Vol. 5, pp. 347–356, 1955.

[16] Desantes José M., López J. Javier, Molina Santiago and López-Pintor Darío. "Validity of the Livengood & Wu correlation and theoretical development of an alternative procedure to predict ignition delays under variable thermodynamic conditions". *Energy Conversion and Management*, Vol. 105, pp. 836–847, 2015.

[17] Desantes José M., López J. Javier, Molina Santiago and López-Pintor Darío. "Theoretical development of a new procedure to predict ignition delays under transient thermodynamic conditions and validation using a Rapid Compression-Expansion Machine". *Energy Conversion and Management*, Vol. 108, pp. 132–143, 2016.

[18] Desantes José M., Bermúdez Vicente, López J. Javier and López-Pintor Darío. "A new method to predict high and low-temperature ignition delays under transient thermodynamic conditions and its experimental validation using a Rapid Compression-Expansion Machine". *Energy Conversion and Management*, Vol. 123, pp. 512–522, 2016.

[19] Glassman Irvin. *Combustion*. Academic Press, Orlando [Fla.], 2nd ed edition, 1987.

[20] Müller U. C., Peters N. and Liñán A. "Global kinetics for n-heptane ignition at high pressures". *Twenty-Fourth Symposium (International) on Combustion-The Combustion Institute*, pp. 777–784, 1992.

[21] Baeuerle B., Warnatz J. and Behrendt F. "Time-resolved investigation of hot spots in the end gas of an S.I. engine by means of 2-D double-pulse LIF of formaldehyde". *Symposium (International) on Combustion*, Vol. 2, pp. 2619–2626, 1996.

# Chapter 5

# Experimental results

Contents

## 5.1 Experimental measurements of the ignition delay

The ignition delay trends that have been experimentally obtained are analyzed in this section. The consistence of the experimental data with the well-known ignition delay behavior has been studied in the following paragraphs, including not only the high-temperature ignition delay, but also the ignition delay referred to cool flames and the NTC behavior.

The parametric study performed and a detailed description of the methodological approach can be found in Chapter 3, Sections 3.2 and 3.3. Furthermore, the information related to the investigation discussed in this section has been already published in [1–3].

Figs. 5.1, 5.2 and 5.3 show the ignition delay trends versus temperature for PRF25, PRF50 and PRF75, respectively, under different compression ratios (pressure levels) and oxygen molar fractions. As expected [4, 5], it can be seen that the ignition delay decreases if the temperature is increased except in the Negative Temperature Coefficient (NTC) zone. Despite the fact that the NTC behavior can be smooth enough to avoid an increase of the ignition delay (such as under $F_r = 0.6$, CR = 19, $X_{O_2} = 0.21$ for the three fuels), the ignition delay decreasing rate is usually affected by this phenomenon, changing the slope of the curve. Higher temperature implies higher collision frequency and collision energy and, therefore, higher specific accumulation rate of chain carriers and shorter ignition delay. During the NTC zone, the accumulation of chain carriers competes with the formation of stable long-chain olefins by the alkyl radicals, which causes a decrease of reactivity that results in longer ignition delays.

The dependence of the ignition delay on the compression ratio can be also seen in Figs. 5.1, 5.2 and 5.3 for PRF25, PRF50 and PRF75, respectively. The ignition delay decreases when the compression ratio is increased, since higher pressure and temperature is reached. Moreover, Fig. 5.1 shows that, in general, the NTC zone becomes less pronounced if the pressure is increased. The end of the NTC zone is controlled by the unimolecular fall-off reaction $H_2O_2 + M = OH + OH + M$, which is a third body reaction the specific reaction rate of which increases if pressure is increased.

The effect of the equivalence ratio on the ignition delay under low temperature conditions is also plotted in Figs. 5.1, 5.2 and 5.3 for PRF25, PRF50 and PRF75, respectively. The ignition delay referred to the high-exothermic stage of the process decreases when the equivalence ratio is increased, since ignition is triggered when a critical concentration of chain

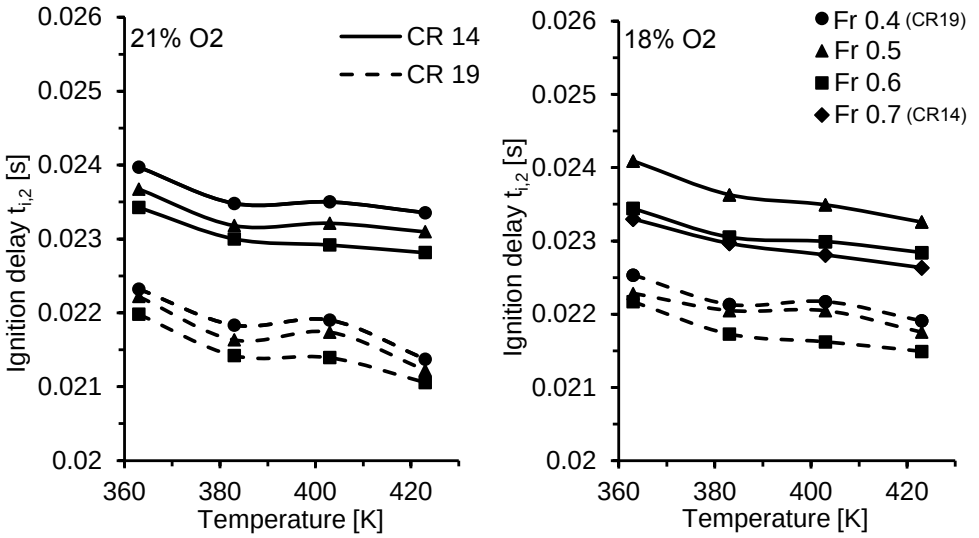


***Figure 5.1.*** *Ignition delay, $t_{i,2}$, versus initial temperature for PRF25. Both compression ratios are plotted. Left.- $X_{O_2} = 0.21$. Right.- $X_{O_2} = 0.18$.*

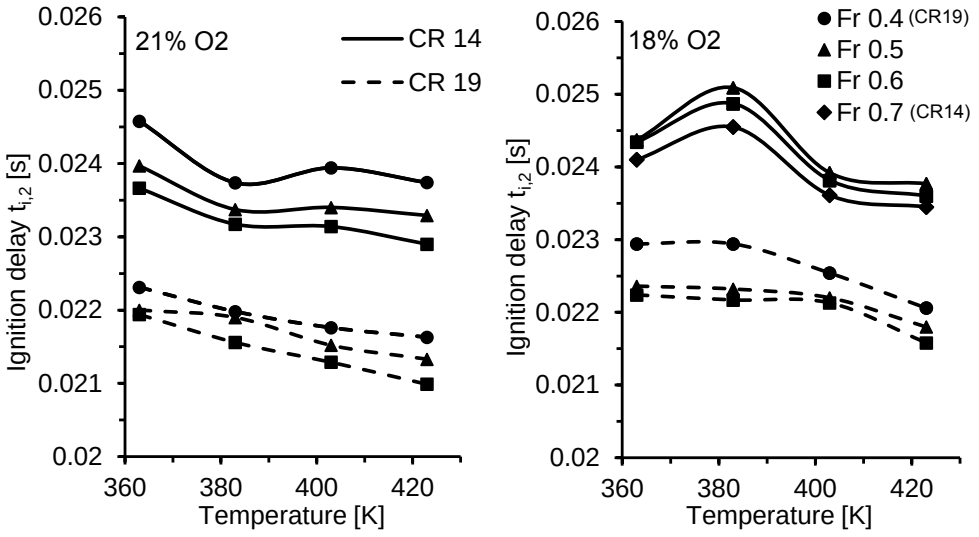


***Figure 5.2.*** *Ignition delay, $t_{i,2}$, versus initial temperature for PRF50. Both compression ratios are plotted. Left.- $X_{O_2} = 0.21$. Right.- $X_{O_2} = 0.18$.*

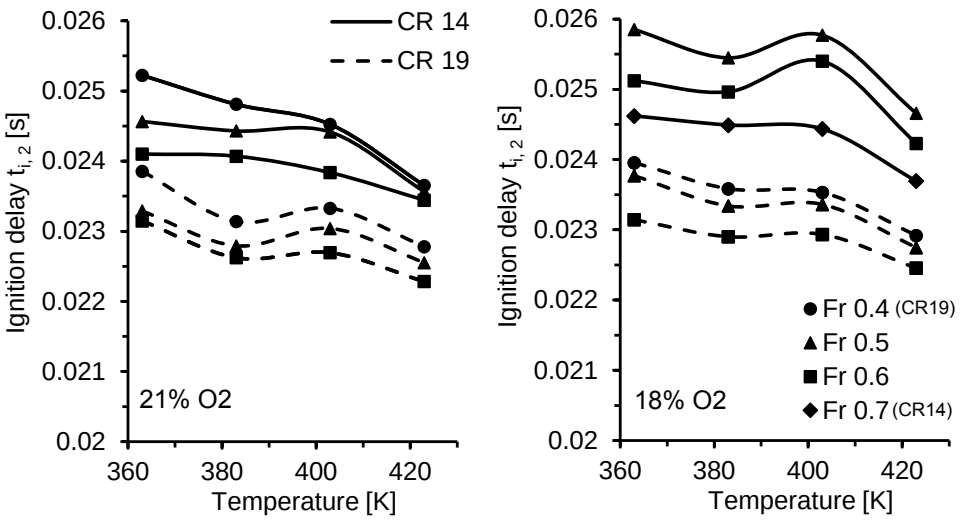


***Figure 5.3.*** *Ignition delay, $t_{i,2}$, versus initial temperature for PRF75. Both compression ratios are plotted. Left.- $X_{O_2} = 0.21$. Right.- $X_{O_2} = 0.18$.*

carriers is reached. The accumulation of chain carriers depends on the amount of fuel, so that the higher the equivalence ratio, the higher the generation rate of chain carriers and the shorter the ignition delay. Moreover, ignition delay can be generally scaled with the equivalence ratio and the oxygen content by $\tau \sim Fr^{-a}X_{O_2}^{-b}$, where $a$ and $b$ are positive numbers [6]. Thus, the higher the equivalence ratio, the lower its effect on the ignition time, being the ignition delay almost constant if the equivalence ratio is varied around the stoichiometric value. The lower the compression ratio or the lower the amount of oxygen, the higher the effect of the equivalence ratio on the ignition delay. Thus, the ignition delay is more sensitive to changes in the equivalence ratio if the reactivity of the mixture is reduced, since the low-temperature chain branching reactions, which depend on the amount of fuel, are more dominant. Besides, it can be seen in the figures that the NTC zone becomes less pronounced if the equivalence ratio is increased, so that the ignition can be characterized by the absence of such phenomenon for equivalence ratios near the stoichiometric value.

Fig. 5.4 shows the dependence of the ignition delay on the oxygen concentration. The chromatographic analysis of the test samples shows that the coefficient of variation of the oxygen content is lower than 1.6%, which

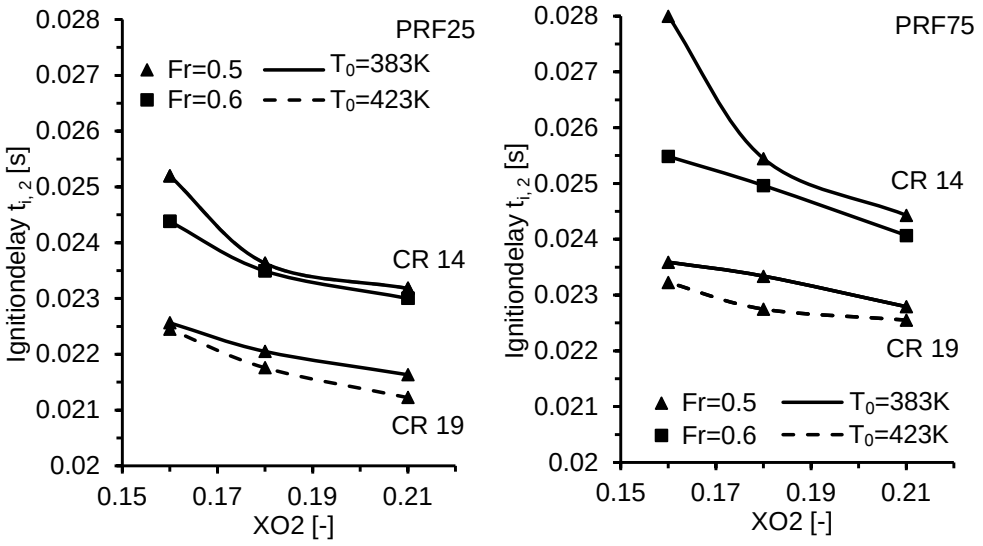


***Figure 5.4.*** *Ignition delay, $t_{i,2}$, versus molar fraction of oxygen for different fuels under different conditions. Triangular marks.- $F_r = 0.5$. Square marks.- $F_r = 0.6$. Dashed line.- $T_0 = 423\ K$. Solid line.- $T_0 = 383\ K$. Left.- PRF25. Right.- PRF75. Both compression ratios are plotted.*

guarantees the consistence between operating points. Ignition delay increases when the molar fraction of oxygen of the mixture is reduced, since lower amount of oxidizer implies lower reactivity. Moreover, the effect of the oxygen molar fraction becomes stronger if the equivalence ratio or the compression ratio are decreased. I.e. the ignition delay is more sensitive to changes in the oxygen content if the reactivity of the mixture is reduced, since the low-temperature chain branching reactions, which include the $O_2$ addition, are more dominant. In the same way, it can be clearly seen in Fig. 5.2 that the NTC zone is moved to lower temperature and it becomes more pronounced if the oxygen content is reduced.

Finally, the effects of the octane number on the ignition delay can be seen by comparing Figs. 5.1, 5.2 and 5.3. The higher the octane number, the longer the ignition delay, since the octane number represents, with strong non-linearity, the resistance of a certain fuel to autoignite. Differences in octane number are reflected in differences in cool flames intensity. Higher low-temperature heat release and higher $H_2O_2$ concentration are correlated with earlier ignition and lower octane values [7]. Furthermore, the fuel composition strongly affects the existence or not of a NTC behavior smooth enough to

avoid a two-stage ignition pattern. In general, the higher the octane number the less prone is the fuel to show an NTC zone. Thus, the NTC behavior is a common phenomenon for alkanes. Finally, it should be noted that all fuels auto-ignite under low temperature conditions following chemical paths that include the NTC behavior. However, if the characteristic time (or relevance) of such phenomenon is short enough, it cannot be distinguished and an apparent single-stage ignition pattern occurs.

According to cool flames, this phenomenon has shown to be highly dependent on temperature. Fig. 5.5 shows the ignition delay referred to cool flames for PRF25 under different working conditions. It can be seen that the ignition delay referred to cool flames is shorter if the compression ratio is increased, since higher temperature and pressure is reached. Moreover, the ignition delay sensitivity to the equivalence ratio of the mixture is really low despite the ignition delay referred to cool flames seems to decrease if the equivalence ratio increases. On the one hand, the higher the equivalence ratio, the higher the reactivity of the mixture at low temperature. On the other hand, the higher the equivalence ratio, the higher the heat capacity of the mixture and, therefore, the higher the thermal sink effect, leading to lower temperature. The result of these two phenomena is that cool flames are only slightly affected by the equivalence ratio. It should be mentioned that differences in heat capacity associated to different equivalence ratios are not important enough to see any effect on the ignition delay referred to the high exothermic stage. Finally, the ignition delay referred to cool flames is also shorter if the percent of oxygen is increased. However, the effect of the amount of oxygen on the ignition delay for cool flames is lower than for the high-temperature stage. Cool flames occur due to the slightly exothermic reactions of the initial low-temperature branching mechanism. The H-abstraction of the fuel, $RH$, by its combination with the molecular oxygen, $RH + O_2 = R + HO_2$, is endothermic [8]. Thus, this reaction becomes less relevant when enough active radicals are generated, so that the oxygen content becomes less relevant for cool flames.

The experimental trends obtained when the operating conditions are varied for both ignition delays, referred to cool flames and referred to the high-temperature stage, as well as for the NTC zone, are summarized in Table 5.1. It can be seen that the observed behavior is consistent with the autoignition theory explained in Chapter 2, Section 2.2.2.

Comparing the ignition delay referred to cool flames and referred to the high-temperature stage, both can be scaled with the equivalence ratio and the oxygen content by $\tau \sim Fr^{-a} X_{O_2}^{-b}$ as indicated before, where $a$ and $b$ are

| | **T** ↑ | **P** ↑ | **CR** ↑ | $\mathbf{F}_r$ ↑ | $\mathbf{X}_{O_2}$ ↑ | **ON** ↑ |
|---|---|---|---|---|---|---|
| $\mathbf{t}_{i,1}$ | ↓ | ↓ | ↓ | ↓ | ↓ | ↑ |
| $\mathbf{t}_{i,2}$ | It depends on NTC<br>In general, ↓ | ↓ | It depends on NTC<br>In general, ↓ | Low T cond. ↓<br>High T cond. ↑ | ↓ | ↑ |
| **NTC** | - | Smoother | Smoother | Smoother | Smoother | Smoother |

***Table 5.1.*** *Ignition delay and NTC zone trends when increasing temperature, $T$, pressure, $P$, compression ratio, $CR$, equivalence ratio, $F_r$, oxygen molar fraction, $X_{O_2}$, and octane number value, $ON$.*

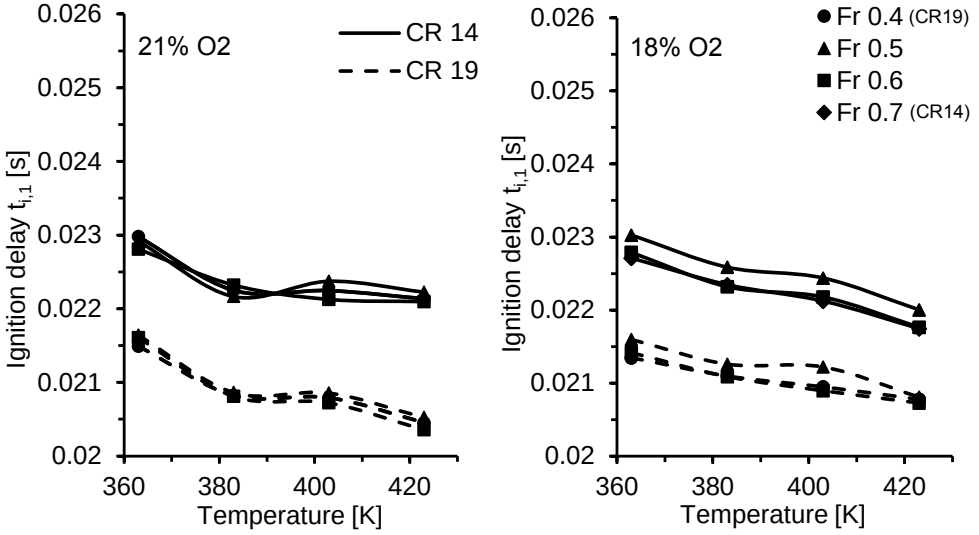


***Figure 5.5.*** *Ignition delay referred to cool flames, $t_{i,1}$, versus initial temperature for PRF25. Both compression ratios are plotted. Left.- $X_{O_2} = 0.21$. Right.- $X_{O_2} = 0.18$.*

positive numbers. Kumar et al. [6] checked that $a_{cool\ flames} < a_{high\ T}$ and $b_{cool\ flames} < b_{high\ T}$. Therefore, the sensitiveness of cool flames to the oxygen content and to the amount of fuel is much lower than for the high-temperature stage, being cool flames a phenomenon mainly controlled by temperature.

## 5.2 Validation of the predictive methods

The accuracy of the different methods to predict ignition delays proposed in this Thesis will be analyzed by comparison to the results of a wide

parametric study performed in an RCEM following this methodology: for a certain case, the evolution of both the in-cylinder temperature and pressure are experimentally obtained under motoring conditions. Then, the ignition delay, $\tau$, and the critical concentration, $[CC]_{crit}$, are obtained for each thermodynamic state by simulation in a perfectly stirred reactor. The ignition delay under transient conditions is then predicted by using the alternative procedures proposed in this investigation and the Livengood & Wu integral method. Besides, the ignition delay under transient conditions is obtained experimentally and it is also calculated by simulating it in an internal combustion engine reactor (direct chemical simulation) solving the corresponding chemical kinetics mechanism. Finally, the predicted ignition delays and the values obtained from the direct chemical simulations are compared directly to the experimental results.

The parametric study performed and a detailed description of the methodological approach can be found in Chapter 3, Sections 3.2 and 3.3.3. Finally, the theoretical development of the proposed predictive methods for cool flames and for the high-temperature stage can be found in Chapter 4, Section 4.2. Furthermore, the information related to the investigation discussed in this section has been already published in [2, 3, 9].

### 5.2.1 Predictive methods applied to cool flames

Ignition delays referred to cool flames are obtained experimentally and by direct chemical kinetic simulation in CHEMKIN. Besides, two different predictive methods have been evaluated. First, the integral method described by Eq. 4.42 has been used assuming $HO_2$ as chain carrier. It is not necessary to evaluate Eq. 4.43, since no disappearance of chain carriers occurs at the same instant than cool flames. Finally, the Livengood & Wu integral method (Eq. 2.6) has been applied by using a $\tau$ function referred to cool flames. It should be noted that cool flames cannot be clearly identified for PRF75 and iso-octane. Therefore, these two fuels are not present in the following analyses.

The percentage deviation in ignition delay, $\epsilon$, was calculated in order to compare more easily experimental and simulation results. This deviation is defined as follows:

$$\epsilon = \frac{t_{i,1x} - t_{i,1RCEM}}{t_{i,1RCEM}} 100 \tag{5.1}$$

where $t_{i,1}$ represents the time of ignition (ignition delay under transient conditions) referred to cool flames. The subscript $x$ can represent either

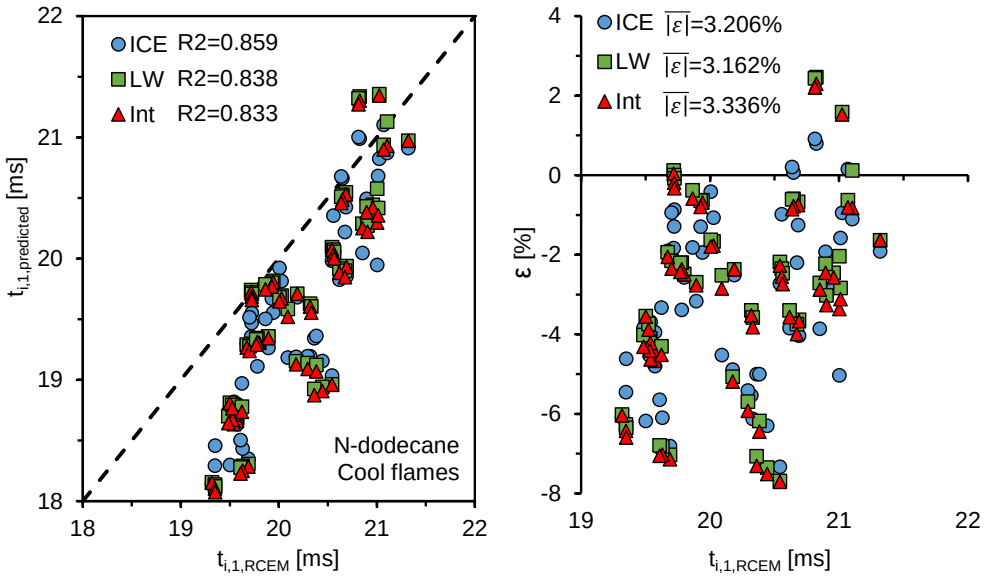


***Figure 5.6.*** *Left.- Simulated and predicted versus experimental ignition delay referred to cool flames. Right.- Ignition delay deviation referred to cool flames for CHEMKIN simulations and for each predictive procedure.* ***The fuel used is n-dodecane****. All the operating conditions are plotted.*

data obtained from a chemical simulation with CHEMKIN using a closed 0-D IC-engine reactor, $ICE$, from the new predictive method, $Int$, or from the Livengood & Wu integral method, $LW$. Finally, the subscript $RCEM$ represents data obtained experimentally from the RCEM.

Figs. 5.6, 5.7, 5.8 and 5.9 to the left show the ignition delay simulations and predictions versus the experimental ignition delay referred to cool flames for n-dodecane, n-heptane, PRF25 and PRF50, respectively. The line $y = x$, which represents a perfect match between values, has also been plotted in the figure. Finally, the Pearson's coefficient of correlation, $R^2$, has been calculated for each method and its value has been added to the figure. Furthermore, the ignition delay deviations, $\epsilon$, versus the experimental ignition delay are shown in Figs. 5.6, 5.7, 5.8 and 5.9 to the right for all cases that show a two-stage ignition pattern. The mean absolute deviations, $|\bar{\epsilon}| = \sum|\epsilon|/N$, have been calculated for each procedure and each fuel, and their values can be seen in the corresponding figure. Furthermore, the confidence intervals of $|\bar{\epsilon}|$ with a confidence level of 95% have been calculated and they are summarized in Table 5.2.

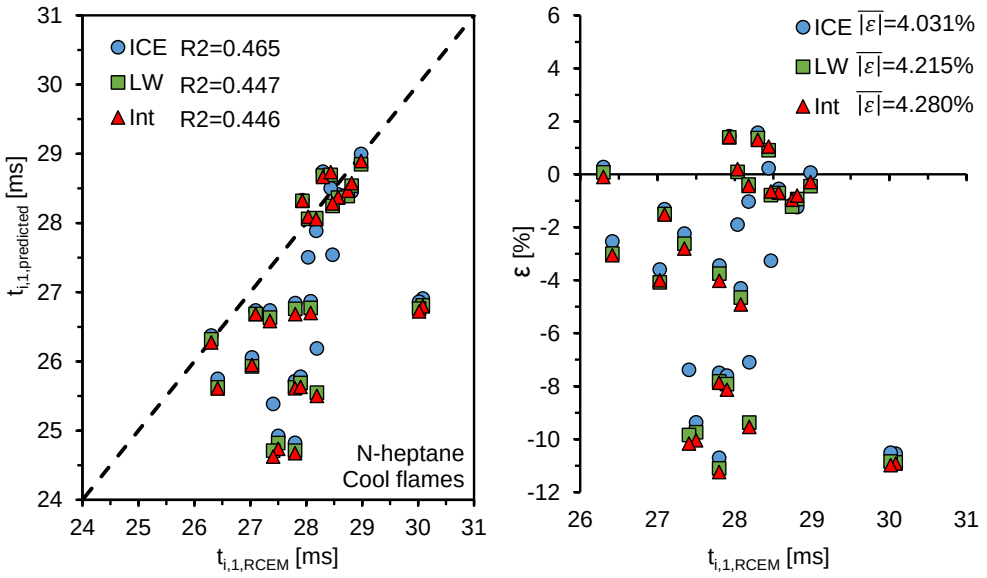


***Figure 5.7.*** *Left.- Simulated and predicted versus experimental ignition delay referred to cool flames. Right.- Ignition delay deviation referred to cool flames for CHEMKIN simulations and for each predictive procedure.* ***The fuel used is n-heptane****. All the operating conditions are plotted.*

| | *ICE* | | *LW* | | *Int* | |
|---|---|---|---|---|---|---|
| | $\overline{\lvert\epsilon\rvert}$ [%] | **CI 95%** [%] | $\overline{\lvert\epsilon\rvert}$ [%] | **CI 95%** [%] | $\overline{\lvert\epsilon\rvert}$ [%] | **CI 95%** [%] |
| **N-dodecane** | 3.206 | [2.702 - 3.710] | 3.162 | [2.622 - 3.702] | 3.336 | [2.796 - 3.877] |
| **N-heptane** | 4.031 | [2.535 - 5.528] | 4.215 | [2.537 - 5.893] | 4.280 | [2.567 - 5.994] |
| **PRF25** | 2.204 | [1.805 - 2.602] | 2.124 | [1.787 - 2.462] | 2.113 | [1.750 - 2.476] |
| **PRF50** | 1.653 | [1.267 - 2.039] | 1.761 | [1.366 - 2.155] | 2.097 | [1.657 - 2.537] |

***Table 5.2.*** *Mean absolute deviations, $\overline{\lvert\epsilon\rvert}$, and confidence interval of $\overline{\lvert\epsilon\rvert}$ with a confidence level of 95% for the ignition delay referred to cool flames. CHEMKIN simulations and predictive methods are included in the table.*

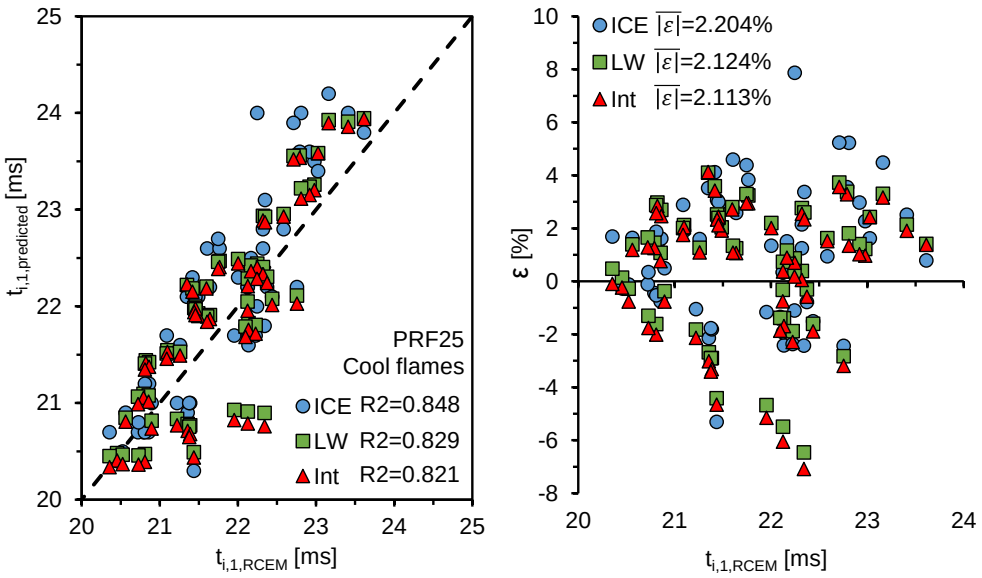


***Figure 5.8.*** *Left.- Simulated and predicted versus experimental ignition delay referred to cool flames. Right.- Ignition delay deviation referred to cool flames for CHEMKIN simulations and for each predictive procedure.* ***The fuel used is PRF25****. All the operating conditions are plotted.*

The values of $|\bar{\epsilon}|$ are very similar to each other, meaning that both predictive methods are able to predict the ignition delay referred to cool flames with approximately the same accuracy than the detailed chemical kinetic mechanism. Therefore, $HO_2$ seems to be a good tracer of cool flames. Furthermore, it should be noted that the Livengood & Wu integral method can be used to predict cool flames without having high deviations, even if a two-ignition pattern occurs, since cool flames are a phenomenon that occurs before the NTC zone.

As it can be seen, the ignition delay is underestimated by predictions and simulations for n-dodecane and n-heptane, specially for short ignition delay values. This is mainly caused by the absence of wall effects in CHEMKIN, which lead to higher pressure rise rates and, therefore, to an underestimation of the ignition delay. However, this effect is only present in n-dodecane and n-heptane. Ignition delays from predictions and simulations of PRF25 and PRF50 show an aleatory distribution around the line $y = x$, which means that ignition delay deviations are caused partly by the chemical kinetic mechanism used and partly by the experimental uncertainties mainly associated to the

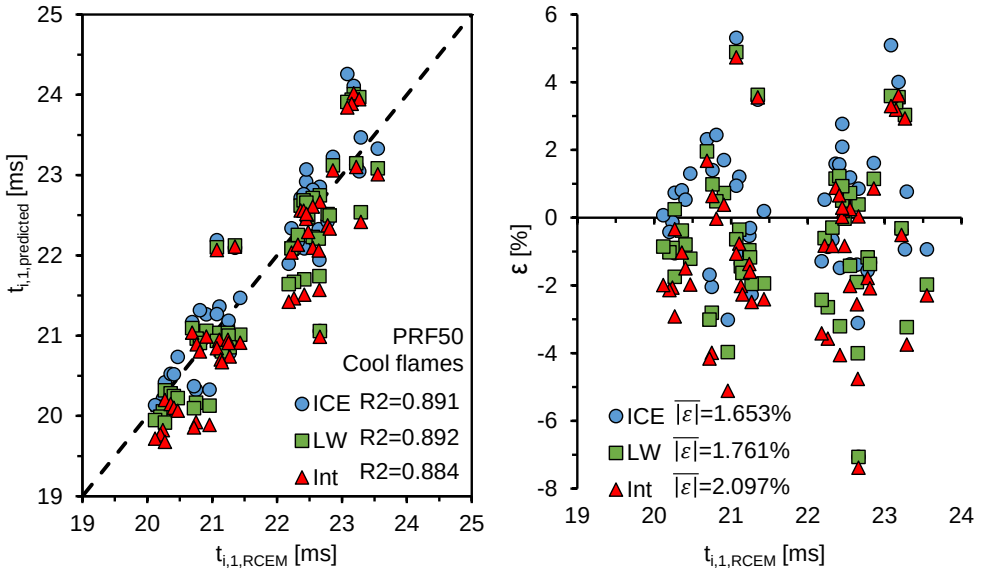


***Figure 5.9.*** *Left.- Simulated and predicted versus experimental ignition delay referred to cool flames. Right.- Ignition delay deviation referred to cool flames for CHEMKIN simulations and for each predictive procedure.* ***The fuel used is PRF50****. All the operating conditions are plotted.*

calculation of the effective volume and the heat losses in the RCEM. The chemical mechanism that was used for PRF mixtures has been designed from the detailed chemical kinetics of n-heptane [10] and iso-octane [11]. Moreover, the mechanism of iso-octane is based on that of n-heptane, where in order to reproduce the very low reactivity observed experimentally at low temperatures (600 $K$ - 700 $K$) the rates of alkyl-peroxyl radical isomerization and peroxy-alkylhydroperoxyl radical isomerization have been artificially decreased by a factor of three (relative to those of n-heptane) [10]. The reason why the isomerization rates of iso-octane are slower than those of n-heptane is not clear (this is probably caused by alternative chemical paths that occur at low temperature and that are not described in the mechanism). This reduction of isomerization rates leads to longer ignition delays when iso-octane is involved, which compensates wall effects for PRF25 and PRF50.

### 5.2.2 Predictive methods applied to the high exothermic stage

Ignition delays referred to the high-temperature stage of the autoignition process are obtained experimentally and by direct chemical kinetic simulation in CHEMKIN. Besides, two different predictive methods have been evaluated. First, the integral method described by Eqs. 4.42 and 4.43 has been used assuming $CH_2O$ as chain carrier. It should be noted that two consecutive integrals have to be evaluated now, one for the accumulation and another for the consumption of chain carriers. Finally, the Livengood & Wu integral method (Eq. 2.6) has been applied by using a $\tau$ function referred to the maximum pressure rise rate.

The percentage deviation in ignition delay, $\epsilon$, was calculated in order to compare more easily experimental and simulation results. This deviation is defined as follows:

$$\epsilon = \frac{t_{i,2x} - t_{i,2RCEM}}{t_{i,2RCEM}} 100 \tag{5.2}$$

where $t_{i,2}$ represents the time of ignition (ignition delay under transient conditions) referred to the high-temperature stage. As before, the subscript $x$ can represent either data obtained from a chemical simulation with CHEMKIN using a closed 0-D IC-engine reactor, $ICE$, from the new predictive method, $Int$, or from the Livengood & Wu integral method, $LW$. Finally, the subscript $RCEM$ represents data obtained experimentally from the RCEM.

Figs. 5.10, 5.11, 5.12, 5.13, 5.14 and 5.15 to the left show the ignition delay simulations and predictions versus the experimental ignition delay referred to the high-temperature stage for n-dodecane, n-heptane, PRF25, PRF50, PRF75 and iso-octane, respectively. The line $y = x$, which represents a perfect match between values, has also been plotted in the figure. Finally, the Pearson's coefficient of correlation, $R^2$, has been calculated for each method and its value has been added to the figure. Furthermore, the ignition delay deviations, $\epsilon$, versus the experimental ignition delay are shown in Figs. 5.10, 5.11, 5.12, 5.13, 5.14 and 5.15 to the right for all cases. The mean absolute deviations, $|\bar{\epsilon}| = \sum|\epsilon|/N$, have been calculated for each procedure and each fuel, and their values can be seen in the corresponding figure. Furthermore, the confidence intervals of $|\bar{\epsilon}|$ with a confidence level of 95% have been calculated and they are summarized in Table 5.3.

The results show that direct chemical kinetic simulations are able to reproduce the experimental ignition delays with quite good accuracy. As before, ignition delay deviations are caused partly by the chemical kinetic

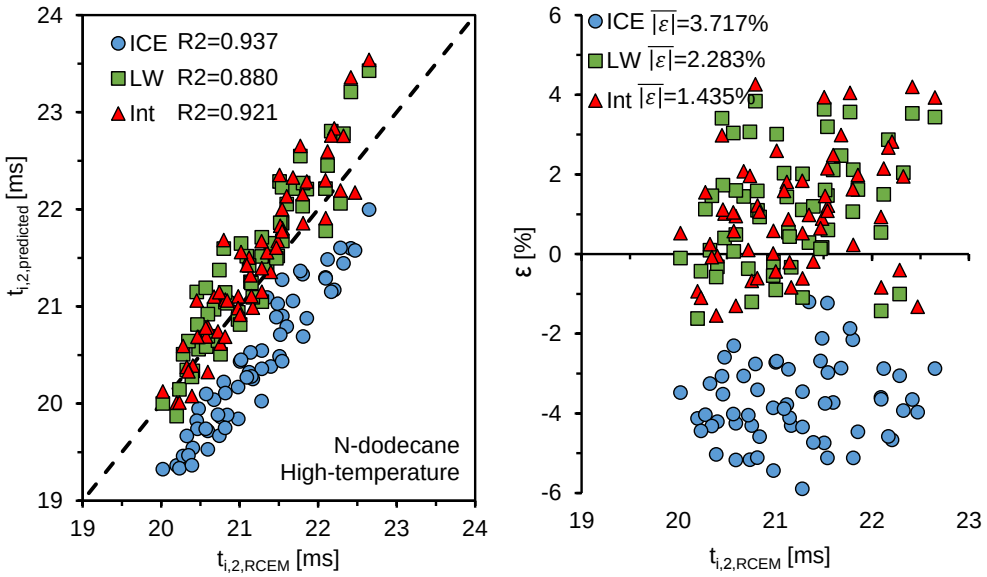


***Figure 5.10.*** *Left.- Simulated and predicted versus experimental ignition delay referred to the high-temperature stage. Right.- Ignition delay deviation referred to the high-temperature stage for CHEMKIN simulations and for each predictive procedure.* ***The fuel used is n-dodecane****. All the operating conditions are plotted.*

| | *ICE* | | *LW* | | *Int* | |
|---|---|---|---|---|---|---|
| | $\overline{\lvert\epsilon\rvert}$ [%] | **CI 95%** [%] | $\overline{\lvert\epsilon\rvert}$ [%] | **CI 95%** [%] | $\overline{\lvert\epsilon\rvert}$ [%] | **CI 95%** [%] |
| **N-dodecane** | 3.717 | [3.453 - 3.980] | 2.283 | [1.104 - 3.463] | 1.435 | [1.148 - 1.722] |
| **N-heptane** | 1.719 | [1.217 - 2.221] | 10.124 | [5.894 - 14.354] | 2.719 | [1.752 - 3.687] |
| **PRF25** | 1.768 | [1.430 - 2.107] | 5.680 | [4.908 - 6.452] | 2.905 | [2.192 - 3.618] |
| **PRF50** | 2.586 | [1.846 - 3.326] | 8.439 | [6.700 - 10.178] | 4.923 | [4.093 - 5.753] |
| **PRF75** | 3.019 | [2.365 - 3.672] | 2.355 | [1.949 - 2.762] | 3.421 | [2.826 - 4.016] |
| **Iso-octane** | 1.738 | [1.206 - 2.270] | 2.814 | [1.428 - 4.200] | 2.278 | [1.453 - 3.103] |

***Table 5.3.*** *Mean absolute deviations, $\overline{\lvert\epsilon\rvert}$, and confidence interval of $\overline{\lvert\epsilon\rvert}$ with a confidence level of 95% for the ignition delay referred to the high-temperature stage. CHEMKIN simulations and predictive methods are included in the table.*

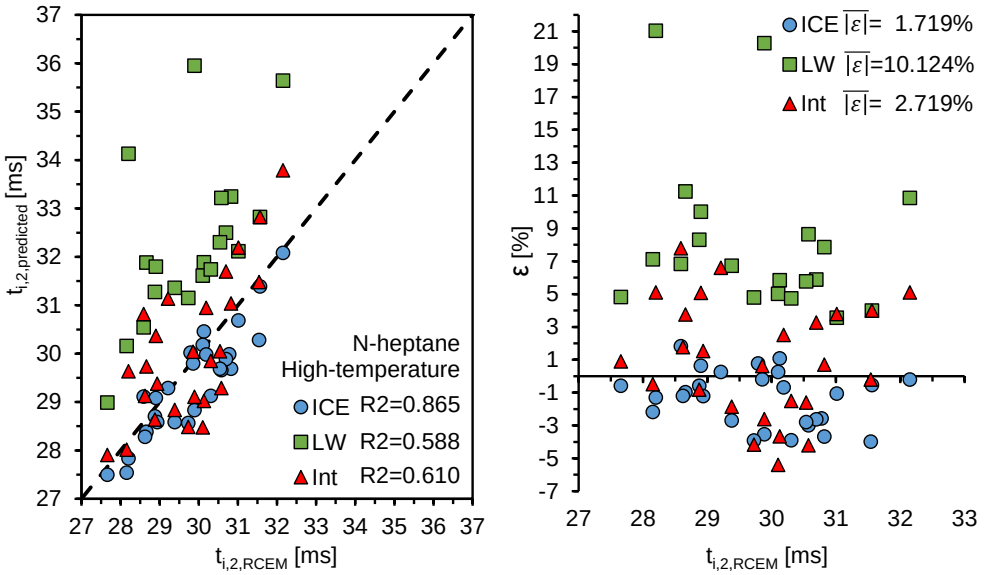


***Figure 5.11.*** *Left.- Simulated and predicted versus experimental ignition delay referred to the high-temperature stage. Right.- Ignition delay deviation referred to the high-temperature stage for CHEMKIN simulations and for each predictive procedure.* ***The fuel used is n-heptane****. All the operating conditions are plotted.*

mechanism used and partly by the uncertainties in the calculation of the effective volume and the heat losses in the RCEM. It can be seen that the ignition delay referred to a maximum pressure rise is slightly underestimated for n-heptane but slightly overestimated for iso-octane. As explained above, this fact can be caused by the isomerization rates of alkyl-peroxyl radicals and peroxy-alkylhydroperoxyl radicals, which have been decreased by a factor of three compared to n-heptane in the case of the iso-octane sub-mechanism. Thus, higher percentage of iso-octane implies more overestimated ignition delays. Regarding n-dodecane, it should be taken into account that the experimental results are affected by wall effects that are not included in the simulations. Thus, more sudden heat release rates are presented in the numerical results, which lead to a certain trend to under-predict the ignition time.

The new integral method proposed in this paper shows good agreement with the experiments. However, the accuracy of the Livengood & Wu integral method shows a strong dependence on the type of fuel. It can be seen that the Livengood & Wu integral is able to predict accurately the ignition

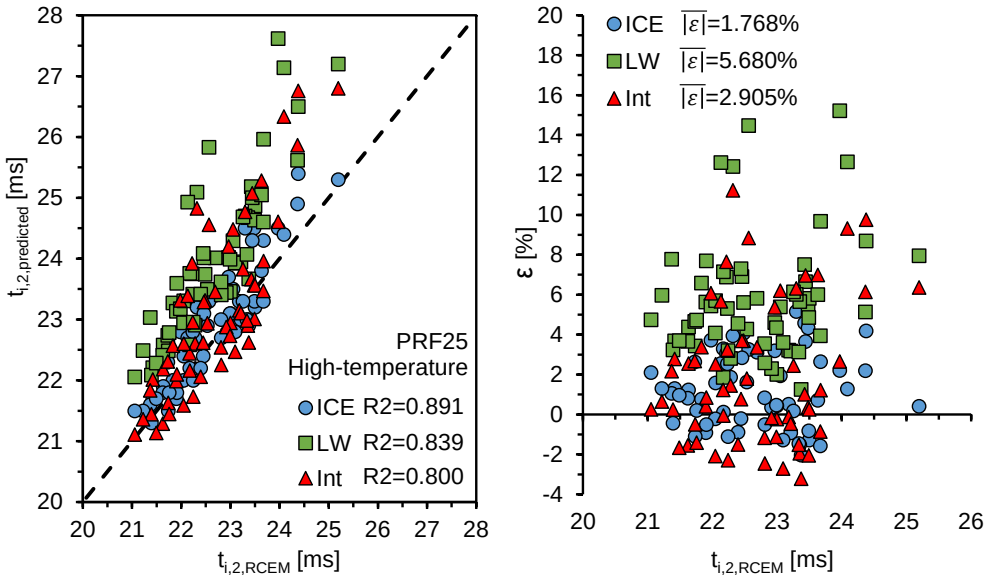


***Figure 5.12.*** *Left.- Simulated and predicted versus experimental ignition delay referred to the high-temperature stage. Right.- Ignition delay deviation referred to the high-temperature stage for CHEMKIN simulations and for each predictive procedure.* ***The fuel used is PRF25****. All the operating conditions are plotted.*

delay referred to the high exothermic stage of combustion if the fuel shows a single-stage ignition pattern (PRF75 and iso-octane), but the predictive capability is significantly reduced when a two-stage ignition process occurs (n-heptane, PRF25 and PRF50). The ignition delay of n-dodecane is also properly predicted by the Livengood & Wu integral, probably because the NTC zone of n-dodecane is placed at higher temperatures than for PRF mixtures. Thus, its influence on the integral method is lower than for other fuels. The Livengood & Wu predictive method assumes that autoignition occurs when a critical concentration of chain carriers is reached. Therefore, only ignition delays referred to a critical concentration can be predicted, which occur at a different stage than the maximum pressure rise rate. Moreover, only information referred to a critical concentration of chain carriers, $\tau$, should be used in the integral by definition of the method itself. These facts cause an intrinsic deviation between predictions and experimental results, which leads to unacceptable predictions for fuels that show cool flames. It should be noted that the smoother the NTC zone, the more similar the ignition delay referred to a critical concentration and referred to a maximum pressure rise rate, so

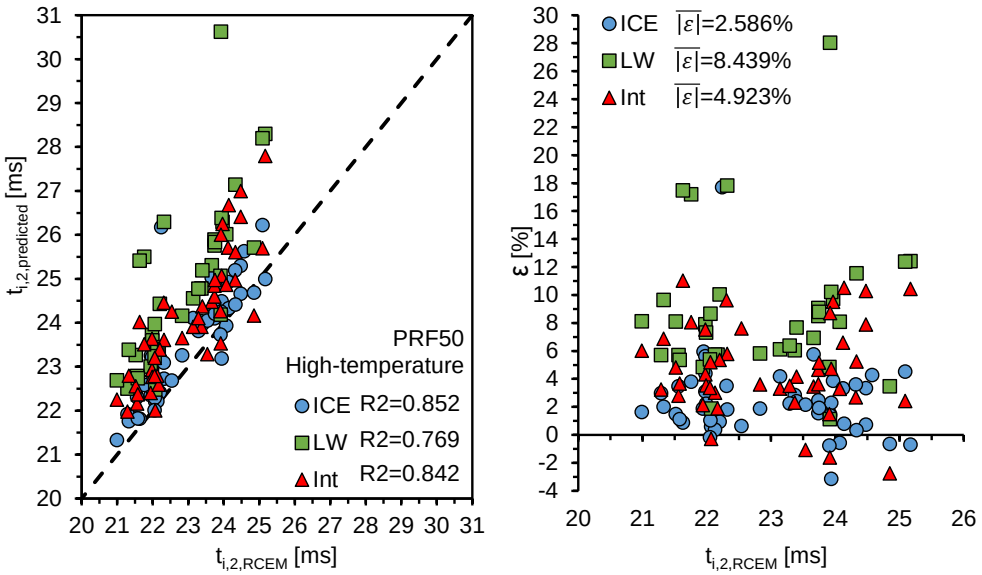


***Figure 5.13.*** *Left.- Simulated and predicted versus experimental ignition delay referred to the high-temperature stage. Right.- Ignition delay deviation referred to the high-temperature stage for CHEMKIN simulations and for each predictive procedure.* ***The fuel used is PRF50****. All the operating conditions are plotted.*

that the accuracy of the Livengood & Wu integral is increased under these conditions.

### 5.2.3 Conclusions

The following conclusions can be deduced from this study:

- Both predictive methods tested in this work can predict with quite good accuracy the ignition time referred to cool flames, demonstrating that $HO_2$ can be taken as a good cool flame tracer under a wide range of octane numbers and that the Livengood & Wu integral method works properly for cool flames.

- The alternative integral method has shown to be able to predict the ignition delays referred to a maximum pressure rise rate when $CH_2O$ is taken as chain carrier. This ignition delay can be experimentally

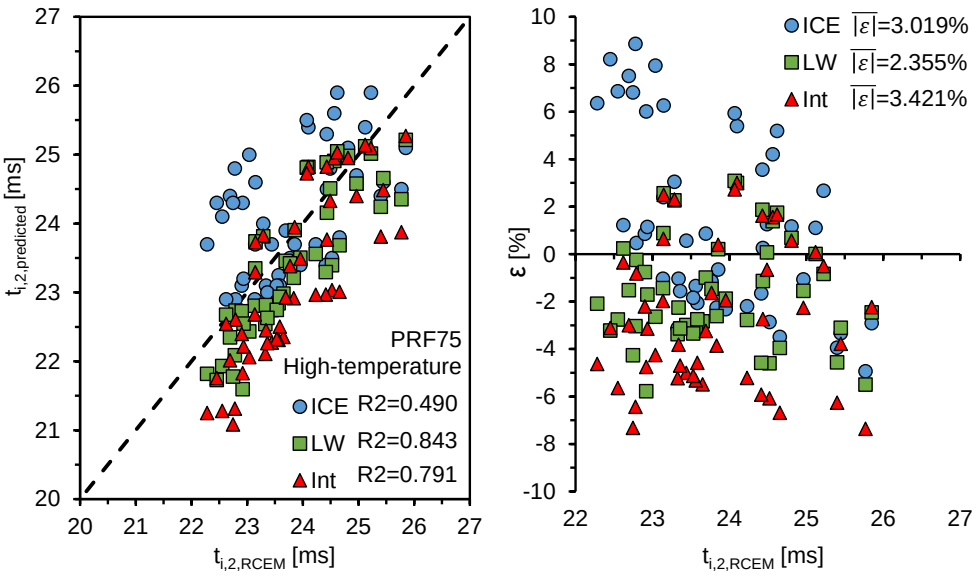


***Figure 5.14.*** *Left.- Simulated and predicted versus experimental ignition delay referred to the high-temperature stage. Right.- Ignition delay deviation referred to the high-temperature stage for CHEMKIN simulations and for each predictive procedure.* ***The fuel used is PRF75****. All the operating conditions are plotted.*

measured, allowing a direct comparison between predictions and experiments.

- The Livengood & Wu integral method is able to predict ignition delays referred to the high exothermic stage of combustion only if the fuel shows a single-stage ignition pattern. This method is originally based on the premise that autoignition occurs when the critical concentration of chain carriers is reached. Therefore, the predicted ignition delays will be referred to this criterion and the information used to obtain the predictions may be also referred to this criterion. Otherwise, an intrinsic deviation between predictions obtained from the Livengood & Wu integral and the experimental results appears, since both ignition delays could be referred to different stages of the combustion process. If the fuel does not present a two-stage ignition pattern or if the NTC zone is very soft, all criteria to define the ignition delay are virtually the same and they can be compared to each other. Thus, the Livengood & Wu integral can be used with high accuracy to predict ignition delays

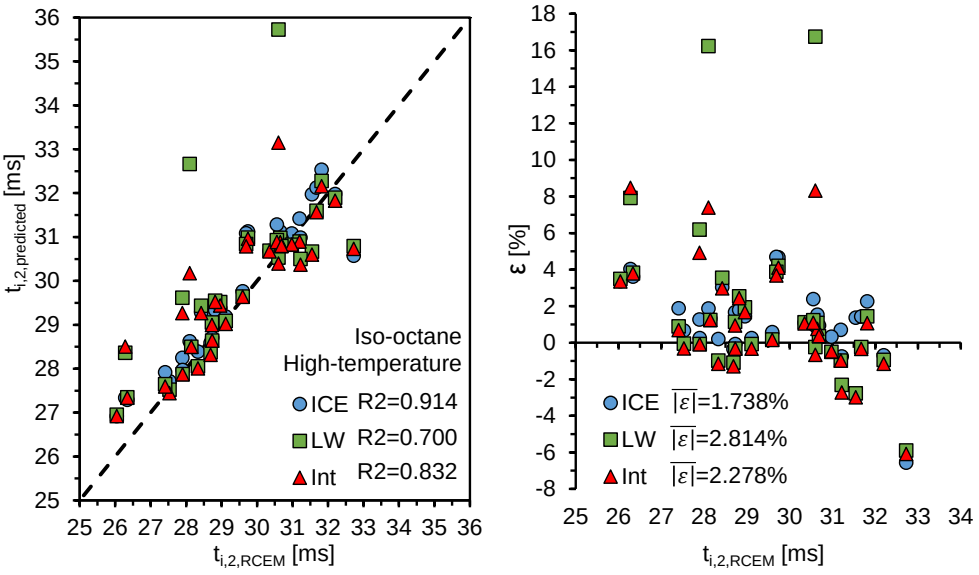


***Figure 5.15.*** *Left.- Simulated and predicted versus experimental ignition delay referred to the high-temperature stage. Right.- Ignition delay deviation referred to the high-temperature stage for CHEMKIN simulations and for each predictive procedure.* ***The fuel used is iso-octane****. All the operating conditions are plotted.*

of single-stage ignition fuels, but not with fuels that show a two-stage ignition pattern.

## 5.3 Generalization of the autoignition event. Autoignition measurements by means of optical techniques

In this section, a spectroscopic analysis of the autoignition event is presented, highlighting the dominant radiation in each stage of the process. First, experimental results from a photo-multiplier and from a high speed camera are compared to chemical simulations, validating an OH* sub-model that allows to distinguish excited and natural state of such species in chemical kinetic simulations. Furthermore, the possibility of measuring ignition delays by means of optical techniques is also explored. Then, the spectroscopic

analysis is carried out. Finally, the generalization of the autoignition event (percent of the combustion chamber ignited) is studied.

A detailed explanation about the methodological approach can be found in Section 3.3.3, while the parametric study performed is described in Section 3.2, both from Chapter 3. Furthermore, the information related to the investigation discussed in this section has been already published in [1, 12].

### 5.3.1 Validation of the OH* sub-model. Optical measurements of the ignition delay

Two additional ignition delays are defined in order to compare the experimental measurements to the chemical simulations using the OH* sub-model:

- $t_{i,CO}$ represents the ignition delay referred to a maximum oxidation rate of $CO + O \Rightarrow CO_2 + hv$, which is an estimator of the $CO$ continuum.
- $t_{i,OH}$ represents the ignition delay referred to a maximum concentration of OH*, which is an estimator of the OH* chemiluminescence.

Both ignition delays are also experimentally obtained by means of a photo-multiplier and by means of a high-speed camera. Thus, the instant at which the maximum integrated radiation occurs is defined as the ignition time.

Both ignition delays are also obtained by simulation from CHEMKIN. The percentage deviation in the ignition delay, $\epsilon$, has been calculated in order to compare more easily experimental and simulation results. This deviation is defined as follows:

$$\epsilon = \frac{t_{i,x,ICE} - t_{i,x,RCEM}}{t_{i,x,RCEM}} 100$$

where $t_{i,x}$ represents the ignition delay time. The subscript $x$ represents one of the definitions, maximum oxidation rate of $CO$ to $CO_2$ (ignition delay referred to $CO$) or maximum concentration of OH* (ignition delay referred to OH*). Finally, the subscript $RCEM$ represents an experimental ignition delay. The ignition delay can be measured by two different ways, by means of the photo-multiplier or by means of the high-speed camera. In this case, data from the photo-multiplier has been used since it has higher temporal resolution. Of course, only the cases that show OH* peak in the spectroscopy analysis are taken into account for the calculation of the ignition delay deviation referred to OH*, and vice versa.

| | $t_{i,OH}$ | | $t_{i,CO}$ | |
|---|---|---|---|---|
| | $\bar{\epsilon}$ [%] | **CI 95%** [%] | $\bar{\epsilon}$ [%] | **CI 95%** [%] |
| **N-heptane** | 1.153 | [0.581 - 1.725] | 1.847 | [1.353 - 2.341] |
| **Iso-octane** | 2.256 | [1.602 - 2.910] | 1.976 | [1.324 - 2.628] |

***Table 5.4.*** *Mean absolute deviations, $|\bar{\epsilon}|$, and confidence interval of $|\bar{\epsilon}|$ with a confidence level of 95% for the ignition delay referred to a peak of radiation.*

The average of the deviations in absolute value ($\bar{\epsilon} = \sum \mid \epsilon \mid /n$), has been calculated for each fuel, as well as its confidence interval with a confidence level of 95 %, the results of which are summarized in Table 5.4.

Of course, the times obtained from the two experimental methods should be virtually the same, since both methods measure the same parameter in parallel. In fact, the confidence interval with a confidence level of 95% of the mean relative deviation between these two methods is equal to [0.069 0.116] % for n-heptane and to [0.112 0.223] % for iso-octane. The existence of a certain deviation between both experimental methods is justified by the different acquisition frequency. More specifically, Fig. 5.16 shows that the profiles obtained from the photo-multiplier and by integrating the luminosity detected by the camera are almost identical. This is a logical results as both detection methods are measuring the same parameter in parallel.

Comparing Tables 5.3 and 5.4, it can be concluded that the aforementioned deviations are mainly caused by a deviation in the autoignition chemistry and not in the accumulation of excited OH*. The excited $OH$ sub-model is able to predict with high accuracy the time at which the OH* is accumulated (high temperature stage of the autoignition process). In fact, Fig. 5.17 shows the time evolution of the normalized OH* intensity from the high speed camera, as well as the normalized OH* molar fraction from CHEMKIN and the oxidation of $CO$ to $CO_2$, for two cases.

Fig. 5.17 to the left shows a case in which the OH* radiation is outshined by the $CO$ oxidation. Therefore, two different sources of radiation can be measured. On the one hand, the luminosity recorded during the combustion belongs to the $CO$ continuum. On the other hand, the decay starting from $\approx$0.03075 $s$, which occurs after the combustion, may belong to the OH* chemiluminescence. Fig. 5.17 to the right shows a case in which the OH* radiation is dominant. Therefore, all the chemiluminescence at 310 $nm$ belongs to this radical. It should be noted that the lifetime of the luminosity is

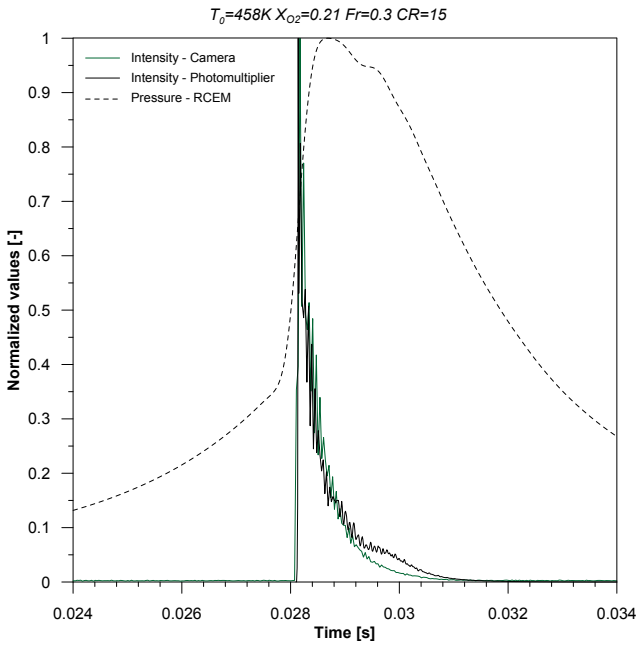


***Figure 5.16.*** *Normalized evolution of the chemiluminescence intensity signal from camera and photomultiplier, and experimental pressure for iso-octane at $CR$=15, $T_0$=458 K, $X_{O_2}$=0.21 and $F_r$=0.3.*

much longer since the decay of the OH* is more gradual. The measured OH* radiation is consistent with the OH* predicted by the chemical kinetic mechanism. However, the lifetime of OH* obtained by CHEMKIN is longer than the obtained experimentally. This is caused by the limitations in the measurements, since the luminous intensity is too low as the temperature decreases. Both experimental methods show similar profiles, and it can be seen that a short lifetime of the luminous intensity is directly related to an absence of a peak of OH* in the spectroscopic analysis, as it will be shown below.

The OH* intensity is directly related to the amount of accumulated OH* and with the thermodynamic conditions in the combustion chamber. The higher the reached temperature and the higher the concentration of OH*, the higher its luminous intensity. The combination of low temperature and small concentration of OH* is the reason why cool flames are not detected by the photo-multiplier nor by the camera.

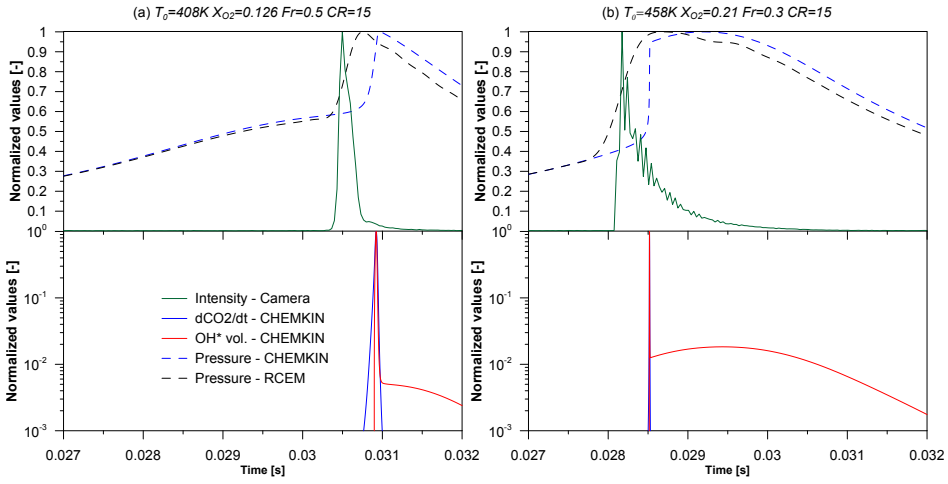


***Figure 5.17.*** *Normalized evolution of the oxidation rate of CO, OH* molar fraction, integrated natural chemiluminescence intensity from camera, and simulated and experimental pressure for two different cases fueled with iso-octane, with and without OH* peak in the spectrographic analysis. Left.- Chemiluminescence belongs to CO continuum. Right.- Chemiluminescence belongs to OH*.*

Finally, Fig. 5.18 shows a comparison between the molar fraction of $OH$ at its ground and excited states for the two cases previously discussed. It can be seen that the peaks take place at the same instant for each of the cases, which corresponds to the maximum chemiluminescence radiation time. Nevertheless, the decay is different for both cases and therefore the lifetime of the radiation will also be different than the lifetime of $OH$ at its ground state. In this sense, a sub-model for the prediction of excited $OH$ is necessary to perform a chemical kinetic analysis of chemiluminescence results.

### 5.3.2 Spectroscopic analysis

A spectroscopic analysis was performed to determine the source of the radiation measured by chemiluminescence at 310 $nm$. The results showed two different scenarios, which can be seen in Fig. 5.19.

On the one hand, for very lean or very low-temperature conditions, the spectrum is dominated by the $CO$ continuum, which covers a range of wavelengths from 300 $nm$ to 550 $nm$. In these cases no peak of intensity

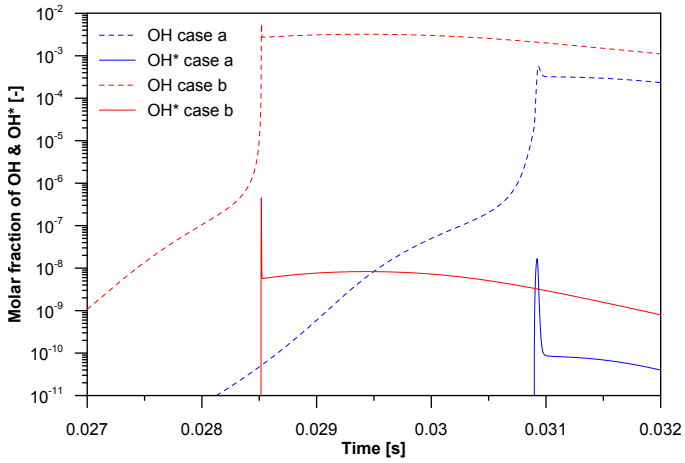


***Figure 5.18.*** *Molar fraction of OH and OH* for the two different cases represented in Fig 5.17.*

can be seen around 310 *nm*, which implies that chemiluminescence at this wavelength belongs to the *CO* continuum and it outshines the OH* radiation. On the other hand, a clear and long-lasting peak of intensity centered at 310 *nm* can be identified when a more intense combustion occurs. Thus, the chemiluminescence measured in these cases may belong to OH*. Therefore, the experiments can be divided in two groups, those that present an OH* peak in the spectroscopic analysis and those that only show the *CO* continuum. These groups are shown in Table 5.5.

Figs. 5.20 and 5.21 show two sequences of images where the evolution of the chemiluminescence at 310 *nm* over time can be seen in terms of intensity and area. Besides, the spectra of the combustion chamber are also shown for each time of the sequences. In Figure 5.20, a peak of OH* in the spectrum of the combustion can be clearly seen, which means that the chemiluminescent radiation measured belongs to the OH* radical. However, the absence of a peak in the spectrum of Fig. 5.21 implies that the measured chemiluminescence belongs to *CO*. Additionally, by linking the information provided by Fig. 5.17, the auto-ignition and combustion process can be described as follows:

i For two-stage ignitions, the so called cool flames start appearing and a small peak in the pressure rise rate can be seen. There is a tiny amount of

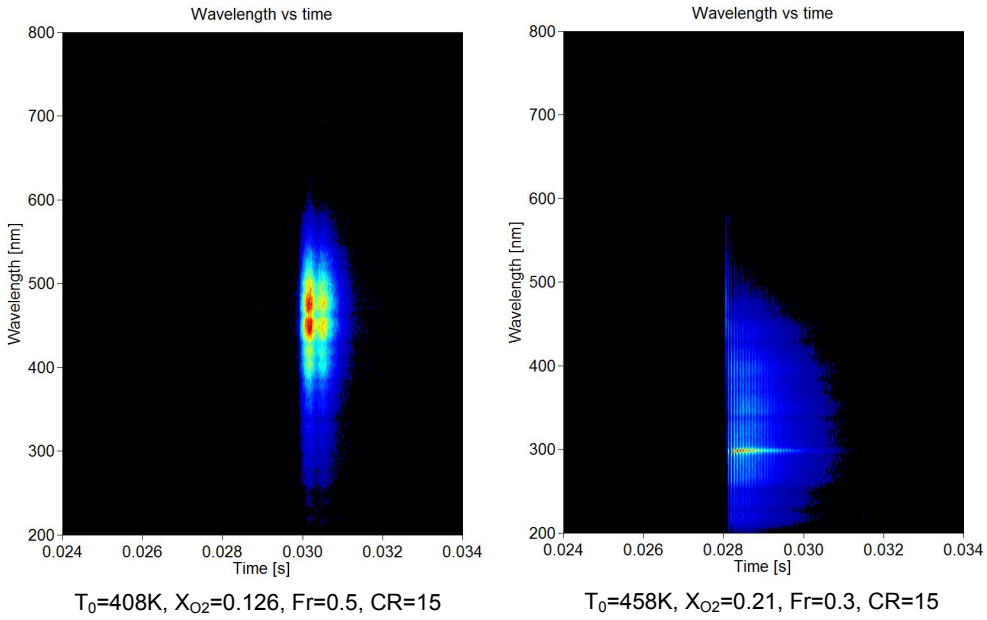


***Figure 5.19.*** *Evolution of the spectrum inside the chamber for two different cases fueled with iso-octane. Left.- without OH* peak at 310 nm. Right.- with OH* peak at 310 nm.*

radicals generated, which added to the low temperature are not enough to generate significant luminosity. In fact, a really small amount of OH* is accumulated according to the validated sub-model, being the main formation reaction of such radical $HO_2 + H \Rightarrow OH + OH^*$. However, $HO_2$ has an accumulation behavior during cool flames and the relevance of the previous reaction is negligible. Moreover, the excited OH* that is formed during this stage reacts with $CH_3$ through the third body reaction $CH_3 + OH^* + M \Rightarrow CH_3OH + M$. Therefore, the decay of excited OH to its ground state is negligible during this stage and no radiation is emitted.

ii With the start of the NTC behavior there is a decrease in reactivity as the formation of chain carriers and formation of olefins are competing against each other, causing a change of slope in the pressure curve. Almost all the exothermic reactions are frozen during this stage, including the generation and decay of OH*. Thus, no radiation can be seen during the NTC zone.

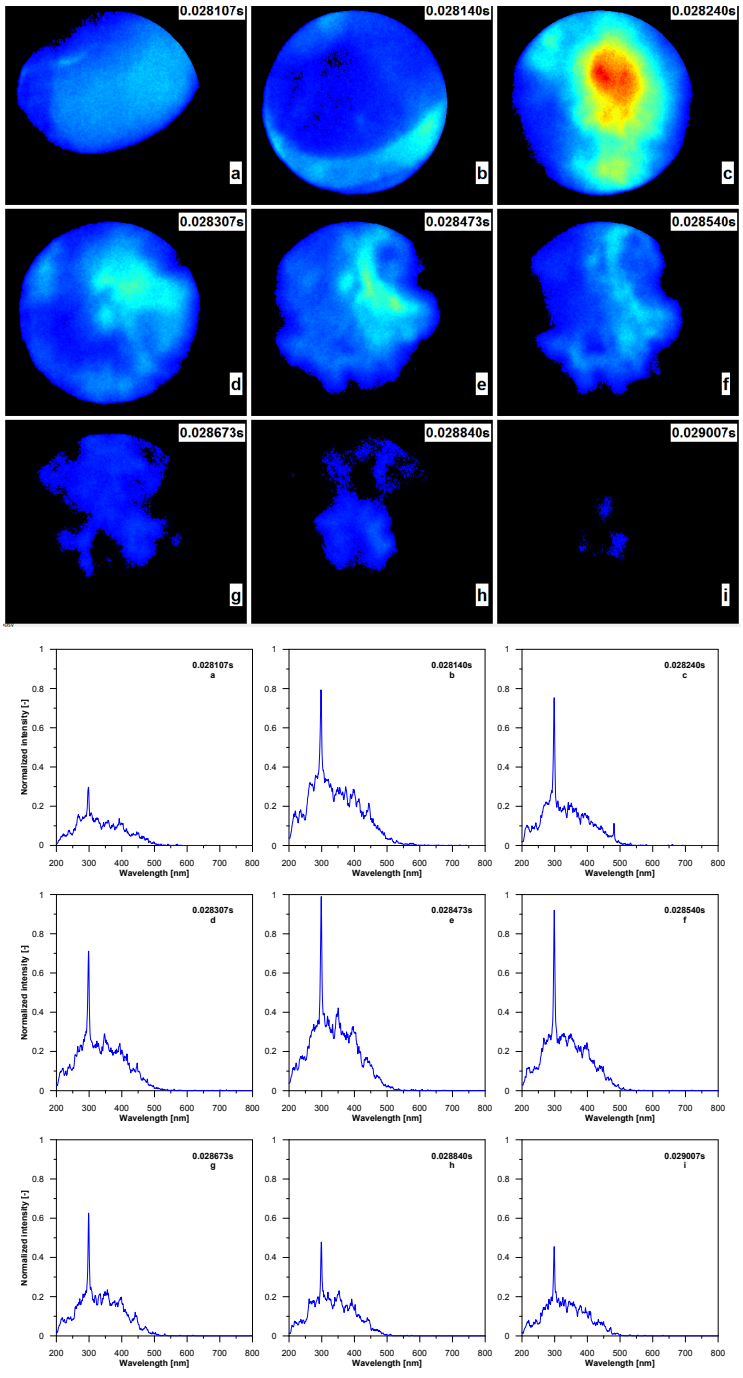


***Figure 5.20.*** *Evolution of chemiluminescence and spectroscopic analysis inside chamber for iso-octane at CR=15, $T_0$=458 K, $X_{O_2}$=0.21 and $F_r$=0.3. Top.- OH* intensity. Bottom.- Spectra.*

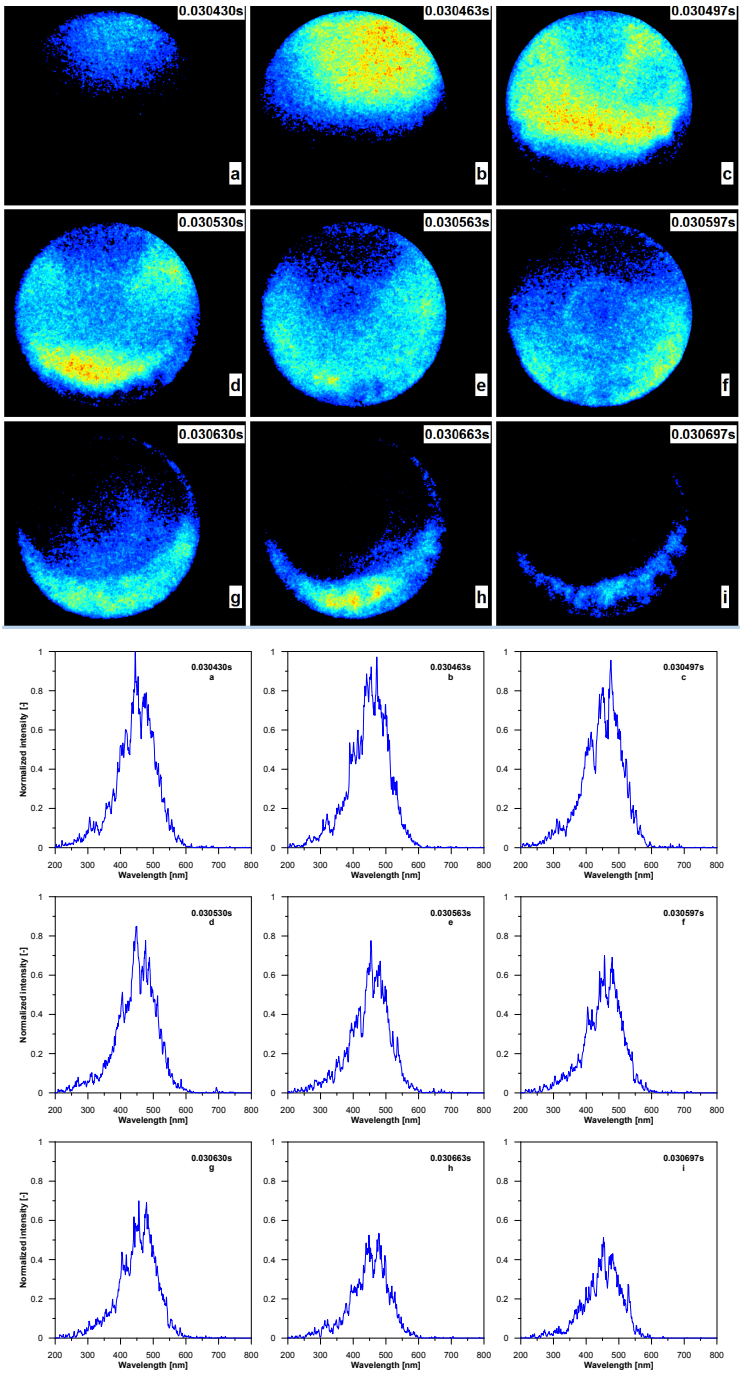


***Figure 5.21.*** *Evolution of chemiluminescence and spectroscopic analysis inside chamber for iso-octane at CR=15, $T_0$ 408 K, $X_{O_2}$=0.126 and $F_r$=0.5. Top.- CO continuum intensity. Bottom.- Spectra.*

| | | $\mathbf{T_0}$ $[K]$ | | | | |
|---|---|---|---|---|---|---|
| | | **358** | **383** | **408** | **433** | **458** |
| $F_r$ [-] | **0.3** | 0.126 | | 0.21, 0.147, 0.126, 0.105 | | 0.126 |
| | **0.4** | 0.21, 0.147, 0.126, 0.105 | 0.126, 0.105 | 0.21, 0.147, 0.126, 0.105 | 0.126,0.105 | 0.21, 0.147, 0.126, 0.105 |
| | **0.5** | 0.126 | 0.126 | 0.126, 0.105 | 0.126 | 0.126 |
| | **0.6** | 0.126 | | 0.126, 0.105 | | 0.126 |
| | **0.7** | | | 0.126, 0.105 | | |
| | **0.8** | | | 0.126, 0.105 | | |

***Table 5.5.*** *Parametric study performed, oxygen molar fractions for different initial temperature values and equivalence ratios for iso-octane and n-heptane. Green.- cases in which there is a peak of OH*. Black.- cases in which the CO continuum outshines the OH*.*

iii The NTC stage comes to an end due to a slight increase in temperature. This phase is controlled by the decomposition of $H_2O_2$ through the third-body reaction $H_2O_2 + M \Rightarrow 2OH + M$. There is still no presence of OH* chemiluminescence as the $OH$ generated is consumed to oxidize formaldehyde into $CO$ instead of forming excited OH*. At this point the high-temperature heat release starts.

iv After its formation, $CO$ starts to oxidize into $CO_2$. As it can be seen in Fig. 5.22, the oxidation of $CO$ is mainly caused by $OH$ through $CO + OH \Rightarrow CO_2 + H$ and by $O$ through $CO + O \Rightarrow CO_2 + hv$ (which is a luminous reaction). Therefore, the so called $CO$ continuum starts. This light emission covers a range of wavelengths from 300 $nm$ to 550 $nm$ and, if it is bright enough, it can outshine the OH* chemiluminescence. At the same time, the $OH$ accumulation mainly starts through reactions $O + H_2O \Rightarrow OH + OH^*$ and $H + O_2 \Rightarrow O + OH$. The appearance of excited OH* is promoted by the accumulation of $OH$ and the chemiluminescence radiation starts. Light is emitted by the decay of OH* to its ground state mainly thanks to its reaction with $O_2$, CO, $CO_2$, $H_2O$ and $N_2$ ($OH^* + M \Rightarrow OH + M$). Regarding the specific reaction rate of the decay reaction for OH*, $H_2O$ is the dominant third body species whereas $N_2$ is the less relevant according to the proposed enhanced third body efficiencies. At the end of this phase the pressure

rise rate reaches a peak (Fig. 5.17) and it is at this instant when the chemiluminescence takes up the whole chamber (Figs. 5.20-c and 5.21-c).

Two different scenarios can be present at this stage, controlled by the temperature through the $HO_2 + H \Rightarrow OH + OH^*$ reaction (Fig. 5.22). For lean equivalence ratios or low-temperature conditions the accumulated OH* is not enough and the natural chemiluminescence at 310 $nm$ belongs to the $CO$ continuum, since no peak can be seen at this wavelength (Fig. 5.21 to the bottom). However, for higher combustion temperature values the active compound $H$ formed during the oxidation of $CO$ terminates with the radical $HO_2$ (last chain carrier to disappear) through $HO_2 + H \Rightarrow OH + OH^*$. The increase of relevance of this reaction at high combustion temperatures causes a higher OH* accumulation, which leads to a brighter OH* emission. In this case, a peak of intensity can be seen at 310 $nm$ (Fig. 5.20to the bottom), which means that the chemiluminescence at this wavelength belongs to OH*.

v Once the $CO$ has been oxidized into $CO_2$ the maximum cycle pressure is reached and the heat release stops (Fig. 5.17). For the cases in which the $CO$ continuum predominates, this instant coincides with the end of the light emission (Fig. 5.21-i). However, for the cases that show peak of OH*, significant amounts of this radical remain in the combustion chamber and the luminous intensity continues during part of the expansion (Fig. 5.20-h).

vi Finally, the excited OH* disappears and the chemiluminescence of OH* stops. Since the $OH$ radical is only stable at high temperatures, it also disappears during the expansion stroke (Fig. 5.20-i) by its recombination with atomic oxygen, $OH + O \Rightarrow O_2 + H$.

The oxidation of $CO$ and the accumulation of OH* occur simultaneously. Therefore, a priori, it is not possible to decide without a spectrograph if the chemiluminescence at 310 $nm$ belongs to OH* or if it is outshined by the $CO$ continuum. However, it should be noted that the lifetime of the luminous intensity is very different in case of belonging to $CO$ continuum or to OH*, as can be seen in Fig. 5.17, where the lifetime of the OH* chemiluminescence is 0.65 $ms$ longer than the $CO$ continuum luminosity. Thus, it is possible to use this parameter as a criterion to determine the source of the radiation.

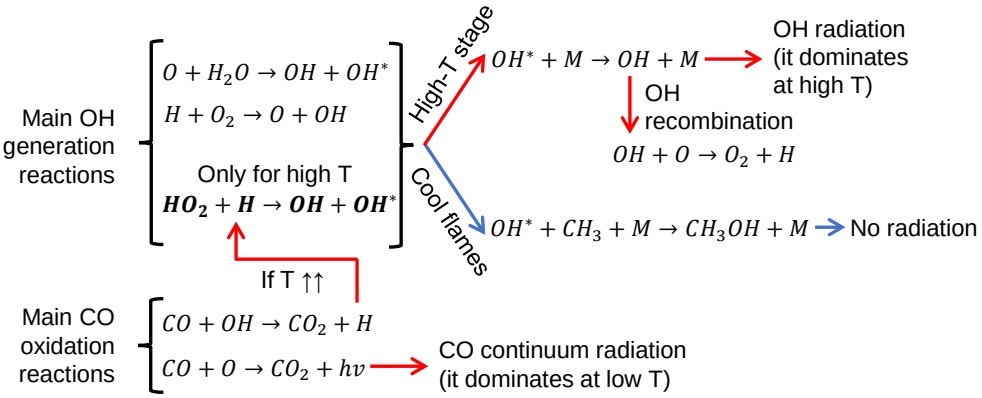


***Figure 5.22.*** *$OH^*$-OH and CO-$CO_2$ scheme. The two radiation sources at 310 nm are described, as well as the key reaction that controls the dominant radiation ($HO_2$ + H ⇒ OH + $OH^*$, in bold).*

### 5.3.3 Generalization and intensity of the auto-ignition

The generalization of the auto-ignition is defined as the percentage of the combustion chamber that has ignited during a certain instant. Simultaneously the instant at which the largest variation of area takes place is also the instant at which the chemiluminescent radiation is the most intense. Moreover, both phenomena also occur at the peak of the pressure rise rate curve. Therefore, the mixture ignites abruptly causing a rise in the pressure while the radiation is maximum and present throughout almost the whole combustion chamber.

Figs. 5.20 and 5.21 show two sequences of images where the evolution of the chemiluminescence over time can be seen in terms of intensity and area. Additionally, it can be seen that the ignition always starts at the top of the combustion chamber. This is caused by the existence of a cooled piezoelectric pressure sensor at the bottom of the cylinder head, which leads to a hot spot at the top of the combustion chamber. It should be mentioned that such effect occurs only in the RCEM available at ETH - Zurich, since an uncooled pressure sensor is used in the facility available at CMT - Motores Térmicos. Nevertheless, the ignition is very quickly generalized, which is consistent with Fig. 5.16. The luminosity ends first at the top, as the combustion begins there, and the last section of the window to show any chemiluminescence is at the bottom. The observed *virtual* propagation velocity is too fast for a

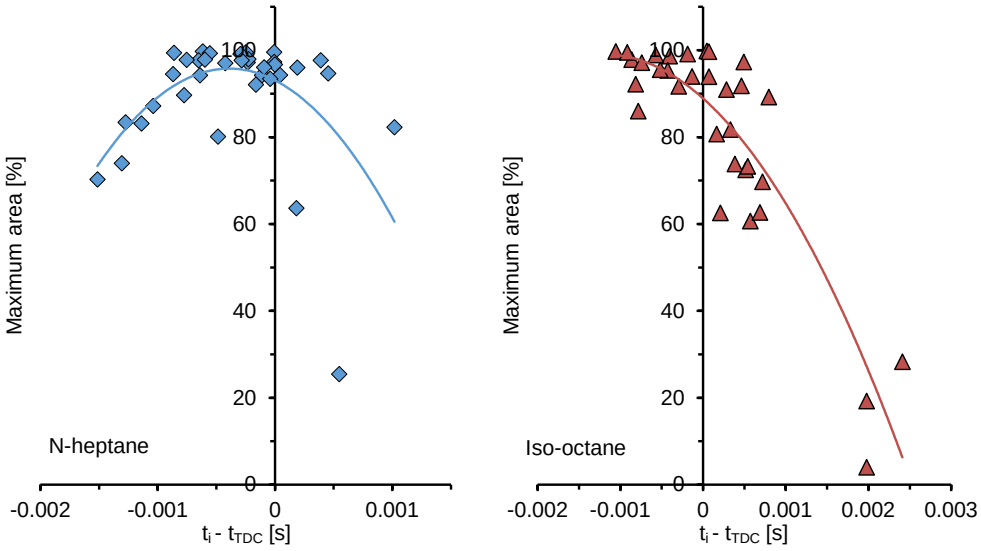


***Figure 5.23.*** *Maximum illuminated area versus the ignition time referred to TDC, $t_i - t_{TDC}$, for both fuels at all conditions.*

turbulent flame front propagation, which supports the argument that it is an autoignition process.

Fig. 5.23 shows the evolution of the maximum area as a function of the instant after TDC at which the ignition occurs. Very reactive or poorly reactive conditions (i.e., ignition events far away of TDC) do not lead to 100% of occupied area because the thermodynamic conditions are not optimal for the generation of radiation. More specifically, the luminous area is maximized if the characteristic propagation time of the reaction front is shorter than the life time of the radiation (which is an estimator of the combustion duration). Thus, depending on the reactivity gradient established in the chamber at the ignition time, the propagation of the autoignition front will lead to slower ignitions and areas below 100%. With this in mind, the trends presented in Fig. 5.23 summarize the hypotheses of area vs time relationship. It can be seen for n-heptane, which has ignition times close to TDC, that most values are very high and close to 100% (Fig. 5.23 to the left), while the values that occur either too soon or too late have smaller areas. For iso-octane the trend is also similar, however the values are not. Since for this second fuel ignition times mostly occur after TDC, hence the fitted line points downwards instead of being balanced on the center (Fig. 5.23 to the right).

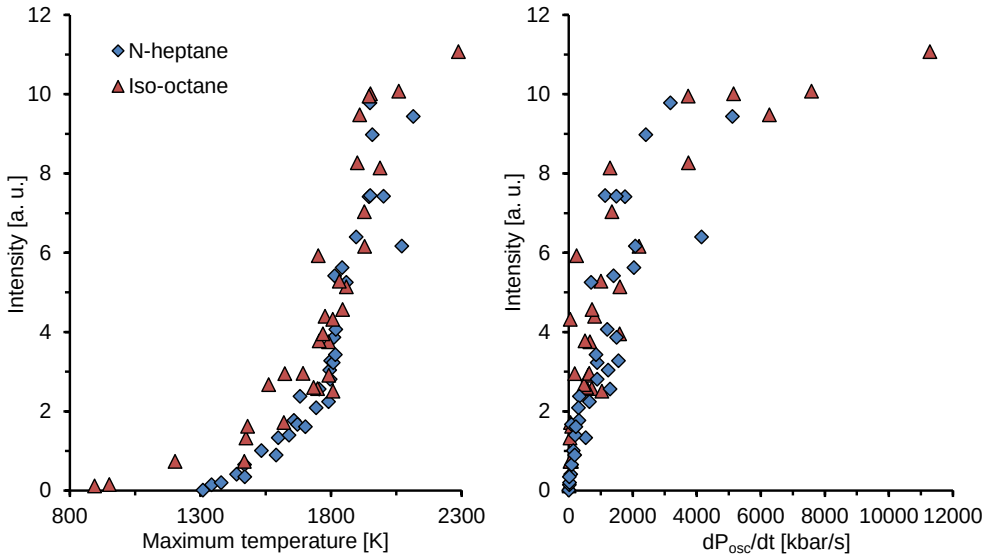


***Figure 5.24.*** *Maximum luminous intensity from the photo-multiplier. Left.- versus maximum temperature reached in the cycle. Right.- versus maximum pressure rise rate of pressure oscillations, $dP_{osc}/dt$.*

The maximum luminous intensity is analyzed as an estimator of the combustion intensity. As Fig. 5.24 to the left shows, the maximum intensity strongly correlates with the maximum temperature reached in the cycle. Moreover, the luminous intensity is higher in case of iso-octane for the same temperature because iso-octane is more prone to show knocking in the in-cylinder pressure signal. In fact, Fig. 5.24 to the right shows the maximum luminous intensity versus the maximum pressure rise rate of pressure oscillations, $dP_{osc}/dt$. As expected, the higher the combustion intensity (combustion temperature or $dP_{osc}/dt$) the higher the maximum radiation intensity. Furthermore, assuming a knocking limit in pressure rise rate equal to 120 $kbar/s$ (20 $bar/CAD$ at 1000 $rpm$, which is a typical limit in engines), it can be seen that most of the experiments are located in the knocking regime. Thus, pressure waves seems to be relevant for the autoignition propagation.

### 5.3.4 Conclusions

The following conclusions can be deduced from this study:

- The experimental ignition delays obtained by means of optical techniques have been reproduced by using an OH* sub-model linked to a detailed chemical kinetic mechanism. The OH* sub-model shows similar accuracy when simulations are compared to optical measurements than the detailed mechanism when simulations are compared to in-cylinder pressure measurements, which validates the sub-model.

- The spectroscopic analysis showed that there were two types of luminous emissions: one dominated by the $CO$ continuum and another from the OH*. $CO$ radiation was seen to appear at lean equivalence ratios and low temperatures, while OH* was present at high combustion temperatures. The reaction $HO_2 + H \Rightarrow OH + OH^*$ becomes more relevant at high combustion temperatures, which causes higher accumulation of OH* and therefore higher luminosity. Additionally, the fuel also showed a big influence on the type of luminosity generated. The cases with iso-octane presented a more violent combustion that lead to more OH* generation, whereas the luminous emission from cases with n-heptane was more prone to be dominated by the $CO$ continuum. Therefore, the cases can be separated into two groups (OH* and $CO$) based on the boundary conditions and fuel tested.

- Cool flames cannot be seen by OH* chemiluminescence by keeping constant the camera gain during all the combustion process, because both the OH* concentration and the temperature are too low. OH* luminous intensity starts when the $CO$ starts oxidizing into $CO_2$. The maximum intensity appears very close to the maximum oxidation rate of the $CO$ to $CO_2$, which virtually coincides with the time of maximum pressure rise rate. This makes it difficult to separate one from the other by just measuring luminosity. Nevertheless, it has been seen that the lifetime of OH* is much longer than that of $CO$. So, the lifetime seems to be a good indicator of the source of luminosity.

- The maximum area occupied by natural chemiluminescence is highly dependent on where ignition occurs. For ignitions far away of TDC, the thermodynamic conditions in the combustion chamber are not optimal for the propagation of the auto-ignition front, leading to slower ignition processes and areas below 100%.

- The maximum luminous intensity strongly correlates with the maximum temperature reached in the cycle, being higher in case of using iso-octane for the same temperature. Moreover, the maximum luminous intensity

seems to be also an estimator of the maximum amplitude of pressure oscillations reached in the combustion chamber.

## 5.4 Autoignition propagation: a phenomenological explanation

A phenomenological explanation about the autoignition propagation under HCCI conditions is developed in this section. To do so, diffusive effects from the burned zones to the fresh mixture, pressure waves based effects and expansion effects caused by combustion have been taken into account. Additionally, different Damköhler numbers have been defined in order to characterize the phenomenon and quantify the relevance of each effect. The theoretical explanation has been evaluated by means of the chemiluminescence measurements carried out in the RCEM, which allow to estimate the velocity of propagation of the autoignition front. The structure of this section is the following: first, the phenomenological analysis of the autoignition propagation phenomenon is explained. Afterwards, the phenomenological description is evaluated by means of $OH^*$ chemiluminescence experimental results. Finally, the conclusions of this study are shown.

A detailed explanation about the methodological approach can be found in Section 3.3.3, while the parametric study performed is described in Section 3.2, both from Chapter 3. Furthermore, the information related to the investigation discussed in this section has been already published in [13].

### 5.4.1 Theory and calculations

A phenomenological model to explain the autoignition propagation, so called sequential autoignition or propagation of the reaction front, under HCCI conditions is described in this section. To do so, the combustion chamber is assumed to be composed by two different fluids: burned gases (indicated by the subscript $b$) and unburned mixture (indicated by the subscript $u$). The burned fuel is calculated by means of the cumulated heat release and the reaction heat of the global combustion reaction. Thus, the amount of each fluid can be obtained by solving a mass balance. On the one hand, the temperature of the unburned mixture is obtained assuming a polytropic evolution starting from the ignition point. On the other hand, the temperature of the burned gases is obtained by solving an energy balance in the combustion chamber. Further details about this procedure can be found in [14].

Different characteristic physical and chemical velocities are evaluated, defining the following Damköhler numbers:

$$Da_1 = \frac{u_{prop} - u_b}{u_b} \tag{5.3}$$

$$Da_2 = \frac{u_{prop} - u_b}{a} \tag{5.4}$$

$$Da_3 = \frac{u_{prop} - u_b}{u_{TC}} \tag{5.5}$$

where $u_{prop}$ is the velocity of propagation of the autoignition front, which is an apparent chemical velocity experimentally measured, while $u_b$ is the mean expansion speed of the burned gas. Thus, the combustion speed of the reaction front is equal to $u_{comb} = u_{prop} - u_b$. Besides, $a = \sqrt{\gamma_u R_g T_u}$ represents the speed of sound, where $\gamma_u$ is the adiabatic coefficient of the unburned gas, $R_g = R/MW_u$ is the gas constant of the unburned gas (universal gas constant divided by the molecular weight of the unburned gas) and $T_u$ is the unburned gas temperature. Finally, $u_{TC}$ represents the turbulent combustion velocity of a flame front dominated by diffusive effects.

The dimensionless number $Da_1$ relates the combustion velocity associated to the reaction front with the mean expansion speed of the burned gas. Thus, $Da_1$ quantifies the relevance of expansion effects on the propagation velocity. If $Da_1 >> 1$, the expansion of the burned gases caused by the pressure rise associated to the combustion process is negligible compared to the combustion velocity, which means that the propagation of the reaction front is controlled by the chemical kinetics of the mixture.

The dimensionless number $Da_2$ relates the combustion velocity associated to the reaction front with the speed of sound. Thus, $Da_2$ quantifies the relevance of pressure gradients in the chamber (pressure waves based phenomena). If $Da_2 << 1$, pressure waves propagate much faster than the reaction front and constant pressure can be assumed in the chamber (null pressure gradients), otherwise, the existence of pressure waves has to be taken into account.

The dimensionless number $Da_3$ relates the combustion velocity associated to the reaction front with the turbulent combustion velocity from a flame front dominated by diffusive effects. $Da_3$ quantifies the relevance of diffusion on the autoignition propagation. If $Da_3 >> 1$, the reaction front propagates much faster than a typical flame front, meaning that mass and thermal diffusion have no influence on the autoignition propagation (diffusion phenomena are too slow), otherwise, the diffusion from the reaction front to the unburned mixture has to be taken into account.

The mean expansion speed of the burned gas, $u_b$, is calculated from the variation of unburned mixture mass as follows [15]:

$$u_b = \frac{V_u}{\gamma_u P A_f} \frac{dP}{dt} \tag{5.6}$$

where $V_u$ is the unburned mixture volume and $A_f$ is the area of the reaction front. Since the ignition is promoted by a hot spot located at the top of the combustion chamber that acts as an ignition spot, a spherical shape reaction front can be assumed, the volume of which is the volume of the burned gases (obtained from their mass and thermodynamic conditions, derived as explained above). Thus, the radius of the equivalent sphere is obtained from the burned volume, $V_b$, and the area of the reaction front is calculated from such equivalent radius:

$$A_f = 4\pi \left( \frac{3V_b}{4\pi} \right)^{2/3} \tag{5.7}$$

The turbulent combustion velocity, $u_{TC}$, is calculated from the laminar burning velocity of a flame, $u_{LC}$, using the Schelkin's scaling law: $u_{TC}/u_{LC} \propto \sqrt{1 + \nu_T/\nu} \approx 32$, where $\nu_T/\nu$ is the turbulent-to-molecular kinematic viscosity ratio, which is estimated at $10^3$ at TDC by CFD calculations. Besides, the laminar burning velocity is calculated by means of the Metghalachi-Keck correlation for iso-octane [16]:

$$\begin{aligned} u_{LC} = & \left( 0.2632 - 0.8472 \left( F_r - 1.13 \right)^2 \right) \left( \frac{T_u}{298} \right)^{2.18 - 0.8(F_r - 1)} \cdot \\ & \cdot \left( \frac{P}{1.01325} \right)^{-0.16 + 0.22(F_r - 1)} (1 - 2.1 Y_{EGR}) \end{aligned} \tag{5.8}$$

where $F_r$ is the working equivalence ratio, $T_u$ is the temperature of the unburned mixture in $K$, $P$ is the pressure in *bar* and $Y_{EGR}$ is the mass fraction of the inert diluent (in case of working with synthetic EGR). Despite the fact that Eq. 5.8 has been experimentally validated only up to 50.7 *bar* and 700 $K$, extrapolations can be performed to obtain estimators of the turbulent combustion velocity, since just an order of magnitude of $Da_3$ is intended to be obtained.

Finally, the autoignition propagation velocity is assumed to be a chemical velocity controlled by the chemical kinetics of the mixture, i.e., by the ignition delay distribution in the combustion chamber. Thus, the velocity of propagation of the reaction front can be estimated as [17]:

$$u_{chem} = \left( \frac{d\tau}{dx} \right)^{-1} \tag{5.9}$$

where $\tau$ represents the ignition delay under certain thermodynamic conditions and $x$ represents the direction of propagation of the front (in this study, from the top to the bottom of the combustion chamber).

The ignition delay is obtained for each ignition condition by means of chemical simulations in CHEMKIN. The Curran's detailed chemical kinetic mechanism for iso-octane and n-heptane [10, 11], which consists of 1034 species and 4238 reactions, has been solved in a homogeneous closed reactor (perfectly stirred reactor, PSR), which works with constant pressure and uses the energy equation to solve the temperature temporal evolution. Ignition is defined as the instant at which the maximum temperature rise rate occurs, and the resulting ignition delays have been parameterized using the Levenberg-Marquardt algorithm for minimizing the sum of the squares of the deviations. The least-squares curve fitting results in the following expressions for iso-octane (Eq. 5.10) and n-heptane (Eq. 5.11), respectively:

$$\tau = 6.2697 \cdot 10^{-11} P^{-0.504} X_{O_2}^{-1.946} F_r^{-0.836} exp\left(\frac{14940}{T}\right) \tag{5.10}$$

$$\tau = 1.5931 \cdot 10^{-6} P^{-1.316} X_{O_2}^{-1.637} F_r^{-0.548} exp\left(\frac{8756}{T}\right) \tag{5.11}$$

where the ignition delay, $\tau$, is in seconds, $P$ is the pressure in $bar$, $F_r$ is the working equivalence ratio, $X_{O_2}$ is the oxygen molar fraction, and $T$ is the temperature in $K$.

Fig. 5.25 shows the simulated ignition delays versus the ones obtained by means of Eqs. 5.10 and 5.11 for all the ignition points and both fuels. The line $y = x$, which represents a perfect match between values, has been also plotted in the figure. Finally, the Pearson's coefficient of correlation, $R^2$, has been calculated and its value has been added to the figure. It can be seen that the matching between simulations and correlations is quite good in the range of thermodynamic conditions of interest.

Assuming that the sequential autoignition is caused by the temperature gradient under HCCI conditions [18], the chemical velocity can be finally obtained as:

$$u_{chem} = \left(\frac{d\tau}{dT}\frac{dT}{dx}\right)^{-1} = \left(-\tau\frac{T_a}{T^2}\frac{dT}{dx}\right)^{-1} \tag{5.12}$$

where $T_a$ represents the activation temperature, which is equal to 14940 $K$ for iso-octane and to 8756 $K$ for n-heptane. Furthermore, the temperature gradient, $dT/dx$, has been estimated in -160 $K/m$ by means of CFD calculations.

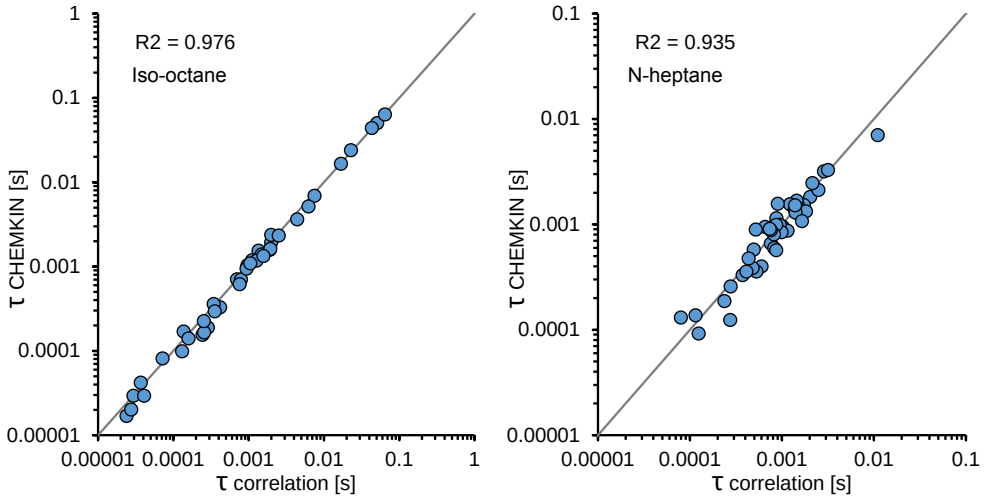


***Figure 5.25.*** *Ignition delays from chemical simulations with CHEMKIN versus ignition delays from Eqs. 5.10 and 5.11.*

Thus, the velocity ratio $u_{chem}/u_{comb}$, where $u_{comb} = u_{prop} - u_b$ is obtained from experimental measurements, is the control parameter to evaluate the accuracy of the phenomenological description derived by $Da_2$ and $Da_3$ and that will be discussed in the following section.

### 5.4.2 Results and discussion

Fig. 5.26 shows the maximum combustion velocity of the autoignition front versus the maximum in-cylinder average temperature (Fig. 5.26 to the left) and versus the ignition time referred to TDC, $t_i - t_{TDC}$, (Fig. 5.26 to the right) for iso-octane (top) and n-heptane (bottom). Despite the fact that the reaction front propagation is controlled by the thermodynamic conditions reached at the instant of ignition, the ignition time is controlled by the successive thermodynamic conditions reached during the ignition delay. Thus, for a certain engine configuration, the propagation velocity is mainly controlled by the ignition delay under constant conditions, $\tau$, evaluated at the thermodynamic conditions of the ignition point. It can be seen that the higher the maximum temperature reached the faster the combustion velocity. However, earlier ignitions are not necessarily related to a faster propagation. The propagation velocity increases if the ignition is advanced for iso-octane, since the smooth NTC behavior of this fuel causes that the higher

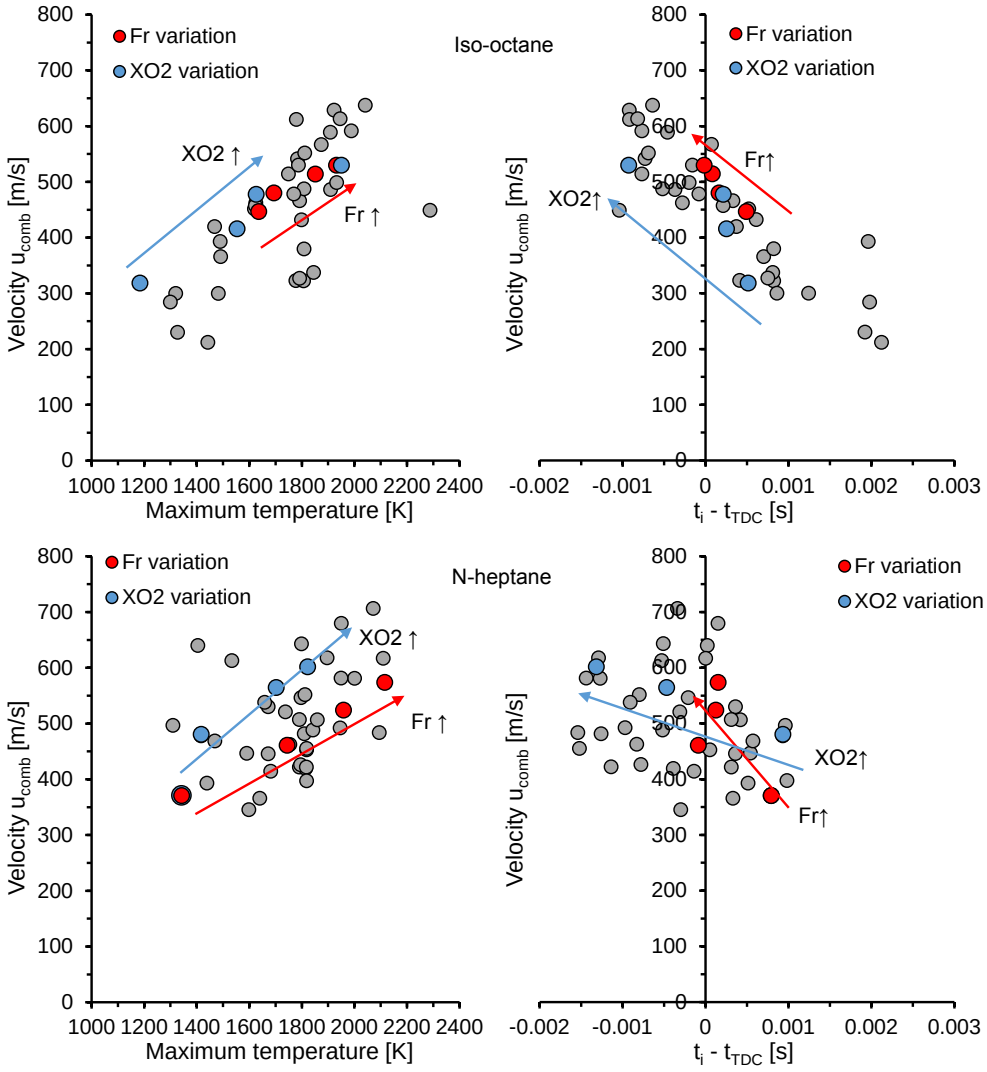


***Figure 5.26.*** *Maximum combustion velocity of the autoignition front. Left.- versus the maximum in-cylinder average temperature. Right.- versus the ignition time referred to TDC, $t_i - t_{TDC}$. Top.- iso-octane, $F_r \epsilon\{0.5, 0.6, 0.7, 0.8\}$ in red and $X_{O_2}\epsilon\{0.21, 0.147, 0.126, 0.105\}$ in blue. Bottom.- n-heptane, $F_r \epsilon\{0.3, 0.4, 0.5, 0.6\}$ in red and $X_{O_2}\epsilon\{0.21, 0.147, 0.126, 0.105\}$ in blue.*

the reactivity (the earlier the ignition), the shorter the ignition delay at the ignition conditions and the faster the autoignition propagation. Nevertheless, the strong NTC behavior of n-heptane can lead to longer ignition delays at the ignition conditions even if the global reactivity is increased (earlier ignitions). Besides, it can be seen by comparing Fig. 5.23 to Fig. 5.26 that the maximum luminous area and the maximum combustion velocity are related, being all figures consistent to each other. Finally, Fig. 5.26 shows, in red, the effect of the equivalence ratio on the combustion velocity, while it shows the effect of the oxygen concentration in blue. It can be seen that the higher the equivalence ratio or the higher the oxygen content (the higher the reactivity under LTC conditions), the faster the propagation.

The repeatability of the phenomenon has been studied in order to identify if the variability of the results is caused by physical aspects or if it is promoted by the measurement methods. Thus, the semi-amplitude of the confidence interval with a 95% of level of confidence, $\mu$, has been calculated for the maximum propagation velocity, $u_{prop}$, for the corresponding pressure rise rate, $dP/dt$, and for the ignition delay, $t_i$, as a way to evaluate the cycle-to-cycle variation. Fig. 5.27 shows the values of $\mu$ normalized by the averaged maximum propagation velocity, the averaged pressure rise rate, and the averaged ignition delay, respectively, versus the ignition time referred to TDC, $t_i - t_{TDC}$, for both fuels. It can be seen that, while the ignition delay has a very good repeatability, the sequential autoignition shows very high variability. In fact, the mean value of $\mu/\bar{x}$ has been calculated for the propagation velocity, the pressure rise rate and the ignition delay, for iso-octane and n-heptane, the results of which are summarized in Table 5.6. This is an expected result, since the autoignition propagation is controlled by combustion, which is a source of turbulence and, therefore, which has a random behavior by definition. Moreover, the corresponding pressure rise rate shows the same repeatability than the combustion velocity, which means that such dispersion is intrinsic to the physical phenomenon and it is not caused by the post-processing. Moreover, Table 5.6 shows that the sequential autoignition of iso-octane has higher cycle-to-cycle deviation. As it has been explained above, iso-octane leads to more intense combustion events and it is more prone to show pressure oscillations. Therefore, turbulence and the subsequent fluctuations of the local thermodynamic conditions are higher for this fuel, leading to poorer repeatability.

In order to describe the sequential autoignition by a chemical propagation velocity, the question is what are the thermodynamic conditions in front of the reaction front, i.e., what thermodynamic conditions should be used to evaluate Eq. 5.12. To do so, diffusive and pressure-based effects are quantified

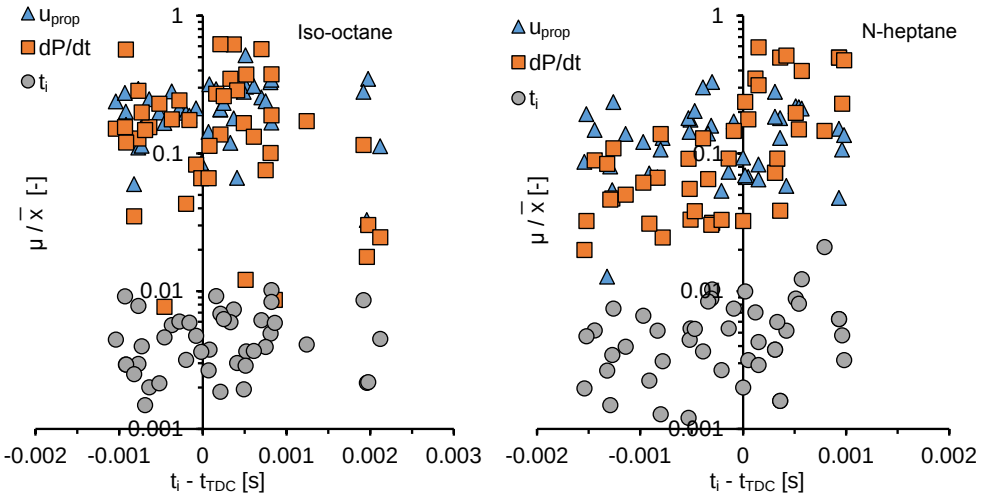


***Figure 5.27.*** *Semi-amplitude of the confidence interval with a 95% of level of confidence, $\mu$, for the maximum propagation velocity, $u_{prop}$, for the corresponding pressure rise rate, $dP/dt$, and for the ignition delay, $t_i$, normalized by the averaged values, $\bar{x}$, versus the ignition time referred to TDC, $t_i - t_{TDC}$. Left.- iso-octane. Right.- n-heptane.*

| | **Iso-octane** | **N-heptane** |
|---|---|---|
| | **Averaged** $\mu/\bar{x}$ | **Averaged** $\mu/\bar{x}$ |
| **Propagation velocity,** $u_{prop}$ | 21.7% | 13.7% |
| **Pressure rise rate,** $dP/dt$ | 19.2% | 16.2% |
| **Ignition delay,** $t_i$ | 0.468% | 0.539% |

***Table 5.6.*** *Repeatability analysis of propagation velocity, pressure rise rate and ignition delay by means of the averaged value of $\mu/\bar{x}$ for iso-octane and n-heptane.*

by means of different Damköhler numbers. Figs. 5.28, 5.29 and 5.30 show the three dimensionless Damköhler numbers defined in Section 5.4.1. It can be seen that $Da_1 >> 1$ for all cases, which means that, contrary to what occurs in spark-ignition engines, the propagation velocity of the reaction front is dominated and controlled by the chemical kinetics of the mixture. This is an expected result, since autoignition is characterized to be a chemically-controlled phenomenon.

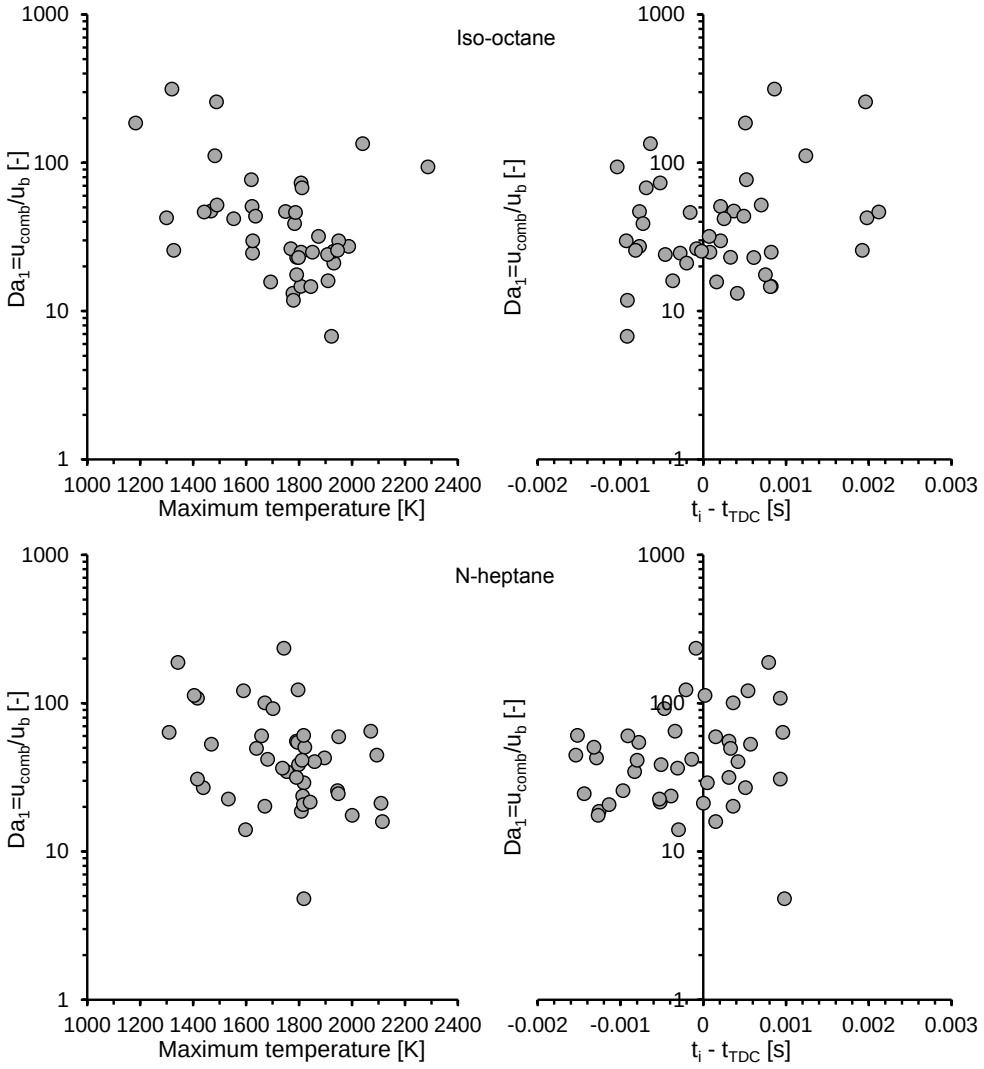


***Figure 5.28.*** *$Da_1 = u_{comb}/u_b$. Left.- versus the maximum in-cylinder average temperature. Right.- versus the ignition time referred to TDC, $t_i - t_{TDC}$. Top.- iso-octane. Bottom.- n-heptane.*

It can be seen in Fig. 5.29 to the left that $Da_2 = u_{comb}/a$ increases if the maximum in-cylinder average temperature is increased, specially for iso-octane. Furthermore, Fig. 5.29 to the right shows that $Da_2$ follows similar trends than the combustion velocity and the luminous area. $Da_2 > 0.75$ is reached in most cases, meaning that pressure gradients in the combustion chamber have to be taken into account.

Fig. 5.30 shows the same behavior for $Da_3 = u_{comb}/u_{TC}$ than for $Da_2$. However, $Da_3 > 4$ for all cases, meaning that diffusive effects are too slow compared to the propagation of the reaction front. Thus, the influence of mass and thermal diffusion on the autoignition propagation can be neglected under the conditions tested in this investigation. In fact, a critical propagation velocity of a flame front controlled by diffusive effects can be estimated, so that propagation velocities higher than the critical one imply that diffusive effects can be neglected. To do so, the temperature distribution from the burned gas to the unburned mixture is estimated by means of the hybrid theory of laminar flame propagation developed by Zeldovich and Frank-Kamanetskii and published by Semenov [19]. From this expression, the critical propagation velocity is estimated for the instant $j$ taking into account the position of the reaction front at the instant $j+1$ (from the propagation velocity experimentally measured) and assuming a difference between the temperature reached at this position and the temperature far away from the front of 1% ($\Delta$T=0.01T$_\infty$) as follows:

$$u_{crit} = \sqrt{-\frac{\alpha_T}{\Delta t} ln\left(\frac{0.01T_\infty}{T_b - T_\infty}\right)} < 55[m/s] \tag{5.13}$$

where $\alpha_T$ represents the turbulent thermal diffusivity (estimated in 0.01 $m^2/s$ at TDC from CFD calculations) and $\Delta t$ is the experimental time step. Besides, $T_b$ and $T_\infty$ represent the temperature of the burning gas and the temperature far away from the reaction front, respectively. $u_{crit}$ seems to be lower than 55 $m/s$ in the present study, which means that, regarding Fig. 5.26, the reaction front propagates at $T_\infty$ and diffusive effects are negligible. Finally, it should be noted that $T_\infty$ has to be calculated from the temperature of the unburned mixture, $T_u$, taking into account the effect of the pressure waves generated in the chamber, as demonstrated by $Da_2$.

The chemical velocity that describes the autoignition propagation, $u_{chem}$ (Eq. 5.12), has to be evaluated taking into account the thermodynamic conditions reached in front of the reaction front, which are affected by the pressure waves generated by the sequential ignition. Thus, three different scenarios have to be considered, all of them described in Fig. 5.31:

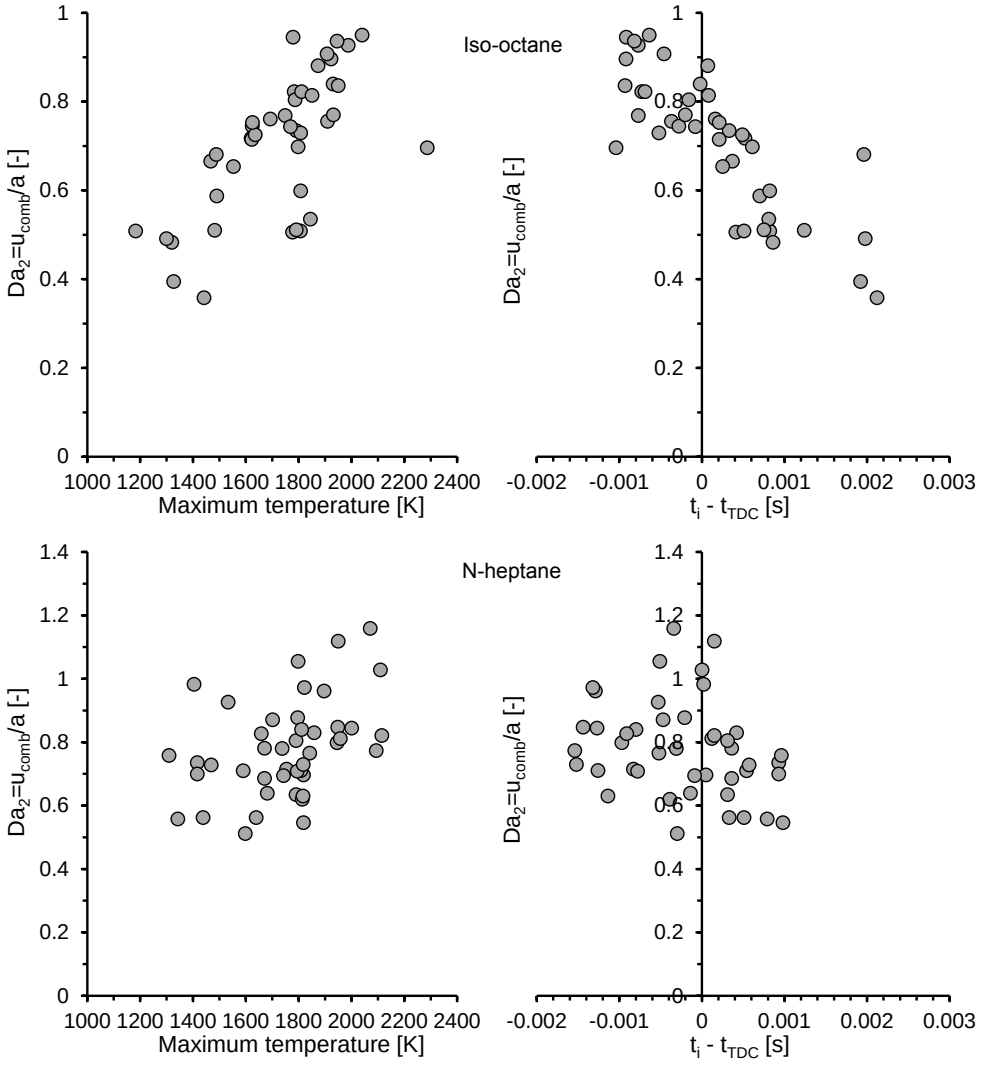


***Figure 5.29.*** *$Da_2 = u_{comb}/a$. Left.- versus the maximum in-cylinder average temperature. Right.- versus the ignition time referred to TDC, $t_i - t_{TDC}$. Top.- iso-octane. Bottom.- n-heptane.*

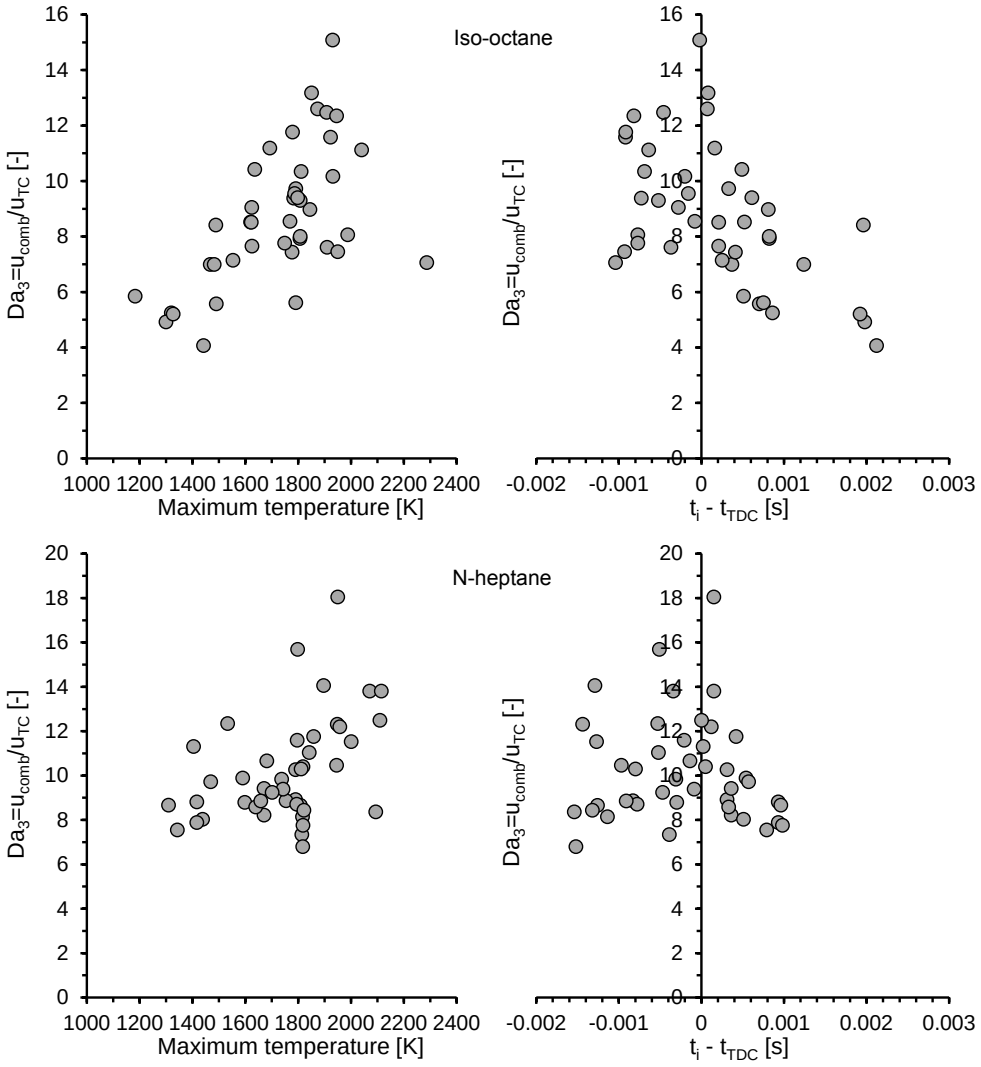


***Figure 5.30.*** *$Da_3 = u_{comb}/u_{TC}$. Left.- versus the maximum in-cylinder average temperature. Right.- versus the ignition time referred to TDC, $t_i - t_{TDC}$. Top.- iso-octane. Bottom.- n-heptane.*

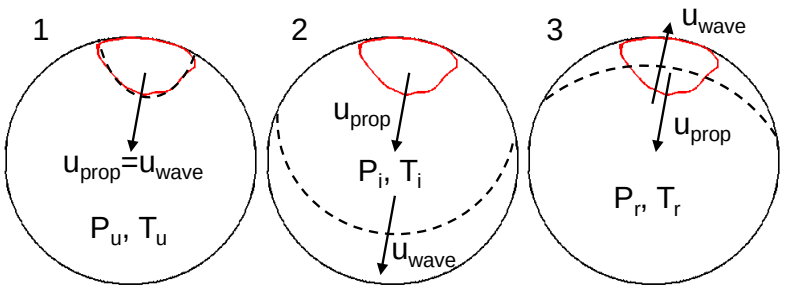


***Figure 5.31.*** *The three different scenarios that can be present in the combustion chamber. 1.- Reaction front and pressure front propagate together. 2.- The thermodynamic conditions established in front of the reaction front are controlled by the incident pressure front. 3.- The thermodynamic conditions established in front of the reaction front are controlled by the reflected pressure front.*

1. The incident pressure wave generated by the sequential ignition and the reaction front have the same propagation velocity. Therefore, the thermodynamic conditions used in Eq. 5.12 are the ones referred to the unburned mixture, as shown in Fig. 5.31 1.

2. The incident pressure wave generated by the sequential ignition is faster than the reaction front, but the reflected wave is not fast enough to interact with the reaction front. Therefore, the thermodynamic conditions used in Eq. 5.12 are the ones behind the incident pressure wave, as shown in Fig. 5.31 2.

3. The incident pressure wave generated by the sequential ignition is faster than the reaction front and the reflected wave is also fast enough to interact with the reaction front. Therefore, the thermodynamic conditions used in Eq. 5.12 are the ones behind the reflected pressure wave, as shown in Fig. 5.31 3.

The intensity of the incident pressure wave has to be estimated in order to evaluate the three different scenarios described above. Fig. 5.32 shows the raw in-cylinder pressure, its spectrum, and the filtered pressure waves for a certain case. It can be seen that 2000 $Hz$ seems to be a proper value to decouple the high frequency pressure oscillations from the in-cylinder pressure pedestal signal measured by the piezo-electric sensor. A zero-phase digital high-pass filter is used to obtain the pressure oscillations, the order of which has been selected as $f_{ac}/1000$, where $f_{ac}$ represents the acquisition frequency. Since the

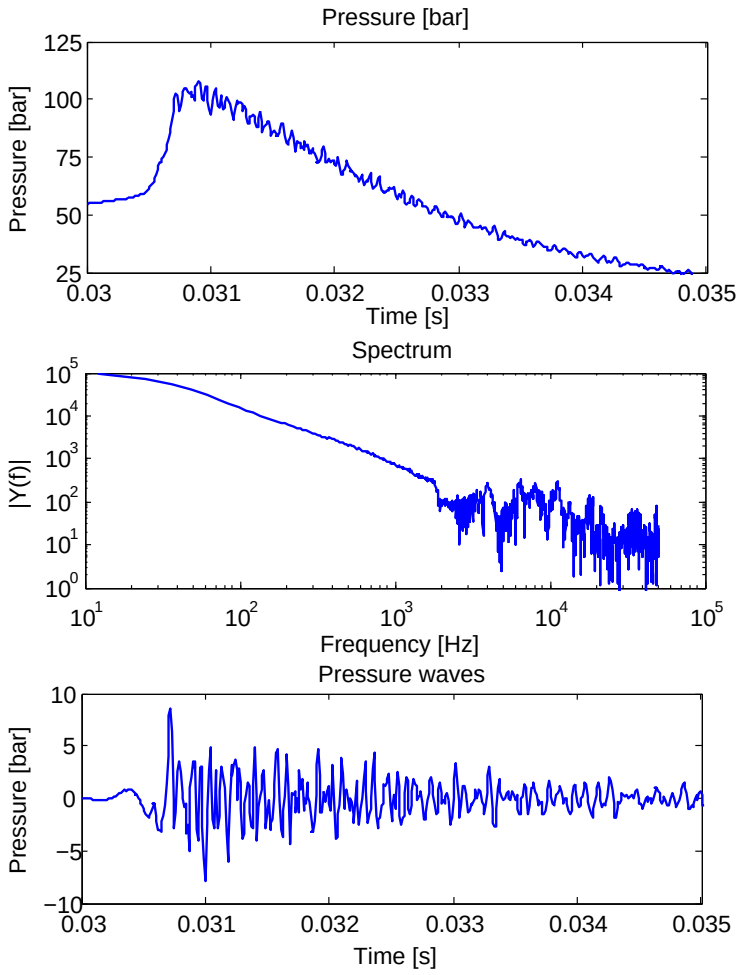


***Figure 5.32.*** *Raw in-cylinder pressure, its spectrum, and the filtered pressure waves (high-pass filter, $f_c$=2000 Hz) for $T_0$=408K, $P_0$=1.4bar, CR=15, $X_{O_2}$=0.126 and $F_r$=0.5.*

sensor is located near the liner, the maximum measured pressure wave will be assumed to be an estimator of the pressure behind the reflected wave. Thus, the incident wave is indistinguishable, since the reflected wave is generated just on the sensor. However, the propagation velocity of the incident wave, the propagation velocity of the reflected wave and the intensity of the incident wave can be obtained by means of the Rankine-Hugoniot equations, since the pressure behind the reflected wave and the pressure in front of the incident

wave are measured. To do so, the following system of equations has to be solved:

$$\frac{P_r}{P_i} = \frac{2\gamma_u M_r^2 - (\gamma_u - 1)}{\gamma_u + 1} \tag{5.14}$$

$$\frac{P_i}{P_u} = \frac{2\gamma_u M_i^2 - (\gamma_u - 1)}{\gamma_u + 1} \tag{5.15}$$

$$\sqrt{1 + \frac{2(\gamma_u - 1)}{(\gamma_u + 1)^2}\left(\gamma_u M_i^2 - \frac{1}{M_i^2} - (\gamma_u - 1)\right)} = \frac{M_i - 1/M_i}{M_r - 1/M_r} \tag{5.16}$$

where the subscript $u$ refers to the unburned mixture, $i$ refers to the thermodynamic conditions behind the incident pressure wave and $r$ refers to the thermodynamic conditions behind the reflected pressure wave. Besides, $M = u/a_u$ is the Mach number of the pressure wave, which relates the propagation velocity of the wave to the speed of sound of the mixture in front of the wave (i.e., under unburned mixture conditions). Thus, the Mach number of the incident wave, $M_i$, the Mach number of the reflected wave, $M_r$ and the pressure behind the incident wave, $P_i$ have to be calculated, while the pressure of the unburned mixture, $P_u$ and the pressure behind the reflected wave, $P_r$, are measured by the piezoelectric sensor.

Finally, the temperature behind the incident pressure wave can be obtained as follows:

$$\frac{T_i}{T_u} = \frac{P_i}{P_u}\frac{(\gamma_u - 1)M_i^2 + 2}{(\gamma_u + 1)M_i^2} \tag{5.17}$$

Fig. 5.33 shows the velocity ratio between the propagation velocity of the reaction front and of the incident pressure front. Points where $u_{prop}/u_{wave} = 1$, with a confidence interval with a level of confidence of 95%, are plotted in red, and the reaction front is assumed to propagate at the same velocity than the pressure front under these conditions. Thus, red dots in Fig. 5.33 represent detonations while grey dots represent deflagrations. Furthermore, it should be noted that the propagation velocity of the reaction front cannot be higher than the propagation velocity of the pressure waves generated by the combustion event, since the reaction front itself promotes new pressure fronts. It can be seen that detonations are only present for n-heptane, which shows higher propagation velocities. Furthermore, calculations show that in this study all deflagrations are affected by the incident pressure wave generated by the ignition but not by the reflected wave. Thus, the thermodynamic conditions ($P_i$, $T_i$) are the ones established in front of the reaction front for deflagrations and, therefore, the chemical velocity (Eq. 5.12) has to be evaluated using ($P_i$,

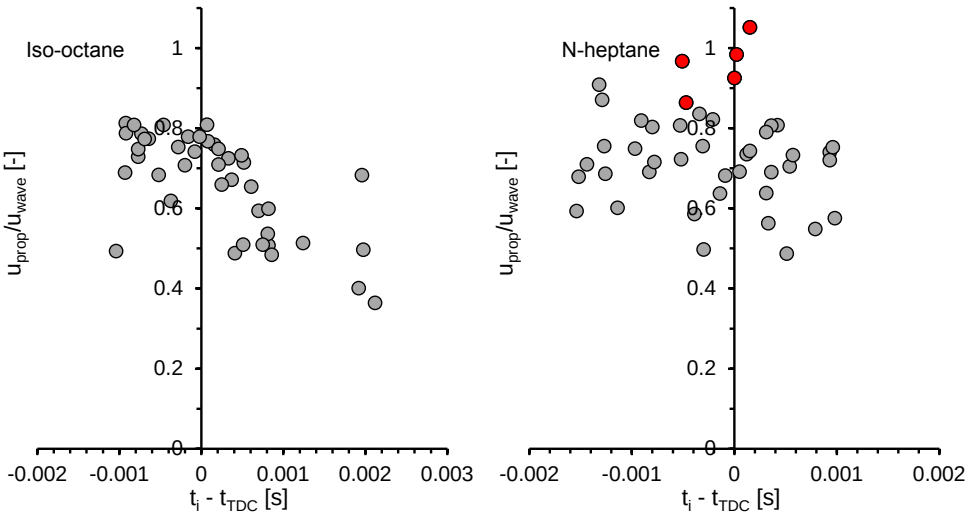


***Figure 5.33.*** *Velocity ratio, $u_{prop}/u_{wave}$, between the propagation velocities of the reaction front and of the incident pressure front versus the ignition time referred to TDC, $t_i - t_{TDC}$. Left.- iso-octane. Right.- n-heptane.*

$T_i$). In fact, the chemical velocity reaches values far away of the measurements if the pressure effects are not taken into account.

Fig. 5.34 shows the $u_{chem}/u_{comb}$ ratio, where $u_{comb}$ is obtained from the experimental results. It can be seen that most of the data are located in the interval [0.75, 1.25], which means that the autoignition propagation can be described by the chemical velocity affected by the incident pressure wave promoted by the sequential autoignition. It should be noted that incomplete combustion events as the ones that occur during the expansion stroke lead to a $u_{chem}/u_{comb}$ ratio near to zero. On the one hand, this can be caused by the complexity in measuring the velocity of propagation, since very low radiation is recorded for these experiments. On the other hand, the ignition delay, $\tau$, is more difficult to be predicted under these low-reactive conditions, leading to unrealistic $u_{chem}$ values. Finally, the high variability of the autoignition propagation phenomenon (Fig. 5.27) contributes also to obtain values for $u_{chem}/u_{comb}$ different from 1.

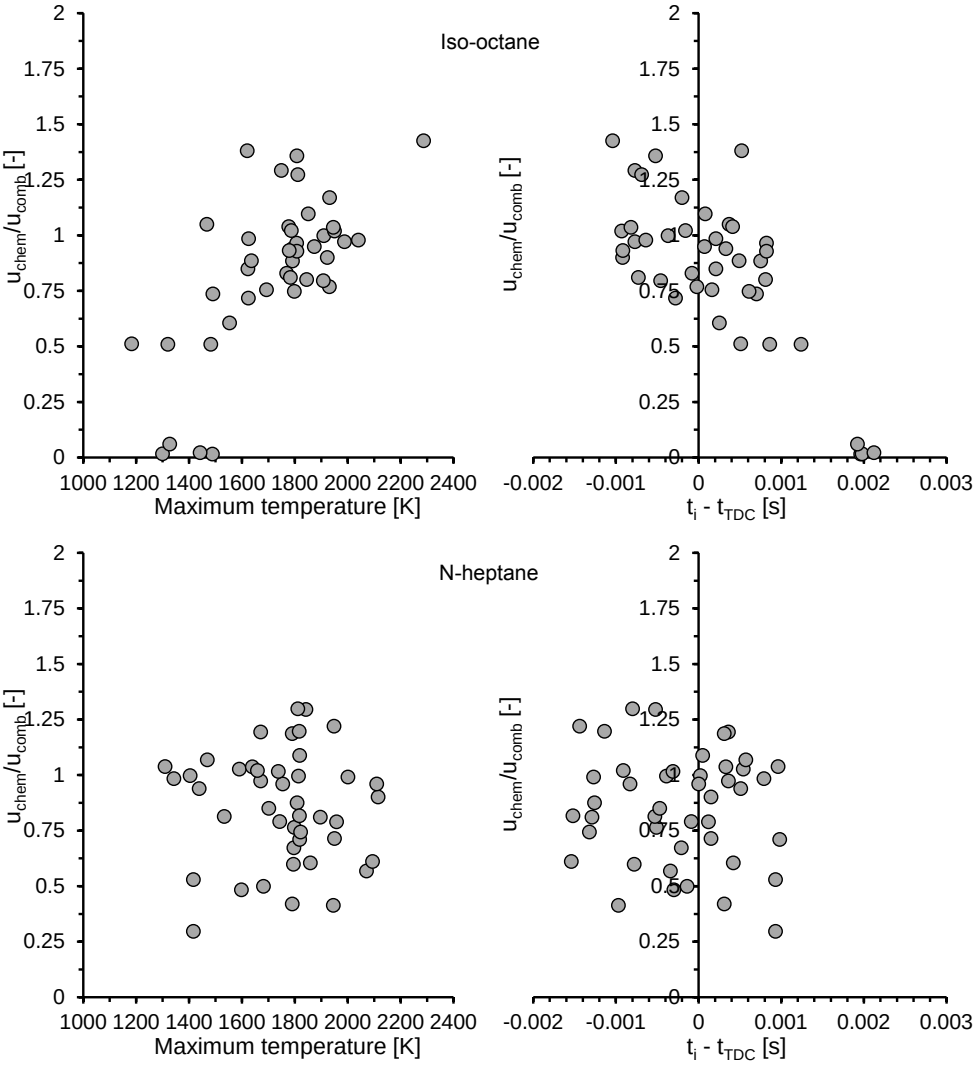


***Figure 5.34.*** *Velocity ratio, $u_{chem}/u_{comb}$, between the estimated and the measured combustion velocities of the reaction front. Left.- versus the maximum in-cylinder average temperature. Right.- versus the ignition time referred to TDC, $t_i - t_{TDC}$. Top.- iso-octane. Bottom.- n-heptane.*

### 5.4.3 Conclusions

In this work a phenomenological explanation about the autoignition propagation under HCCI conditions is developed. Diffusive effects from the burned zones to the fresh mixture, pressure waves based effects and expansion effects caused by combustion have been taken into account for the determination of the chemical velocity that describes the sequential autoignition. Besides, the relevance of each effect has been quantified by means of three different Damköhler numbers. Finally, the theoretical description has been compared to experimental propagation velocities obtained from chemiluminescence measurements in an RCEM.

The following conclusions can be deduced from this study:

- The maximum combustion velocity of the reaction front is controlled by the ignition delay, $\tau$, evaluated at the ignition conditions, which is highly affected by the NTC behavior of the fuel. Thus, the earlier the ignition the faster the propagation of the reaction front for iso-octane, while a maximum of propagation velocity seems to occur near TDC for n-heptane.

- The sequential autoignition is characterized by very high variability, since it depends on the local conditions established by the combustion process. This leads to low repeatability, since combustion is a turbulent phenomenon and, therefore, it has a local random behavior.

- On the one hand, expansion effects are negligible and, therefore, the measured propagation velocity and the combustion velocity of the reaction front are almost the same. On the other hand, the contribution of diffusive phenomena on the propagation is negligible, since the characteristic time of diffusion is too long compared to the characteristic time of the autoignition propagation.

- The sequential autoignition under HCCI conditions can be described by a chemical velocity, which is controlled by the thermodynamic conditions established in front of the reaction front by the pressure waves generated by the combustion phenomenon. In fact, the characteristic time of the autoignition propagation is too short to assume the absence of pressure gradients in the combustion chamber.

# References

[1] Desantes José M., García-Oliver José M., Vera-Tudela Walter, López-Pintor Darío, Schneider Bruno and Boulouchos Konstantinos. "Study of ignition delay time and generalization of auto-ignition for PRFs in an RCEM by means of natural chemiluminescence". *Energy Conversion and Management*, Vol. 111, pp. 217–228, 2016.

[2] Desantes José M., Bermúdez Vicente, López J. Javier and López-Pintor Darío. "Experimental validation of an alternative method to predict high and low-temperature ignition delays under transient thermodynamic conditions for PRF mixtures using a Rapid Compression-Expansion Machine". *Energy Conversion and Management*, Vol. 129, pp. 23–33, 2016.

[3] Desantes José M., Bermúdez Vicente, López J. Javier and López-Pintor Darío. "Sensitivity analysis and validation of a predictive procedure for high and low-temperature ignition delays under engine conditions for n-dodecane using a Rapid Compression-Expansion Machine". *Energy Conversion and Management*, Vol. 145, pp. 64–81, 2017.

[4] Mittal Gaurav. *A Rapid Compression Machine design, characterization, and autoignition investigations*. Doctoral Thesis, Case Western Reserve University, 2006.

[5] Baumgardner M. E., Sarathy S. M. and Marchese A. J. "Autoignition characterization of Primary Reference Fuels and n-heptane/n-butanol mixtures in a constant volume combustion device and Homogeneous Charge Compression Ignition engine". *Energy and Fuels*, Vol. 27, pp. 7778–7789, 2013.

[6] Kumar Kamal, Mittal Gaurav and Sung Chih-Jen. "Autoignition of n-decane under elevated pressure and low-to-intermediate temperature conditions". *Combustion and Flame*, Vol. 156, pp. 1278–1288, 2009.

[7] Blin-Simiand N., Rigny R., Viossat V., Circan S. and Sahetchian K. "Autoignition of hydrocarbon/air mixtures in a CFR engine: Experimental and modeling study". *Combustion Science and Technology*, Vol. 88, pp. 329–348, 1993.

[8] Lü Xing-Cai, Chen Wei and Huang Zhen. "A fundamental study on the control of the HCCI combustion and emissions by fuel design concept combined with controllable EGR. Part 1. The basic characteristics of HCCI combustion". *Fuel*, Vol. 84, pp. 1074–1083, 2005.

[9] Desantes José M., Bermúdez Vicente, López J. Javier and López-Pintor Darío. "A new method to predict high and low-temperature ignition delays under transient thermodynamic conditions and its experimental validation using a Rapid Compression-Expansion Machine". *Energy Conversion and Management*, Vol. 123, pp. 512–522, 2016.

[10] Curran H. J., Gaffuri P., Pitz W. J. and Westbrook C. K. "A comprehensive modeling study of n-heptane oxidation". *Combustion and Flame*, Vol. 114, pp. 149–177, 1998.

[11] Curran H. J., Gaffuri P., Pitz W. J. and Westbrook C. K. "A comprehensive modeling study of iso-octane oxidation". *Combustion and Flame*, Vol. 129, pp. 253–280, 2002.

[12] Desantes José M., García-Oliver José M., Vera-Tudela Walter, López-Pintor Darío, Schneider Bruno and Boulouchos Konstantinos. "Study of the auto-ignition phenomenon of PRFs under HCCI conditions in an RCEM by means of spectroscopy". *Applied Energy*, Vol. 179, pp. 389–400, 2016.

[13] Desantes José M., López J. Javier, García-Oliver José M. and López-Pintor Darío. "A phenomenological explanation on the autoignition propagation under HCCI conditions". *Fuel*, Vol. 206, pp. 43–57, 2017.

[14] Desantes J.M., Arregle J., Molina S. and Lejeune M. "Influence of the EGR rate, oxygen concentration and equivalent fuel/air ratio on the combustion behavior and pollutant emissions of a heavy-duty diesel engine". *SAE Technical Paper 2000-01-1813*, 2000.

[15] Heywood John B. *Internal combustion engine fundamentals*. McGraw-Hill series in mechanical engineering. McGraw-Hill, New York, 1988.

[16] Metghalchi M. and Keck J.C. "Burning Velocities of Mixtures of Air with Methanol, Isooctane, and Indolene at High Pressure and Temperature". *Combustion and Flame*, Vol. 48, pp. 191–210, 1982.

[17] Zeldovich Y.B. "Regime classification of an exothermic reaction with nonuniform initial conditions". *Combustion and Flame*, Vol. 39, pp. 211–214, 1980.

[18] Sjoberg M., Dec J.E. and Cernansky N.P. "Potential of thermal stratification and combustion retard for reducing pressure-rise rates in HCCI engines, based on multi-zone modeling and experiments". *SAE Technical Paper 2005-01-0113*, 2005.

[19] Semenov N. "Thermal theory of combustion and explosion III. Theory of normal flame propagation". *Progress of Physicai Science (USSR)*, Vol. 24, pp. 433, 1940.

# Chapter 6

# Conclusions and future works

**Contents**



## 6.1 Conclusions

The main conclusions derived from this Thesis are summarized in this chapter, including both theoretical and experimental results and highlighting the contributions of this work to the scientific community. Furthermore, the extent to which the objectives established in Chapter 1 have been fulfilled is also analyzed in the following paragraphs.

Specifically, the main objective of the Thesis was:

– *To improve the knowledge about the autoignition phenomenon under LTC conditions by developing an alternative numerical method to predict ignition delays under transient thermodynamic conditions and by studying the ignition propagation under working conditions with real applications.*

Several gaps of knowledge can be deduced from the literature review discussed in Chapter 2, the investigation of which leads to improve the scientific knowledge about the autoignition phenomenon under LTC

conditions. On the one hand, the validity of the Livengood & Wu predictive method for the ignition delay has been widely analyzed. Moreover, new predictive procedures have been proposed in order to be able to accurately predict ignition delays under transient conditions referred to peaks of heat release rate, which allow to distinguish between cool flames and the high-temperature stage of the ignition in case of having a two-stage ignition pattern. Thus, the first part of the main objective of this Thesis has been fulfilled. On the other hand, the autoignition propagation has been studied by means of optical techniques. First, an spectroscopic analysis of the autoignition event under LTC conditions has been carried out. The different sources of radiation that dominate the spectrum have been identified and a diagnosis of the phenomenon has been performed by linking the optical results to chemical kinetics. Afterwards, the generalization and propagation of the autoignition phenomenon have been analyzed by means of chemiluminescence measurements. Sequential autoignition has been described taken into account the different physical and chemical phenomena that contribute to the ignition propagation. Thus, the second part of the main objective of this Thesis has also been fulfilled. Finally, the methodological approach to meet the desired objectives had to be properly defined. To do so, the RCEM used in this investigation had been widely validated by means of CFD simulations and by comparing its results to other experimental measurements from similar facilities. Different models were developed in order to perform a full diagnosis of the combustion process. Besides, a rigorous experimental methodology was designed in order to obtain reliable results from the experiments.

The main objective of the Thesis can be decoupled in several goals:

i **To design a criterion to define the proper composition of the synthetic EGR for autoignition studies.**

A method to create synthetic mixtures simulating the EGR of an engine has been designed. These mixtures can later be used in experimental facilities to study the autoignition phenomenon in both standard and low temperature conditions.

The method developed and presented here is based on using five different species: $N_2$, $O_2$, $CO_2$, $H_2O$ and Ar. However, it is possible to work with the following simplified mixtures, with deviations in the ignition delay lower than 1%:

- Mixture formed by $N_2$ + $O_2$: it is valid for oxygen molar fractions higher than or equal to 0.205.

- Mixture formed by $N_2 + O_2 + CO_2$: it is valid for oxygen molar fractions higher than or equal to 0.20.
- Mixture formed by $N_2 + O_2 + H_2O$: it is valid for oxygen molar fractions higher than or equal to 0.12 if the fuel used is n-heptane, and higher than or equal to 0.10 if the fuel used is iso-octane.
- Mixture formed by $N_2 + O_2 + CO_2 + H_2O$: in case of using iso-octane, it is valid for all the oxygen molar fractions simulated. In case of using n-heptane, it is valid for oxygen molar fractions higher than or equal to 0.07.

The ignition delay changes when any species is obviated due to a combination of two opposite effects: a thermodynamic and a chemical effect. On the one hand, the thermodynamic effect leads to shorter ignition delays when $HO_2$ or $CO_2$ are obviated, because of their larger heat capacity, while longer ignition delays are obtained if Ar is neglected. Besides, this effect predominates at low and at high initial temperatures and for rich mixtures. On the other hand, the chemical effect leads to longer ignition delays when $HO_2$ or $CO_2$ are obviated. This effect predominates at medium initial temperatures and for lean mixtures. Finally, it has been checked that $H_2O$ is, by far, the species with the major influence on the ignition delay for the proportions used in this study.

This objective has been discussed and fulfilled in Chapter 4, Section 4.1.

ii **To develop a new alternative procedure to predict ignition delays under transient thermodynamic conditions.**

New alternative methods to predict ignition delays under variable conditions from those obtained under constant conditions have been developed. These methods have been theoretically deduced from the Glassman's model for autoignition and they allow to predict ignition delays referred to a critical concentration of chain carriers, to cool flames or to the high-temperature stage of the process.

It should be noted that predictive methods based on the premise that autoignition occurs when the critical concentration of chain carriers is reached lead to predicted ignition delays referred to this very criterion. Moreover, the information used to obtain the predictions may be also referred to the same criterion. Therefore, care should be taken in comparing the predictions obtained from these methods with experimental results, since both ignition

delays could be referred to different stages of the combustion process. Thus, these methods (which includes the classical Livengood & Wu correlation) are, in principle, complex to be validated versus experimental ignition delays. For this reason, predictive procedures based on a maximum pressure rise rate are more convenient, since the pressure trace can be easily measured in almost all experimental facilities.

The Livengood & Wu integral is valid for an engine-like temperature and pressure evolution despite the hypothesis of constant critical concentration of chain carriers. The largest contribution to the integral method is made in a narrow time interval in which the assumption of constant critical concentration is not catastrophic. However, since all the predictive methods based on a critical concentration proposed in this Thesis have been deduced from models that cannot reproduce the NTC zone, the more pronounced the NTC regime, the higher the prediction deviations. In fact, when autoignition occurs in the NTC regime, better predictions can be obtained from the Livengood & Wu integral method than for more sophisticated procedures due to, to some extent, a compensation of errors.

The predictive procedure for ignition delays referred to a maximum pressure rise rate proposed in this Thesis is composed by two different consecutive integrals:

$$1 = \frac{1}{[CC]_{crit,t_{i,CC}}} \int_0^{t_{i,CC}} \frac{[CC]_{crit}}{\tau_{CC}} dt \tag{6.1}$$

$$1 = \frac{1}{[CC]_{crit,t_{i,CC}}} \int_{t_{i,CC}}^{t_{i,2}} \frac{[CC]_{crit}}{\tau_2 - \tau_{CC}} dt \tag{6.2}$$

where $t_{i,CC}$ is the ignition delay of the process referred to a maximum concentration of chain carriers and $t_{i,2}$ is the ignition delay referred to the high-temperature stage of combustion. Besides, $\tau_2$, $\tau_{CC}$ and $[CC]_{crit}$ are the ignition delay referred to the high exothermic stage, the ignition delay referred to a maximum of chain carriers and the critical concentration of chain carriers, respectively, under constant conditions of pressure and temperature for the successive thermodynamic states.

The method is decoupled in two steps depending on the stage of the ignition to predict. On the one hand, a predictive method for cool flames is based on the accumulation of chain carriers up to reach the critical concentration. $HO_2$ is selected as chain carrier since it seems to be a good tracer of such phenomenon ($CC$=$HO_2$). The accumulation of $HO_2$ is modeled by Eq. 6.1, in which $\tau_{CC}$ and $[CC]_{crit}$ are related to this species. The upper limit of

the integral represents the instant at which the maximum concentration of $HO_2$ occurs, which corresponds to the ignition delay referred to cool flames. On the other hand, a predictive method for the high-temperature stage of the combustion process is based on the accumulation of chain carriers up to the critical concentration (Eq. 6.1), and the subsequent consumption from this maximum of concentration (Eq. 6.2). Thus, two different consecutive integrals have to be solved in this method. $CH_2O$ is selected as chain carrier ($CC$=$CH_2O$), since formaldehyde is widely recognized as an autoignition tracer and the maximum heat release rate occurs when this species is almost consumed. The instant at which the maximum concentration of $CH_2O$ is reached is obtained by solving Eq. 6.1, whereas the consumption of $CH_2O$ is modeled by Eq. 6.2. Obviously, $\tau_{CC}$ and $[CC]_{crit}$ have to be related to this species. The upper limit of the integral in Eq. 6.2 represents the time at which all formaldehyde is consumed, which corresponds to the ignition delay referred to the high-temperature stage.

This objective has been discussed and fulfilled in Chapter 4, Sections 4.2 and 4.3.

iii **To validate different chemical kinetic mechanisms, as well as different predictive methods for the ignition delay, by comparison to experimental data.**

The predictive capability of the different procedures previously described has been compared to the accuracy of direct chemical simulations when experiments are numerically replicated.

All the predictive methods tested in this work can predict with quite good accuracy the ignition time referred to cool flames, demonstrating that $HO_2$ can be taken as a good cool flames tracer under a wide range of octane numbers, and that the Livengood & Wu integral method works properly for cool flames. Furthermore, the new alternative integral method proposed in this Thesis has shown to be able to predict the ignition delays referred to a maximum pressure rise rate when $CH_2O$ is taken as chain carrier. This ignition delay can be experimentally measured, allowing a direct comparison between predictions and experiments. However, the Livengood & Wu integral method is able to predict ignition delays referred to the high exothermic stage of combustion only if the fuel shows a single-stage ignition pattern. This method is originally based on the premise that autoignition occurs when the critical concentration of chain carriers is reached. Therefore, the predicted ignition delays will be referred to this criterion and the information used to obtain the predictions may be also referred to this criterion. Otherwise, an

intrinsic deviation between predictions obtained from the Livengood & Wu integral and the experimental results appears, since both ignition delays could be referred to different stages of the combustion process. If the fuel does not present a two-stage combustion or if the NTC zone is very soft, all criteria to define the ignition delay are virtually the same, and they can be compared to each other. Thus, the Livengood & Wu integral can be used with high accuracy to predict ignition delays of single-stage ignition fuels, but not with fuels that show a two-stage ignition pattern.

Specifically, chemical simulations can reproduce ignition delays referred to cool flames and to the high-temperature stage with deviations lower than 4.1% and 3.8%, respectively. The new predictive method proposed in this Thesis can predict the cool flames and the high-temperature ignition with deviations lower than 4.3% and 5%, respectively. Finally, the Livengood & Wu integral leads to ignition delay deviations lower than 4.3% for cool flames, but from 5.7% to 10.2% for the high-temperature ignition of fuels that show a clear two-stage ignition pattern.

This objective has been discussed and fulfilled in Chapter 5, Section 5.2.

iv **To study the generalization of the autoignition event and the propagation of the autoignition front in experimental facilities under realistic conditions.**

First, a study on the generalization of auto-ignition has been performed in the RCEM by means of OH*-CO chemiluminescence. The percent of the combustion chamber ignited was related to the ignition time. Besides, the luminous intensity was studied, comparing the experimental results from a photo-multiplier and from a high speed camera with chemical simulations. The experimental ignition delays obtained by means of optical techniques have been reproduced by solving an OH* sub-model linked to a detailed chemical kinetic mechanism. The OH* sub-model showed similar accuracy when simulations were compared to optical measurements than the detailed mechanism when simulations were compared to in-cylinder pressure measurements, which validates the sub-model.

A spectroscopic analysis has been performed in order to study the sources of radiation under LTC conditions. Results showed that there were two types of emission: one dominated by the $CO$ continuum and another from the OH*. $CO$ radiation was seen to appear at lean equivalence ratios and low temperatures, while on the other hand, OH* was present at high combustion temperatures. Reaction $HO_2 + H \Rightarrow OH + OH^*$ was seen to become more

relevant at high combustion temperatures, which caused higher accumulation of OH* and therefore higher luminosity. Additionally, the fuel also showed a big influence on the type of luminosity generated. The cases with iso-octane presented a more violent combustion which lead to more OH* generation, whereas the luminous emission from cases with n-heptane was more prone to be dominated by the $CO$ continuum. Therefore, the cases can be separated into two groups (OH* and $CO$) based on the boundary conditions and fuel tested.

Cool flames cannot be seen by OH* chemiluminescence by keeping constant the gain during all the combustion process because both the OH* concentration and the temperature are too low. OH* luminous intensity starts when the CO starts oxidizing into $CO_2$, since before all the generated OH* is consumed by the generation of CO. The maximum intensity appears very close to maximum oxidation rate of the CO to $CO_2$, which virtually coincides with the time of maximum pressure rise rate. This makes it difficult to separate one from the other by just measuring luminosity. Nevertheless, it has been seen that the lifetime of OH* is much longer than that of CO. So, the lifetime seems to be a good indicator of the source of radiation.

Furthermore, the maximum area occupied by chemiluminescence seemed to be dependent on where ignition occurred. For ignitions far away of TDC, the thermodynamic conditions in the combustion chamber were not optimal for the propagation of the auto-ignition front, leading to slower ignitions and areas below 100%. Furthermore, the maximum luminous intensity showed a good correlation with the maximum temperature reached in the cycle, being higher in case of using iso-octane for the same temperature. Moreover, the maximum luminous intensity seemed to be also an estimator of the maximum amplitude of pressure oscillations reached in the combustion chamber.

Secondly, a phenomenological explanation about the autoignition propagation under HCCI conditions has been developed. Diffusive effects from the burned zones to the fresh mixture, pressure waves based effects and expansion effects caused by combustion have been taken into account for the determination of the chemical velocity that describes the sequential autoignition. Besides, the relevance of each effect has been quantified by means of three different Damköhler numbers. Finally, the theoretical description has been compared to experimental combustion velocities obtained from the chemiluminescence measurements.

It was demonstrated that the maximum combustion velocity of the reaction front is controlled by the ignition delay, $\tau$, evaluated at the ignition conditions, which is highly affected by the NTC behavior of the fuel. Thus, the earlier the

ignition the faster the propagation of the reaction front for iso-octane, while a maximum of propagation velocity seems to occur near TDC for n-heptane. However, sequential autoignition is characterized by very high variability, since it depends on the local conditions established by the combustion process. This leads to low repeatability, since combustion is a turbulent phenomenon and, therefore, it has a local random behavior.

Finally, it was found that the sequential autoignition under HCCI conditions can be described by a chemical velocity, which is controlled by the thermodynamic conditions established in front of the reaction front by the pressure waves generated by the combustion phenomenon. In fact, the characteristic time of the autoignition propagation is too short to assume the absence of pressure gradients in the combustion chamber. On the one hand, expansion effects are negligible and, therefore, the measured propagation velocity and the combustion velocity of the reaction front are almost the same. On the other hand, the contribution of diffusive phenomena on the propagation is negligible, since the characteristic time of diffusion is too long compared to the characteristic time of the autoignition propagation.

This objective has been discussed and fulfilled in Chapter 5, Sections 5.3 and 5.4.

## 6.2 Future works

Future works and extensions of this Thesis are proposed in this section in order to indicate directions for new studies related to the autoignition phenomenon. The following ideas are focused on improving the quality of some measurements and also on answering new questions derived from this work. More specifically, five different future investigations are proposed:

1. The experimental study on the sequential autoignition by means of chemiluminescence measurements has shown that autoignition propagation has an intrinsic cycle-to-cycle variability because it depends on the local thermodynamic conditions established in the combustion chamber by turbulent phenomena, which have a random behavior by definition. Thus, despite the fact that the experiments have been repeated enough times to guarantee statistically robust ignition delay measurements, the number of repetitions should be increased in order to obtain reliable results for the propagation velocity. Therefore, the experimental results shown in Chapter 5, Section 5.4 can be highly

improved by increasing the number of tests in order to mitigate the effects of the cycle-to-cycle variability on the propagation characteristics.

Furthermore, the sequential autoignition is promoted in this investigation by a cooled piezo-electric pressure sensor located at the bottom of the cylinder head of the RCEM available at ETH - Zurich. The phenomenological description of the autoignition propagation phenomenon can be better evaluated by means of experimental results in which the boundary conditions are better controlled. Thus, if the temperature distribution and, more specifically, the hot spot that promotes the ignition is fully controlled, the temperature gradients and, therefore, the chemical propagation velocities will be better estimated.

In summary, chemiluminescence measurements to study the autoignition propagation should be carried out under more controlled conditions and performing enough repetitions to obtain a narrower confidence interval for the propagation velocities.

2. 0-D chemical kinetic simulations in CHEMKIN that try to replicate the RCEM conditions cannot reproduce the heat release and combustion efficiency since wall effects and other inhomogeneities cannot be taken into account in 0-D reactors. Thus, if a complete diagnosis of the combustion process wants to be carried out in CHEMKIN, multi-zone models should be used in order to take into account the effects of incomplete combustion events because of cold walls and heat losses. Multi-zone reactors can be designed and calibrated for certain experimental facilities, and its use can widely improve the chemical kinetic analyses performed in CHEMKIN, as well as the diagnosis capabilities of the autoignition studies carried out in the RCEM.

   A 5-zone model to replicate in-cylinder conditions of the RCEM has already been designed and tested. In fact, its comparison to 1-zone models and to experimental measurements can be read in [1].

3. The predictive methods proposed in Chapter 4, Section 4.2 use the ignition characteristics under constant thermodynamic conditions to estimate the ignition delay under transient conditions, $t_i$. The ignition characteristics under constant conditions include the ignition delay, $\tau$, and the critical concentration of chain carriers, $[CC]_{crit}$, which compose the database needed to apply the predictive procedures. This database has been generated by solving chemical kinetic mechanisms in perfectly stirred reactors with CHEMKIN. Thus, the predictive accuracy of the

numerical methods depends, in some way, on the chemical mechanisms used to create the database.

A sensitivity analysis about the effects of varying the database on the predictions obtained by means of the new procedures proposed in this Thesis should be done. Thus, it can be checked if deviations between databases are magnified when the predictive methods are applied, and also such deviations can be compared to deviations from direct chemical kinetic simulations performed with different mechanisms. This work, the results of which can be read in [2], has already been carried out.

4. The database of ignition delays and critical concentrations of chain carriers under constant thermodynamic conditions can be parameterized as a function of temperature, pressure, equivalence ratio, oxygen molar fraction and type of fuel. This way, the implementation of the predictive methods proposed in this Thesis will be easier, since interpolations and extrapolations are avoided. There are two main possibilities to parameterize the database: by means of fitting mathematical correlations or by means of neural networks. On the one hand, mathematical correlations are simply and easy to use. However, they have to be re-fitted if the database is extended. On the other hand, neural networks are more complex to use but easy to train. Thus, the application limits can be easily extended.

   Correlations for the different ignition delays and critical concentrations have been obtained and their prediction capability has been compared to the original database. These results can be read in [3].

5. The predictive methods proposed in this Thesis have been validated for homogeneous reactive mixtures under engine-like conditions. However, it is really interesting to test these predictive procedures in CFD applications. Thus, autoignition chemistry can be avoided leading to shorter computing times. Furthermore, these methods can be implemented in an ECU in order to improve the ignition models for engine control. Finally, the predictive procedures can be linked to 1-D fuel spray models in order to predict the ignition event of direct injection sprays as those used in Diesel engines.

   In summary, future works should be focused on implementing the predictive procedures in scientific applications and test their accuracy compared to other autoignition models.

# References

[1] Desantes José M., López J. Javier, García-Oliver José M. and López-Pintor Darío. "A 5-zone model to improve the diagnosis capabilities of a Rapid Compression-Expansion Machine (RCEM) in autoignition studies". *SAE Technical Paper 2017-01-0730*, 2017.

[2] Desantes José M., Bermúdez Vicente, López J. Javier and López-Pintor Darío. "Sensitivity analysis and validation of a predictive procedure for high and low-temperature ignition delays under engine conditions for n-dodecane using a Rapid Compression-Expansion Machine". *Energy Conversion and Management*, Vol. 145, pp. 64–81, 2017.

[3] Desantes José M., Bermúdez Vicente, López J. Javier and López-Pintor Darío. "Correlations for the ignition characteristics of six different fuels and their application to predict ignition delays under transient thermodynamic conditions". *Energy Conversion and Management, in press*, 2017.

# Chapter 7

# Appendices

Contents



## 7.1 Appendix: Evaluation of the homogeneity in temperature at the RCEM by CFD calculations

A CFD analysis on the filling of the machine has been carried out in ANSYS Fluent in order to evaluate the homogeneity in initial temperature of the machine. Furthermore, a dynamic simulation taking into account the compression stroke of the piston has been also solved, in order to know the in-cylinder air movement and the temperature distribution near TDC. Besides, an

additional CFD analysis of the injection and vaporization processes has been performed in OpenFOAM in order to characterize the time of stratification of the mixture because of gravitational effects. A brief summary about the methods and results of both studies are shown in the following paragraphs. A more detailed explanation is avoided since the CFD simulation of the RCEM is not the main topic of this Thesis.

### 7.1.1 Evolution of the in-cylinder temperature during the filling and compression processes

The evolution of the in-cylinder thermodynamic conditions during the filling have been studied in order to evaluate the grade of homogeneity in temperature of the RCEM. Moreover, a complete compression stroke has been also simulated in order to know the velocity and temperature fields near TDC. These two studies have been carried out in the software for CFD simulations ANSYS Fluent.

First, the inlet flow has been experimentally measured for different strokes (i.e, initial volumes) and wall temperatures. This inlet flow has been imposed in the simulations as a boundary condition in the intake pipes. Besides, since sonic conditions are reached in the intake valves, the inlet flow is constant for all simulations (it depends only on the conditions upstream the valves, which are constant). The filling time up to reach the desired initial pressure has been also measured and the duration of the simulations has been selected according to this parameter. Obviously for a certain desired pressure, the smaller the initial volume or the higher the wall temperature, the shorter the filling time. The desired filling pressure has been fixed to 3 $bar$ for both, measurements and simulations. Two different strokes have been evaluated: 120 $mm$ (minimum stroke) and 240 $mm$ (almost maximum stroke). Finally, two different wall temperatures have been tested for each stroke: 373 $K$ (typical value in engines) and 353 $K$ (minimum value to ensure all the fuel vaporization).

The combustion chamber, including the intake pipes, the optical accesses and the piston bowl, have been modeled in the software for computer-aided design (CAD) SolidWorks. The physical domain can be seen in Fig. 7.1. The CAD model has been imported to ANSYS Fluent for its discretization. Fig. 7.2 shows the mixed mesh generated, detailing the intake ducts (top) and the lateral optical accesses (bottom). On the one hand, a structured grid has been used in the simple cylindrical domain, which includes the piston bowl. On the other hand, an unstructured mesh is applied in the volume near TDC, which contains the pipes and the lateral windows. Despite the fact that

the volume covered by the structured mesh is several times larger than the volume defined by the unstructured mesh, this last is composed by a much higher number of cells, since the cell size is smaller in order to adapt the mesh to the more complex geometry and to know with higher accuracy the flow characteristics in this area (in which the flow will be more complex due to the inlet pipes). The number of elements of the structured mesh depends on the selected stroke, since the same cell size ($\Delta x$=1 $mm$) is kept.

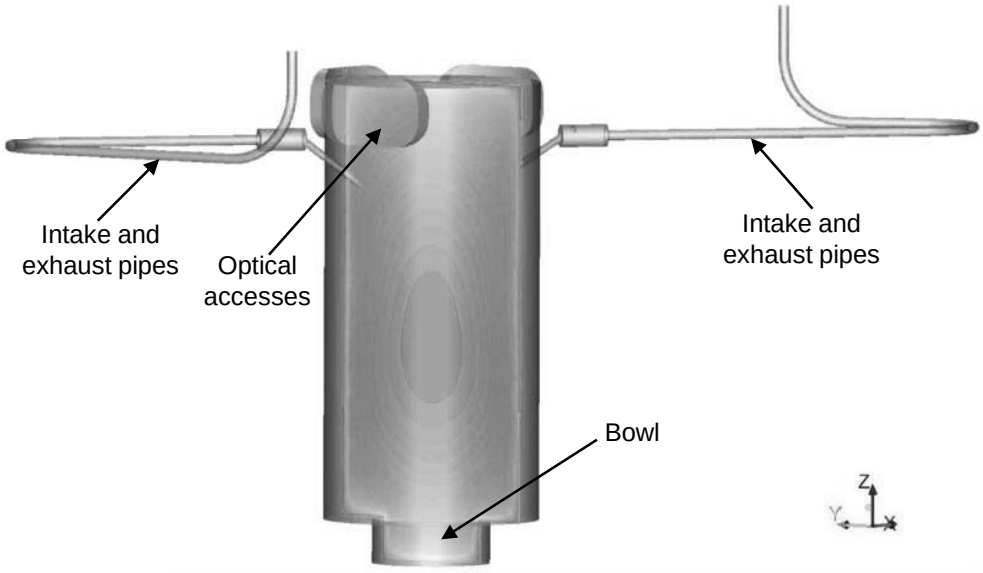


***Figure 7.1.*** *Physical domain.*

The mesh quality has been evaluated by its orthogonality, which measures the angle between the line that links the centroids of two consecutive cells and the normal vector of the contact surface of such cells. ANSYS Fluent gives the orthogonality as the cosine of such angle, thus, a value equal to 1 implies the best mesh quality according to this parameter. The orthogonality value of the mesh used in this simulation work is 0.912, with a standard deviation of 0.097.

The turbulence model applied in the simulations is the $k$-$\epsilon$ standard, which is a second order two-equation RANS model in which the turbulent viscosity emerging from the Reynolds averaged Navier-Stokes equations is characterized by a turbulent kinetic energy, $k$, and a dissipation rate of such turbulent kinetic energy, $\epsilon$. The $k$-$\epsilon$ equations include the following five adjustable constants:

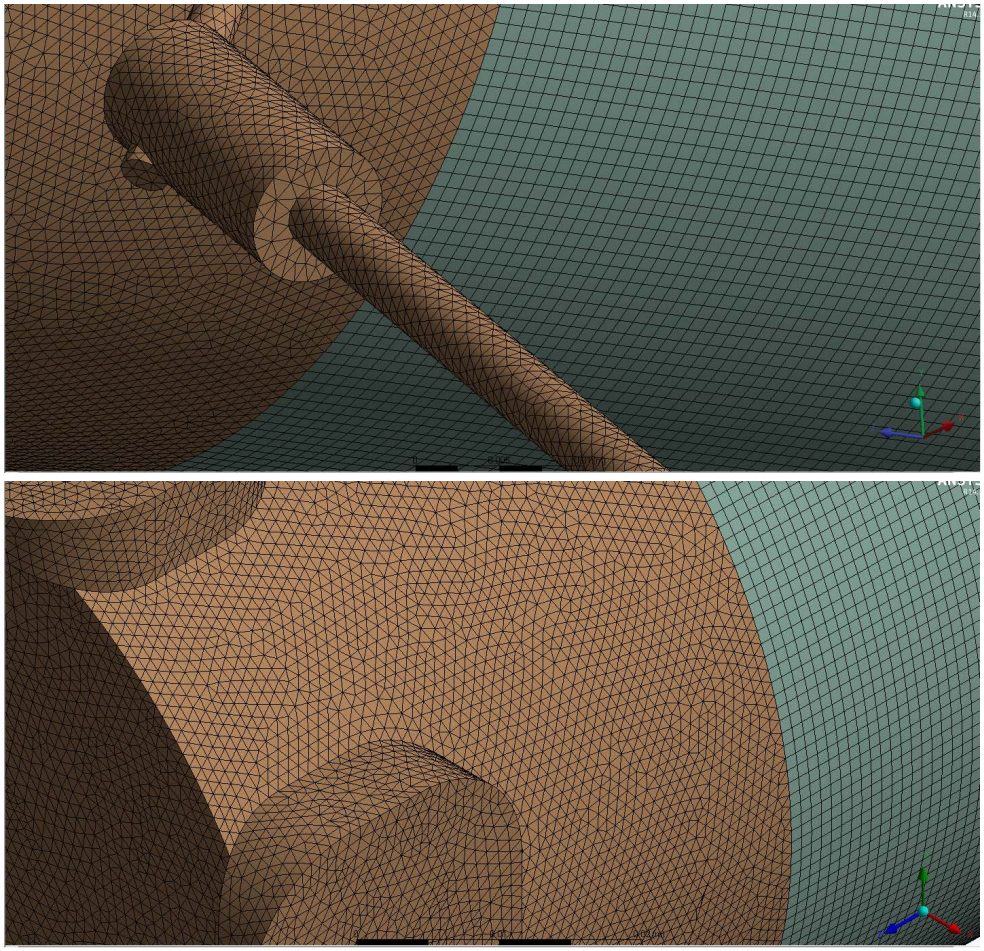

***Figure 7.2.*** *Mixed mesh designed for the discretization of the physical domain. Top.- Detail of the intake ducts. Bottom.- Detail of the lateral optical accesses.*

$C_\mu$, $\sigma_k$, $\sigma_\epsilon$, $C_{1\epsilon}$ and $C_{2\epsilon}$, the values of which have been assumed as the standard values that can be seen in [1] and that have been obtained by fitting a wide range of turbulent flows. Moreover, a constant time step equal to $10^{-4}$ $s$ has been selected, which leads to a maximum Courant number in the ducts equal to $C = u\Delta t/\Delta x \approx 0.5$, while the results have been saved each 0.25 $s$ due to memory restrictions.

Finally, the initial and boundary conditions have been set in order to replicate the RCEM behavior. They are summarized in Table 7.1, in which

| | | |
|---|---|---|
| **Boundary conditions** | **Stroke** | 120 & 240 $mm$ |
| | **Wall temperature** | 353 & 373 $K$ |
| | **Inlet flow** | 0.01984 $g/s$ |
| | **Inlet temperature** | 293 $K$ |
| **Initial conditions** | **Initial pressure** | 1 $bar$ |
| | **Initial temperature** | 293 $K$ |
| | **Initial velocity** | 0 $m/s$ |
| | **Initial turbulent kinetic energy** | 0 $m^2/s^2$ |
| | **Initial turbulent kinetic energy dissipation rate** | 0 $m^2/s^3$ |
| **k-$\epsilon$ standard constants** | $C_\mu$ | 0.09 |
| | $\sigma_k$ | 1.00 |
| | $\sigma_\epsilon$ | 1.30 |
| | $C_{1\epsilon}$ | 1.44 |
| | $C_{2\epsilon}$ | 1.92 |

***Table 7.1.*** *Initial and boundary conditions, as well as default values for the k-$\epsilon$ standard turbulent model for the CFD simulations with ANSYS Fluent.*

the inlet flow has been experimentally measured and the initial temperature has been selected as the ambient temperature in order to reproduce the most unfavorable conditions, in which the air remains cold after the cleaning of the combustion chamber (i.e. no time between the cleaning and the filling procedures is considered). Moreover, an initial quiescent environment (null velocity) has been selected, which implies null initial values for the turbulent kinetic energy and the rate of dissipation of the turbulent kinetic energy, according to [2]. The wall temperature is assumed to be constant during the whole process, which is ensured by the electrical heaters located in the liner and in the bowl, as well as the thermal inertia of the material.

The average in-cylinder temperature evolution during the filling process is plotted in Fig. 7.3 versus the normalized filling time for all cases. As it can be seen, the temperature before the end of the filling process reached values similar to the wall temperature (inside the interval $T_w \pm 3\ K$). The in-cylinder temperature rises up to a maximum value in the $\approx 25\%$ of the filling time, which corresponds to an in-cylinder pressure of around 1.4 $bar$. This maximum is caused by the turbulent kinetic energy dissipation and, from this instant on, the temperature decreases up to reach the asymptotic value of the wall temperature. Assuming an uncertainty in temperature equal to $\pm 3\ K$, a mean initial temperature similar to the wall temperature is reached

from ≈ 10% of the filling time, which corresponds to an increment in pressure, $\Delta P = P - P_0$, of around 0.25 *bar* over the initial condition. I.e., the initial temperature can be assumed as the wall temperature if the filling pressure is higher than 1.25 *bar*.

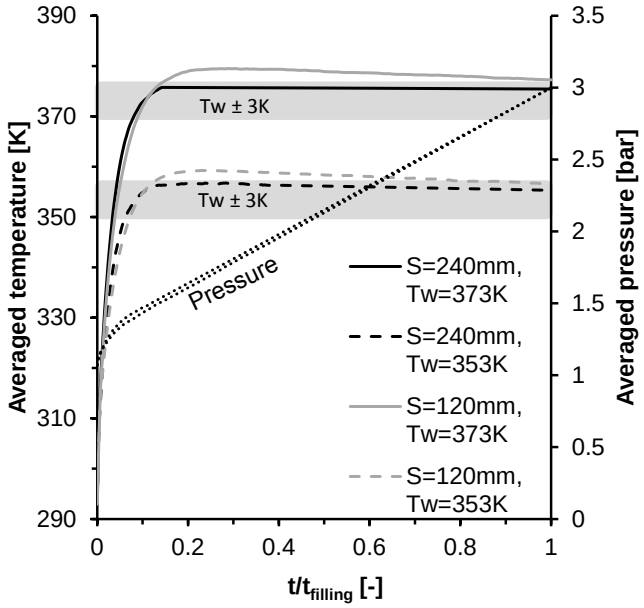


***Figure 7.3.*** *Average in-cylinder temperature (solid and dashed lines) and pressure (dotted lines) during the filling process versus the normalized filling time for both strokes and both wall temperatures.*

Moreover, Fig. 7.3 shows that the smaller the initial volume, the higher the maximum temperature reached during the filling. For the same turbulent kinetic energy dissipation rate, if the volume is reduced, a smaller amount of gas has to be heated and, therefore, higher temperature is reached.

The temperature distributions in the axial and radial planes, both including the inlet ducts and represented by a dashed line in the opposite projection, are shown in Fig. 7.4 for a selected stroke of 240 *mm* and a wall temperature equal to 373 *K*. If the scale is fixed from the initial temperature up to the wall temperature for all the different instants, it can be seen that from $t/t_{filling}$ ≈0.143 the temperature distribution in the whole chamber is almost constant. In fact, the corresponding image for $t/t_{filling}$=0.143 is shown in Fig. 7.5 using an adjusted scale from the minimum to the maximum value reached in the chamber at such instant. A clear cylindrical

symmetric temperature distribution is presented, and the resulting differences in temperature between all cells are lower than 3 $K$.

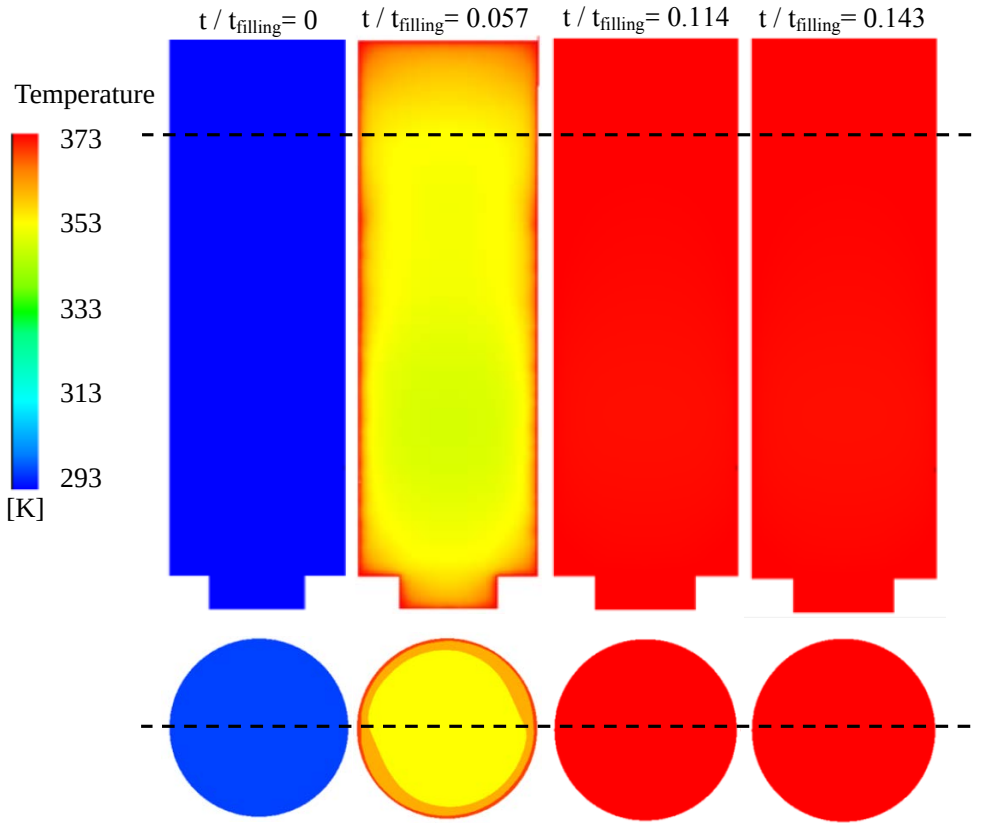


***Figure 7.4.*** *Temperature distributions in the axial and radial planes, both including the inlet ducts, for different times during the filling process. the stroke is equal to 240 mm and the wall temperature is equal to 373 K.*

The evolution of the in-cylinder temperature up to reach similar values than the wall temperature is caused by the intense heat transfer between gas and wall, which is promoted by the turbulent regime present in the combustion chamber. In fact, the turbulent viscosity defined by the $k$-$\epsilon$ standard turbulence model is two orders of magnitude higher than the laminar dynamic viscosity of the fluid. Moreover, the turbulence is caused by the inlet flow, which generates a swirl motion due to the inlet angle of the intake pipes, as shown in Fig. 7.6. I.e., since the intake pipes are designed to induce a swirl motion (they are tangentially connected to the combustion chamber), the inlet

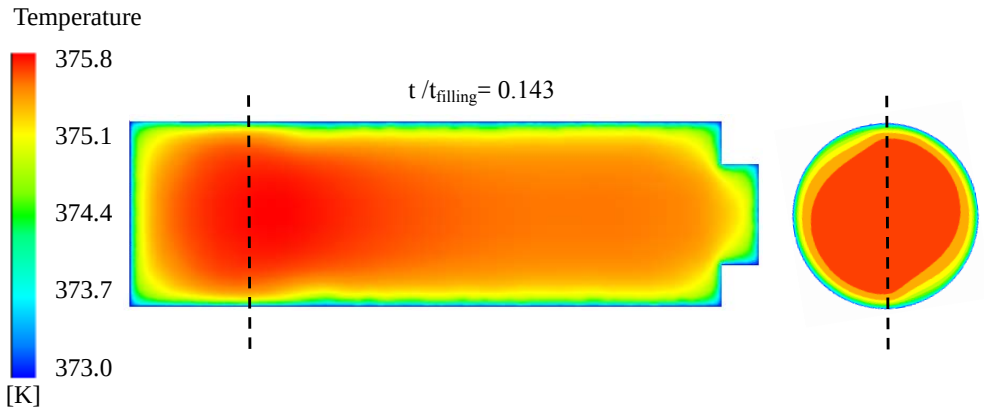


***Figure 7.5.*** *Cylindrical symmetric temperature distribution in the axial and radial planes, both including the inlet ducts, using an adjusted scale from the minumin to the maximum values reached in the chamber for $t/t_{filling}$=0.143. The stroke is equal to 240 mm and the wall temperature is equal to 373 K.*

flow is directed to the wall, promoting the heat transfer. Thus, a homogeneous initial environment in terms of temperature is guaranteed, so that the average temperature (equal to the wall temperature) can be used to calculate the mass trapped inside the cylinder by means of the equation of state.

After this first study under static conditions, a dynamic mesh has been implemented in the physical domain and the compression stroke under motoring conditions has been reproduced in ANSYS Fluent. The initial conditions are defined by the filling procedure previously described. The temporal evolution of the combustion chamber volume is imposed, so that the compression stroke is simulated. The mesh is deformed in order to adapt the cells to the piston movement. The mesh deformation is obtained by the moment distribution method (MDM), in which a dynamic layering of cell sizes, characterized by an appropriate layering constant, is assumed. In the dynamic case, the same constant $\Delta t$ equal to $10^{-4}$ $s$ has been selected, while the results have been saved at each time step.

The temperature and velocity distributions near TDC have been studied, as well as the evolution of the average in-cylinder pressure and temperature. Fig. 7.7 shows the temperature distribution at TDC for 120 $mm$ of stroke and 353 $K$ of wall temperature. A high-temperature homogeneous core can be seen in the domain, the average temperature of which can be assumed as the in-cylinder temperature in a 0-D analysis.

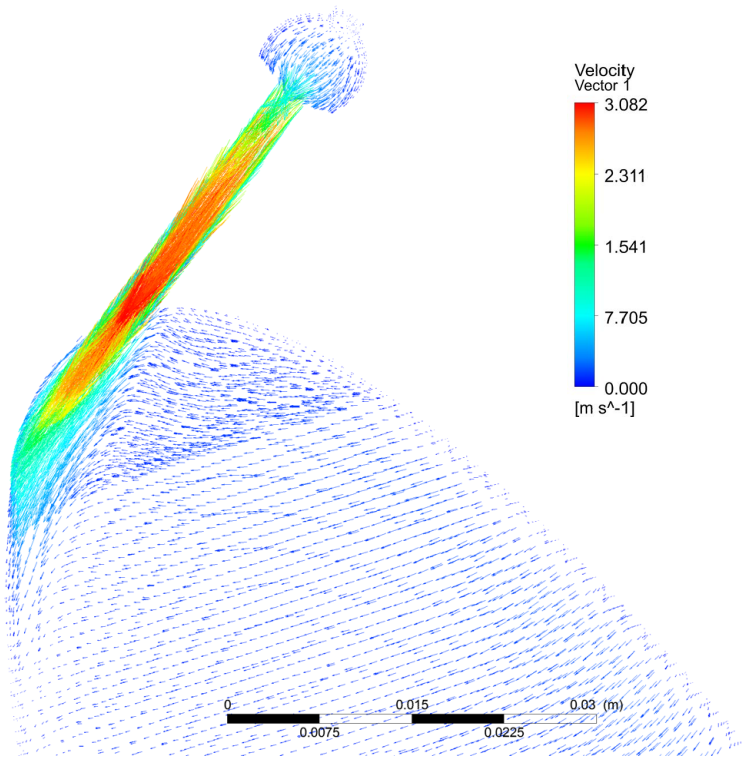


***Figure 7.6.*** *Detail of the inlet velocity vectors in one of the intake pipes. The flow is directed to the wall, promoting the heat transfer.*

The turbulent viscosity reaches values three orders of magnitude higher than the laminar kinematic viscosity. Such a high level of turbulence is promoted by the squish movement of the fluid from the cylinder head to the piston bowl. As it can be seen in Fig. 7.8, the piston design promotes the existence of two recirculation zones that cover most of the cylinder volume. Thus, a well-mixed environment is achieved and a homogeneous temperature core is obtained thanks to this stirring effect.

Finally, it should be noted that for chemical kinetic studies, a homogeneous environment is highly desirable, since it allows to perform 0-D simulations with detailed mechanisms to properly describe the oxidation paths of the air - fuel mixture. Thus, the higher the homogeneity in temperature, the more reliable the results from 0-D simulations. The results obtained from this CFD study ensure the existence of an initial homogeneous environment, in which the initial

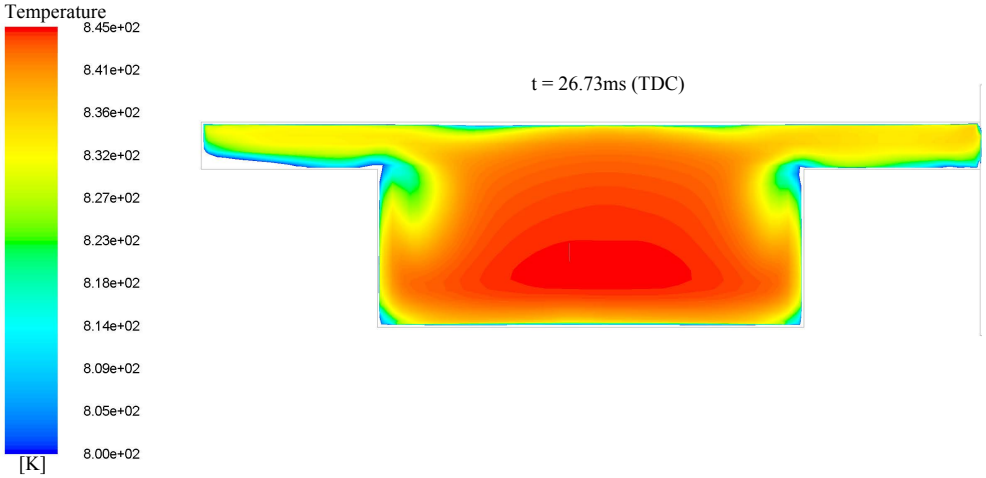


***Figure 7.7.*** *Temperature distribution at TDC. A high-temperature homogeneous core can be clearly identified.*

temperature is very similar to the wall temperature. Moreover, the analysis of the compression stroke shows the existence of a homogeneous core, which covers most of the cylinder volume and the temperature of which is highly representative of the thermodynamic conditions reached in the combustion chamber. Therefore, it can be concluded that the RCEM has been validated in terms of temperature to perform autoignition studies assuming homogeneous conditions and, thereby, for the validation of chemical kinetics mechanisms by using its experimental data.

### 7.1.2 Fuel vaporization, mixing and stratification characteristic times

The evolution of the fuel during the filling of the facility has been studied, including the injection phenomenon, the vaporization of the fuel and the mixing time, in order to define a characteristic time for stratification of the mixture due to gravitational effects. Both the mesh generation as well as the CFD calculations have been carried out in the open-access software OpenFOAM.

The combustion chamber is meshed using the *blockMesh* utility, whereby simple domains can be discretized by means of a structured grid. Fig. 7.9 shows the generated mesh, in which two different blocks can be distinguished:

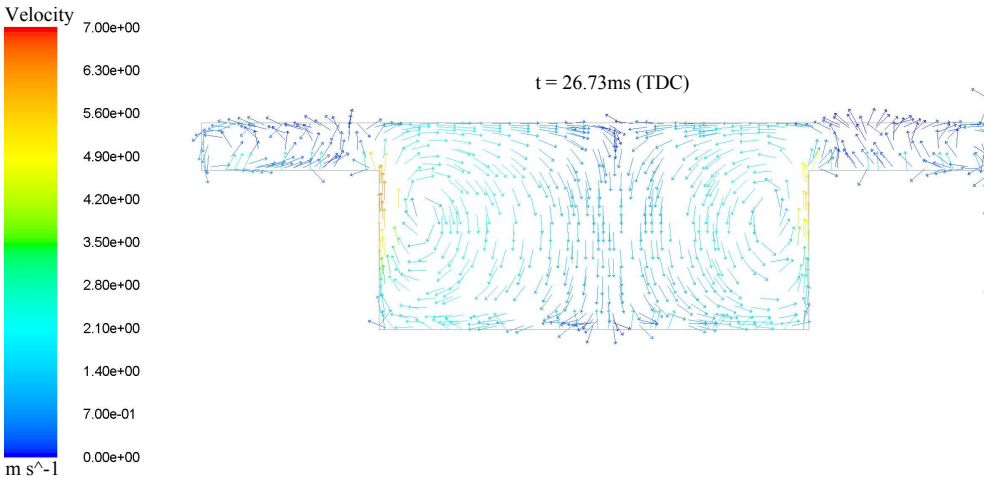


***Figure 7.8.*** *Velocity field at TDC. Two recirculation zones are generated by the piston movement and the geometry of the combustion chamber.*

a central core with rectangular shape and a surrounding volume that defines the liner wall. The selected stroke is 249 $mm$, which leads to the maximum initial volume and, therefore, to the most unfavorable conditions for the fuel homogenization. Such stroke results in a mesh composed by 976,752 cells, with a mean size of $\Delta x = 1.07\ mm$, which is almost orthogonal.

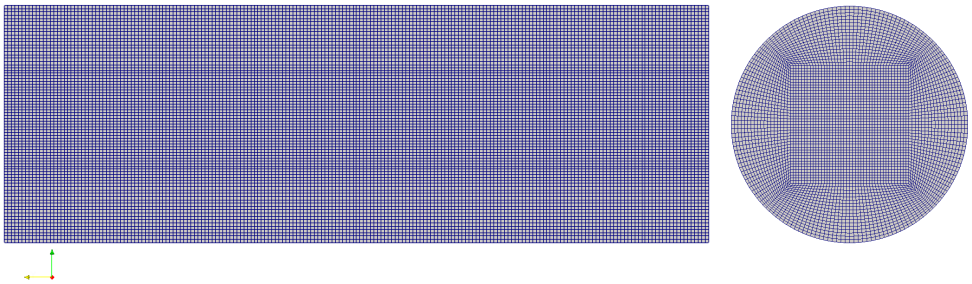

***Figure 7.9.*** *Structured mesh used to study the fuel stratification and mixing times in OpenFOAM.*

The solver used is the standard *sprayFOAM*, which allows the study of liquid sprays from a Lagrangian point of view. This solver includes different models for injection, atomization, evaporation and mixing of a liquid spray

injected in a gaseous domain. It is able to solve compressible, reactive, turbulent and transient flows by linking the physical equations with chemical kinetic mechanisms. In this study, chemistry is deactivated and the turbulence is modeled by assuming a $k$-$\epsilon$ standard model, whereas the thermodynamic properties of the species involved in the calculation, including the fuel, are defined by means of NASA polynomials [3]. Besides, since the stratification of the mixture wants to be solved, it is mandatory to take into account the gravitational effects.

Two different approaches are involved in the simulation work. On the one hand, the gas phase is solved from an Eulerian point of view, assuming it as a continuous phase and applying the finite volume method (FVM). On the other hand, the liquid phase is solved from a Lagrangian point of view, assuming the liquid droplets as single particles that are grouped in *parcels* according to their size. These *parcels* are randomly injected in the gas phase, causing certain loss of symmetry, which is the reason why the full combustion chamber has been simulated (instead of only a 2-D sheet). Finally, a second order implicit method is used for the spatial discretization, while a first order explicit method is used for the temporal discretization.

The initial and boundary conditions are summarized in Table 7.2, whereas the default values for the constants of the $k$-$\epsilon$ standard turbulent model can be seen in Table 7.1. A quiescent environment is assumed, in which the initial pressure is the ambient pressure and the initial temperature is varied in order to reproduce different conditions. The injected mass of fuel, which is assumed as n-heptane ($C_7H_{16}$), is varied from 10 to 300 $mg$, while it is assumed to be injected following a trapezoidal injection rate in which the opening and closure times are equal to 250 $\mu s$, which are typical values in direct injection systems. Besides, the total time of injection is defined assuming an injection pressure of 500 $bar$, which is the typical value used in the RCEM for the generation of homogeneous mixtures. Finally, the fuel is injected through a 135 $\mu m$ nozzle by inserting $20{\cdot}10^6$ parcels per second into the domain, assuming a Rosin-Rammler droplets size distribution from $1\mu m$ to $135\mu m$ that results in a statistical mode of $88\mu m$.

The vaporization and homogenization times are plotted in Fig. 7.10 versus the injected mass of n-heptane for an ambient temperature equal to 353 $K$. Specifically, the vaporization time is defined as the instant at which only 5% of the fuel remains in liquid phase. Besides, the homogenization time is defined as the instant at which the coefficient of variation of the fuel molar fraction in the whole chamber is lower than 2%.

| | | |
|---|---|---|
| **Boundary conditions** | **Stroke** | 249 $mm$ |
| | **Wall temperature** | 353 & 373 $K$ |
| **Initial conditions** | **Initial pressure** | 1 $bar$ |
| | **Initial temperature** | 353 & 373 $K$ |
| | **Initial velocity** | 0 $m/s$ |
| | **Initial turbulent kinetic energy** | 0 $m^2/s^2$ |
| | **Initial turbulent kinetic energy dissipation rate** | 0 $m^2/s^3$ |

***Table 7.2.*** *Initial and boundary conditions for the CFD simulations with OpenFOAM.*

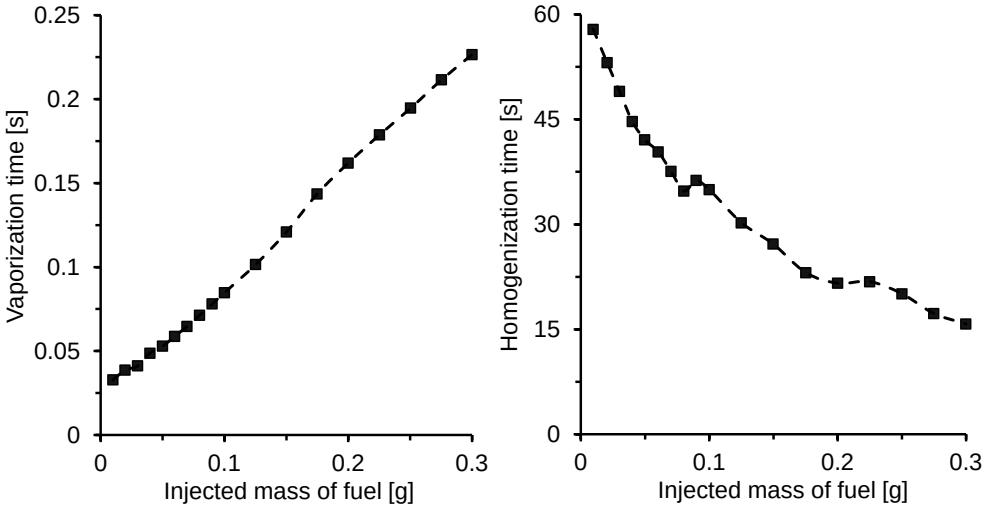


***Figure 7.10.*** *Characteristic times of the process versus injected fuel mass. Left.- Vaporization time. Right.- Homogenization time.*

As expected, the vaporization time increases linearly with the injected mass of fuel, since the injection duration also increases linearly with the injected mass. It can be seen that the vaporization times are negligible compared to the homogenization times, so that the generation of a homogeneous gas mixture in the combustion chamber is controlled by the mixing time.

Three different phenomena affect the mixing time: convective effects, mass diffusivity effects and gravitational effects. On the one hand, convective effects are related to the dynamics of the spray, which causes the dependence of

the homogenization time on the injected mass of fuel. They are extremely relevant only during the first stage of the process, since the characteristic time of the turbulence (defined as the time at which the turbulent and laminar viscosities coincide) is lower than 10 $s$ in all cases. I.e., the dissipation rate of the turbulent kinetic energy causes that convective effects are not dominant in the mixing process, but their contribution causes the behavior of the mixing time with the mass of fuel, since the higher the mass of fuel injected, the larger the area of air perturbed by the spray. On the other hand, the mass diffusivity effects are related to the trend to homogenize of heterogeneous mixtures because of gradients of concentration, while the gravitational effects are related to the trend to stratify the fuel because of its higher molecular weight compared to air. It should be noted that mass diffusivity and gravity cause opposite effects. It can be checked that the evolution of the coefficient of variation of the fuel molar fraction with time for a certain amount of fuel always decreases, which means that the diffusive effects are the dominant ones and a clear trend to homogenize is always present during the simulated time. Thus, although the stratification due to gravitational effects can be seen in an adjusted scale, as shown in Fig. 7.11, it is negligible in a global scale. Moreover, since the molecular weights of the different fuels used in the Thesis compared to the air always have the same order of magnitude, this result can be extrapolated to any of these fuels and it is not only valid for n-heptane.

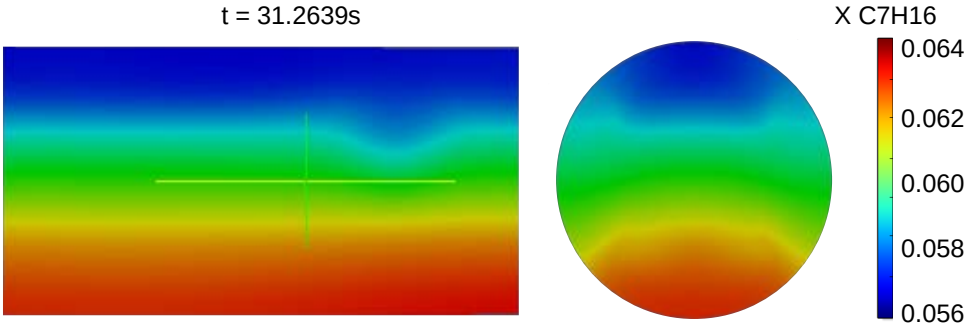


***Figure 7.11.*** *Effects of stratification in the n-heptane molar fraction because of differences in molecular weight for 100 mg of injected fuel mass and a wall temperature equal to 353 K.*

Fig. 7.12 shows the spray development in terms of fuel molar fraction, as well as both the liquid and vapor phases in the whole domain. Since the fuel liquid droplets are treated from a Lagrangian point of view, they appear as

discrete red spheres in the figure. Since the turbulence generated by the spray is not enough to reach the condition of homogeneity and the mass diffusion is a very slow process, the mixing time reach really long values. However, the long duration of the filling procedure ($\approx$40 $s$) and the delay between the end of the filling and the rapid compression stroke ensure the existence of a homogeneous environment not only in terms of temperature (see 7.1.1), but also in terms of equivalence ratio.

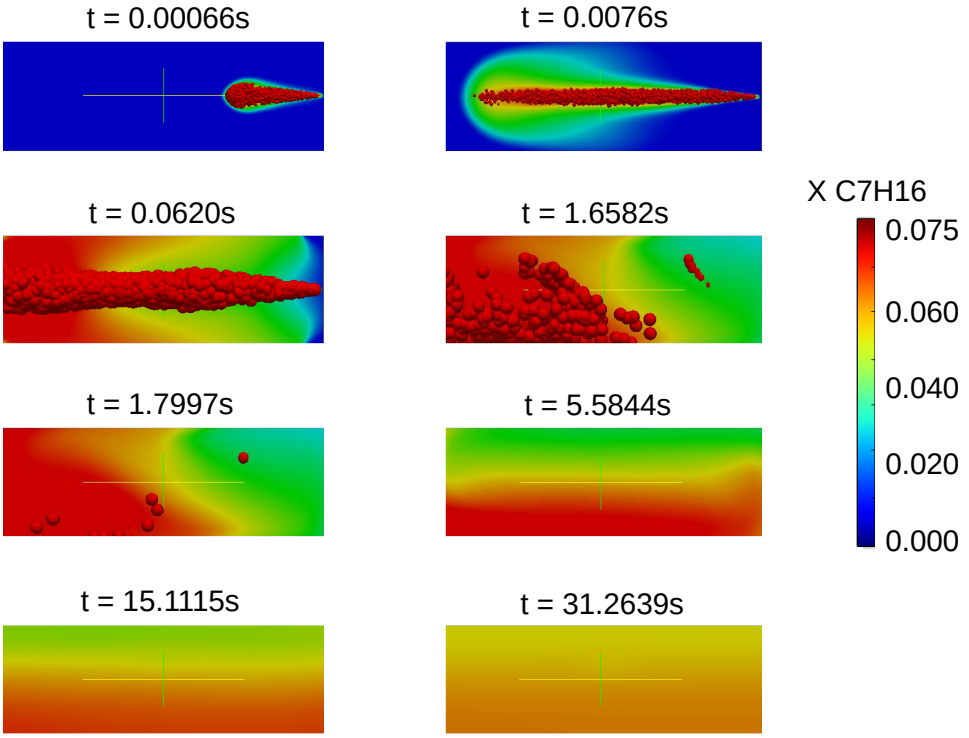


***Figure 7.12.*** *Evolution of the fuel molar fraction for both the liquid and vapor phase in the combustion chamber.*

## 7.2 Appendix: N-dodecane evaporation characteristic time in RCEM experiments

The characteristic evaporation time of n-dodecane under the working conditions performed in the RCEM is estimated in this section. N-dodecane is

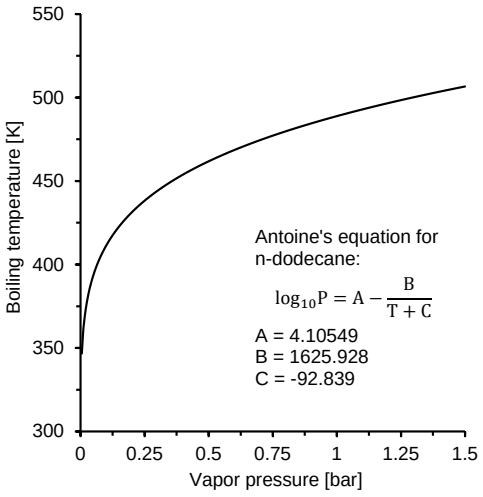


***Figure 7.13.*** *Boiling temperature versus vapor pressure for n-dodecane. Data obtained by solving the Antoine's equation.*

a long-chain hydrocarbon, the boiling temperature of which (489 $K$ at 1 $bar$) is usually higher than the initial temperature of the combustion chamber. Thus, it is mandatory to check if the filling time and the initial thermodynamic conditions are high enough to allow the vaporization of the fuel, since a homogeneous vapor-phase mixture wants to be obtained.

A vacuum pump is available to clean the combustion chamber before a filling procedure, ensuring the no contamination of the mixture. The minimum pressure than can be reached in the chamber is equal to 13 $mbar$, so that the fuel can be injected at very low in-cylinder pressure conditions, occurring a flash-boiling and avoiding any liquid phase. Specifically, the boiling temperature of n-dodecane under different pressures can be obtained by solving the Antoine's equation [4], the solution of which can be seen in Fig. 7.13. Thus, vapor fuel is ensured for initial temperatures higher than 365 $K$ if the injection of n-dodecane is performed when the combustion chamber is under vacuum conditions (13 $mbar$).

However, in some cases the fuel injection cannot be performed before the filling procedure due to the trend to stratify of heavy fuels under long filling times. Thus, it is mandatory to be able to evaporate the fuel during the mixing time, which should be long enough to obtain a homogeneous mixture but short enough to avoid stratification problems. In order to check the viability of such

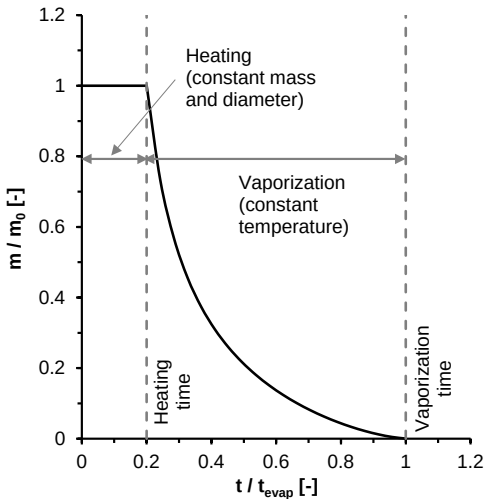


***Figure 7.14.*** *Schematic of the estimation of the heating and vaporization times. The evolution of the droplet mass, m, with time is plotted.*

methodology, the vaporization time of a fuel droplet is solved under the most unfavorable conditions and the resulting value is compared to the characteristic filling time ($\approx 40\ s$). The following conditions have been assumed:

- Ambient temperature, $T_\infty$: 403 $K$.
- Ambient pressure, $P_\infty$: 1.5 $bar$.
- Fuel initial temperature, $T_0$: 300 $K$.
- Droplet initial diameter, $\phi_0$: 135 $\mu s$.

$T_\infty$ and $P_\infty$ represent the lowest initial temperature and the highest initial pressure in the parametric study performed, respectively, which lead to the worst ambient conditions for fuel vaporization. Besides, the initial temperature of the fuel has been assumed as the storage temperature, while the initial diameter of the fuel droplet has been assumed as the nozzle diameter.

Under the previous conditions, two different phenomena have been independently taken into account: the heating and the vaporization of the droplet.

Fig. 7.14 shows a schematic of the estimation of the heating and vaporization times. The characteristic heating time, $t_{heating}$, has been

estimated assuming that the vaporization is negligible during the heating stage, being the mass and the diameter of the droplet constant. Moreover, the thermal properties (Nusselt number and heat capacity) are also assumed as being constant. Thus, the following expression for the heating time can be obtained by integrating the energy equation in the droplet:

$$t_{heating} = \frac{mC\phi_0}{Nu\lambda A} ln\left(\frac{T_\infty - T_0}{T_\infty - 0.99T_\infty}\right) \tag{7.1}$$

where $m$ represents the mass and $A$ represents the external area of the droplet (assuming spherical shape). $Nu$, $\lambda$ and $C$ represent the Nusselt number, the thermal conductivity and the heat capacity, respectively. Finally, the heating of the droplet is assumed to end when the fuel reaches a 99% of the ambient temperature. Assuming natural convection ($Nu \approx 2$) and computing the thermal properties of n-dodecane at $T = (T_\infty + T_0)/2$, the resulting heating time is equal to 0.053 $s$.

According to the model shown in Fig. 7.14, the vaporization starts once the droplet has reached the ambient temperature. The characteristic vaporization time can be obtained as follows:

$$t_{vap} = \frac{\phi_0^2}{K_v} \tag{7.2}$$

where $K_v$ is the vaporization constant, which is described by the following equation:

$$K_v = 8\frac{\bar{\rho}}{\rho_f} Dln\left(1 + \frac{Y_{f0} - Y_{f\infty}}{1 - Y_{f0}}\right) \tag{7.3}$$

where $\bar{\rho}$ represents the averaged density of the environment, which is assumed as the air density (the amount of fuel is assumed to be negligible), and $\rho_f$ represents the fuel density. $D_{j,k}$ is the mass diffusion coefficient of species $j$ through species $k$ (in this case n-dodecane through air), and $B = (Y_{f0} - Y_{f\infty})/(1 - Y_{f0})$ is the Spalding's transfer number, in which $Y_{f0}$ is the mass fraction of fuel on the droplet surface and $Y_{f\infty}$ is the mass fraction of fuel in the environment. Finally, $Y_{f0}$ is defined by the fuel vapor pressure, which can be estimated by solving the Clausius-Clapeyron equation. Thus, a vaporization time equal to 1.33 $s$ has been obtained.

It should be noted that $t_{heating} \ll t_{vap}$, so that no vaporization during the heating time seems a reasonable assumption. Finally, the total time that the fuel needs to be in vapor phase is $t_{heating} + t_{vap}$=1.383 $s$, which is much shorter than the typical filling time (40 $s$).

## 7.3 Appendix: Post-processing of the experimental data from the RCEM

The different models involved in the post-processing of experimental results from the RCEM are described in this appendix. Besides, the fitting procedure performed to obtain the characteristic constants of each model is also presented. Finally, the calculation of diagnosis parameters as the heat release rate or the combustion efficiency is also shown.

### 7.3.1 Models and their fitting procedure

Three different models are taken into account in the post-processing of RCEM data: a heat losses model, a deformation model and a leakage model.

- Heat losses model.

The heat losses model is based on the Woschni correlation [5], which defines a global convection coefficient, $h$, for the whole combustion chamber with temporal resolution as follows:

$$\begin{aligned} h =& 0.013 d^{-0.2} P^{0.8} T^{-0.53} \cdot \\ & \cdot \left( C_{11} C_m + C_{12} u_{swirl} + C_2 \frac{V_d T_{ref}}{V_{ref} P_{ref}} (P - P_{motored}) \right)^{0.8} \end{aligned} \tag{7.4}$$

where $d$ is the piston bore, and $P$ and $T$ are the in-cylinder pressure and temperature, respectively. The last bracket of the expression represents a characteristic velocity of the gas in the combustion chamber, where $C_m = 2Sn$ is the mean piston speed, $u_{swirl}$ is the swirl velocity (which is assumed to be negligible in the RCEM), $V_d$ is the displacement volume, $T_{ref}$, $V_{ref}$ and $P_{ref}$ are temperature, volume and pressure at reference conditions (which are assumed as the initial conditions in the RCEM), and $P_{motored}$ represents the in-cylinder pressure under motoring conditions (without combustion). Finally, $C_{11}$, $C_{12}$ and $C_2$ are constants that have to be fitted according to the operating conditions. On the one hand, $C_{11}$ and $C_{12}$ represent the in-cylinder air movement caused by geometrical aspects of the machine. Since the kinematics of the machine is not controlled by any mechanism (e.g., the piston-rod-crank mechanism in an engine) and TDC is defined by compensation of forces between the driving gas pressure, the inertia and the in-cylinder pressure, different working conditions lead to different geometrical configurations (clearance volume and compression ratio), which

implies different values for $C_{11}$ and $C_{12}$. Thus, these constant should be fitted for each operating point. On the other hand, $C_2$ represents the turbulence generated by the combustion process and the standard value proposed by Woschni has been assumed here.

It should be noted that the move law of the RCEM shows two different equivalent engine speeds, one for the compression stroke and another for the expansion stroke. Thus, two different mean engine speeds, $C_m$ are defined, which results in a discontinuity in the heat losses evolution at TDC.

Once the convection coefficient has been obtained, heat losses can be easily calculated by applying the Newton's law of cooling, $\dot{Q}_{lost} = hA(T_w - T)$, where the liner, cylinder head, piston and bowl are taken into account to evaluate the heat transfer area, $A$, while the wall temperature, $T_w$, is assumed to be uniform and constant during the whole cycle.

- Deformation model.

The deformation model is based on the deformation of a beam under compression strain, in which the stiffness constant is fitted in order to model the mechanical deformation of the whole combustion chamber, including thermal expansions. Thus the stiffness constant, $K$, loses its physical meaning and can reach positive or negative values (depending on the relative deformation between piston and cylinder head and between compression strains and thermal expansions).

The deformation of the combustion chamber, $\delta$, is calculated assuming that the whole deformation can be computed as the deformation of the piston, which modifies the piston position. $\delta$ is obtained assuming two different forces: in-cylinder pressure force and inertia. The deformation that occurs between the position sensor and the combustion chamber cannot be read by the position sensor and it should be estimated by the model, as shown in Fig. 7.15. Thus, only the mass of a section of the piston tube (driver piston) has to be computed.

The following expression is used to obtain the deformation of the combustion chamber:

$$\begin{aligned} \delta &= K\left(F_{pressure} + F_{inertia}\right)(0.455 - x) = \\ &= K\left(P\frac{\pi}{4}d^2 + \left(m_{piston} + \lambda L\right)a\right)(0.455 - x) \end{aligned} \tag{7.5}$$

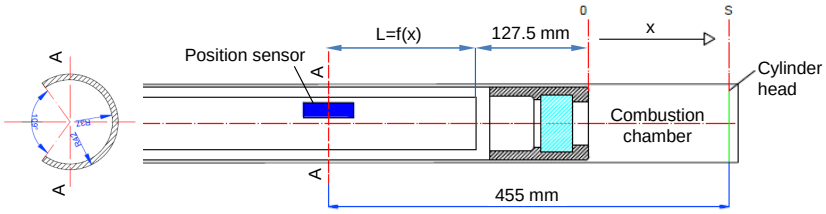


***Figure 7.15.*** *Schematic of the section of the piston tube that has to be coomputed in the model.*

where $K$ is the stiffness constant, which has to be experimentally fitted for each operating point since it depends on the wall temperature and on the oil pressure in the hydraulic closing mechanism. $P$ represents the in-cylinder pressure and $d$ is the piston bore. $m_{piston}$ is the mass of the experimental piston (striped section in Fig. 7.15), $\lambda$ represents the lineal density of the piston tube and $L = 0.3275 - x$ defines the length of piston tube that has to be taken into account to compute the inertia, in meters. Finally, $a$ represents the piston acceleration.

Thus, the volume of the combustion chamber is obtained by the following equation:

$$V = \frac{\pi}{4} d^2 \left(S - (x - \delta)\right) \tag{7.6}$$

where $S$ represents the selected stroke.

- Leakage model.

The leakage model is based on the flow through a nozzle, which represents the clearance between liner and sealing rings. Specifically, the problem can be described as Fig. 7.16 shows. Assuming that the ambient pressure is equal to 1 *bar* and an adiabatic coefficient, $\gamma$, equal to 1.4 (dry air at standard conditions), the in-cylinder pressure needed to reach sonic conditions in the nozzle is equal to 1.89 *bar*, which means that sonic velocity is established in the leakage area during almost all the cycle.

Therefore, the leakage flux can be assumed as the flow through a nozzle under critical conditions:

$$\dot{m}_{leakage} = A_{throat} \rho_{throat} a_{throat} \tag{7.7}$$

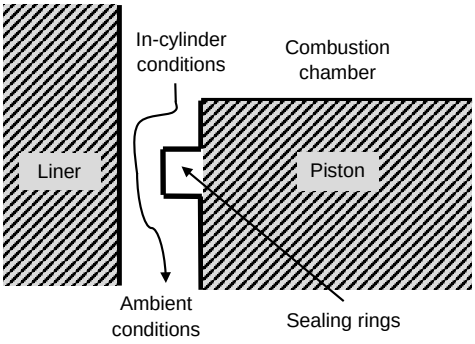


***Figure 7.16.*** *Schematic of the leakage model.*

where $A_{throat}$ represents the leakage area, $\rho_{throat}$ is the gas density in the throat and $a_{throat}$ is the speed of sound under critical conditions. Thus:

$$\rho_{throat} = \frac{P_{crit} MW}{R T_{crit}} \tag{7.8}$$

$$a_{throat} = \sqrt{\gamma \frac{R}{MW} T_{crit}} \tag{7.9}$$

where $P_{crit} = P\,(2/(\gamma+1))^{\gamma/(\gamma-1)}$ represents the critical pressure (which depends on the in-cylinder pressure, $P$) and $T_{crit} = T\,(2/(\gamma+1))$ represents the critical temperature (which depends on the in-cylinder temperature, $T$).

Finally, the leakage area has been experimentally estimated by measuring the in-cylinder pressure losses during a frame of time when the chamber is filled up to a certain pressure. Thus, the mass flow through the clearance between piston and liner can be calculated and a leakage area can be obtained. These experiments have been carried out for in-cylinder pressures up to 20 *bar* and the leakage from the combustion chamber has proved to be negligible. In fact, once the leakage model was calibrated, assuming standard compression conditions of 50 *bar* and 800 $K$ during the whole cycle ($\approx$30 $ms$), the mass losses represent less than 0.25% of the in-cylinder initial mass. However, the leakage model is implemented and taken into account in the post-processing routine.

- Fitting procedure for models.

Two different constants have to be experimentally fitted for the calibration of the models: $C_{11}$ for the heat losses and $K$ for the deformation model.

Despite the fact that the intake pipes are tangentially connected to the combustion chamber, the swirl motion promoted during the filling dissipates during the slow compression process. Thus, $C_{12}$ is not used in the expression that defines the convection coefficient since the swirl velocity, $u_{swirl}$, is assumed to be zero in the RCEM. Besides, since $C_{11}$ and $K$ depend on the working conditions, both constants should be fitted for each operating point.

To do so, an experiment under motoring conditions (without combustion) is carried out. Thus, the heat release rate is null during the whole cycle and the temperature evolution can be calculated by applying both the equation of state and the energy equation. Taking into account that the air-fuel mixture can be assumed as ideal gas, the in-cylinder temperature can be obtained by solving:

$$T = \frac{PV}{mR}MW = \frac{P\frac{\pi}{4}d^2\left(S-(x-\delta)\right)}{mR}MW \tag{7.10}$$

or

$$\frac{d}{dt}\left(mC_vT\right) = \dot{Q}_{lost} - P\frac{dV}{dt} = hA(T_w - T) - P\frac{d}{dt}\left(\frac{\pi}{4}d^2\left(S-(x-\delta)\right)\right) \tag{7.11}$$

where $m$ is the mass trapped, which can be calculated by applying the leakage model, and $C_v$ is the heat capacity at constant volume of the mixture. The stiffness constant, $K$, from the deformation model, is involved in the calculation of $\delta$, as it has been explained previously. Besides, $C_{11}$, from the heat losses model, is involved in the calculation of the convection coefficient, $h$, as also explained above. Moreover, $C_2$ is not involved in the calculation of heat losses since, under motoring conditions, the corresponding term is null. Thus, different values of $K$ and $C_{11}$ lead to different temperature profiles.

An iterative procedure is performed to minimize the differences between both temperature profiles, the one obtained by the equation of state and the one obtained by the energy equation. Once the best matching between profiles is reached, the corresponding values for $K$ and $C_{11}$ are the fitted values. Starting form certain initial values for both constants, $K_0$ and $C_{11,0}$, the minimum area enclosed by the temperature curves is reached by modifying these initial values according to two indicators, both shown in Fig. 7.17.

On the one hand, the instant at which the maximum temperature occurs can be shifted in the energy equation by modifying the heat losses. Specifically, the temperature profile obtained by the energy equation moves to north-est (higher temperature reached nearer TDC) when $C_{11}$ decreases. This is an expected result, since the lower the value of $C_{11}$, the lower the heat losses and the higher the temperature. Moreover, the thermodynamic lag between maximum pressure and minimum volume is related to heat losses [6], being

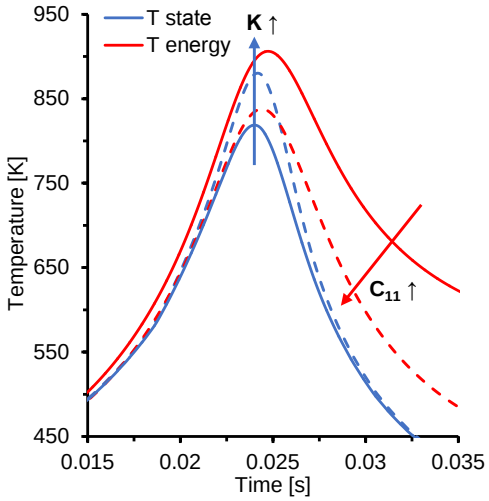


***Figure 7.17.*** *Effects of $K$ and $C_{11}$ on temperature profiles.*

smaller if heat losses decreases. Thus, $C_{11}$ can be modified imposing that both maximums of temperature (from energy equation and from equation of state) occur at the same instant.

On the other hand, the maximum temperature reached by solving the equation of state can be modified by changing the deformation. Specifically, the temperature profile obtained by the equation of state is shifted to higher values while keeping the maximum in the same instant if the deformation constant, $K$, increases. Besides, $K$ does not have relevant influence on the temperature profile obtained by the energy equation. The higher the value of $K$, the higher the deformation and the higher the volume, resulting in higher temperature. It should be noted that, since the deformation mainly depends on the in-cylinder pressure, they are relevant only around TDC. Thus, $K$ can be modified imposing that both maximums of temperature (from energy equation and from equation of state) reach the same value.

Fig. 7.18 shows the resulting temperature paths from the equation of state and from the energy equation once the constants $C_{11}$ and $K$ have been fitted, i.e., once both models have been calibrated. A very good matching between both temperature profiles can be seen in the figure, which proves the good accuracy of the models. Furthermore, the heat release rate, which should be null, is also a good indicator of the models accuracy. Fig. 7.19, which will be explained in the next paragraph, shows the heat release rate for an

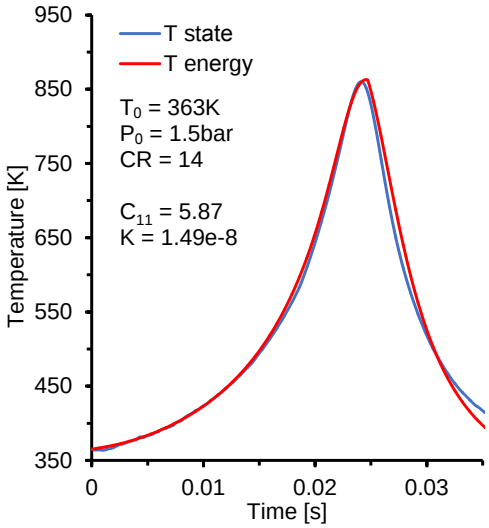


***Figure 7.18.*** *Temperature profiles from equation of state and energy equation once* $C_{11}$ *and* $K$ *have been fitted.*

experiment performed with n-dodecane and the corresponding signal under motoring conditions. It can be seen that the resulting heat release rate under motoring conditions is almost null.

### 7.3.2 Calculation of diagnosis parameters

The equation of state and the energy equation are applied to obtain the temperature profile and the heat release rate from the experimental data. Equations are discretized in time using a first order explicit method, in which the information of the previous instant is used to calculate the information of the current one.

It should be noted that the move law of the RCEM during an experiment includes a slow compression phase (piston position from 0 $mm$ to 29 $mm$) and the fast compression phase (piston position from 29 $mm$ to TDC). Thus, the initial conditions after the filling have to be extrapolated to the instant at which the piston reaches 29 $mm$, which is the time reference instant ($t = 0$). The in-cylinder temperature when $t = 0$ can be calculated using the equation of state, since the volume of the combustion chamber is known thanks to the position sensor and the relative in-cylinder pressure evolution during the

slow compression phase measured by the piezoelectric sensor, the base value of which is measured by a piezoresistive sensor (filling pressure). Moreover, deformation and leakages can be neglected during this slow compression phase due to the low in-cylinder pressure. Thus, the conditions when the piston reaches 29 $mm$ will be assumed as the initial conditions from now on.

From a certain instant, $i$, in which all the parameters are known (e.g., the initial conditions), the following equations are solved at each instant to obtain the calculated parameters:

$$T_{i+1} = \frac{P_i V i}{m_i R} MW_i \tag{7.12}$$

where $R$ represents the universal gas constant and $MW_i$ represents the molecular weight. The pressure evolution, $P_i$, is measured and the volume, $V_i$, is calculated by solving Eq. 7.6. The mass trapped, $m_i$, is obtained as $m_{i+1} = m_i - \dot{m}_{leakage}\Delta t$, where the leakage flow, $\dot{m}_{leakage}$ is calculated by solving Eq. 7.7 and the time step, $\Delta t$, is defined by the acquisition frequency. The molecular weight, $MW_i$, is calculated assuming a mixture between fresh mixture (fuel and synthetic air) and combustion products from a complete combustion reaction. Thus, $MW_i = \sum X_j MW_j$.

The combustion products fraction is determined by estimating the instantaneous fuel consumption as follows:

$$m_{fuel\ consumed,\,i} = \frac{Q_{accumulated,\,i}}{LHV} \tag{7.13}$$

where $Q_{accumulated,\,i}$ represents the accumulated heat release that results from integrating the heat release rate and $LHV$ is the lower heating value of the fuel. Thus:

$$m_{fresh\ mixture\ consumed,\,i} = m_{fuel\ consumed,\,i}\left(1 + \frac{\lambda_{st}}{Y_{O_2}}\right) \tag{7.14}$$

where $\lambda_{st} = (m_{O_2}/m_{fuel})_{st}$ is the $O_2$-to-fuel ratio under stoichiometric conditions and $Y_{O_2}$ is the oxygen mass fraction in the synthetic air. Therefore, the instantaneous mass of fresh mixture and combustion products will be:

$$m_{combustion\ products,\,i} = m_{fresh\ mixture\ consumed,\,i} \tag{7.15}$$

$$m_{fresh\ mixture,\,i} = m_i - m_{fresh\ mixture\ consumed,\,i} \tag{7.16}$$

where $m_i$ is the mass trapped taking into account the leakage model.

It should be noted that not only the molecular weight of the gas mixture can be determined by combining Eqs. 7.15 and 7.16, but also both heat

capacities ($C_p$ and $C_v$) and the mean temperature of both fresh mixture and combustion products. The heat capacity can be calculated similarly to the molecular weight, $C_{p,\,i} = \sum X_j C_{p,\,j}$, where the heat capacity of each species is defined by NASA polynomials [3]. On the one hand, the mean temperature of the fresh mixture is obtained assuming a polytropic evolution in which the pressure is considered to be uniform and equal to the measured in-cylinder pressure, while the polytropic index is defined by the compression stroke up to the start of ignition, including in this way the heat losses. On the other hand, the mean temperature of the combustion products can be obtained by solving an energy balance between fresh mixture and combustion products as follows:

$$\begin{aligned} m_i C_{p,\,i} T_i = {} & m_{fresh\ mixture,\,i} C_{p\ fresh\ mixture,\,i} T_{fresh\ mixture,\,i} + \\ & + m_{combustion\ products,\,i} C_{p\ combustion\ products,\,i} T_{combustion\ products,\,i} \end{aligned} \tag{7.17}$$

where $T_i$ is the averaged in-cylinder temperature obtained from Eq. 7.12, while $T_{fresh\ mixture,\,i}$ and $T_{combustion\ products,\,i}$ represent the mean temperature of fresh mixture and combustion products, respectively.

Finally, the heat release rate, $HRR$, can be calculated directly from the energy equation as follows:

$$HRR_{i+1} = \frac{C_{v,\,i}}{R} V_i \frac{dP}{dt}_{i} + \frac{C_{p,\,i}}{R} P_i \frac{dV}{dt}_{i} - \dot{Q}_{lost,\,i} \tag{7.18}$$

where the pressure and volume time derivatives are calculated as $\Delta P/\Delta t$ and $\Delta V/\Delta t$, respectively, and the heat losses, $\dot{Q}_{lost,\,i}$, are obtained as explained above. Once the heat release rate is obtained, the accumulated heat release is easily calculated by a numeral integration: $Q_{accumulated,\,i+1} = Q_{accumulated,\,i} + HRR_i \Delta t$. Furthermore, the combustion efficiency is defined as $\eta_{comb} = max(Q_{accumulated})/(m_{fuel} LHV)$.

Fig. 7.19 shows the heat release rate (solid line) and the accumulated heat release (dashed line) for an experiment fueled with PRF25 under the following conditions: $T_0$=363 $K$, $P_0$=1.5 $bar$, $CR$=14 and $F_r$=0.4. The values of the constants that characterize the deformation model and the heat losses model can be also seen in the figure, as well as the resulting combustion efficiency. Finally, the heat release rate under motoring conditions is plotted in red color. It can be seen that it is almost null or negligible if it is compared to the heat release rate with combustion (blue), which is an indicator of the accuracy of the fitting procedure performed to determine the characteristic constants $K$ and $C_{11}$ that define the models.

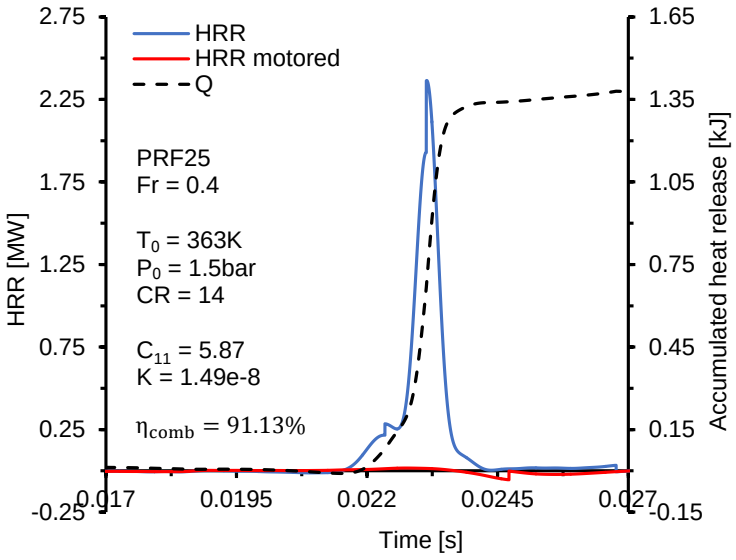


***Figure 7.19.*** *Heat release rate obtained with the post-processing routine for PRF25 and under motoring conditions.*

# References

[1] Versteeg Henk Kaarle and Malalasekera Weeratunge. *An Introduction to Computational Fluid Dynamics: The Finite Volume Method*. Pearson Education, 2007.

[2] Flórez-Orrego D., Arias W., López D. and Vel'asquez H. "Experimental and CFD study of a single phase cone-shaped helical coiled heat exchanger: an empirical correlation". *Proceedings of ECOS 2012 - The 25th International Confereence on Efficiency, Cost, Optimization, Simulation and Environmental Impact of Energy Systems*, 2012.

[3] Gordon S. and McBride B. J. "Computer program for calculation of complex chemical equilibrium compositions, rocket performance, incident and reflected shocks and Chapman-Jouguet detonations". *NASA Report*, Vol. SP-273, 1971.

[4] Several Authors. "NIST Chemistry WebBook". *http://webbook.nist.gov/chemistry*, 2016.

[5] Woschni G. "A universally applicable equation for the instantaneous heat transfer coefficient in the internal combustion engine". *SAE Technical Papers 670931*, 1967.

[6] Payri F., Molina S., Martín J. and Armas O. "Influence of measurement errors and estimated parameters on combustion diagnosis". *Applied Thermal Engineering*, Vol. 26, pp. 226–236, 2006.

# References


**Allen Casey, Toulson Elisa, Edwards Tim and Lee Tonghun**.
Application of a novel charge preparation approach to testing the autoignition characteristics of JP-8 and camelina hydroprocessed renewable jet fuel in a rapid compression machine.
*Combustion and Flame*, Vol. 159, pp. 2780–2788, 2012. (cited on p. 58)

**Allen Casey, Valco Daniel, Toulson Elisa, Yoo Ji Hyung and Lee Tonghun**.
JP-5 and HRJ-5 Autoignition Characteristics and Surrogate Modeling.
*Energy & Fuels*, Vol. 27, pp. 7790–7799, 2013. (cited on p. 54)

**Anderlohr J.M., Piperel A., Pires da Cruz A., Bounaceur R., Battin-Leclerc F., Dagaut P. and Montagne X.**
Influence of EGR compounds on the oxidation of an HCCI-diesel surrogate.
*Proceedings of the Combustion Institute*, Vol. 32, pp. 2851–2859, 2009.
(cited on pp. 106, 147)

**Asad Usman, Tjong Jimi and Zheng Ming**.
Exhaust gas recirculation - Zero dimensional modelling and characterization for transient diesel combustion control.
*Energy Conversion and Management*, Vol. 86, pp. 309–324, 2014. (cited on p. 14)

**Augusta R., Foster D. E., Ghandhi J. B., Eng J. and Najt P. M.**
Chemiluminescence measurements of homogeneous charge compression ignition (HCCI) combustion.
*SAE Technical Papers 2006-01-1520*, 2006. (cited on pp. 56, 76)

**Babajimopoulos A., Lavoie G. A. and Assanis D. N.**
Modeling HCCI combustion with high levels of residual gas fraction. A comparison of two VVA strategies.
*SAE Technical Papers 2003-01-3220*, 2003. (cited on p. 60)

**Baert R. S. G., Frijters P. J. M., Somers B., Luijten C. C. M. and de Boer W.**
Design and operation of a high pressure, high temperature cell for HD Diesel spray diagnostics: Guidelines and results.
*SAE Technical Papers 2009-01-0649*, 2009. (cited on p. 41)

**Baeuerle B., Warnatz J. and Behrendt F.**
Time-resolved investigation of hot spots in the end gas of an S.I. engine by means of 2-D double-pulse LIF of formaldehyde.
*Symposium (International) on Combustion*, Vol. 2, pp. 2619–2626, 1996.
(cited on pp. 21, 174)

**Bahlouli Keyvan, Atikol Ugur, Khoshbakhti Saray R. and Mohammadi Vahid**.
A reduced mechanism for predicting the ignition timing of a fuel blend of natural-gas and n-heptane in HCCI engine.
*Energy Conversion and Management*, Vol. 79, pp. 85–96, 2014. (cited on pp. 5, 14)

**Bamford C. H., Compton R. G. and Tipper C. F. H.**
*The Formation and Decay of Excited Species*.
Elsevier Science, 1st edition, 1969. (cited on pp. 114, 141)

**Bansal G. and Im H.G.**
Autoignition and front propagation in low temperature combustion engine environments.
*Combustion and Flame*, Vol. 158, pp. 2105–2112, 2011. (cited on p. 55)

**Bardi Michele, Payri Raul, Malbec Louis Marie, Bruneaux Gilles, Pickett Lyle M., Manin Julien, Bazyn Tim and Genzale Caroline L.**
Engine combustion network: comparison of spray development, vaporization, and combustion in different combustion vessels.
*Atomization and Sprays*, Vol. 22, 2012. (cited on p. 41)

**Barroso G., Escher A. and Boulouchos K.**
Experimental and numerical investigations on HCCI-combustion.
*SAE Technical Papers 2005-24-038*, 2005. (cited on pp. 49, 93)

**Baumgardner M. E., Sarathy S. M. and Marchese A. J.**
Autoignition characterization of Primary Reference Fuels and n-heptane/n-butanol mixtures in a constant volume combustion device and Homogeneous Charge Compression Ignition engine.
*Energy and Fuels*, Vol. 27, pp. 7778–7789, 2013.

**Benajes J., Olmeda P., Martín J. and Carreño R.**
A new methodology for uncertainties characterization in combustion diagnosis and thermodynamic modelling.
*Applied Thermal Engineering*, Vol. 71, pp. 389–399, 2014.

**Benajes J., Pastor J. V., García A. and Monsalve-Serrano J.**
An experimental investigation on the influence of piston bowl geometry on RCCI performance and emissions in a heavy-duty engine.
*Energy Conversion and Management*, Vol. 103, pp. 1019–1030, 2015. (cited on p. 5)

**Bendu H. and Murugan S.**
Homogeneous charge compression ignition (HCCI) combustion: Mixture preparation and control strategies in diesel engines.
*Renewable and Sustainable Energy Reviews*, Vol. 38, pp. 732–746, 2012. (cited on p. 4)

**Bessonette P.W., Schleyer C.H., Duffy K.P., Hardy W.L. and Liechty M.P.**
Effects of fuel property changes on heavy-duty HCCI combustion.
*SAE Technical Paper 2007-01-0191*, 2007. (cited on p. 5)

**Blin-Simiand N., Rigny R., Viossat V., Circan S. and Sahetchian K.**
Autoignition of hydrocarbon/air mixtures in a CFR engine: Experimental and modeling study.
*Combustion Science and Technology*, Vol. 88, pp. 329–348, 1993. (cited on pp. 31, 199)

**Blomberg Christopher, Mitakos Dimitrios, Bardi Michele, Boulouchos Konstantinos, Wright Yuri M. and Vandersickel Annelies**.
Extension of the phenomenological 3-Arrhenius auto-ignition model for six surrogate automotive fuels.
*SAE Technical Papers 2016-01-0755*, 2016. (cited on p. 36)

**Bradley D. and Kalghatgi G.T.**
Influence of autoignition delay time characteristics of different fuels on pressure waves and knock in reciprocating engines.
*Combustion and Flame*, Vol. 156, pp. 2307–2318, 2009. (cited on p. 37)

**Bradley D., Lawes M. and Materego M.**
Interpretation of auto-ignition delay times measured in different Rapid Compression Machines.
*25th International Colloquium on the Dynamics of Explosions and Reactive systems*, 2015. (cited on p. 47)

**Bradley D., Morley C., Gu X.J. and Emerson D.R.**
Amplified Pressure Waves During Autoignition: Relevance to CAI Engines.
*SAE Technical Paper 2002-01-2868*, 2002. (cited on p. 54)

**Bradley Derek and Head R.A.**
Engine autoignition: The relationship between octane numbers and autoignition delay times.
*Combustion and Flame*, Vol. 147, pp. 171–184, 2006.

**Bradley J.**
*Shock Waves in Chemistry and Physics*.
Chapman and Hall, London, 1962. (cited on p. 43)

**Burke Ultan, Metcalfe Wayne K., Burke Sinead M., Heufer K. Alexander, Dagaut Philippe and Curran Henry J.**
A detailed chemical kinetic modeling, ignition delay time and jet-stirred reactor study of methanol oxidation.
*Combustion and Flame*, Vol. 165, pp. 125–136, 2016. (cited on p. 44)

**Challen Bernard, Baranescu Rodica and others**.
*Diesel Engine Reference Book*.
Digital Designs. (cited on p. 14)

**Chen J.H., Hawkes E.R., Sankaran R., Mason S.D. and Im H.G.**
Direct numerical simulation of ignition front propagation in a constant volume with temperature inhomogeneities I. Fundamental analysis and diagnostics.
*Combustion and Flame*, Vol. 145, pp. 128–144, 2006. (cited on p. 54)

**Chen L., Li T., Yin T. and Zheng B.**
A predictive model for knock onset in spark-ignition engines with cooled EGR.
*Energy Conversion and Management*, Vol. 87, pp. 946–955, 2014. (cited on p. 35)

**Chen R. and Milovanovic N.**
A computational study into the effect of exhaust gas recycling on homogeneous charge compression ignition combustion in internal combustion engines fuelled with methane.
*International Journal of Thermal Sciences*, Vol. 41, pp. 805–813, 2002. (cited on p. 60)

**Cheng Yu, Hu Erjiang, Deng Fuquan, Yang Feiyu, Zhang Yingjia, Tang Chenglong and Huang Zuohua**.
Experimental and kinetic comparative study on ignition characteristics of 1-pentene and n-pentane.
*Fuel*, Vol. 172, pp. 263–272, 2016.

**Cho Gyubaek, Jeong Dongsoo, Moon Gunfeel and Bae Choongsik**.
Controlled auto-ignition characteristics of methane-air mixture in a Rapid Intake Compression and Expansion Machine.
*Energy*, Vol. 35, pp. 4184–4191, 2010.

**Choi Y. and Chen J.-Y.**
Fast prediction of start-of-combustion in HCCI with combined artificial neural networks and ignition delay model.
*Proceedings of the Combustion Institute*, Vol. 30, pp. 2711–2718, 2005. (cited on p. 37)

**Clarkson J., Griffiths J. F., MacNamara J. P. and Whitaker B. J.**
Temperature fields during the development of combustion in a Rapid Compression Machine.
*Combustion and Flame*, Vol. 125, pp. 1162–1175, 2001. (cited on p. 55)

**Colin Olivier, Pires da Cruz Antonio and Jay Stephane**.
Detailed chemistry-based auto-ignition model including low temperature phenomena applied to 3-D engine calculations.
*Proceedings of the Combustion Institute*, Vol. 30, pp. 2649–2656, 2005. (cited on p. 65)

**Curran H. J., Gaffuri P., Pitz W. J. and Westbrook C. K.**
A comprehensive modeling study of n-heptane oxidation.
*Combustion and Flame*, Vol. 114, pp. 149–177, 1998.
(cited on pp. 19, 24, 31, 71, 114, 121, 140, 157, 161, 174, 206, 231)

**Curran H. J., Gaffuri P., Pitz W. J. and Westbrook C. K.**
A comprehensive modeling study of iso-octane oxidation.
*Combustion and Flame*, Vol. 129, pp. 253–280, 2002. (cited on pp. 19, 121, 206)

**Curran Henry, Simmie John M., Dagaut Philippe, Voisin David and Cathonnet Michel**.
The ignition and oxidation of allene and propyne: Experiments and kinetic modeling.
*Symposium (International) on Combustion*, Vol. 26, pp. 613–620, 1996. (cited on p. 24)

**Curran H.J., Pitz W.J., Westbrook C.K., Callahan C.V. and Dryer F.L.**
Oxidation of automotive primary reference fuels at elevated pressures.
*Symposium (International) on Combustion*, Vol. 37, pp. 379–389, 1999. (cited on p. 155)

**Dagaut P., Reuillon M. and Cathonnet M.**
Experimental study of the oxidation of n-heptane in a jet stirred reactor from low to high temperature and pressures up to 40 atm.
*Combustion and Flame*, Vol. 101, pp. 132–140, 1995. (cited on p. 52)

**Dagaut Philippe, Reuillon Marcelline and Cathonnet Michel**.
Experimental study of the oxidation of n-heptane in a jet stirred reactor from low to high temperature and pressures up to 40 atm.
*Combustion and Flame*, Vol. 101, pp. 132–140, 1995. (cited on pp. 22, 24)

**Darcy D., Nakamura H., Tobin C.J., Mehl M., Metcalfe W.K., Pitz W.J., Westbrook C.K. and Curran H.J.**
A high-pressure Rapid Compression Machine study of n-propylbenzene ignition.
*Combustion and Flame*, Vol. 161, pp. 65–74, 2014. (cited on pp. 33, 45)

**Davidson D. F., Gauthier B. M. and Hanson R. K.**
Shock tube ignition measurements of iso-octane/air and toluene/air at high pressures.
*Proceedings of the Combustion Institute*, Vol. 30, pp. 1175–1182, 2005. (cited on p. 42)

**Davidson D. F. and Hanson R. K.**
Interpreting shock tube ignition data.
*International Journal of Chemical Kinetics*, Vol. 36, pp. 510–523, 2004. (cited on p. 42)

**Dec John E.**
A computational study of the effects of low fuel loading and EGR on heat release rates and combustion limits in HCCI engines.
*SAE Technical Papers 2002-01-1309*, 2002. (cited on pp. 38, 60)

**Dec John E. and Sjöberg Magnus**.
Isolating the effects of fuel chemistry on combustion phasing in an HCCI engine and the potential of fuel stratification for ignition control.
*SAE Technical Papers 2004-01-0557*, 2004. (cited on p. 67)

**Dernotte J., Dec J. and Ji C.**
Investigation of the Sources of Combustion Noise in HCCI Engines.
*SAE Technical Paper 2014-01-1272*, 2014. (cited on p. 54)

**Desantes J.M., Arregle J., Molina S. and Lejeune M.**
Influence of the EGR rate, oxygen concentration and equivalent fuel/air ratio on the combustion behavior and pollutant emissions of a heavy-duty diesel engine.
*SAE Technical Paper 2000-01-1813*, 2000. (cited on p. 228)

**Desantes J.M., López J.J., Redón P. and Arrégle J.**
Evaluation of the thermal NO formation mechanism under low temperature diesel combustion conditions.
*International Journal of Engine Research*, Vol. 13, pp. 531–539, 2012. (cited on p. 3)

**Desantes José M., Bermúdez Vicente, López J. Javier and López-Pintor Darío**.
Experimental validation of an alternative method to predict high and low-temperature ignition delays under transient thermodynamic conditions for PRF mixtures using a Rapid Compression-Expansion Machine.
*Energy Conversion and Management*, Vol. 129, pp. 23–33, 2016.

**Desantes José M., Bermúdez Vicente, López J. Javier and López-Pintor Darío**.
A new method to predict high and low-temperature ignition delays under transient thermodynamic conditions and its experimental validation using a Rapid Compression-Expansion Machine.
*Energy Conversion and Management*, Vol. 123, pp. 512–522, 2016. (cited on p. 202)

**Desantes José M., Bermúdez Vicente, López J. Javier and López-Pintor Darío**.
Correlations for the ignition characteristics of six different fuels and their application to predict ignition delays under transient thermodynamic conditions.
*Energy Conversion and Management, in press*, 2017. (cited on p. 258)

**Desantes José M., Bermúdez Vicente, López J. Javier and López-Pintor Darío**.
Sensitivity analysis and validation of a predictive procedure for high and low-temperature ignition delays under engine conditions for n-dodecane using a Rapid Compression-Expansion Machine.
*Energy Conversion and Management*, Vol. 145, pp. 64–81, 2017. (cited on p. 258)

**Desantes José M., García-Oliver José M., Vera-Tudela Walter, López-Pintor Darío, Schneider Bruno and Boulouchos Konstantinos**.
Study of ignition delay time and generalization of auto-ignition for PRFs in an RCEM by means of natural chemiluminescence.
*Energy Conversion and Management*, Vol. 111, pp. 217–228, 2016.
(cited on pp. 196, 214)

**Desantes José M., García-Oliver José M., Vera-Tudela Walter, López-Pintor Darío, Schneider Bruno and Boulouchos Konstantinos**.
Study of the auto-ignition phenomenon of PRFs under HCCI conditions in an RCEM by means of spectroscopy.
*Applied Energy*, Vol. 179, pp. 389–400, 2016.

**Desantes José M., López J. Javier, García-Oliver José M. and López-Pintor Darío**.
A 5-zone model to improve the diagnosis capabilities of a Rapid Compression-Expansion Machine (RCEM) in autoignition studies.
*SAE Technical Paper 2017-01-0730*, 2017. (cited on p. 257)

**Desantes José M., López J. Javier, García-Oliver José M. and López-Pintor Darío**.
A phenomenological explanation on the autoignition propagation under HCCI conditions.
*Fuel*, Vol. 206, pp. 43–57, 2017. (cited on p. 228)

**Desantes José M., López J. Javier, Molina Santiago and López-Pintor Darío**.
Design of synthetic EGR and simulation study of the effect of simplified formulations on the ignition delay of isooctane and n-heptane.
*Energy Conversion and Management*, Vol. 96, pp. 521–531, 2015. (cited on p. 147)

**Desantes José M., López J. Javier, Molina Santiago and López-Pintor Darío**.
Validity of the Livengood & Wu correlation and theoretical development of an alternative procedure to predict ignition delays under variable thermodynamic conditions.
*Energy Conversion and Management*, Vol. 105, pp. 836–847, 2015.
(cited on pp. 164, 179)

**Desantes José M., López J. Javier, Molina Santiago and López-Pintor Darío**.
Theoretical development of a new procedure to predict ignition delays under transient thermodynamic conditions and validation using a Rapid Compression-Expansion Machine.
*Energy Conversion and Management*, Vol. 108, pp. 132–143, 2016.

**Di Haisheng, He Xin, Zhang Peng, Wang Zhi, Wooldridge Margaret S., Law Chung K., Wang Cuiping, Shuai Shijin and Wang Jianxin**.
Effects of buffer gas composition on low temperature ignition of iso-octane and n-heptane.
*Combustion and Flame*, Vol. 161, pp. 2531–2538, 2014. (cited on pp. 61, 160)

**Doménech Llopis Vicente**.
*Estudio de nuevas estrategias para el control de la combustion en modos parcialmente premezclados en motores de encendido por compresión.*
Doctoral Thesis, 2013. (cited on p. 14)

**Dreizler A., Lindenmaier S., Maas U., Hult J., Aldén M. and Kaminski C. F.**
Characterisation of a spark ignition system by planar laser-induced fluorescence of OH at high repetition rates and comparison with chemical kinetic calculations.
*Applied Physics B*, Vol. 70, pp. 287–294, 2000. (cited on p. 40)

**Dubreuil A., Foucher F. and Mounam-Rousselle C.**
Analysis of flame and OH natural emissions of n-heptane combustion in a Homogeneous Charge Compression Ignition (HCCI) engine: Effect of burnt gas dilution.
*Energy and Fuels*, Vol. 23, pp. 1406–1411, 2009. (cited on pp. 16, 57)

**Edenhofer R., Lucka K. and Kohne H.**
Low temperature oxidation of diesel-air mixtures at atmospheric pressure.
*Proceedings of the Combustion Institute*, Vol. 31, pp. 2947–2954, 2007.
(cited on pp. 38, 74)

**Egusquiza J. C. Cuisano, Braga S. Leal, Braga C. V. Maciel, Villela A. C. Scardini and Moura N. Reis de**.
Experimental investigation of the natural gas / Diesel dual-fuel combustion using a Rapid Compression Machine.
*SAE Technical Papers 2011-36-0360*, 2011. (cited on pp. 45, 50, 93)

**Falk K. George**.
The ignition temperatures of hydrogen-oxygen mixtures.
*Journal of the American Chemical Society*, Vol. 28, pp. 1517 – 1534, 1906.
(cited on p. 45)

**Fathi Morteza, Saray R. Khoshbakhti and Checkel M. David**.
The influence of Exhaust Gas Recirculation (EGR) on combustion and emissions of n-heptane/natural gas fueled Homogeneous Charge Compression Ignition (HCCI) engines.
*Applied Energy*, Vol. 88, pp. 4719–4724, 2011. (cited on pp. 60, 160)

**Flórez-Orrego D., Arias W., López D. and Vel'asquez H.**
Experimental and CFD study of a single phase cone-shaped helical coiled heat exchanger: an empirical correlation.
*Proceedings of ECOS 2012 - The 25th International Confereence on Efficiency, Cost, Optimization, Simulation and Environmental Impact of Energy Systems*, 2012.
(cited on p. 265)

**Floyd R., Kotrba A., Martin S. and Prodin K.**
Material corrosion investigations for urea SCR diesel exhaust systems.
*SAE Technical Paper 2009-01-2883*, 2009. (cited on p. 3)

**Frassoldati A, Faravelli T and Ranzi E**.
Kinetic modeling of the interactions between NO and hydrocarbons at high temperature.
*Combustion and Flame*, Vol. 135, pp. 97–112, 2003.

**Gauthier B.M., Davidson D.F. and Hanson R.K.**
Shock tube determination of ignition delay times in full-blend and surrogate fuel mixtures.
*Combustion and Flame*, Vol. 139, pp. 300–311, 2004. (cited on p. 68)

**Gaydon A. G.**
*The Spectroscopy of Flames.*
Chapman and Hall, 1974. (cited on pp. 97, 110)

**Gaydon Alfred Gordon and Hurle Ian Roy**.
*The shock tube in high-temperature chemical physics.*
Chapman and Hall, 1963. (cited on p. 43)

**Ghojel Jamil I. and Tran Xuan-Thien**.
Ignition Characteristics of Diesel-Water Emulsion Sprays in a Constant-Volume Vessel: Effect of Injection Pressure and Water Content.
*Energy & Fuels*, Vol. 24, pp. 3860–3866, 2010. (cited on p. 40)

**Gibson C., Gray P., Griffiths J. F. and Hasko S. M.**
Spontaneous ignition of hydrocarbon and related fuels: A fundamental study of thermokinetic interactions.
*Symposium (International) on Combustion*, Vol. 20, pp. 101–109, 1985. (cited on p. 21)

**Glarborg P. and Bentzen L. L. B.**
Chemical effects of high CO2 concentration in oxy-fuel combustion of methane.
*Energy and Fuels*, Vol. 22, pp. 291–296, 2008.

**Glassman Irvin**.
*Combustion*.
Academic Press, Orlando [Fla.], 2nd ed edition, 1987. (cited on pp. 15, 164, 172, 190)

**Goldsborough S. Scott**.
A crevice blow-by model for a Rapid Compression Expansion Machine used for chemical kinetic (HCCI) studies.
*SAE Technical Papers 2007-01-1052*, 2007. (cited on p. 58)

**Gordon S. and McBride B. J.**
Computer program for calculation of complex chemical equilibrium compositions, rocket performance, incident and reflected shocks and Chapman-Jouguet detonations.
*NASA Report*, Vol. SP-273, 1971. (cited on pp. 272, 287)

**Gray Jeffrey A. and Westbrook Charles K.**
High-temperature ignition of propane with MTBE as an additive: Shock tube experiments and modeling.
*International Journal of Chemical Kinetics*, Vol. 26, pp. 757–770, 1994. (cited on p. 32)

**Gu X. J., Haq M. Z., Lawes M. and Woolley R.**
Laminar burning velocity and Markstein lengths of methane-air mixtures.
*Combustion and Flame*, Vol. 121, pp. 41–58, 2000. (cited on p. 40)

**Gu X.J., Emerson D.R. and Bradley D.**
Modes of reaction front propagation from hot spots.
*Combustion and Flame*, Vol. 133, pp. 63–74, 2003. (cited on p. 54)

**Gupta Sreenath and Singh Gurpreet**.
Rapid Compression Machine - A key experimental device to dffectively collaborate with basic energy sciences.
*ACE 2011 Program Review, Washington D.C., USA*, 2011. (cited on p. 45)

**Hall J. M. and Petersen E. L.**
An optimized kinetics model for OH chemiluminescence at high temperatures and atmospheric pressures.
*International Journal of Chemical Kinetics*, Vol. 38, pp. 714–724, 2006.
(cited on pp. 114, 141)

**Han Dong, Guang Huanyu, Yang Zheng, Lu Xingcai and Huang Zhen**.
Premixed ignition characteristics of blends of gasoline and diesel-like fuels on a Rapid Compression Machine.
*Thermal Science*, Vol. 17, pp. 1–10, 2013.

**Hanson R.K.**
Quantitative laser diagnostics for combustion chemistry and propulsion: Shock tube techniques and applications.
*Princeton, New Jersey, USA*, 2015. (cited on pp. 43, 44)

**Herbinet Olivier, Husson Benoit, Serinyel Zeynep, Cord Maximilien, Warth Valérie, Fournet René, Glaude Pierre-Alexandre, Sirjean Baptiste, Battin-Leclerc Frédérique, Wang Zhandong, Xie Mingfeng, Cheng Zhanjun and Qi Fei**.
Experimental and modeling investigation of the low-temperature oxidation of n-heptane.
*Combustion and Flame*, Vol. 159, pp. 3455–3471, 2012. (cited on p. 19)

**Hernandéz J. J., Lapuerta M. and Sanz-Argent J.**
Autoignition prediction capability of the Livengood-Wu correlation applied to fuels of commercial interest.
*International Journal of Engine Research*, Vol. 15, pp. 817–829, 2014. (cited on p. 38)

**Hernández J. J., Sanz-Argent J., Carot J. M. and Jabaloyes J. M.**
Ignition delay time correlations for a diesel fuel with application to engine combustion modelling.
*International Journal of Engine Research*, Vol. 11, pp. 199–206, 2010. (cited on p. 36)

**Herzler J. and Naumann C.**
Shock tube study of the influence of NOx on the ignition delay times of natural gas at high pressure.
*Combustion Science and Technology*, Vol. 184, pp. 1635–1650, 2012.
(cited on pp. 60, 158)

**Heufer K. A., Bugler J. and Curran H. J.**
A comparison of longer alkane and alcohol ignition including new experimental results for n-pentanol and n-hexanol.
*Proceedings of the Combustion Institute*, Vol. 34, pp. 511–518, 2013.
(cited on pp. 45, 62)

**Heywood John B.**
*Internal combustion engine fundamentals.*
McGraw-Hill series in mechanical engineering. McGraw-Hill, New York, 1988.
(cited on pp. 1, 230)

**Higgins Brian, Siebers Dennis L. and Aradi Allen**.
Diesel-spray ignition and premixed-burn behavior.
*SAE Technical Papers 2000-01-0940*, 2000. (cited on p. 40)

**Hillion M., Chauvin J. and Petit N.**
Control of highly diluted combustion in Diesel engines.
*Control Engineering Practice*, Vol. 19, pp. 1274–1286, 2011. (cited on p. 37)

**Hoepke Bjoern, Jannsen Stefan, Kasseris Emmanuel and Cheng Wai K.**
EGR effects on boosted SI engine operation and knock integral correlation.
*SAE Technical Papers 2012-01-0707*, 2012. (cited on pp. 36, 38)

**Hwang W., Dec J. and Sjöberg M.**
Spectroscopic and chemical-kinetic analysis of the phases of HCCI autoignition and combustion for single- and two-stage ignition fuels.
*Combustion and Flame*, Vol. 154, pp. 387–409, 2008. (cited on pp. 55, 57)

**Ihme Matthias**.
Reconcile discrepancies of current syngas kinetics models by considering turbulence effects on ignition delay at gas-turbine relevant operating conditions.
*49th AIAA Aerospace Sciences Meeting including the New Horizons Forum and Aerospace Exposition*, 2011. (cited on p. 55)

**Iijima A. and Shoji H.**
A spectroscopic analysis of combustion in Homogeneous Charge Compression Ignition engine.
*ASME-JSME Thermal Engineering Summer Heat Transfer Conference*, Vol. HT2007-32552, 2007. (cited on p. 56)

**Imamori Y., Endo H., Sakaguchi K. and Yanagi J.**
Development of combustion system in low speed two-stroke diesel engine using CFD.
*International Council on Combustion Engines*, 2004. (cited on p. 37)

**Jerzembeck S., Petersa N., Pepiot-Desjardins P. and Pitsch H.**
Laminar burning velocities at high pressure for primary reference fuels and gasoline: Experimental and numerical investigation.
*Combustion and flame*, Vol. 156, pp. 292–301, 2009. (cited on p. 116)

**Kee Robert J., Dixon-Lewis Graham, Warnatz Jurgen, Coltrin Michael E., Miller James A. and Moffat Harry K.**
A FORTRAN computer code package for the evaluation of gas-phase, multicomponent transport properties.
*Sandia National Laboratories Report*, Vol. SAND86-8246B, 1998.

**Kee Robert J., Rupley Fran M., Meeks Ellen and Miller James A.**
CHEMKIN-III: A FORTRAN chemical kinetics package for the analysis of gas phase chemical and plasma kinetics.
*Sandia National Laboratories Report*, Vol. UC-405 SAND96-8216, 1996. (cited on p. 70)

**Kim B., Kaneko M., Ikeda Y. and Nakajima T.**
Detailed spectral analysis of the process of HCCI combustion.
*Proceedings of the Combustion Institute*, Vol. 29, pp. 671–677, 2002. (cited on p. 56)

**Kobashi Y., Tanaka D., Maruko T. and Kato S.**
Effects of mixedness and ignition timings on PCCI combustion with a dual fuel operation.
*SAE Technical Papers 2011-01-1768*, 2011. (cited on p. 38)

**Koert David N., Pit William J., Boelli Joseph W. and Cernansky Nicholas P.**
Chemical kinetic modeling of high-pressure propane oxidation and comparison to experimental results.
*Symposium (International) on Combustion*, Vol. 26, pp. 633–640, 1996. (cited on p. 21)

**Krehl Peter O. K.**
*History of Shock Waves, Explosions and Impact: A Chronological and Biographical Reference.*
Springer Science & Business Media, 2008. (cited on p. 42)

**Krishnan Sundar Rajan, Srinivasan Kalyan Kumar and Stegmeir Matthew**.
Characterization of Diesel and Gasoline Compression Ignition Combustion in a Rapid Compression-Expansion Machine using OH* Chemiluminescence Imaging.
*Bulletin of the American Physical Society*, Vol. 60, 2015. (cited on p. 50)

Kuhl A. L., editor.
*Dynamics of reactive systems.*
Progress in astronautics and aeronautics. American Institute of Aeronautics and Astronautics, Washington, DC, 1988. (cited on p. 15)

**Kukkadapu Goutham, Kumar Kamal, Sung Chih-Jen, Mehl Marco and Pitz William J.**
Experimental and surrogate modeling study of gasoline ignition in a Rapid Compression Machine.
*Combustion and Flame*, Vol. 159, pp. 3066–3078, 2012. (cited on p. 26)

**Kukkadapu Goutham, Kumar Kamal, Sung Chih-Jen, Mehl Marco and Pitz William J.**
Autoignition of gasoline and its surrogates in a Rapid Compression Machine.
*Proceedings of the Combustion Institute*, Vol. 34, pp. 345–352, 2013. (cited on p. 39)

**Kumar Kamal, Mittal Gaurav and Sung Chih-Jen**.
Autoignition of n-decane under elevated pressure and low-to-intermediate temperature conditions.
*Combustion and Flame*, Vol. 156, pp. 1278–1288, 2009.
(cited on pp. 16, 27, 32, 198, 201)

**Kumar Kamal and Sung Chih-Jen**.
An experimental study of the autoignition characteristics of conventional jet fuel-oxidizer mixtures: Jet-A and JP-8.
*Combustion and Flame*, Vol. 157, pp. 676–685, 2010.

**Lü Xing-Cai, Chen Wei and Huang Zhen**.
A fundamental study on the control of the HCCI combustion and emissions by fuel design concept combined with controllable EGR. Part 1. The basic characteristics of HCCI combustion.
*Fuel*, Vol. 84, pp. 1074–1083, 2005. (cited on pp. 16, 200)

**Lü Xing-Cai, Chen Wei and Huang Zhen**.
A fundamental study on the control of the HCCI combustion and emissions by fuel design concept combined with controllable EGR. Part 2. Effect of operating conditions and EGR on HCCI combustion.
*Fuel*, Vol. 84, pp. 1084–1092, 2005. (cited on pp. 157, 190)

**Ladommatos N., Abdelhalim S., Zhao H. and Hu Z.**
The dilution, chemical, and thermal effects of Exhaust Gas Recirculation on Diesel engine emissions - Part 1: Effect of reducing inlet charge oxygen.
*SAE Technical Papers 961165*, 1996. (cited on p. 59)

**Ladommatos N., Abdelhalim S., Zhao H. and Hu Z.**
The dilution, chemical, and thermal effects of Exhaust Gas Recirculation on Diesel engine emissions - Part 2: Effects of carbon dioxide.
*SAE Technical Papers 961167*, 1996.

**Ladommatos N., Abdelhalim S., Zhao H. and Hu Z.**
The dilution, chemical, and thermal effects of Exhaust Gas Recirculation on Disesel engine emissions - Part 4: Effects of carbon dioxide and water vapour.
*SAE Technical Papers 971660*, 1997.

**Ladommatos N., Abdelhalim S., Zhao H. and Hu Z.**
The dilution, chemical, and thermalt effects of Exhaust Gas Recirculation on Diesel engine emissions - Part 3: Effects of water vapour.
*SAE Technical Papers 971659*, 1997.

**Lapuerta Magín, Sanz-Argent Josep and Raine Robert**.
Heat release determination in a constant volume combustion chamber from the instantaneous cylinder pressure.
*Applied Thermal Engineering*, Vol. 63, pp. 520–527, 2014. (cited on p. 40)

**Lapuerta Magín, Sanz-Argent Josep and Raine Robert R.**
Ignition Characteristics of Diesel Fuel in a Constant Volume Bomb under Diesel-Like Conditions. Effect of the Operation Parameters.
*Energy & Fuels*, Vol. 28, pp. 5445–5454, 2014. (cited on p. 40)

**Le Cong T. and Dagaut P.**
Experimental and detailed kinetic modeling of the oxidation of natural gas, natural gas/syngas mixtures, and effect of burnt gas recirculation.
*Proceedings of the European Combustion Meeting, July 23-27, 2007, Poitiers, France.* (cited on p. 60)

**Lee Changyoul, Vranckx Stijn, Heufer Karl A., Khomik Sergey V., Uygun Yasar, Olivier Herbert and Fernandez Ravi X.**
On the chemical kinetics of ethanol oxidation: Shock tube, Rapid Compression Machine and detailed modeling study.
*Zeitschrift für Physikalische Chemie*, Vol. 226, pp. 1–28, 2012. (cited on p. 47)

**Lee Daeyup and Hochgreb Simone**.
Rapid Compression Machines: Heat transfer and suppression of corner vortex.
*Combustion and Flame*, Vol. 114, pp. 531–545, 1998. (cited on p. 46)

**Lezanski T., Seczyk J. and Wolanski P.**
Design of the rapid compression machines for combustion researches in spark ignition engines.
*Journal of KONES*, Vol. 19, pp. 379–391, 2012. (cited on pp. 45, 53)

**Li G., Bo T., Chen C. and Johns R.**
CFD simulation of HCCI combustion in a 2-stroke DI gasoline engine.
*SAE Technical Papers 2003-01-1855*, 2003. (cited on p. 52)

**Li G., Bo T., Chen C. and Johns R.J.R.**
CFD Simulation of HCCI Combustion in a 2-Stroke DI Gasoline Engine.
*SAE Technical Papers 2003-01-1855*, 2003. (cited on p. 37)

**Li T., Wu D. and Xu M.**
Thermodynamic analysis of EGR effects on the first and second law efficiencies of a boosted spark-ignited direct-injection gasoline engine.
*Energy Conversion and Management*, Vol. 70, pp. 130–138, 2013. (cited on pp. 3, 14)

**Liang Long and Reitz Rolf D.**
Spark ignition engine combustion modeling using a level set method with detailed chemistry.
*SAE Technical Papers 2006-01-0243*, pág. 0243, 2006. (cited on pp. 38, 74)

**Liu H. F., Yao M. F., Jin C., Zhang P., Li Z. M. and Zheng Z.Q.**
Chemiluminescence spectroscopic analysis of homogeneous charge compression ignition combustion processes.
*Spectroscopy and Spectral Analysis*, Vol. 30, pp. 2611–2615, 2010. (cited on pp. 56, 76)

**Liu Hao, Zhang Hongguang, Shi Zhicheng, Lu Haitao, Zhao Guangyao and Yao Baofeng**.
Performance characterization and auto-ignition performance of a Rapid Compression Machine.
*Energies*, Vol. 7, pp. 6083–6104, 2014. (cited on p. 45)

**Liu Y., Li L., Ye J., Deng J. and Wu Z.**
Ion current signal and characteristics of ethanol/gasoline dual fuel HCCI combustion.
*Fuel*, Vol. 166, pp. 42–50, 2016. (cited on p. 54)

**Livengood J. C. and Wu P. C.**
Correlation of autoignition phenomena in internal combustion engines and rapid compression machines.
*Symposium (International) on Combustion*, Vol. 5, pp. 347–356, 1955.
(cited on pp. 6, 33, 74, 164, 170, 177)

**Lopez J.J., Novella R., Garcia A. and Winklinger J.F.**
Investigation of the ignition and combustion processes of a dual-fuel spray under diesel-like conditions using computational fluid dynamics (CFD) modeling.
*Mathematical and Computer Modelling*, Vol. 57, pp. 1897–1906, 2013. (cited on p. 65)

**Lu T. and Law C.K.**
Linear time reduction of large kinetic mechanisms with directed relation graph: n-neptane and iso-octane.
*Combustion and Flame*, Vol. 144, pp. 24–36, 2006. (cited on p. 71)

**Lunt S. T., Marston G. and Wayne R. P.**
Formation of $O_2(a^1\Delta_g)$ and vibrational excited OH in the reaction between O atoms and $HO_x$ species.
*Journal of the Chemical Society, Faraday Transactions 2: Molecular and Chemical Physics*, Vol. 84(7), pp. 899–912, 1988. (cited on p. 141)

**Machrafi Hatim**.
Experimental validation of a kinetic multi-component mechanism in a wide HCCI engine operating range for mixtures of n-heptane, iso-octane and toluene: Influence of EGR parameters.
*Energy Conversion and Management*, Vol. 49, pp. 2956–2965, 2008.

**Manasra Salih and Brueggemann Dieter**.
Effect of injection pressure and timing on the in-cylinder soot formation characteristics of low CR neat GTL-fueled DI Diesel engine.
*SAE Technical Papers 2011-01-2464*, 2011. (cited on pp. 49, 93)

**Mancaruso E. and Vaglieco B. M.**
Optical investigation of the combustion behaviour inside the engine operating in HCCI mode and using alternative diesel fuel.
*Experimental Thermal and Fluid Science*, Vol. 34, pp. 346–351, 2010. (cited on p. 56)

**Mancaruso E. and Vaglieco B. M.**
Spectroscopic measurements of premixed combustion in diesel engine.
*Fuel*, Vol. 90, pp. 511–520, 2011. (cited on p. 56)

**Mastorakos Epaminondas**.
Ignition of turbulent non-premixed flames.
*Progress in Energy and Combustion Science*, Vol. 35, pp. 57–97, 2009.
(cited on pp. 16, 102)

**Mehl Marco, Pitz William J., Westbrook Charles K. and Curran Henry J.**
Kinetic modeling of gasoline surrogate components and mixtures under engine conditions.
*Proceedings of the Combustion Institute*, Vol. 33, pp. 193–200, 2011.
(cited on pp. 24, 70)

**Meijer Maarten, Somers Bart, Johnson Jaclyn, Naber Jeffrey, Lee Seong-Young, Malbec Louis Marie, Bruneaux Gilles, Pickett Lyle M., Bardi Michele, Payri Raul and Bazyn Tim**.
Engine Combustion Network (ECN): Characterization and comparison of boundary conditions for different combustion vessels.
*Atomization and Sprays*, Vol. 22, pp. 777–806, 2012. (cited on pp. 40, 52)

**Metghalchi M. and Keck J.C.**
Burning Velocities of Mixtures of Air with Methanol, Isooctane, and Indolene at High Pressure and Temperature.
*Combustion and Flame*, Vol. 48, pp. 191–210, 1982. (cited on p. 230)

**Milovanovic N. and Chen R.**
A review of experimental and simulation studies on Controlled Auto-Ignition Combustion.
*SAE Technical Paper 2001-01-1890*, 2001. (cited on p. 4)

**Mitakos D., Blomberg C., Vandersickel A., Wright Y., Schneider B. and Boulouchos K.**
Ignition delays of different homogeneous fuel-air mixtures in a Rapid Compression Expansion Machine and comparison with a 3-stage-ignition model parametrized on shock tube data.
*SAE Technical Papers 2013-01-2625*, 2013. (cited on pp. 58, 67, 136)

**Mitakos Dimitrios Angelos, Blomberg Christopher, Wright Yuri M., Obrecht Peter, Schneider Bruno and Boulouchos Konstantinos**.
Integration of a cool-flame heat release rate model into a 3-stage ignition model for HCCI applications and different fuels.
*SAE Technical Papers 2014-01-1268*, 2014. (cited on pp. 50, 93)

**Mittal Gaurav**.
*A Rapid Compression Machine design, characterization, and autoignition investigations.*
Doctoral Thesis, Case Western Reserve University, 2006. (cited on p. 196)

**Mittal Gaurav, Chaos Marcos, Sung Chih-Jen and Dryer Frederick L.**
Dimethyl ether autoignition in a Rapid Compression Machine: Experiments and chemical kinetic modeling.
*Fuel Processing Technology*, Vol. 89, pp. 1244–1254, 2008.

**Mittal Gaurav and Chomier Mickael**.
Effect of crevice mass transfer in a Rapid Compression Machine.
*Combustion and Flame*, Vol. 161, pp. 398–404, 2014. (cited on pp. 46, 54)

**Mittal Gaurav and Chomier Mickael**.
Interpretation of experimental data from Rapid Compression Machines without creviced pistons.
*Combustion and Flame*, Vol. 161, pp. 75–83, 2014. (cited on p. 46)

**Mittal Gaurav, Davies Varun Anthony and Parajuli Bikash**.
Autoignition of ethanol in a Rapid Compression Machine.
*8th U.S. National Combustion Meeting - Western States Section of the Combustion Institute*, Vol. Paper 070RK-0222, 2013. (cited on p. 53)

**Mittal Gaurav and Sung Chih-Jen**.
A Rapid Compression Machine for chemical kinetics studies at elevated pressures and temperatures.
*Combustion Science and Technology*, Vol. 179, pp. 497–530, 2007. (cited on p. 53)

**Müller U. C., Peters N. and Liñán A.**
Global kinetics for n-heptane ignition at high pressures.
*Twenty-Fourth Symposium (International) on Combustion-The Combustion Institute*, pp. 777–784, 1992. (cited on pp. 19, 169, 190)

**Munsin Ronnachart, Laoonual Yossapong, Jugjai Sumrerng, Matsuki Masataka and Kosaka Hidenori**.
Investigation of effects of ignition improvers on ignition delay time of ethanol combustion with Rapid Compression and Expansion Machine.
*SAE Technical Papers 2012-01-0854*, 2012. (cited on p. 39)

**Murase E., Hanada K., Miyaura T. and Ikeda J.**
Photographic observation and emission spectral analysis of Homogeneous Charge Compression Ignition combustion.
*Combustion Science and Technology*, Vol. 177, pp. 1699–1723, 2005. (cited on p. 57)

**Nakamura Hisashi, Darcy Daniel, Mehl Marco, Tobin Colin J., Metcalfe Wayne K., Pitz William J., Westbrook Charles K. and Curran Henry J.**
An experimental and modeling study of shock tube and rapid compression machine ignition of n-butylbenzene/air mixtures.
*Combustion and Flame*, Vol. 161, pp. 49–64, 2014. (cited on pp. 44, 53)

**Narayanaswamy K., Pepiot P. and Pitsch H.**
A chemical mechanism for low to high temperature oxidation of n-dodecane as a component of transportation fuel surrogates.
*Combustion and Flame*, Vol. 161, pp. 866–884, 2014. (cited on p. 114)

**Neuman John**.
*Development of a Rapid Compression Controlled-Expansion Machine for chemical ignition studies.*
Doctoral Thesis, University of Wisconsin, 2015. (cited on p. 45)

**Nicolas Ghassan and Metghalchi Hameed**.
Comparison between RCCE and shock tube ignition delay times at low temperatures.
*Journal of Energy Resources Technology*, Vol. 137, pp. 062203–062203, 2015. (cited on pp. 44, 53)

**Novella R., Garcia A., Pastor J. M. and Domenech V.**
The role of detailed chemical kinetics on CFD diesel spray ignition and combustion modelling.
*Mathematical and Computer Modelling*, Vol. 54, pp. 1706–1719, 2011.

**Ohyama Y.**
Engine control using a combustion model.
*Seoul 2000 FISITA World Automotive Congress*, 2000. (cited on p. 37)

**Onishi S., Jo S. H., Shoda K., Jo P. D. and Kato S.**
Active thermo-atmosphere combustion (ATAC) - A new combustion process for internal combustion engines.
*SAE Technical Papers 790501*, 1979. (cited on p. 16)

**Pastor J. V., García-Oliver J. M., García A., Micó C. and Durrett R.**
A spectroscopy study of gasoline partially premixed compression ignition spark assisted combustion.
*Applied Energy*, Vol. 104, pp. 568–575, 2013. (cited on p. 23)

**Payri F. and Desantes J.M.**
*Motores de combustión interna alternativos.*
Reverté, 2012. (cited on p. 3)

**Payri F., Margot X., Patouna S., Ravet F. and Funk M.**
Use of a single-zone thermodynamic model with detailed chemestry to study a natural gas fueled Homogeneous Charge Compression Ignition engine.
*Energy Conversion and Management*, Vol. 53, pp. 298–304, 2012. (cited on p. 115)

**Payri F., Molina S., Martín J. and Armas O.**
Influence of measurement errors and estimated parameters on combustion diagnosis.
*Applied Thermal Engineering*, Vol. 26, pp. 226–236, 2006. (cited on pp. 108, 283)

**Payri R., Salvador F.J., Gimeno J. and Bracho G.**
A new methodology for correcting the signal cumulative phenomenon on injection rate measurements.
*Experimental Techniques*, Vol. 32, pp. 46–49, 2008. (cited on p. 96)

**Payri Raul, García-Oliver Jose M., Bardi Michele and Manin Julien**.
Fuel temperature influence on diesel sprays in inert and reacting conditions.
*Applied Thermal Engineering*, Vol. 35, pp. 185–195, 2012. (cited on p. 41)

**Payri Raul, Gimeno Jaime, Viera Juan P. and Plazas Alejandro H.**
Needle lift profile influence on the vapor phase penetration for a prototype diesel direct acting piezoelectric injector.
*Fuel*, Vol. 113, pp. 257–265, 2013. (cited on p. 40)

**Payri Raul, Viera Juan Pablo, Pei Yuanjiang and Som Sibendu**.
Experimental and numerical study of lift-off length and ignition delay of a two-component diesel surrogate.
*Fuel*, Vol. 158, pp. 957–967, 2015. (cited on p. 69)

**Pei Y., Mehl M., Liu W., Lu T., Pitz W. J. and Som S.**
A multicomponent blend as a Diesel fuel surrogate for compression ignition engine applications.
*Journal of Engineering for Gas Turbines and Power*, Vol. 137, pp. 111502–111502, 2015. (cited on p. 114)

**Pei Y., Mehl M., Liu W., Lu T.F., Pitz W.J. and Som S.**
A multi-component blend as a diesel fuel surrogate for compression ignition engine applications.
*Proceedings of the ASME 2014 Internal Combustion Engine Division Fall Technical Conference*, Vol. ICEF2014, 2014. (cited on p. 114)

**Pepiot Perrine and Pitsch Heinz**.
Systematic reduction of large chemical mechanisms.
*4th Joint Meeting of the U.S. Sections of the Combustion Institute*, 2005. (cited on p. 71)

**Peters N.**
*Turbulent Combustion.*
Cambridge University Press, 2000. (cited on p. 15)

**Petrucci R. H., Harwood W. S. and Herring F. G.**
*General Chemistry.*
Prentice Hall, 2001. (cited on p. 27)

**Pickett Lyle M. and Siebers Dennis L.**
Soot in diesel fuel jets: effects of ambient temperature, ambient density, and injection pressure.
*Combustion and Flame*, Vol. 138, pp. 114–135, 2004. (cited on p. 40)

**Pickett Lyle M., Siebers Dennis L. and Idicheria Cherian A.**
Relationship between ignition processes and the lift-off length of diesel fuel jets.
*SAE Technical Papers 2005-01-3843*, 2005. (cited on p. 39)

**Pöschl M. and Sattelmayer T.**
Influence of temperature inhomogeneities on knocking combustion.
*Combustion and Flame*, Vol. 153, pp. 562–573, 2008. (cited on pp. 49, 94)

**Rausen D. J., Stefanopoulou A. G., Kang J.-M., Eng J. A. and Kuo T.-W.**
A mean-value model for control of Homogeneous Charge Compression Ignition (HCCI) engines.
*Journal of Dynamic Systems, Measurement, and Control*, Vol. 127, pp. 355, 2005. (cited on p. 37)

**Redón P.**
*Modelling of the nitogen oxides formation process applicable to several diesel combustion modes.*
Doctoral Thesis, Universitat Politècnica de València, Valencia (Spain), 2013. (cited on p. 115)

**Reitz Rolf D.**
CFD combustion models for IC engines.
*Engine Research Center Symposium*, 2007. (cited on p. 72)

**Reyes M., Tinaut F.V., Andrés C. and Pérez A.**
A method to determine ignition delay times for Diesel surrogate fuels from combustion in a constant volume bomb: Inverse Livengood-Wu method.
*Fuel*, Vol. 102, pp. 289–298, 2012. (cited on pp. 37, 40, 52)

**Salaun Erwan, Apeloig Julien, Grisch Frédéric, Yvonnet Charles-Edouard, Nicolas Baptiste and Dionnet Frederic**.
Optical Investigation of Ignition Timing and Equivalence Ratio in Dual-Fuel CNG/Diesel Combustion.
*SAE Technical Papers 2016-01-0772*, 2016. (cited on p. 50)

**Samuelsen S., McDonell V., Greene M. and Beerer D.**
Correlation of ignition delay with natural gas and IGCC type fuels.
*University of California*, Vol. DOE Award Number: DE-FC26-02NT41431 UTSR Project Number: 03-01-SR112, 2006. (cited on p. 65)

**Sarathy S.M., Westbrook C.K., Mehl M., Pitz W.J., Togbe C., Dagaut P., Wang H., Oehlschlaeger M.A., Niemann U., Seshadri K., Veloo P.S., Ji C., Egolfopoulos F.N. and Lu T.**
Comprehensive chemical kinetic modeling of the oxidation of 2-methylalkanes from C7 to C20.
*Combustion and Flame*, Vol. 158, pp. 2338–2357, 2011. (cited on pp. 71, 114)

**Schlatter Stephanie, Schneider Bruno, Wright Yuri and Boulouchos Konstantinos**.
Experimental study of ignition and combustion characteristics of a Diesel pilot spray in a lean premixed methane/air charge using a Rapid Compression Expansion Machine.
*SAE Technical Papers 2012-01-0825*, 2012. (cited on pp. 49, 97)

**Schlatter Stephanie, Schneider Bruno, Wright Yuri M. and Boulouchos Konstantinos**.
Comparative study of ignition systems for lean burn gas engines in an optically accessible Rapid Compression Expansion Machine.
*SAE Technical Papers 2013-24-0112*, 2013. (cited on p. 49)

**Semenov N.**
Thermal theory of combustion and explosion III. Theory of normal flame propagation.
*Progress of Physicai Science (USSR)*, Vol. 24, pp. 433, 1940. (cited on p. 237)

**Several Authors**.
CANTERA description.
*http://cantera.org*, 2016. (cited on p. 72)

**Several Authors**.
CHEMKIN-PRO description.
*http://reactiondesign.com/products/chemkin/chemkin-pro*, 2016. (cited on p. 72)

**Several Authors**.
CMT - Motores Termicos RCEM.
*cmt.upv.es*, 2016. (cited on p. 50)

**Several Authors**.
Lawrence Livermore National Laboratories Chemical Kinetic Mechanisms.
*http://combustion.llnl.gov/mechanisms*, 2016. (cited on pp. 19, 71)

**Several Authors**.
NIST Chemistry WebBook.
*http://webbook.nist.gov/chemistry*, 2016. (cited on p. 276)

**Several Authors**.
TESTEM GMBH.
*http://www.testem.de/26/Einhubtriebwerk/*, 2016. (cited on p. 49)

**Siebers D.**
Ignition delay characteristics of alternative Diesel fuels: Implications on cetane number.
*SAE Technical Papers 852102*, 1985. (cited on p. 40)

**Siebers Dennis L., Higgins Brian and Pickett Lyle**.
Flame lift-off on direct-injection diesel fuel jets: oxygen concentration effects.
*SAE Technical Papers 2002-01-0890*, 2002. (cited on p. 39)

**Simmie John M.**
Detailed chemical kinetic models for the combustion of hydrocarbon fuels.
*Progress in Energy and Combustion Science*, Vol. 29, pp. 599–634, 2003. (cited on p. 19)

**Sjoberg M., Dec J.E. and Cernansky N.P.**
Potential of thermal stratification and combustion retard for reducing pressure-rise rates in HCCI engines, based on multi-zone modeling and experiments.
*SAE Technical Paper 2005-01-0113*, 2005. (cited on pp. 54, 231)

**Sjöberg Magnus and Dec John E.**
An investigation into lowest acceptable combustion temperatures for hydrocarbon fuels in HCCI engines.
*Proceedings of the Combustion Institute*, Vol. 30, pp. 2719–2726, 2005. (cited on p. 114)

**Sjöberg Magnus and Dec John E.**
Effects of EGR and its constituents on HCCI autoignition of ethanol.
*Proceedings of the Combustion Institute*, Vol. 33, pp. 3031–3038, 2011. (cited on p. 60)

**Sjöberg Magnus and Dec John E.**
Effects of EGR and its constituents on HCCI autoignition of ethanol.
*Proceedings of the Combustion Institute*, Vol. 33, pp. 3031–3038, 2011. (cited on p. 160)

**Sjöberg Magnus, Dec John E. and Hwang Wontae**.
Thermodynamic and chemical effects of EGR and its constituents on HCCI autoignition.
*SAE Technical Papers 2007-01-0207*, 2007. (cited on p. 60)

**Skeen Scott A., Manin Julien, Pickett Lyle M., Cenker Emre, Bruneaux Gilles, Kondo Katsufumi, Aizawa Tets, Westlye Fredrik, Dalen Kristine, Ivarsson Anders, Xuan Tiemin, Garcia-Oliver Jose M, Pei Yuanjiang, Som Sibendu, Hu Wang, Reitz Rolf D., Lucchini Tommaso, D'Errico Gianluca, Farrace Daniele, Pandurangi Sushant S., Wright Yuri M., Chishty Muhammad Aqib, Bolla Michele and Hawkes Evatt**.
A progress review on soot experiments and modeling in the Engine Combustion Network (ECN).
*SAE Technical Papers 2016-01-0734*, 2016. (cited on p. 55)

**Soloukhin Rem Ivanovich**.
*Shock waves and detonations in gases.*
Mono Book Corp., Baltimore, 1966. (cited on p. 42)

**Steinhilber T. and Sattelmayer T.**
The effect of water addition on HCCI Diesel combustion.
*SAE Technical Papers 2006-01-3321*, 2006. (cited on pp. 50, 93)

**Strehlow Roger A. and Cohen Arthur**.
Initiation of detonation.
*Physics of Fluids (1958-1988)*, Vol. 5, pp. 97–101, 1962. (cited on p. 42)

**Sung Chih-Jen and Curran Henry J.**
Using Rapid Compression Machines for chemical kinetics studies.
*Progress in Energy and Combustion Science*, Vol. 44, pp. 1–18, 2014.
(cited on pp. 39, 45, 47)

**Swan K., Shahbakhti M. and Koch C.R.**
Predicting start of combustion using a modified knock integral method for an HCCI engine.
*SAE Technical Papers 2006-01-1086*, 2006. (cited on pp. 35, 38)

**Syed I., Mukherjee A. and Naber J.**
Numerical Simulation of Autoignition of Gasoline-Ethanol/Air Mixtures under Different Conditions of Pressure, Temperature, Dilution, and Equivalence Ratio.
*SAE Technical Paper 2011-01-0341*, 2011. (cited on p. 72)

**Tanaka Shigeyuki, Ayala Ferran, Keck James C. and Heywood John B.**
Two-stage ignition in HCCI combustion and HCCI control by fuels and additives.
*Combustion and Flame*, Vol. 132, pp. 219–239, 2003. (cited on p. 62)

**Taylor Charles Fayette**.
*The internal combustion engine in theory and practice.*
M.I.T. Press, Cambridge, Mass, 2nd ed., rev edition, 1985. (cited on p. 2)

**Terashima H. and Koshi M.**
Mechanisms of strong pressure wave generation in end-gas autoignition during knocking combustion.
*Combustion and Flame*, Vol. 162, pp. 1944–1956, 2015. (cited on p. 54)

**Turns S. R.**
*An Introduction to Combustion.*
McGraw-Hill. (cited on p. 16)

**Turányi T.**
Reduction of large reaction mechanisms.
*New Journal of Chemistry*, Vol. 14, pp. 795–803, 1990. (cited on p. 71)

**Turányi T.**
Sensitivity analysis of complex kinetic systems. Tools and applications.
*Journal of Mathematical Chemistry*, Vol. 5, pp. 203–248, 1990. (cited on p. 71)

**Union Eurpoean**.
On type-approval of motor vehicles and engines with respect to emissions from heavy duty vehicles (Euro VI) and on access to vehicle repair and maintenance information and amending Regulation (EC) No 715/2007 and Directive 2007/46/EC and repealing Directives 80/1269/EEC and 2005/78/EC.
*Official Journal of the European Union. Regulation*, 2009. (cited on p. 2)

**Vajda S., Valko P. and Turányi T.**
Principal component analysis of kinetic models.
*International Journal of Chemical Kinetics*, Vol. 17, pp. 55–81, 1985. (cited on p. 71)

**Vandersickel A., Hartmann M., Vogel K., Wright Y.M., Fikri M., Starke R., Schulz C. and Boulouchos K.**
The autoignition of practical fuels at HCCI conditions: High-pressure shock tube experiments and phenomenological modeling.
*Fuel*, Vol. 93, pp. 492–501, 2012. (cited on p. 36)

**Vermeersch M.L., Held T.J., Stein Y. and Dryer F.L**.
Auto-ignition chemistry studies of n-butane in a variable pressure flow reactor.
*SAE Technical Papers 912316*, 1991. (cited on p. 52)

**Versteeg Henk Kaarle and Malalasekera Weeratunge**.
*An Introduction to Computational Fluid Dynamics: The Finite Volume Method.*
Pearson Education, 2007. (cited on p. 264)

**Villela A. C. Scardini, Braga S. Leal, Egusquiza J. C. Cuisano and Machado G. Bastos**.
Rapid Compression Machine tests for brazilian Otto cycle fuels.
*SAE Technical Papers 2011-36-0349*, 2011. (cited on pp. 49, 53, 93)

**W. Sun and Z. Chen, Gou X. and Ju Y.**
A path flux analysis method for the reduction of detailed chemical kinetic mechanisms.
*Combustion and Flame*, Vol. 157, pp. 1298–1307, 2010. (cited on p. 71)

**Wagnon Scott W. and Wooldridge Margaret S.**
Effects of buffer gas composition on autoignition.
*Combustion and Flame*, Vol. 161, pp. 898–907, 2014. (cited on p. 160)

**Wang H. and Frenklach M.**
Detailed reduction of reaction mechanisms for flame modeling.
*Combustion and Flame*, Vol. 87, pp. 365–370, 1991. (cited on p. 71)

**Weber Bryan W., Kumar Kamal, Zhang Yu and Sung Chih-Jen**.
Autoignition of n-butanol at elevated pressure and low-to-intermediate temperature.
*Combustion and Flame*, Vol. 158, pp. 809–819, 2011. (cited on pp. 61, 75)

**Weber Bryan William**.
*Autoigniton of n-butanol at low to intermediate temperature and elevated pressure.*
Doctoral Thesis, University of Connecticut, 2010. (cited on pp. 15, 18)

**Weisser German Andreas**.
*Modelling of combustion and nitric oxide formation for medium-speed DI diesel engines.*
Doctoral Thesis, Diss., Technische Wissenschaften ETH Zürich, Nr. 14465, 2002, 2001.
(cited on p. 36)

**Westbrook Charles K.**
Chemical kinetics of hydrocarbon ignition in practical combustion systems.
*Proceedings of the Combustion Institute*, Vol. 28, pp. 1563–1577, 2000.
(cited on pp. 15, 48)

**Westbrook Charles K., Pitz William J., Herbinet Olivier, Curran Henry J. and Silke Emma J.**
A comprehensive detailed chemical kinetic reaction mechanism for combustion of n-alkane hydrocarbons from n-octane to n-hexadecane.
*Combustion and Flame*, Vol. 156, pp. 181–199, 2009.

**Woschni G.**
A universally applicable equation for the instantaneous heat transfer coefficient in the internal combustion engine.
*SAE Technical Papers 670931*, 1967. (cited on pp. 108, 279)

**Yates Andy D. B., Swarts André and Viljoen Carl L.**
Correlating auto-ignition delays and knock-limited spark-advance data for different types of fuel.
*SAE Technical Papers 2005-01-2083*, 2005. (cited on pp. 38, 74)

**Yoo C.S., Lu T., Chen J.H. and Law C.K.**
Direct numerical simulations of ignition of a lean n-heptane/air mixture with temperature inhomogeneities at constant volume: Parametric study.
*Combustion and Flame*, Vol. 158, pp. 1727–1741, 2011. (cited on p. 54)

**Zeldovich Y.B.**
Regime classification of an exothermic reaction with nonuniform initial conditions.
*Combustion and Flame*, Vol. 39, pp. 211–214, 1980. (cited on p. 230)

**Zhao H., Peng Z., Williams J. and Ladommatos N.**
Understanding the effects of recycled burnt gases on the Controlled Autoignition (CAI) combustion in four-stroke gasoline engines.
*SAE Technical Papers 2001-01-3607*, 2001. (cited on p. 59)

**Zheng Z and Yao M**.
Numerical study on the chemical reaction kinetics of n-heptane for HCCI combustion process.
*Fuel*, Vol. 85, pp. 2605–2615, 2006. (cited on pp. 22, 25)

**Zheng Zunqing, Yue Lang, Liu Haifeng, Zhu Yuxuan, Zhong Xiaofan and Yao Mingfa**.
Effect of two-stage injection on combustion and emissions under high EGR rate on a diesel engine by fueling blends of diesel/gasoline, diesel/n-butanol, diesel/gasoline/n-butanol and pure diesel.
*Energy Conversion and Management*, Vol. 90, pp. 1–11, 2015. (cited on p. 14)

**Zhou L. and Wei H.**
Chemistry acceleration with tabulated dynamic adaptive chemistry in a realistic engine with a primary reference fuel.
*Fuel*, Vol. 171, pp. 186–194, 2016. (cited on p. 54)